

Mechanical and Tribological Characterization of Borohydride Reduced Electroless Nickel Coatings

Thesis submitted by

MANIK BARMAN

**Doctor of Philosophy
(Engineering)**

**DEPARTMENT OF MECHANICAL ENGINEERING
FACULTY COUNCIL OF ENGINEERING & TECHNOLOGY
JADAVPUR UNIVERSITY
KOLKATA, INDIA**

2024

JADAVPUR UNIVERSITY
KOLKATA-700032, INDIA

INDEX NO. 39/22/E

1. Title of Thesis:

Mechanical and Tribological Characterization of Borohydride Reduced Electroless Nickel Coatings

2. Name, Designation & Institution of the Supervisor: Prof.

Tapan Kumar Barman

Professor, Department of Mechanical Engineering, Jadavpur
University, Kolkata-700032

Prof. Prasanta Sahoo

Professor, Mechanical Engineering Department, Jadavpur
University, Kolkata-700032

3. List of Publications (Referred Journals):

3.1 Journals Published

1. Barman, M., Barman, T. K., & Sahoo, P. (2024). Effects of W and Mo Concentrations on Mechanical Behaviour of Ni-B Based Coatings - A Comparative Study. Journal of the Institution of Engineers (India): Series D, 1-18. <https://doi.org/10.1007/s40033-024-00696-7>. **Indexing: Scopus**
2. Barman, M., Barman, T. K., & Sahoo, P. (2023). Tribological Behavior of Electroless Ni-B Ternary and Quaternary Coatings with Inclusion of W and Mo. Physica Scripta, 99(2), 025924. <https://doi.org/10.1088/1402-4896/ad19bc>. **Indexing: SCIE**
3. Barman, M., Barman, T. K., & Sahoo, P. (2023). Corrosion Behaviour of Borohydride Reduced Ni-B, Ni-B-W, Ni-B-Mo, Ni-B-W-Mo Coatings with Varying Composition: A Comparison. Journal of the Institution of Engineers (India): Series D, 1-19. <https://doi.org/10.1007/s40033-023-00574-8>. **Indexing: Scopus**
4. Barman, M., Barman, T. K., & Sahoo, P. (2023). Tribo-Mechanical Behaviour of Electroless Ni-B-Mo Coatings with Varying Bath Composition. Engineering Research Express, 5(2), 025072. <https://doi.org/10.1088/2631-8695/acdd52>. **Indexing: ESCI**
5. Barman, M., Barman, T. K., & Sahoo, P. (2023). Tribo-Mechanical Characterisation of Borohydride Reduced Ni-B-W Coatings. Journal of the Institution of Engineers (India): Series D,

1-21. <https://doi.org/10.1007/s40033-023-00471-0>. **Indexing: Scopus**

6. Barman, M., Barman, T. K., & Sahoo, P. (2023). Effect of Heat-Treatment Temperature and Borohydride Concentration on Corrosion Behaviour of ENB Coating. Proceedings of the Institution of Mechanical Engineers, Part C: Journal of Mechanical Engineering Science, 237(1), 183-200. <https://doi.org/10.1177/09544062221117677>. **Indexing: SCI**
7. Barman, M., Barman, T. K., & Sahoo, P. (2022). Tribo-Mechanical Characterization of ENB Alloy Coatings: Effect of Heat-treatment Temperature and Sodium Borohydride Concentration. Facta Universitatis, Series: Mechanical Engineering. <https://doi.org/10.22190/FUME220814041B>. **Indexing: SCI**
8. Barman, M., Barman, T. K., & Sahoo, P. (2022). Effect of Coating Bath Parameters on Properties of Electroless Nickel-Boron Alloy Coatings. International Journal of Surface Engineering and Interdisciplinary Materials Science (IJSEIMS), 10(1), 1-26. [DOI: 10.4018/IJSEIMS.2022010101](https://doi.org/10.4018/IJSEIMS.2022010101). **Indexing: Scopus**
9. Barman, M., Barman, T. K., & Sahoo, P. (2019). Effect of Borohydride Concentration on Tribological and Mechanical Behavior of Electroless Ni-B Coatings. Materials Research Express, 6(12), 126575. <https://doi.org/10.1088/2053-1591/ab58b7>. **Indexing: SCI**

4. List of Patents: Nil

5. List of Presentations in National / International Conferences:

1. Barman, M., Barman, T. K., & Sahoo, P. (2024). “Corrosion Resistance of Electroless Ni-B-W Coatings” Proceedings of the 2nd International Conference on Mechanical Engineering (INCOM 2024), Jadavpur University, Kolkata, 5-6 January 2024: Paper No. INCOM405.
2. Barman, M., Barman, T. K., & Sahoo, P. (2023). “Optimization of Tribo-Mechanical Properties of ENB Coatings using GRA And ANOVA” Book of Abstracts of 1st International Conference on Mechanical Design and Manufacturing (ICMDM 2023), April 27-28, 2023, IEST Shibpur, INDIA, Paper ID: ICMDM 2023-232.
3. Barman, M., & Barman, T. K. (2021). “Optimization of Mechanical Properties of Electroless Ni-B Coatings using Grey Relational Analysis.” Paper presented at National Conference on Sustainable Development and Circular Economy in Civil Engineering (SDCE 2021), Heritage Institute of Technology, Kolkata, 16-17 December 2021.

4. Barman, M., Barman, T. K., & Sahoo, P. (2020). “Change in Tribological Behaviour of Electroless Ni-B Coatings with Bath Composition and Heat Treatment Temperature” Paper presented at International Conference on Thermal Engineering and Management Advances (ICTEMA 2020), Jalpaiguri Govt. Engineering College, India, December 19-20, 2020.
5. Barman, M., Barman, T. K., & Sahoo, P. (2020). “Variation of Corrosion Resistance of Electroless Ni-B Coatings with Reducing Agent and Heat Treatment Temperature” e-Proceedings of International Conference on Advancements in Mechanical Engineering (ICAME 2020), Aliah University, Kolkata, 16-18 January 2020: Paper No. ICAME 00031 (63-68).

6. List of Book Chapters: Nil

This page is intentionally left blank

STATEMENT OF ORIGINALITY

I, **MANIK BARMAN** registered on **22.04.2022** do hereby declare that this thesis entitled “**Mechanical and Tribological Characterization of Borohydride Reduced Electroless Nickel Coatings**” contains literature survey and original research work done by the undersigned candidate as part of Doctoral studies.

All information in this thesis have been obtained and presented in accordance with existing academic rules and ethical conduct. I declare that, as required by these rules and conduct, I have fully cited and referred all materials and results that are not original to this work.

I also declare that I have checked this thesis as per the “Policy on Anti Plagiarism, Jadavpur University, 2019”, and the level of similarity as checked by iThenticate software is 2%.

Signature of Candidate: Manik Barman 16/07/24

(**MANIK BARMAN**)

Date: 16th July 2024

Certified by Supervisor: Tapan Kr. Barman 16/07/24
(Signature with date, seal) (**Dr. Tapan Kumar Barman**)

Professor
Dept. of Mechanical Engineering
Jadavpur University, Kolkata-32

Certified by Supervisor: Prasanta Sahoo 16/7/24
(Signature with date, seal) (**Dr. Prasanta Sahoo**)

Professor
Dept. of Mechanical Engineering
Jadavpur University, Kolkata-32

This page is intentionally left blank

CERTIFICATE FROM THE SUPERVISORS

This is to certify that the thesis entitled “*Mechanical and Tribological Characterization of Borohydride Reduced Electroless Nickel Coatings*” submitted by **MANIK BARMAN**, who got his name registered on **22.04.2022** for the award of Ph.D. (Engineering) degree of Jadavpur University is absolutely based upon his own work under the supervision of **Prof. Tapan Kumar Barman** and **Prof. Prasanta Sahoo** and that neither his thesis nor any part of the thesis has been submitted for any degree/diploma or any other academic award anywhere before.

Tapan Kr. Barman
16/07/24

(Prof. Tapan Kumar Barman)

Signature of the Supervisor
and date with Office Seal

Professor
Dept. of Mechanical Engineering
Jadavpur University, Kolkata-32

Prasanta Sahoo
16/7/24.

(Prof. Prasanta Sahoo)

Signature of the Supervisor
and date with Office Seal

Professor
Dept. of Mechanical Engineering
Jadavpur University, Kolkata-32

This page is intentionally left blank

Electroless nickel (EN) plating is a deposition process by chemical reaction of reducing agent present in the coating bath itself without the use of electricity. It has received widespread attention for industrial applications due to its high hardness, good corrosion resistance, uniformity of coatings, etc. EN coatings can be classified into three main categories, namely pure nickel, alloy, and composite coatings. Several research studies have been already carried out to investigate the characteristics of EN Pure coating, binary (Ni-B, Ni-P, etc.), and ternary alloy coatings (Ni-W-P, Ni-Cu-P, etc.). Metallic elements like tungsten (W), Cobalt (Co), molybdenum (Mo) have been incorporated to form binary, ternary, or quaternary alloys to improve the properties like thermal stability, hardness, tribological behavior, and corrosion resistance. Nanoparticles like Al_2O_3 , SiO_2 , ZrO_2 , TiO_2 , and SiC are being widely used due to their excellent wear resistance and hardness. TiN also can be an ideal candidate for coating due to its high hardness, chemical resistance, and high melting point. Carbon nanotube (CNT) and Carbon nanofibers (CNFs) are being used since they possess outstanding electrochemical and mechanical properties including high tensile strength and elastic modulus. The electroless nickel-based alloy coatings were investigated based on coating deposition rate, coating thickness, surface morphology, phase structure, tribological and mechanical behaviors of coatings. The deposition rate and coating thickness were observed to vary with coating bath parameter concentration as well as operating conditions. The surface morphology and phase structure were also observed to depend on coating bath composition. The surface morphology, as well as phase structure ultimately, lead to a change in coating characteristics.

It was observed from the literature survey that electroless Ni-B (ENB) coatings deposited with low sodium borohydride in the coating bath exhibit a crystalline structure. The same transformed into an amorphous structure with the rise in sodium borohydride concentration leading to an increase in surface hardness of the coatings. The surface hardness also improved due to the rise in boron content in the coatings with the increase in sodium borohydride concentration in the coating bath solution. Hence, the variation of the coating bath parameters and concentration may impact the coating composition. The coating composition may lead to a change in surface roughness, surface morphology, and phase structure which may ultimately lead to a change in coating characteristics. The present work explores the dependencies of bath parameters on the coating characteristics of different electroless nickel coatings such as Ni-B,

Ni-B-W, and Ni-B-Mo, etc.

In the present work, an attempt is made to deposit Electroless Ni-B, Ni-B-W, and Ni-B-Mo, etc. coatings on mild steel substrate. Analysis of the performance of the coatings in terms of mechanical properties and tribological characteristics are made. The surface roughness of the coatings is compared with the surface roughness of the uncoated substrate. The friction and wear behavior of coatings are evaluated using a tribo-tester. Surface hardness, as well as scratch test, are carried out. Mechanical properties like Elastic modulus, nano-hardness are evaluated using the nanoindentation technique. Scanning electron microscope (SEM), X-ray diffraction technique (XRD) and energy dispersive X-ray (EDAX) analysis are used to study surface morphology, microstructure, and composition, respectively. Finally, a comparative study is conducted to compare the performances of Ni-B, Ni-B-W, and Ni-B-Mo, etc.

The present thesis contains seven chapters. Chapter 1 introduce electroless nickel coatings and surveys the relevant literature to arrive at the specific objectives. Chapter 2 presents the materials and methods used I the present study. Chapter 3, 4 and 5 considers the mechanical and tribological behaviour of Ni-B, Ni-B-W and Ni-B-Mo coatings, respectively. For each of these variants, coating thickness, surface morphology, chemical composition, phase structure, surface roughness, hardness, scratch-resistance, friction, wear and corrosion resistance have been considered in detail. Chapter 6 presents a comparative study of these alloy coatings. Finally, the set of conclusions and scope of future study are presented in Chapter 7.

About the Author

The author Shri **Manik Barman** was born in Alipurduar, a district place of West Bengal state in the year 1989. He spent his childhood days and completed 10+2 education from the same place. He graduated in Mechanical Engineering (B. Tech) in 2011 from Jalpaiguri Government Engineering College, Jalpaiguri, West Bengal. He completed Master of Technology (M. Tech) in Mechanical Engineering (Production Technology and Management) from Jalpaiguri Government Engineering College, Jalpaiguri, West Bengal in 2015. After post-graduation, he started his career as a teaching faculty in the Department of Mechanical Engineering of Heritage Institute of Technology. He is currently pursuing PhD (Engineering) at Jadavpur University Kolkata.

This page is intentionally left blank

Acknowledgement

The present thesis is the result of the doctoral research work carried out in the last few years. It has been never been easy. Though, a number of people have supported me during this journey to complete the doctoral research work. Thus, it is my humble duty to convey my sincere thanks to all who were directly or indirectly associated with this research work and showed their faith, support as well as motivated me.

Firstly, I would like to pay my heartfelt gratitude to my respected supervisor, Prof. Tapan Kumar Barman sir, without whom this research work wouldn't have been possible. It was not easy for me to adapt to the environment coming from a background where there was no idea of research and no such educational background. But, the methodical and visionary guidance from him helped me a lot in enriching myself during the period of work. His continuous help, support and motivation during all these days made things simpler. I feel blessed to have the opportunity to work under his supervision. He never missed to correct the smallest mistakes in the research papers. Thus, he has showed me the path towards perfection. He also has ample of time and patience to hear all my issues.

I would like to thank my co-supervisor Prof. Prasanta Sahoo Sir as well. I feel myself fortunate enough for considering me to be a suitable candidate to work under his supervision and receiving his guidance throughout my journey of doctoral research. His advice, little inputs about the research paper and even in personal life enriched me a lot. His dedication, work ethics, approach towards work and life is a lifetime learning experience for me.

I would like to thank the Lab-in-Charge of Machine Elements Lab of Mechanical Engineering Department of Jadavpur University where the majority of the research work was carried out. I also thank to the technical staffs of the Machine Element Lab for their appreciation during my research work. I must specially thank to HOD Sir, Department of Mechanical Engineering for allowing me to carry out the research work and for providing time to time assistance. I also thank to the Department of Mechanical Engineering, Jadavpur University for providing the financial support to carry out research works smoothly.

In this regard, I must thank Dr. Arkadeb Mukhopadhyay, who introduced me to this world

of research activities and motivated me to start the research activity. I have learned my preliminary knowledge of coating. I have received my hands on training by him on coating deposition process, basic coating characterizations to be carried out, the tests to be carried out, from where to carry out and whom to contact and how to approach. He also taught me how to write research papers with ease. This way, his continuous support, constructive suggestions and positive inputs smoothened my journey a lot. Even today, he is always there to help me out whenever I am stuck in any difficult situation. Thus, he deserves special thanks since he is one of the key persons behind my doctoral research work.

I must not forget the person with whom I have started my journey. He is our beloved Dr. Deviprasanna Mohanty. He has always been very kind and very helpful throughout my journey. During this period, I have learned a lot from him and I am thankful to him for his continuous, selfless supports and suggestions whenever needed. He is another person who helped me a lot to carry out experiments starting from the use of Tribo-tester, Scratch Tester and Hardness Tester. His calm and cool nature in any circumstances is also a learning experience for me.

I spent the initial days of my research work in the lab with Dr. Brajesh Panigrahi, Dr. Priyambada Nayek, Dr. Suswagata Poria, Dr. Sushanta Ghuku, Dr. Hareram Lohar, Dr. Tamonash Jana, Dr. Sudip Banerjee. I really admire their dedication, passion and enthusiasm to work continuously which inspired me a lot to work harder. I would also like to thank Dr. Abhijit Biswas, Mr. Palash Biswas with whom I spent a lot of time in Lab. I also thank to all of my lab mates Rakesh Da, Vikram Sir with whom I spent the latter stages of my research work. I am also thankful to Shashi Kumar Prithwi, Ranjit, Anurag, Arindam, Sudip, Morselim, Sagar da, Sagnik, Rohit with whom I spent the last days of my research work.

During my research activities, I have met many people from different Institutions for different purposes like testing of materials, and material characterisation work. In this context, I must appreciate the support received from the technical staff (Krishanu, Dipanjan) at IEST Shibpur, MMMF lab for carrying out SEM, EDS, Nano-indentation tests. I also thank the technical staff of S N Bose National Centre for Basic Sciences and NIT, Durgapur for allowing to use their test facilities which are key part of my research work.

I am thankful to Dr. Sukanta Sarkar, HOD, Department of Mechanical Engineering, Heritage Institute of Technology for supporting me in different ways which helped me to carry out the research work. I would also like to thank the Management of Heritage Institute of Technology for providing a half day on duty leave per week to carry out the research work outside institution. I also thank to all my colleagues of Heritage Institute of Technology especially Vishnu and Pritam who directly or indirectly helped me time to time whenever needed. They always helped by adjusting my class whenever I have taken leave for research work or went outside for my research work.

I am also thankful to the past researchers in this field whose published literatures helped me to understand the topic in a better way and decide my path of action needed to carry out my doctoral research work. I would also like to thank those who directly or indirectly helped me throughout this journey.

Finally, last but certainly not the least, I would like to thank my parents beloved family members for understanding me when I was busy in research work in the Lab instead of being at home even during the vacations. I also thank to my well-wishers and friends for their patience and constant support without which this work couldn't have been completed. Please do forgive me if I have forgotten to mention anyone who has been a part of this journey. Thanks a lot again.

Manik Barman 16/07/24
MANIK BARMAN

This page is intentionally left blank

*Dedicated to My Parents
Supervisors and
Beloved Wife*

This page is intentionally left blank

Table of Contents

Content	Page No.
List of Publications and Presentations from the Thesis	i-iii
Statement of Originality	iv
Certificate from the Supervisors	v
Abstract	vi-vii
About the Author	viii
Acknowledgement	ix-xi
Table of Contents	xii-xvi
List of Figures	xvii-xxiii
List of Tables	xxiv
Chapter 1: Surface Modification – Electroless Coating and Its Evolution	1-39
1.1 Introduction	1
1.2 Surface Modification	2
1.3 Electroless Coating Process	5
1.4 Bath Composition and Deposition of Electroless Coatings	9
1.5 Development of Electroless Coating Process with Time	13
1.6 Application of Electroless Coatings	15
1.7 Literature Review on Nickel Based Electroless Coatings	16
1.7.1 Influence of Parameters on Deposition Rate	17
1.7.2 Surface Morphology, Phase Structure	21
1.7.3 Physical and Mechanical Properties	25
1.7.3.1 Surface Roughness	25
1.7.3.2 Surface Hardness	26

1.7.3.3 Ductility and Tensile Strength	27
1.7.4 Tribological Test	28
1.7.5 Corrosion Resistance Test	31
1.7.6 Nanocomposite Coatings	32
1.7.7 Lead Free Coatings with the use of Green Bath	33
1.8 Summary of Literature Review	36
1.9 Research Work Plan	38
1.10 Research Objectives	38
1.11 Research Work Methodology	38
1.12 Closure	39
Chapter 2: Materials and Methods	40-62
2.1 Introduction	40
2.2 Sample Preparation	41
2.3 Bath Composition and Coating Deposition	41
2.4 Coating Characterisation	45
2.4.1 Coating Thickness	45
2.4.2 Surface Morphology	46
2.4.3 Chemical Composition	48
2.4.4 Phase Structure	50
2.5 Physical and Mechanical Behaviours	51
2.5.1 Surface Roughness	51
2.5.2 Nano-indentation Test	53
2.5.3 Micro-Scratch Test	55
2.6 Tribological Test	57
2.7 Corrosion Resistance Test	59

2.7.1	Potentiodynamic Polarization	60
2.7.2	Electrochemical Impedance Spectroscopy	62
2.8	Closure	64
Chapter 3: Electroless Ni-B Alloy Coatings		65-88
3.1	Introduction	65
3.2	Experimental Details	65
3.3	Coating Characterisation	66
3.3.1	Coating Thickness	66
3.3.2	Surface Morphology	67
3.3.3	Chemical Composition	69
3.3.4	Phase Structure	71
3.4	Physical and Mechanical Behaviours	73
3.4.1	Surface Roughness	73
3.4.2	Nano-indentation Test	74
3.4.3	Micro-Scratch Test	77
3.5	Tribological Test	78
3.6	Corrosion Resistance Test	84
3.7	Closure	89
Chapter 4: Electroless Ni-B-W Alloy Coatings		91-118
4.1.	Introduction	91
4.2.	Experimental Details	91
4.3.	Coating Characterisation	92
4.3.1	Coating Thickness	92
4.3.2	Surface Morphology	93

4.3.3	Chemical Composition	95
4.3.4	Phase Structure	97
4.4	Physical and Mechanical Behaviours	99
4.4.1	Surface Roughness	99
4.4.2	Nano-indentation Test	101
4.3.3	Micro-Scratch Test	105
4.5	Tribological Test	107
4.6	Corrosion Resistance Test	113
4.7	Closure	118
Chapter 5: Electroless Ni-B-Mo Alloy Coatings		119-150
5.1	Introduction	117
5.2	Experimental details	117
5.3	Coating Characterisation	120
5.3.1	Coating Thickness	120
5.3.2	Surface Morphology	121
5.3.3	Chemical Composition	123
5.3.4	Phase Structure	125
5.4	Physical and Mechanical Behaviours	127
5.4.1	Surface Roughness	127
5.4.2	Nano-indentation Test	129
5.4.3	Micro-Scratch Test	136
5.5	Tribological Test	136
5.6	Corrosion Resistance Test	144
5.7	Closure	149

Chapter 6: Comparison of Electroless Ni-B, Ni-B-W and Ni-B-Mo Alloy Coatings	151-185
6.1 Introduction	151
6.2 Experimental Details	151
6.3 Coating Characterisation	153
6.3.1 Coating Thickness	153
6.3.2 Surface Morphology	155
6.3.3 Chemical Composition	158
6.3.4 Phase Structure	159
6.4 Physical and Mechanical Behaviours	162
6.4.1 Surface Roughness	162
6.4.2 Nano-indentation Test	164
6.4.3 Micro-Scratch Test	168
6.5 Tribological Test	169
6.6 Corrosion Resistance Test	180
6.7 Closure	185
Chapter 7. Conclusions and Future Scope	186-192
7.1 Conclusions	186
7.2 Future scope	192
References	193-209
Publications from the Thesis	210-218

This page is intentionally left blank

List of Figures

Figure no.	Figure Caption	Page No.
Figure 1.1	Surface Modification Technique used in Industries	3
Figure 1.2	Various Coating Techniques	3
Figure 1.3	A Schematic Diagram of a Typical Electroless Coating Set up	7
Figure 1.4	Electroless Coating Deposition Mechanism, (a) Ion Reduction & Deposition Mechanism and (b) Columnar Structure Development Mechanism	12
Figure 1.5	Development and Modification of Electroless Ni-B Since Evolution	14
Figure 1.6	Coating Deposition Rate vs Bath Temperature Plot	18
Figure 1.7	Coating Deposition Rate vs Coating Bath Solution pH Plot	19
Figure 1.8	Coating Deposition Rate vs Sodium Phosphate Concentration Plot	20
Figure 1.9	Typical Surface Morphology of Electroless Ni-P-Cu Coatings, (a) As-deposited (800X), (b) As-deposited (2500X), (c) Heat Treated (800X) and (d) Heat Treated (2500X) Conditions	21
Figure 1.10	XRD Spectrum of Electroless Ni-P-Cu Coatings, (a) As-deposited and (b) Heat-treated Conditions	23
Figure 1.11	Typical Surface Morphology of Electroless Ni-B Coatings Obtained at Sodium Borohydride Concentration of (a) 0.50 g/l and (b) 1.0 g/l	23
Figure 1.12	XRD Spectrum of As-deposited and Heat Treated Electroless Ni-B Coatings	24
Figure 1.13	Ductility vs Phosphorous Content Plot for Electroless Ni-P Coatings	27
Figure 1.14	Tensile Strength vs Phosphorous Content Plot for Electroless Ni-P Coatings	28
Figure 1.15	Research Work Plan	37
Figure 1.16	Research Methodology to be Followed	39

Figure 2.1	Flowchart of Sample Preparation	40
Figure 2.2	Flowchart of Coating Deposition	42
Figure 2.3	Coating Deposition Set up	44
Figure 2.4	(a) Prepared Cylindrical Specimen and (b) Weighing Balance	44
Figure 2.5	Coated Substrates	45
Figure 2.6	Schematic Diagram of Coated Layer Thickness	45
Figure 2.7	SEM, S3400N, HITACHI	46
Figure 2.8	FESEM, SIGMA, CARL ZEISS	47
Figure 2.9	SEM Image of Coated Surface Morphology, (a) SEM Image and (b) FESEM Image	47
Figure 2.10	Representative EDAX Mapping Images of Coated Surface	48
Figure 2.11	Representative EDAX Spectrum of Coatings	49
Figure 2.12	X-ray Diffraction (XRD) Instrument (D8ADVANCED, BRUKER, USA)	50
Figure 2.13	XRD Spectrum of Coatings	51
Figure 2.14	Surface Roughness Tester (Surftonic3+, Taylor Hobson)	52
Figure 2.15	Nano-indentation Test Setup (NHT-1, CSM)	53
Figure 2.16	A Typical Loading-unloading Curve	54
Figure 2.17	Micro-Scratch Tester (TR-101-IAS, DUCOM, India)	55
Figure 2.18	Schematic Diagram of Scratch Test Process	56
Figure 2.19	Typical Image of Scratch Width	57
Figure 2.20	Schematic Diagram of Pin-on-disk Tribo-Tester	58

Figure 2.21	Pin-on-disk Tribo-Tester (TR-20LE-CHM-400, DUCOM, India)	59
Figure 2.22	Electrochemical Corrosion Test Set up (3 Electrode Potentiostat)	60
Figure 2.23	Typical Tafel Plot	61
Figure 2.24	Randle's Circuit Obtained from Gill AC Instrument for (a) Ideal Behaviour and (b) Non-ideal Behaviour	63
Figure 2.25	Typical Nyquist Plot	63
Figure 3.1	SEM Image of Coating Thickness of As-deposited Ni-B Coatings Obtained at (a) Low Level, (b) Mid-Level and (c) High Level Concentrations	67
Figure 3.2	SEM Image of Surface Morphology of As-deposited Ni-B Coatings Obtained at (a) Low Level, (b) Mid-Level and (c) High Level Concentrations	68
Figure 3.3	EDAX Mapping Image of As-deposited Ni-B Coatings Obtained at (a)-(b) Low Level, (c)-(d) Mid-Level and (e)-(f) High Level Concentrations	70
Figure 3.4	EDAX Spectrum of As-deposited Electroless Ni-B Coatings Obtained at (a) Low Level, (b) Mid-Level and (c) High Level Concentrations	71
Figure 3.5	XRD Pattern of As-deposited Ni-B Coatings	72
Figure 3.6	Average Surface Roughness Plot with varying Temperature and (a) Sodium Borohydride and (b) Nickel Chloride Concentrations	73
Figure 3.7	Depth of Indentation vs Applied Load Plot	75
Figure 3.8	Hardness Plot with Varying Temperature and (a) Sodium Borohydride and (b) Nickel Chloride Concentrations	75
Figure 3.9	Elastic Modulus Plot with Varying Temperature and (a) Sodium Borohydride and (b) Nickel Chloride Concentrations	77
Figure 3.10	Scratch-Hardness Plot with Varying Temperature and (a) Sodium Borohydride and (b) Nickel Chloride Concentrations	78
Figure 3.11	Coefficient of Friction (COF) vs Sliding Duration Plot	79

Figure 3.12	Average Coefficient of Friction (COF) Plot with Varying Temperature and (a) Sodium Borohydride and (b) Nickel Chloride Concentrations	79
Figure 3.13	Specific Wear Rate Plot with Varying Temperature and (a) Sodium Borohydride and (b) Nickel Chloride Concentrations	81
Figure 3.14	SEM Image of Worn-out Surface of As-deposited Ni-B Coatings Obtained at (a)-(b) Low Level, (c)-(d) Mid Level and (e)-(f) High Level Concentrations	82
Figure 3.15	EDAX Spectrum of Worn-out Surfaces of As-deposited Ni-B Coatings Obtained at (a) Low Level, (b) Mid Level and (c) High Level Concentrations	83
Figure 3.16	EIS and PDP Test Plot for As-deposited Ni-B Coatings, (a) Nyquist Plot and (b) Tafel Plot	84
Figure 3.17	SEM Image of Corroded Surface of As-deposited Ni-B Coatings Obtained at (a) Low Level, (b) Mid Level and (c) High Level Concentrations	86
Figure 3.18	EDAX Result of Corroded Surface of As-deposited Ni-B Coatings Obtained at (a) Low Level, (b) Mid-Level and (c) High Level Concentrations	89
Figure 4.1	SEM Image of Coating thickness of As-deposited Ni-B-W Coatings Obtained at (a) Low Level, (b) Mid Level and (c) High Level Concentrations	93
Figure 4.2	SEM Image of Surface Morphology for As-deposited Ni-B-W Coatings Obtained at (a) Low Level, (b) Mid Level and (c) High Level Concentrations	94
Figure 4.3	EDAX Mapping Image of As-deposited Ni-B-W Coatings Obtained at (a) Low Level, (b) Mid Level and (c) High Level Concentrations	96
Figure 4.4	EDAX Spectrum of As-deposited Ni-B-W Coatings Obtained at (a) Low Level, (b) Mid Level and (c) High Level Concentrations	97
Figure 4.5	XRD Pattern of As-deposited Ni-B-W Coatings	98
Figure 4.6	Average Surface Roughness Plot with Varying Temperature and (a) Sodium Borohydride, (b) Nickel Chloride and (c) Sodium Tungstate Concentrations	100
Figure 4.7	Depth of Indentation vs Applied Load Plot	101
Figure 4.8	Hardness Plot with Varying Temperature and (a) Sodium Borohydride, (b) Nickel Chloride and (c) Sodium Tungstate Concentrations	103

Figure 4.9	Elastic Modulus Plot with Varying Temperature and (a) Sodium Borohydride, (b) Nickel Chloride and (c) Sodium Tungstate Concentrations	104
Figure 4.10	Scratch-Hardness Plot with Varying Temperature and (a) Sodium Borohydride, (b) Nickel Chloride and (c) Sodium Tungstate Concentrations	106
Figure 4.11	Coefficient of Friction (COF) vs Sliding Duration Plot	107
Figure 4.12	Average Coefficient of Friction (COF) Plot with Varying Temperature with (a) Sodium Borohydride, (b) Nickel Chloride and (c) Sodium Tungstate Concentrations	108
Figure 4.13	Specific Wear Rate Plot with Varying Temperature with (a) Sodium Borohydride, (b) Nickel Chloride and (c) Sodium Tungstate Concentrations	110
Figure 4.14	SEM Image of Worn-out Surface of As-deposited Ni-B-W Coatings Obtained at (a) Low Level, (b) Mid Level and (c) High Level Concentrations	111
Figure 4.15	EDAX Spectrum of Worn-out Surfaces of As-deposited Ni-B-W Coatings Obtained at (a) Low Level, (b) Mid Level and (c) High Level Concentrations	112
Figure 4.16	EIS and PDP Test Plot for As-deposited Ni-B-W Coatings, (a) Tafel Plot and (b) Nyquist Plot	114
Figure 4.17	SEM Image of Corroded Surface of As-deposited Ni-B-W Coatings Obtained at (a) Low Level, (b) Mid-Level and (c) High Level Concentrations	115
Figure 4.18	EDAX Result of Corroded Surface of As-deposited Ni-B-W Coatings Obtained at (a) Low Level, (b) Mid-Level and (c) High Level Concentrations	117
Figure 5.1	SEM Image of Coating thickness of As-deposited Ni-B-Mo Coatings Obtained at (a) Low Level, (b) Mid Level and (c) High Level Concentrations	121
Figure 5.2	SEM Image of Surface Morphology for As-deposited Ni-B-Mo Coatings Obtained at (a) Low Level, (b) Mid Level and (c) High Level Concentrations	122
Figure 5.3	EDAX Mapping Image of As-deposited Ni-B-Mo Coatings Obtained at (a) Low Level, (b) Mid Level and (c) High Level Concentrations	124
Figure 5.4	EDAX Spectrum of As-deposited Ni-B-Mo Coatings Obtained at (a) Low Level, (b) Mid Level and (c) High Level Concentrations	125
Figure 5.5	XRD Pattern of As-deposited Ni-B-Mo Coatings	127

Figure 5.6	Average Surface Roughness Plot with Varying Temperature and (a) Sodium Borohydride, (b) Nickel Chloride and (c) Sodium Molybdate Concentrations	129
Figure 5.7	Depth of Indentation vs Applied Load Plot	130
Figure 5.8	Hardness Plot with Varying Temperature and (a) Sodium Borohydride, (b) Nickel Chloride and (c) Sodium Molybdate Concentrations	132
Figure 5.9	Elastic Modulus Plot with Varying Temperature and (a) Sodium Borohydride, (b) Nickel Chloride and (c) Sodium Molybdate Concentrations	134
Figure 5.10	Scratch-Hardness Plot with Varying Temperature and (a) Sodium Borohydride, (b) Nickel Chloride and (c) Sodium Molybdate Concentrations	135
Figure 5.11	Coefficient of Friction (COF) vs Sliding Duration Plot	137
Figure 5.12	Average Coefficient of Friction (COF) Plot with Varying Temperature with (a) Sodium Borohydride, (b) Nickel Chloride and (c) Sodium Molybdate Concentrations	138
Figure 5.13	Specific Wear Rate Plot with Varying Temperature with (a) Sodium Borohydride, (b) Nickel Chloride and (c) Sodium Molybdate Concentrations	140
Figure 5.14	SEM Image of Worn-out Surface of As-deposited Ni-B-Mo Coatings Obtained at (a) Low Level, (b) Mid Level and (c) High Level Concentrations	142
Figure 5.15	EDAX Spectrum of Worn-out Surfaces of As-deposited Ni-B-Mo Coatings Obtained at (a) Low Level, (b) Mid Level and (c) High Level Concentrations	143
Figure 5.16	EIS and PDP Test Plot for As-deposited Ni-B-Mo Coatings, (a) Tafel Plot and (b) Nyquist Plot	145
Figure 5.17	SEM Image of Corroded Surface of As-deposited Ni-B-Mo Coatings Obtained at (a) Low Level, (b) Mid-Level and (c) High Level Concentrations	146
Figure 5.18	EDAX Result of Corroded Surface of As-deposited Ni-B-Mo Coatings Obtained at (a) Low Level, (b) Mid-Level and (c) High Level Concentrations	149
Figure 6.1	As-deposited Coating Thickness for (a) Ni-B, (b) Ni-B-W and (c) Ni-B-Mo and (d) Comparative Plot	154

Figure 6.2	Surface Morphology of Electroless Coatings Obtained at Low Level of Concentrations (a) Ni-B, (b) Ni-B-W, and (c) Ni-B-Mo	155
Figure 6.3	Surface Morphology of Electroless Coatings Obtained at Mid Level of Concentrations (a) Ni-B, (b) Ni-B-W, and (c) Ni-B-Mo	156
Figure 6.4	Figure 6.4: Surface Morphology of Electroless Coatings Obtained at High Level of Concentrations (a) Ni-B, (b) Ni-B-W, and (c) Ni-B-Mo	157
Figure 6.5	XRD Patterns of As-deposited Electroless Coatings (a) Ni-B, (b) Ni-B-W and (c) Ni-B-Mo	161
Figure 6.6	Comparative Average Surface Roughness (Ra in μm) Plot	163
Figure 6.7	Comparative Hardness Obtained from Nano-indentation	166
Figure 6.8	Comparative Elastic Modulus Obtained from Nano-indentation	167
Figure 6.9	Comparative Scratch Hardness Plot	169
Figure 6.10	Comparative COF Plot at Various Concentration Levels	170
Figure 6.11	Comparative Specific Wear Rate Plot	172
Figure 6.12	SEM Image of Worn-out Surface of As-deposited Coatings Obtained at Low Level Concentrations of (a) Ni-B, (b) Ni-B-W and (c) Ni-B-Mo	174
Figure 6.13	SEM Image of Worn-out Surface of As-deposited Coatings Obtained at Mid-Level Concentrations of (a) Ni-B, (b) Ni-B-W and (c) Ni-B-Mo	175
Figure 6.14	SEM Image of Worn-out Surface of As-deposited Coatings Obtained at High Level Concentration of (a) Ni-B, (b) Ni-B-W and (c) Ni-B-Mo	176
Figure 6.15	EDAX Spectrum of Worn-out Surface of As-deposited Coatings Obtained at Low Level Concentrations of (a) Ni-B, (b) Ni-B-W and (c) Ni-B-Mo	177
Figure 6.16	EDAX Spectrum of Worn-out Surface of As-deposited Coatings Obtained at Mid-Level Concentrations of (a) Ni-B, (b) Ni-B-W and (c) Ni-B-Mo	178
Figure 6.17	EDAX Spectrum of Worn-out Surface of As-deposited Coatings Obtained at High Level Concentrations of (a) Ni-B, (b) Ni-B-W and (c) Ni-B-Mo	179

Figure 6.18	Tafel Plot for As-deposited (a) Ni-B, (b) Ni-B-W and (c) Ni-B-Mo Coatings	181
Figure 6.19	Nyquist Plot for As-deposited (a) Ni-B, (b) Ni-B-W and (c) Ni-B-Mo Coatings	183

List of Tables

Table No.	Table description	Page No.
Table 1.1	A Typical Coating Bath Composition of Electroless Ni-P Coatings	9
Table 1.2	A Typical Coating Bath Composition of Electroless Ni-B Coating	10
Table 1.3	Comparison of Wear Rates against Applied Load and Sliding Speed for Ni-P and Ni-P-TiO ₂	33
Table 2.1	Coating Bath Parameters and their Level of Concentrations	43
Table 6.1	Coating Bath Composition and Concentrations	151
Table 6.2	Coating Types and Bath Elements	152
Table 6.3	Coating Characterisation Techniques	152
Table 6.4	Chemical Composition of Coatings	158

This page is intentionally left blank

Chapter 1: Surface Modification - Electroless Coating and Its Evolution

Outline: 1.1 Introduction, 1.2 Surface Modification, 1.3 Electroless Coating Process, 1.4 Bath Composition and Deposition of Electroless Coatings, 1.5 Development of Electroless Coating Process with Time, 1.6 Application of Electroless Coatings, 1.7 Literature Review on Nickel Based Electroless Coatings, 1.7.1 Influence of Parameters on Deposition Rate, 1.7.2 Surface Morphology, Phase Structure, 1.7.3 Physical and Mechanical Properties, 1.7.3.1 Surface Roughness, 1.7.3.2 Surface Hardness, 1.7.3.3 Ductility and Tensile Strength, 1.7.4 Tribological Test, 1.7.5 Corrosion Resistance Test, 1.7.6 Nanocomposite Coatings, 1.7.7 Lead Free Coatings with the use of Green Bath, 1.8 Summary of Literature Review, 1.9 Research Work Plan, 1.10 Research Objectives, 1.11 Research Work Methodology, 1.12 Closure

1.1 Introduction

A diverse array of material finds their application across industries like housing, agriculture, transportation, and more, catering to both industrial and individual needs. Mild steel is one of them which is widely used in industries. The components made of mild steel may not always perform as desired due to some limitations. Aluminium may have a light weight but it is not suitable for tribological application. Hence, either the aluminium is to be replaced or the surface behaviour of aluminium is to be modified. Therefore, the problem may be resolved by changing the base metal of the components or some sort of surface treatments may be done to improve the surface characteristics as per requirements. The components used in corrosive environments like chemical industries or sea water application are prone to corrosion attack. The mild steel is not a suitable choice for the use in such cases. Hence, it is required to use some other material for such applications which may not be a feasible solution always. The mild steel finds its wide application in industries due to its high strength, light weight, high strength to weight ratio. The mild steel has a lot of disadvantages in some specific applications. Likewise, the other materials are also not always suitable for all application due to specific

limitations. Hence, one material may possess certain advantages but may have certain limitations in terms of surface characteristics. In such cases, the specific material is to be replaced by a suitable one which may not be feasible always. Hence, surface characteristics of the material is required to modify as per requirement to use it for that specific purpose. The surface characteristics may be modified by different methods which is discussed in the following sections.

1.2 Surface Modification

Surface modification is nothing but the modification of its surface behaviours of the base metal which may not possess or may not be sufficient under certain specific applications. The replacement of base metal is not a suitable solution always. Hence, an alternate method is to modify its surface behaviours. The modification of surface leads to generate surfaces with changed properties which is very much different from the base material. Various surface modification techniques have been developed to fulfil the purpose to protect ever-degrading materials. Components made of different materials degrade primarily due to the component-to-component interaction or component-to-environment interaction. There may be different form of degradation but all starts with the surface and hence, the surface modification is necessary. The surfaces modification is done to achieve the required surface properties of the base material leading to enhance the life of the materials. There are various surface modification techniques evolved over the time and successfully is being used in industries which are displayed in **Figure 1.1**. The coatings are nothing but a thin layer provided over a substrate of any material. It is usually used to provide a protective layer over the base metal or to change the surface behaviours of the parent metal. A thin film of coating may improve surface smoothness, tribological behaviour, corrosion resistance, hardness against indentation as well as scratch etc. Therefore, it is better to deposit a coating layer as per the requirement instead of changing the base metal. The soft coatings are used in packaging industries, mobile phone casings, and automotive industries for soft touch feeling purposes etc. The hard coatings are found to be used in automobile industries like bearings, oil seal valves, cylinder liners, piston rings for tribological applications, gas turbine blades and knife

sharpeners against severe conditions. There are several methods displayed in **Figure 1.2** to develop coated layers over any substrate material.

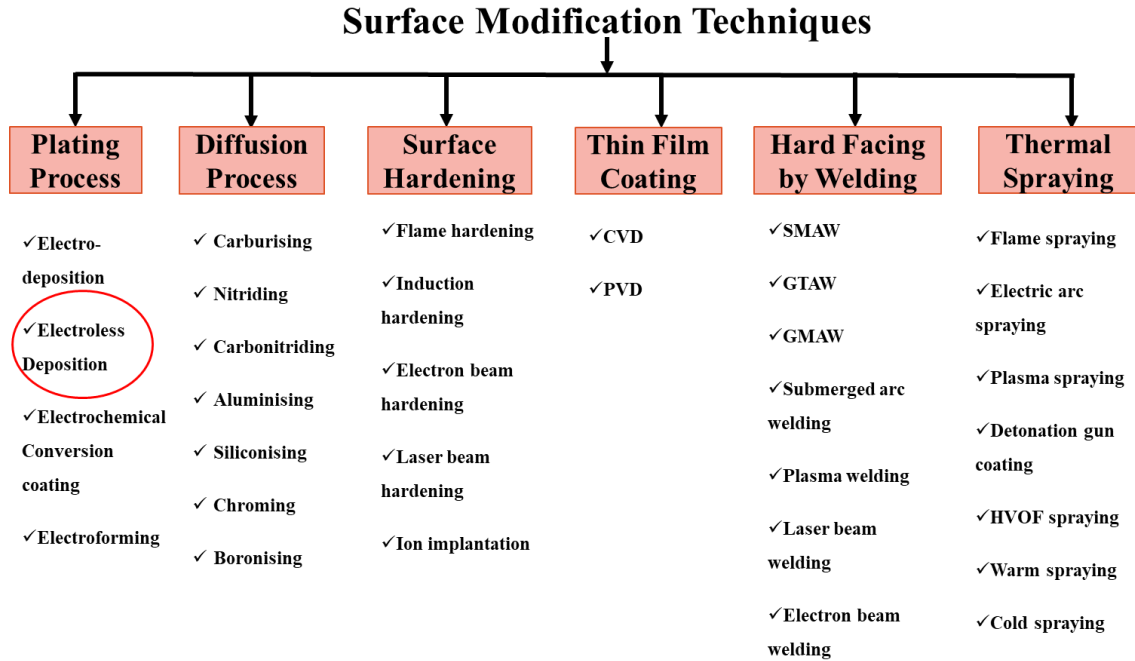


Figure 1.1: Surface Modification Techniques Used in Industries (Budinski, 1988).

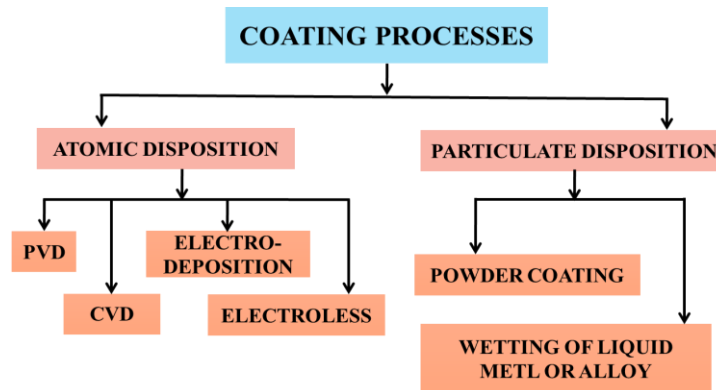


Figure 1.2: Various Coating Techniques

The various coatings are deposited through various deposition techniques like atomic deposition, thermal spray coating, PVD, CVD, electrodeposition, electroless coatings etc.

The particulate deposition techniques is the one in which the dry particles are deposited over the substrate through spontaneous attachment of particles over substrate surfaces. The powder coating is also a particulate deposition technique. These are mainly a surface finishing technique. Powder coatings are used to protect the roughest, toughest machinery as well as the daily household items. The spray paint is also a coating deposition method. It is also an art form using spray paint, traditionally done on posterboard, but can be done on any non-porous material, such as wood, metal, glass, ceramic or plastic. The spray paint also acts as a protective layer against corrosion but does not provide any improvement in surface hardness, scratch hardness or tribological properties.

The atomic Vapor deposition refers to any process in which materials in a vapor state are condensed through condensation, chemical reaction, or conversion to form a solid material. The physical vapour deposition (PVD) method is used for the high-purity, solid coating material such as titanium, chromium and aluminium. The metals are either evaporated by heat or by bombardment with ions (sputtering) to develop the coatings over substrate. PVD methods are clean when carried out under dry vacuum condition. It is known to provide high wear resistance, hardness at high operating temperatures, low friction, anti-sticking properties, scratch resistant purposes. But this method cannot be used to coat bore holes, slots etc. as it can deposit coatings up to a depth equal to the bore diameter or width of the opening. The coating deposit in this method is corrosion resistant only under certain conditions. In order to achieve a uniform coating thickness in this method, the parts are required to be rotated during processing. Whereas, the chemical vapour deposition (CVD) is a widely used method for depositing thin films of a large variety of materials. It is often used in the semiconductor industry to produce thin films. A thin film is a layer of material ranging from fractions of a nanometre to several micrometres in thickness. It also provides high wear resistance and it is suitable for coatings of bore holes, slots etc. But the deposition temperature is very high. It also restricts the deposition of several metals (e.g. TiAlN) together. The coating deposition of sharp edges become rounded after coating deposition in this method. On the other hand, the electrodeposition method uses electric current through a solution called an electrolyte. In this method, two terminals called electrodes are dipped into the electrolyte and

connected them into a circuit with a battery or other power supply. The electricity helps the electrolyte to split up and some of the metal atoms are deposited over the electrode to form a thin layer. All kinds of conducting metals including gold, silver, tin, zinc, copper, cadmium, chromium, nickel, platinum, and lead can be deposited over the substrate. Electrodeposition is used for mainly two purposes - decoration and protective layer. The gold and silver are plated over jewellery to make it cheaper instead of making them from solid gold or silver. While the metals like tin and zinc are deposited over metal substrates as a protective outer layer. The food containers are often tin plated to make them corrosion resistant and several iron made items are plated with zinc (galvanization) for the same reason. Alloys such as brass and bronze can also be plated using the same electrodeposition method. The major problem in electrodeposition is the use of electricity and the non-conducting materials can not be coated with this method. The sharp edges, intricate shapes are difficult to coat with electrodeposition methods. The electroless coating deposition technique is named due to the absence of electricity for coating deposition. The electroless coatings are popular for deposition of various nickel-based coatings like nickel-boron, nickel-phosphorous or many ternary or quaternary coatings. The electroless nickel-boron (ENB) coatings are popular for their tribological and mechanical properties. On the other hand, the surface hardening is done through diffusion to alter the surface properties of the base metal. Thin coatings, hard facing and thermal spraying are used to deposit new materials on top of the base metal. The coatings are provided for shielding of the base material from harsh environment by enhancing the overall property of the parent material. Coatings are generally used to meet particular property needs of the underlying base material and may also enhance the visual appearance of the components. The electroless coating method is one of such surface modification process. The electroless coatings may be used to deposit coatings over any intricate shapes of any materials such as conductive or nonconductive materials, and it can also be used to modify surface behaviours of any substrate surface which makes the electroless coating a better choice than the other coating deposition methods.

1.3 Electroless Coating Process

The coating process was disclosed due to a chemical accident which is distinguished by **Wurtz in 1844**. The use of same method was applied and established as

a coating method by **Brenner and Riddell (1946)**. Electroless coating is nothing but a coated layer development process with the use of chemical reactions and presence of heat. It does not use electricity like electrodeposition. A number of investigations on electroless coatings is already carried out to explore different characteristics like friction and wear for tribological applications, corrosion resistance for anticorrosion use purpose, and mechanical properties for industrial use or decorative uses [**Domínguez et al. 2012; Wang et al. 2014; Fetohi et al. 2015; Wang et al. 2016; Kundu et al. 2018; Lee and Lee, 2018**]. Different electroless coatings are found to improve the wear and corrosion properties of materials which are also used for making different engineering components [**Delaunois and Lienard, 2002; Narayanan and Seshadri, 2004; Gilley et al. 2012; Sudagar et al. 2013; Gadhari and Sahoo, 2016; Ghaderi et al., 2016; Loto, 2016**]. In this chemical reaction process, a reducing agent is required to break the metal salts into metal ions. The same metal ions are deposited over any substrate material to form a uniform coated layer. The electroless process can achieve uniform coated layer thickness over any complicated shapes which is not possible in electrodeposition process. The electroless coating method may also be used to coat nonconducting materials as well. The glass fiber reinforced epoxy resin is a non-conducting material which is used to manufacture printed circuit boards, popularly known as PCB and the copper circuits are printed on the PCB boards through electroless deposition method. The electroless coating process is also used for electromagnetic shielding, decorative coatings, functional coatings for oil and gas, automotive, chemical and aerospace industries [**Das and Sahoo, 2011; Sahoo and Das, 2011; Sha et al., 2011; Bülbül et al. 2012; Domínguez-Ríos et al. 2012; Çelik et al. 2016**]. The electroless coatings is seen to form smooth surface without any effective pitting [**Krishnan et al. 2006; Vitry et al. 2012; Vitry et al. 2012; Bülbül et al. 2013; Madah et al. 2015; Wan et al. 2016**]. In the contrary, a rough surface is also may be formed using electroless coating method [**Vitry et al. 2012; Bülbül et al. 2013; Madah et al. 2015; Wan et al. 2016**]. Both type of surfaces is formed under certain conditions. Hence, a necessary condition for a sound coating is the optimal transfer rate of metal ions onto the substrate from the chemical bath. Generally, slow deposition of metal ion leads to formation of smooth surface and faster deposition or random deposition of metal ions makes the surface rough. The slow deposition of metal

ions occurs usually due to slow reaction rate and leads to low coating thickness. A faster rate of chemical reaction also causes the precipitation of the metal ions.

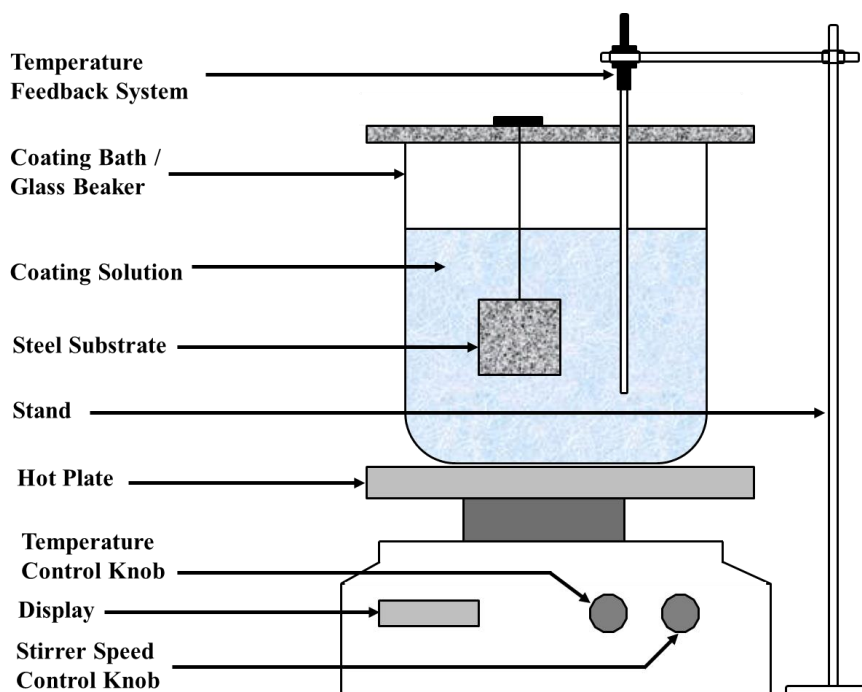


Figure 1.3: A Schematic Diagram of a Typical Electroless Coating Setup

Hence, it is necessary to apply a catalyst to control the reaction kinetics [Szunerits and Thouin, 2007]. The applied catalyst promotes the deposition of metal ions on substrate surface and avoids the precipitation of metal ions in the solution. A lot of studies are also being reported now a days where an attempt is made to improve the electroless coating behaviours with the incorporation of different metallic elements like boron (B), phosphorous (P), tungsten (W), Cobalt (Co), molybdenum (Mo), copper (Cu) etc [Anik et al. 2008; Das and Sahoo, 2011; Afroukhteh et al. 2012; Ranganatha et al. 2012; Arias et al. 2013; Aydeniz et al. 2013; Wang et al. 2015; Mukhopadhyay et al. 2018d]. Various composite coatings are also being developed with the addition of micro particles or nano particles to enhance the properties of these coatings. The mechanical behaviours like hardness, elastic modulus may further be altered with the addition of various nano-particles along with base alloy coating matrix. The nano-particles like TiO_2 , ZrO_2 , Al_2O_3 , ND are a few of the elements seen so far to be used with

the base alloys [Kaya et al. 2008; Radwan et al. 2015; Niksefat and Ghorbani, 2015; Taha-Tijerina et al. 2019]. The addition of these nano-particles is also found to be used to alter tribological behaviours as well [Kaya et al. 2008; Radwan et al. 2015; Niksefat and Ghorbani 2015; Taha-Tijerina et al. 2019]. Recently, few carbon-based nano-particles such as CNT, SiC, WC and graphene are also found to be used as reinforcement material to develop coatings with altered coating characteristics [Ma et al. 2014; Luo et al. 2015; Yazdani et al. 2018].

A schematic diagram of electroless coating deposition setup is displayed in **Figure 1.3**. The electroless coating deposition set up contains a glass beaker, stand to support the temperature feedback system, an electromagnetic heater cum stirrer. The coating bath solution is heated with the help of electric heater. The substrate is suspended with the help of a string and immersed into the coating bath solution. The substrates made of any materials may be coated using the same process even with intricate shapes. The substrates with complicated shapes or sharp edges or made of non-conducting materials may also be coated as it is immersed in the coating solution during coating deposition process. General specimen preparation and coating deposition process is explained step by step as mentioned below.

First Step: Preparation of substrates are as per required shape and size which is polished to achieve smooth surface.

Second Step: The substrate surface cleaning and conditioning are carried out in a 5% NaOH solution.

Third Step: Degreasing with acetone.

Fourth Step: Rust removal with 50% HCl.

Fifth Step: The substrate surface is then catalysed by dipping into 5% NaOH solution.

Sixth Step: The substrate is immersed into coating solution at predefined temperature to deposit coatings with or without magnetic stirrer. Nano-particles are agitated in deionised water prior to addition into coating solution to develop nano-composite coating.

Final Step: The coated substrates are rinsed well with deionized (DI) water to remove any residual coating solution.

1.4 Bath Composition and Deposition of Electroless Coatings

The electroless coating method is used to develop Ni-B and Ni-P alloy coatings. The same coating bath is being used to develop several types of coatings with the addition of few other elements with basic bath composition. The basic coating bath composition to develop electroless Ni-B and Ni-P alloy coatings are displayed in **Table 1.1** and **Table 1.2** for Ni-P and Ni-B coatings, respectively. The specimens are immersed into the coating bath solution after the initial treatments done to the substrate. The coating bath solution contains source of metal ions in the form of metal salts.

Table 1.1: A Typical Coating Bath Composition of Electroless Ni-P Coatings [Park and Kim, 2018]

Bath Parameter	Quantity	Operating Conditions	Quantity
Nickel Sulphate (NiSO_4) in g/l	20-40	pH of the Solution	5.2
Lactic Acid ($\text{C}_2\text{H}_6\text{O}_3$) in g/l	9-15	Bath Temperature in $^\circ\text{C}$	90
Sodium Hypophosphite (NaPO_2H_2) in g/l	20-40	Coating Duration in hours	2
Acetic Acid (CH_3COOH) in g/l	20-30	Bath Volume in mL	500
Lead Nitrate (PbNO_3) in g/l	2	Stirring Rate in rpm	200

The chemical bath compositions are presented in **Table 1.1** and **Table 1.2** contains nickel sulphate and nickel chloride, respectively as primary source of nickel in the coating bath solution. The coating bath also needs a suitable reducing agent which extracts the metal ions in the coating bath solution such as sodium borohydride, sodium hypophosphite etc. Besides, the sodium borohydride and sodium hypophosphite are also used as source of boron and phosphorous in the electroless Ni-B and Ni-P alloy coatings, respectively. The coating bath also contains complexing agent, stabilizers, buffers etc. The function of complexing agent, used in coating bath solution is to prevent the pH to fall drastically and also restricts the nickel ions to precipitate in the solution. Acetic acid, succinic acid and lactic acid are few of the complexing agents found to be used for

electroless nickel-based coatings as reported by **Mallory, 1991** [**Mallory, 1991**]. The coating bath also contain stabilizers which prevents the coating bath to decompose spontaneously.

Table 1.2: A Typical Coating Bath Composition of Electroless Ni-B Coating
[**Mukhopadhyay et al. 2018b**]

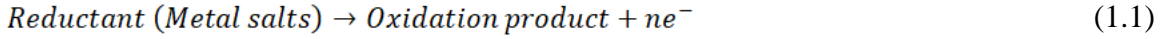
Bath Parameters	Quantity	Operating Conditions	Quantity
Nickel Chloride (NiCl_2) in g/l	20	pH	12.5
Sodium Borohydride (NaBH_4) in g/l	0.80	Coating Duration in hours	4
Lead Nitrate (PbNO_3) in g/l	0.0145	Bath Temperature in $^{\circ}\text{C}$	90 ± 2
Ethylenediamine ($\text{C}_2\text{H}_8\text{N}_2$) in g/l	59	Bath Volume in mL	200
Sodium Hydroxide (NaOH) in g/l	40		

The spontaneous decomposition of coating bath solution may lead to formation of unnecessary hydrogen ions (H^+) as well as the precipitation of nickel. Generally, the heavy metal ions like Sn^{2+} , Sb^{3+} , Hg^+ , Pb^{2+} etc. are known as good coating bath stabilizers [**Mallory, 1991**]. The coating bath solution also contains a buffer which helps to maintain the coating bath pH at required level. Generally, a strong acid or alkali is used to maintain the required bath pH. The coating bath is to be operated at a certain condition to obtain a good coating layer over a substrate. The elements remain present in the coating bath solution do not react with each other. The chemical solution is required to heat for a certain temperature to initiate the chemical reaction process [**Baskaran et al. 2006; Hamid et al. 2010**]. It was observed that the chemical reaction in the coating bath solution starts at around 70°C to deposit electroless Ni-B coatings [**Baskaran et al. 2006; Hamid et al. 2010**].

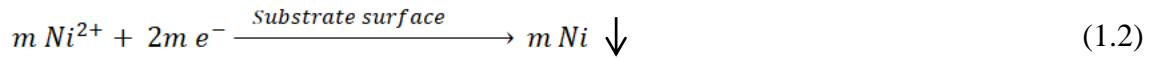
The electroless coatings possess step by step chemical reaction for the extraction of metal ions and the same metal ions are deposited over the substrate. The chemical

reactions during the electroless deposition process involves a combination of reduction reaction and oxidation reaction which is shown below [Mallory, 1991].

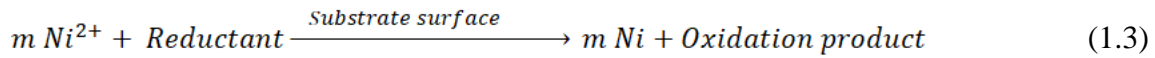
Oxidation:



Reduction:

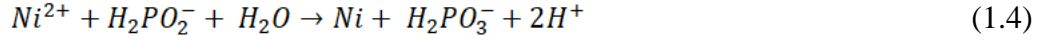


Overall reaction:



The chemical reactions explained through the general equations in **Eq. 1.1, 1.2** and **1.3** show a glimpse of metal ion extraction from metal salts and depositions of those ions over the substrate. **Figure 1.4** also shows the same metal ion extraction and deposition process. The chemical reaction occurs in main two steps where the metal salt releases electron and reduces nickel and hydrogen ions. The same metal ions are deposited on the metal substrate surface and releases some hydrogen. These are not sufficient to understand the complete chemical reactions of the electroless deposition process. The chemical reactions occur during the experimental deposition process are far complicated than the above-mentioned equations. A detailed observation and study on specific reduction process with different reducing agent is required to understand the phenomena during EN plating.

Several numbers of chemical reactions are suggested by various researchers in previous studies in past decades since the evolution of electroless coating deposition. The chemical reactions and metal ion deposition mechanism suggested by **Brenner and Riddell, 1946** is elaborated through two main equations as presented in **Eq. 1.4** and **1.5**. The same equations are popularised as the “Atomic hydrogen mechanism” later. The **Eq. 1.4** and **1.5** shows the deposition of pure nickel without addition of any other metal.



The subsequent experimental evidence disproved this explanation of pure nickel deposition. **Gutzeit (1959)** proposed a solution to resolve this ambiguity. He proposed that the existence of phosphorus could be accounted by the reactions outlined in **Eq. 1.6** and **1.7**.

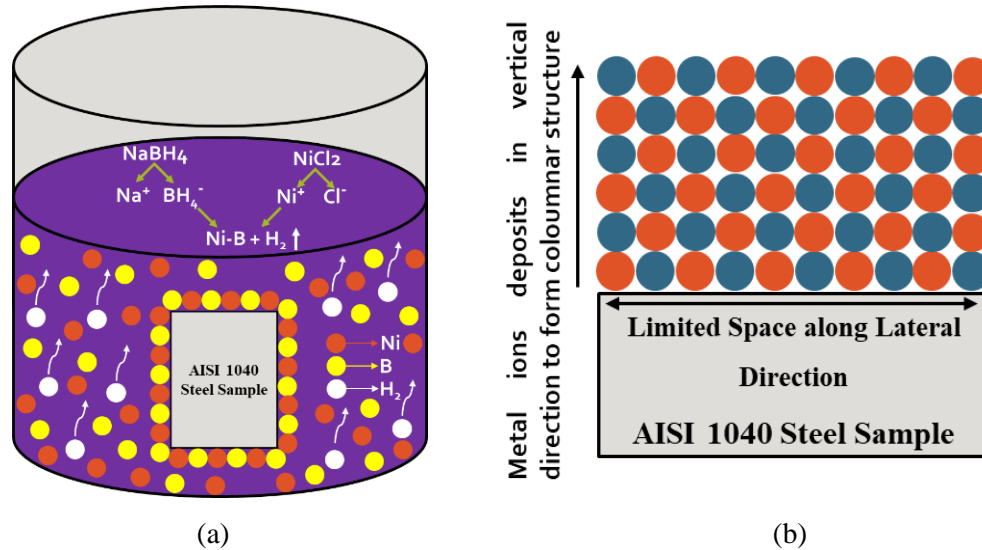
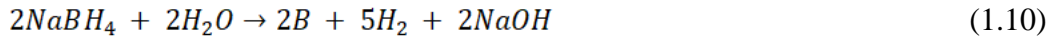
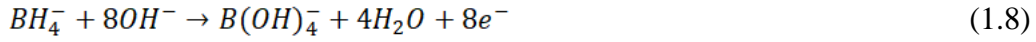


Figure 1.4: Electroless Coating Deposition Mechanism, (a) Ion Reduction & Deposition Mechanism and (b) Columnar Structure Development Mechanism

The chemical reactions show that the NaH_2PO_2 splits up into Na^{2+} and $H_2PO_2^-$ ions. The same $H_2PO_2^-$ ions react with H ions producing H_2O and OH^- ions and leaves P ions to deposit on the substrate surface. It produces OH^- ions which result an increase in the pH of the solution. Due to this increase in pH, the chemical reaction shown in **Eq. 1.7** speeds up and produces more H^+ ions. This way layer-by-layer deposition of electroless coatings over the substrates are achieved. Nevertheless, this mechanism fails to offer a

satisfactory explanation for the concurrent reduction of both Ni and H₂ in the electroless nickel (EN) plating process. But the “Hydride transfer mechanism” proposed by **Gutzeit, 1955** elaborates the continuous reduction of Ni and H₂. Ni-B coatings, formed through the reduction of nickel salts by borohydride (BH₄) ions, typically engage in the reactions illustrated below.



While, the afore mentioned reactions in **Eq. 1.8** and **1.9** illustrates the reduction of Ni but they do not account for the presence of boron in the coatings. **Gourbunova et al. (1973)** have put forth a mechanism involving the reduction by boron, as outlined in **Eq. 1.10**. Several researchers have also reported different mechanism and only a few of them are elaborated in above discussion.

1.5 Development of Electroless Coating Process with Time

The electroless coating deposition method and its application was established by Brenner and Riddell [**Brenner and Riddell, 1946**]. A lot of researchers targeted to explore the different aspects of electroless coatings. Initially, researchers found to be unsuccessful to get a stable coating bath and no coating thickness was achieved. The chemical deposition method was utilised to deposit nickel on small components used in naval purposes by **McLean and Korten (1954)**. **Gutzeit and Mapp (1954)**, recommended the ‘Kanigen’ method to deposit nickel-phosphorus to act against corrosion because of its impermeable nature. The Kanigen method was initially formulated by the engineering department of General American Transportation Corporation in 1947 to replace the complicated electroplating process [**Gutzeit and Mapp, 1954**]. The amorphous phase structure of the nickel deposition was thoroughly studied by **Goldenstein et al., 1957**. It was also reported that the metastable amorphous phase of nickel decomposes into a mixture of Ni₃P and crystalline nickel at a temperature

of 300°C. It was further reported to measure the coating deposition rate by **Minjer and Brenner (1957)**. They further studied the impact of thiourea and a complexing agent on bath chemistry. **Gutzeit (1959)** recommended the electroless nickel deposition process which was initially suggested by Brenner and Riddell. The recommended electroless coating deposition model also explained the role of atomic hydrogen ion to extract the nickel ions to deposit the metal ions over any substrate. Though, it was already demonstrated that various metal ions of copper, nickel, cobalt etc on different substrates made of aluminium, iron, and magnesium by the early 1960s. But still some issues were remained about bath stability, obtain a smooth coated surface and the need of catalytic surface to initiate the chemical reaction. A lot of development of electroless Ni-B coatings and its modifications is done since its evolution in 1949. The development and modification of electroless Ni-B coatings during 1960-1980s have established it as a versatile on the basis of its tribological applications. A lot of research is also reported during 1960-1980s on the chemical bath chemistry. The development of electroless coating and its modifications since its evolution is elaborated in **Figure 1.5**.

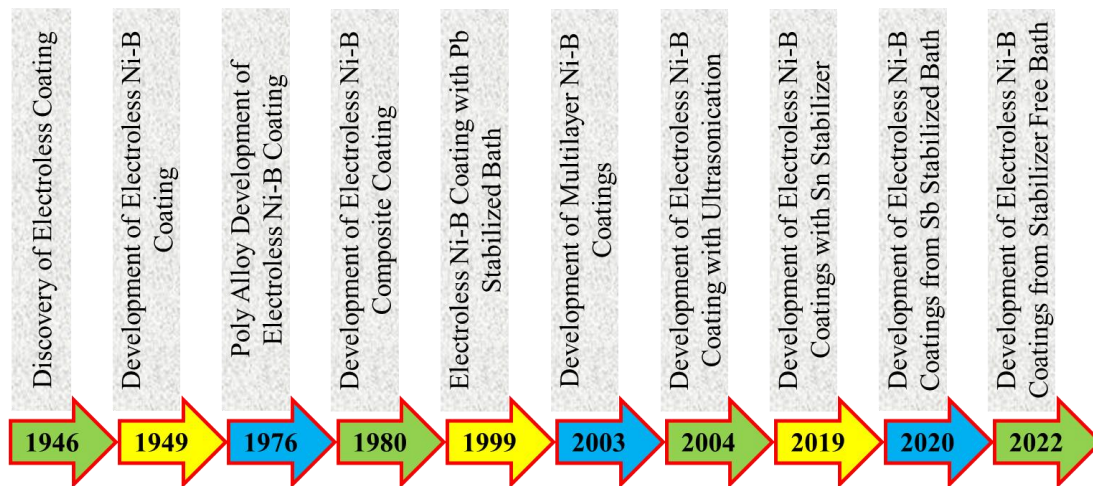


Figure 1.5: Development and Modification of Electroless Ni-B Since Evolution (Vitry et al., 2022)

In recent years, a lot of research is going on the development of Ni-P and Ni-B based alloy or poly-alloy coatings with the addition of different metallic elements like boron (B), phosphorous (P), tungsten (W), Cobalt (Co), molybdenum (Mo), copper (Cu) to achieve high hardness, better corrosion resistance, low COF and high wear resistance

etc. The composite coatings are also being developed with the addition of micro particles or nano-particles of SiC, TiO₂, Al₂O₃, WC, ZrO₂ etc. to understand their characteristics for different applications. Hence, the study of the coating bath chemistry of electroless Ni-B and the impact of different coating bath elements on the characteristics of Ni-B coatings has become important.

1.6 Application of Electroless Coatings

The coatings are normally used to provide a protective layer over the base metal or to change the surface behaviours of the parent metal. A thin film of coating may improve surface smoothness, tribological behaviour, corrosion resistance, hardness against indentation as well as scratch etc. Therefore, it is better to deposit a coating layer as per the requirement instead of changing the base metal. The soft coatings are used in packaging industries, mobile phone casings, automotive industries for soft touch feelings, interior decorative purposes etc. The hard coatings are found to be used in automobile industries like bearings, oil seal valves, cylinder liners, piston rings for tribological applications, gas turbine blades and knife sharpeners against severe conditions. Protecting a soft metallic surface from damage like wear, corrosion, and oxidation, is a significant challenge for the tribology community. While hard tribological coatings effectively prevent surface damage against wear and friction at room temperature. But they frequently found to cease to function at elevated temperatures. Similarly, liquid lubricants also break down at higher temperatures. Therefore, it is necessary to use a coating which may act as a solid lubricant during use.

The electroless coating characteristics vary with their composition. The electroless Ni-B coating with low boron content shows higher electrical conductivity, good solderability but lower contact resistance. The electroless Ni-B coatings with around 3 wt. % boron is suitable for the use in electronic devices. Hence, the electroless Ni-B is used as replacement of gold in many applications of electronic devices. Various particulate matters like PTFE may be co-deposited with nickel which reduces friction coefficient. Water pump motor shafts are often found to be coated with Ni-P-PTFE to enhance the service life by reducing the friction coefficient. On the other hand, hard particles like SiC, B₄C, Si₃N₄ etc may be co-deposited which is useful for the application

in pneumatic cylinders, pump rotors to enhance life. Components used in fuel pumps are also coated with electroless Ni-P with high phosphorous content to enhance the service life by preventing from corrosion. Steel made differential pinions shafts, sleeve liners are also coated with electroless Ni-P coatings having 4 wt. % phosphorous to improve hardness and improve wear resistance which increases its service life. Similarly, fuel injector pipes, nozzles are also coated sometimes with electroless Ni-P coatings by several manufacturers. Hard chromium coatings are widely used in industries due to its high hardness, wear resistance and low friction coefficient. The heat treated electroless Ni-P coatings with high phosphorous content (up to 12 wt. %) is comparable with chromium coatings. Hence, it may act as replacement of chromium coatings.

Therefore, it is clear from the above discussion that the electroless coatings are widely used in industries. Hence, several researchers have developed different coatings with different combinations and composition to obtain different coating characteristics. The studies carried out by several researchers based on different characteristics are discussed in the following sections.

1.7 Literature Review on Nickel Based Electroless Coatings

Electroless nickel plating, in which hypophosphite is used as a reducer, is the most popular process for electroless deposition. Auto catalytic nickel ion reduction by hypophosphite occurs both in acid and in alkaline solutions. The addition of Phosphorus or Boron in the chemical reaction bath solution leads to co-deposition of nickel phosphorous (Ni-P) or nickel boron (Ni-B) over the substrate. The deposition of nickel with addition of boron or phosphorus contributes to the modification of coating behaviours. Generally, the borohydride reduced electroless nickel-boron (Ni-B) coatings show better tribological behaviour due to its surface morphology and it also possess good surface hardness behaviour due to presence of boron like hard elements in the coatings. On the other hand, addition of phosphorous with nickel makes the coatings to possess better strength, ductility. The electroless Ni-P coating with higher phosphorus content coating possess excellent fatigue strength. The electroless Ni-P coatings also possess very good corrosion resistance behaviour [Townsend, 1994]. The coating deposition process

and its characteristics are influenced by various factors like coating bath composition and operating conditions. The same is studied and presented in the following sections.

1.7.1 Influence of Parameters on Deposition Rate

The deposition rate of electroless coatings was observed to be influenced significantly by several coating parameters which was reported by Wolfgang Riedel in 1991 [Riedel, 1991]. In the case of electroless Ni coating, a notable observation proposes a comparable influence of bath temperature on both electroless Ni-B coatings (reduced by borohydride) and Ni-P coatings (reduced by hypophosphite), as reported by Townsend in 1994. Additionally, Glenn O. Mallory [Mallory, 1991] documented the impact of pH on a Ni-B coating (with dimethylamine borane as a reducing agent), highlighting its dependence on specific variables outlined below.

$$\text{Deposition rate} = f \left(\begin{array}{c} \text{Coating Bath Temperature, pH, Concentration of } \text{Ni}^{2+}, \\ \text{Reducing agent, Bath loading} \end{array} \right).$$

The deposition rate of the coatings is most significantly influenced by coating bath temperature. Clearly, the majority of the chemical reactions taking place in the bath during the plating process are endothermic. The metal salts remain present in the coating bath generally do not react at ambient temperature. Therefore, the introduction of heat (an increase in temperature) accelerates the reaction and enhances the deposition rate. Obviously, care should be exercised to avoid over heating the bath, as it can result in the spontaneous decomposition of the coating bath solution. The coating bath temperature is usually kept within the range of 85-95 °C, though the chemical reaction may start much earlier than 85°C. The low temperature coating bath also is maintained even at around 50°C.

Figure 1.6 illustrates the changes in the coating deposition rate with bath temperature, as reported by Townsend in 1994. A little change in coating bath parameters is meant to be a change in coating bath composition. The change in coating composition impacts the coating characteristics which is extensively reported in previous studies [Anik et al. 2008]. The literature also suggests that a change in coating bath

temperature of electroless Ni-B coatings is also plays a significant role to decide the coating characteristics. **Delaunois et al. (2000)** investigated the influence of coating bath temperature on borohydride reduced electroless Ni-B alloy coating deposition on aluminum alloy. The results showed that the coating thickness increased with corresponding increase in the coating bath temperature. Likewise, an increase in coating deposition rate with coating bath temperature or a direct correlation is reported by **Gorbunova et al. (1973)**. **Oraon (2007)** conducted a study that revealed a linear correlation between the coating deposition rate and bath temperature, particularly for shorter immersion periods. In case of longer immersion periods, the deposition rate reaches a saturation point. After reaching saturation, further increases in bath temperature led to a subsequent decline in the deposition rate or decomposition of the coating bath some times.

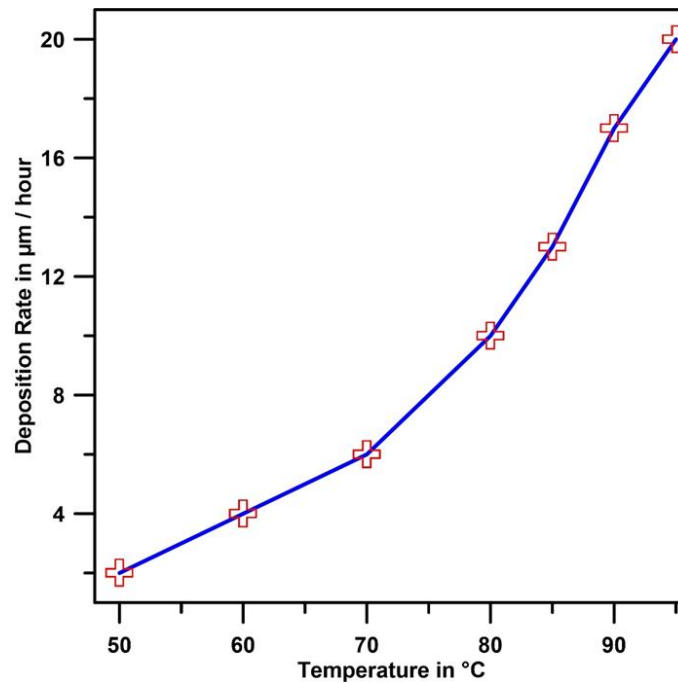


Figure 1.6: Coating Deposition Rate vs Bath Temperature Plot [Townsend, 1994]

While, the influence of coating bath temperature in an acidic bath which uses dimethylaminborane (DMAB) as reducing agent is also reported by **Hamid et al. (2010)**. They endeavoured to develop Ni-B coated layers by submerging copper and steel substrates into the coating bath at temperatures of 60°C and 80°C for different deposition

time. They also observed that the coating deposition rate is low at 60°C which is considered to be low coating bath temperature. The deposition rate does not follow any linear relationship with deposition time rather the deposition rate is observed to decline with time. This decline in deposition rate is occurred due to the decreased concentration of DMAB over time and the remaining in the coating bath solution are the byproducts of chemical reactions. This is the only possible explanation in context to the phenomenon (Hamid et al., 2010).

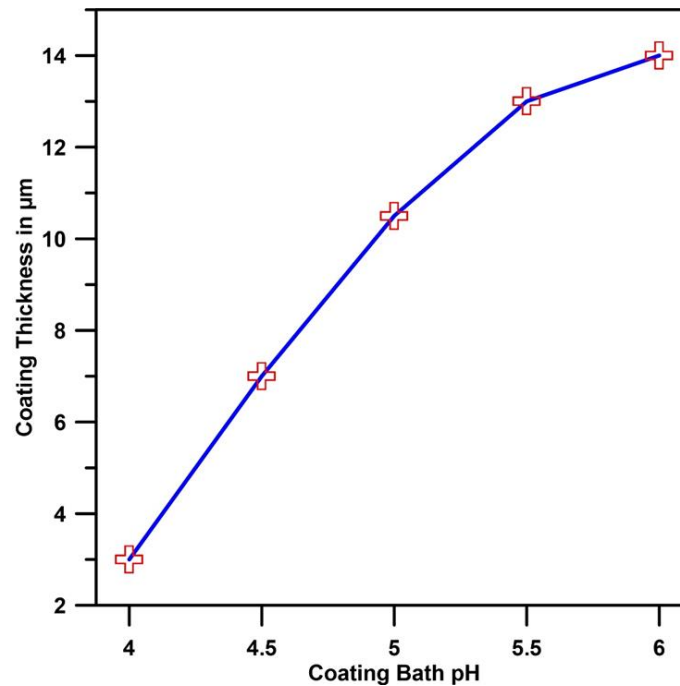


Figure 1.7: Coating Deposition Rate vs Coating Bath Solution pH Plot [Baldwin and Such., 2017]

The electroless nickel phosphorus (ENP) coating deposition method necessitates different chemical reactions which is affected by the change in coating bath solution pH. The reduction reaction is usually improved with the rise in chemical solution pH resulting an improvement in nickel deposition over the substrate but a reduction in phosphorous is observed. The reduction reaction of phosphorous is hindered with rise in chemical solution pH resulting the formation of hydroxide ions as a byproduct of the reduction reaction. The development of electroless nickel-based coatings is mainly controlled by the nickel reduction reaction. Hence, the improvement in deposition rate with the rise in

pH indicates that the deposition rate may be controlled as per requirement with the manipulation of chemical solution pH. The **Figure 1.7** shows an increase in coating thickness with coating bath pH which indicates an increase in deposition rate with the rise in pH as reported by **Baldwin and Such (2017)**.

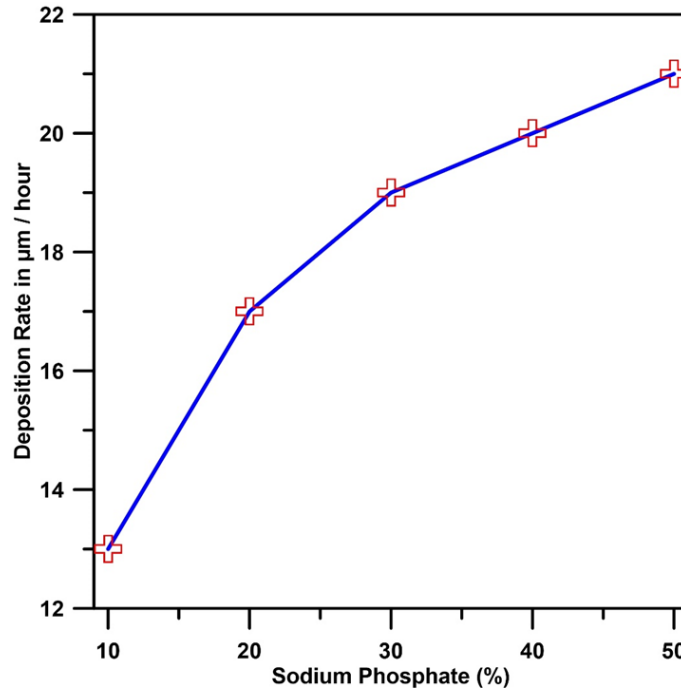


Figure 1.8: Coating Deposition Rate vs Sodium Phosphate Concentration Plot
[Mallory, 1991]

The thickness of electroless nickel (EN) coatings is determined by the duration of substrate immersion in the solution bath. Studies conducted by **Oraon (2007)** and **Vitry et al. (2012)** indicate a direct correlation between immersion time and coating thickness. The deposition rate remains relatively constant for initial 2 hours (approximately) before experiencing a sharp decline without replenishing the coating bath. **Oraon (2007)** concluded that there is a clear relationship between deposition time and coating thickness. Similarly, **Vitry et al. (2012)** observed that during Ni-B electroless deposition, there is an initial increase in coating thickness, with a growth rate exceeding $40\mu\text{m}/\text{min}$ for up to 4 minutes. Subsequently, the coating undergoes densification, resulting in no further increase in thickness for the next 4 to 7 minutes. Following this period, the coating thickness tends to increase almost linearly over the course of 1 hour of

immersion. While the selection of the reducing agent may impact the deposition rate to some extent, particularly up to a certain concentration. The general trend indicates that the deposition rate tends to rise with an increase in the concentration of the reducing agent. **Figure 1.8** illustrates the reported relationship between the coating deposition rate and the concentration of the reducing agent. It is evident from the graph that the deposition rate experiences an upward trend with the concentration of the reducing agent (sodium hypophosphite) until reaching a specific threshold, beyond which the rate stabilizes and remains relatively constant.

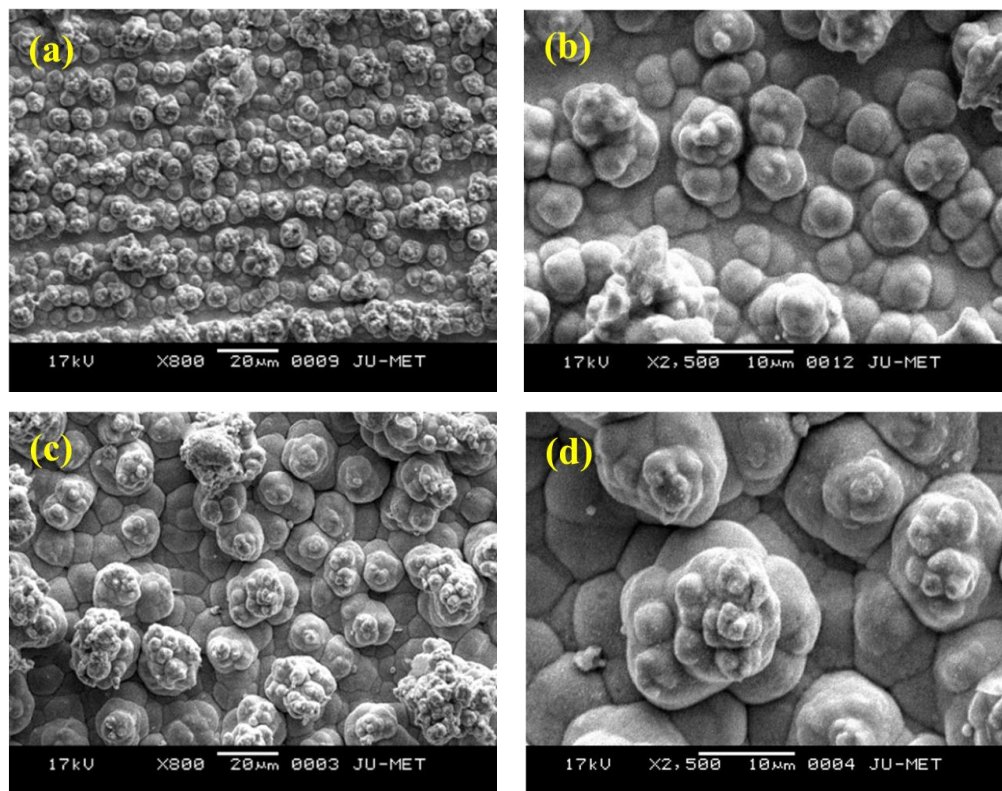


Figure 1.9: Typical Surface Morphology of Electroless Ni-P-Cu Coatings (a) As-deposited (800X), (b) As-deposited (2500X), (c) Heat Treated (800X) and (d) Heat Treated (2500X) Conditions [Duari et al. 2016]

1.7.2 Surface Morphology, Phase Structure

The electroless nickel-based coatings are nothing but the different variant of coatings deposited with addition of phosphorous, boron to form binary nickel-phosphorous (Ni-P), nickel-boron (Ni-B) alloy coatings. Tungsten, molybdenum may

further be incorporated to develop Ni-P based ternary coating (Ni-P-W, Ni-P-Mo) or Ni-B based ternary (Ni-B-W, Ni-B-Mo) alloy coatings. The surface appearance of electroless coating exhibits a characteristics resemblance to cauliflower which is formed with nodules. The amount of phosphorous present in electroless Ni-P based coatings has a notable impact on both their structure and properties [Gould et al., 1981; Fan et al. 2012]. The nodules of the cauliflower-like morphology tend to become larger with increased amount of phosphorus in the coatings [Fan et al., 2012]. Similar types of morphology are also observed for Ni-P based ternary alloy coatings like Ni-P-W [Palaniappa et al. 2008], Ni-P-Mo [Balaraju et al. 2014]. Ni-P-Cu [Duari et al. 2016] coatings are also reported to pass through a grain refinement to modify the surface morphology of Ni-P coatings with the introduction of copper. The **Figure 1.9** shows the surface morphology of electroless Ni-P-Cu coatings at different resolutions [Duari et al. 2016]. An extensive study is reported by **Goldenstein et al. (1957)** on the impact of phosphorus content on Ni-P coatings which suggests that the as-deposited Ni-P alloy coatings having phosphorous content more than 7 wt.% possess amorphous phase structure. Subsequent heat treatment prompts the amorphous phase to crystalline phase with Ni and NiP like crystalline phases [Goldenstein et al. 1957; Sribalaji et al. 2016; Duari et al. 2016]. Heat treatment results in the precipitation of crystalline nickel and its phosphides as can be seen in **Figure 1.10**. Hard phases of crystalline nickel and Ni₃P is precipitated along with a metastable phase of Ni₃P₂ and Ni-Cu solid solution. Similar characteristics has been observed by **Yu et al. 2011** [Yu et al. 2011] for electroless Ni-P-Cu coatings heat treated at 500°C for 1 hour. The **Figure 1.11** represents the coated surface morphology of electroless Ni-B coatings as reported by **Surden et al. 2019** [Surden et al. 2019]. The surface morphology of the electroless Ni-B coatings is reportedly observed to possess an appearance which resembles with cauliflower [Delaunois et al. 2000; Krishnaveni et al. 2005; Baskaran et al. 2006; Vitry et al. 2008; Bülbül et al. 2013; Madah et al. 2015; Wan et al. 2016; Yazdani et al. 2018; Bonin et al. 2019; Sukackiene et al. 2020]. The nodules of the surface are also observed to become larger with boron content into coatings due to rise in sodium borohydride concentration in the coating bath solution [Baskaran et al. 2006]. Usually, electroless Ni-B coatings possess a uniform surface morphology with uniform distribution of

nodules [Delaunois et al. 2000; Krishnaveni et al. 2005; Baskaran et al. 2006; Vitry et al. 2008; Bülbül et al. 2013; Wan et al. 2016].

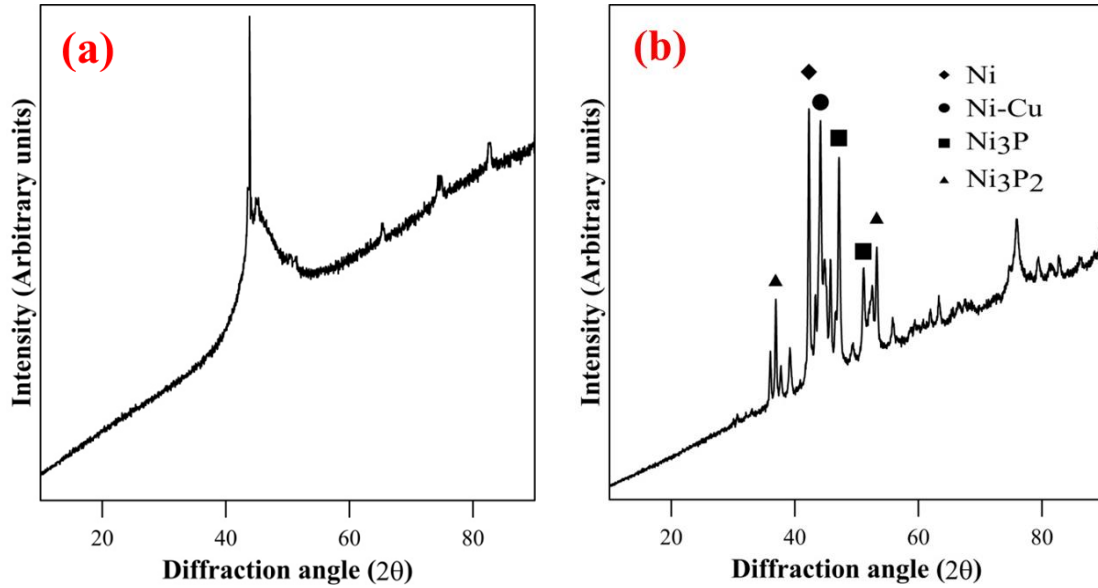


Figure 1.10: XRD Spectrum of Electroless Ni-P-Cu Coatings, (a) As-deposited and (b) Heat-treated Conditions [Duari et al. 2016]

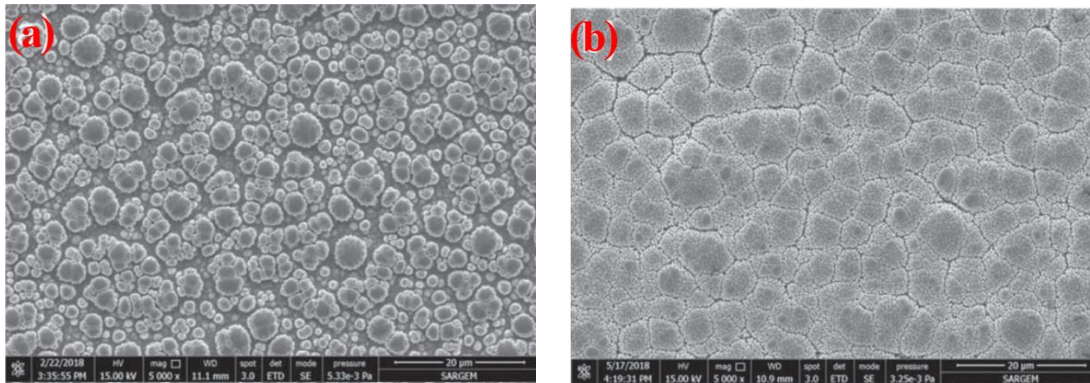


Figure 1.11: Typical Surface Morphology of Electroless Ni-B Coatings Obtained at Sodium Borohydride Concentration of (a) 0.5 g/l and (b) 1.0 g/l [Surden et al. 2019]

The nodules of the surfaces are also found to agglomerate to form clusters upon heat treatment [Bülbül et al. 2013]. This trend may also be observed for electroless Ni-P coatings as well [Duari et al. 2016]. Whereas, electroless Ni-B coatings generally possess amorphous phase with boron content above 4 wt.% and in as-deposited condition

[Baskaran et al. 2006, Bekish et al. 2010, Venkatakrishnan and Karthik 2019]. The same coatings with boron content below 4 wt. % usually found to possess a mixture of amorphous crystalline phase in its as-deposited condition [Baskaran et al. 2006, Bekish et al. 2010, Venkatakrishnan and Karthik 2019].

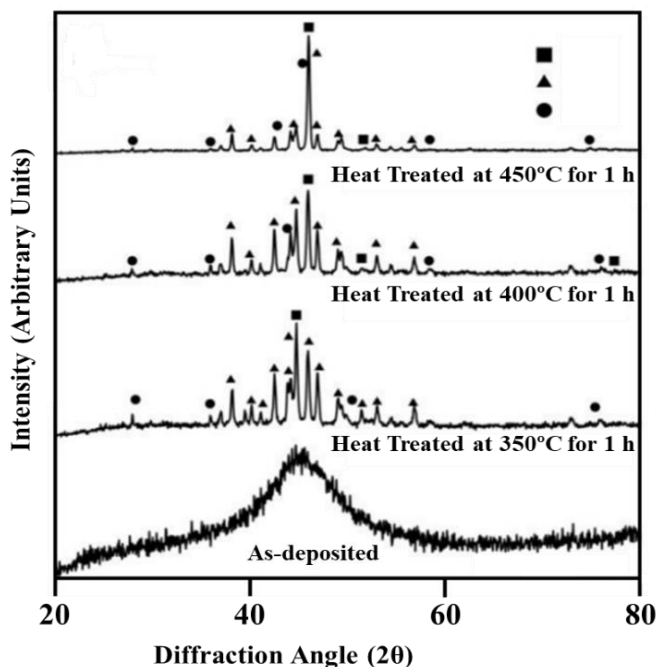


Figure 1.12: XRD Spectrum of As-deposited and Heat-treated Electroless Ni-B Coatings [Mukhopadhyay et al. 2018a]

The same amorphous phase of as-deposited Ni-B coatings get transformed into crystalline phase upon heat treatment. This type of phase transformation upon heat treatment may also be observed in case of electroless Ni-P coatings as reported by Krishnaveni et al. (2012). Krishnaveni et al. (2012) also reported that the as-deposited electroless Ni-P or Ni-B coatings possess a single broad in peak in its XRD spectrum which confirms its amorphous phase. Sharp peak in XRD pattern indicates the presence of crystalline peaks [Cullity, 1978] and the presence of both sharp peaks with broad hump is the indication of coexistence of amorphous phase with crystalline peaks [Delaunois and Lienard, 2002; Dervos et al. 2004; Ziyua et al. 2006]. It is also reported that the electroless Ni-B coatings possess a cauliflower-like surface morphology with columnar structure [Rao et al. 2005]. It was also reported by Watanabe and

Tanabe (1983) that the electroless Ni-B deposits possess amorphous phase which was confirmed through SEM and XRD patterns. The similar findings are also reported by a few other researchers [**Srivastava et al. 1992; Evans and Schlesinger, 1994**]. These surface morphology and phase structure of the electroless Ni-B coatings are also found to depend on the amount of boron present in the coatings [**Gaevskaya et al. 1996; Anik et al. 2008; Vitry, Kanta and Delaunois, 2011; Vitry et al. 2012**]. The **Figure 1.12** shows the typical XRD spectrum which shows the phase transformation of electroless Ni-B coatings with sodium borohydride concentration as well as with the variation in heat treatment temperature.

1.7.3 Physical and Mechanical Properties

1.7.3.1 Surface Roughness

Surface roughness is a critical factor in assessing the tribological behaviour of coatings. Frequently, the level of surface roughness determines whether the friction coefficient between two contacting surfaces will be high or low [**Goettems et al., 2017**]. It is also reported that the COF value decreased for the Ni-P coated samples compared to the uncoated substrate [**Goettems et al., 2017**]. Similar type of reduction in COF value may also be observed upon deposition of Ni-B coatings over aluminium alloy substrate [**Vitry et al., 2008**]. The surface roughness is also reported to be reduced due to surface modifications upon heat treatment [**Vitry et al., 2008**]. The electroless Ni-B coated surface roughness is influenced by the roughness of the substrate. The coatings deposit on the substrate surface and grow in locally perpendicular to the surface to form columnar structure. Therefore, deposition of the coatings in columnar form over a smooth substrate surface led to formation of an even smoother than the substrate itself, as the columns will be parallel to each other. However, the deposition of coatings over rough substrate surface, the columns will tend to form an uneven arrangement in height which acts as the roughness asperities resulting a rougher coated surface than the substrate. The roughness asperities ultimately may impact the friction and wear behaviour of coatings largely.

1.7.3.2 Surface Hardness

The surface hardness of any material surface may be altered with the deposition of coating layer over it. It is reported by **Sha et al. (2011)** that the hardness of electroless Ni-P coated surface varied within the range of 450-500 HV which is improved further upon heat treatment nearly about 1000 HV. It is already mentioned that the amorphous phase of as-deposited Ni-P coatings transform into crystalline phase with some hard phases like Ni and Ni₃P which may have contributed in this improvement in surface hardness. This phase transformation behaviour is observed by several researchers with the help of X-ray diffractometry and this phase transformation might have contributed to the improvement in surface hardness [**Rabizadeh et al. 2010; Islam and Shehbaz, 2011; Ma et al. 2014; Czagány et al. 2017**]. The formation and presence of hard phases like Ni₃P is contingent upon both the phosphorus content in the as-deposited coatings and the temperature of heat treatment [**Rabizadeh et al. 2010; Czagány et al. 2017**]. Moreover, the heat-treatment of electroless Ni-P coatings is reported to enhance the abrasion resistance and promotes better adhesion between the substrate and coating [**Mallory, 1991; Rabizadeh et al. 2010**]. Similarly, electroless Ni-B coatings achieve high hardness and wear resistance through the precipitation of intermetallic phases like Ni₃B upon heat treatment. Several studies suggests that the surface hardness and wear resistance of Ni-B coatings is superior compared to Ni-P coatings deposited with electroless method [**Riedel, 1991; Pal and Jayaram, 2018**].

It is reported that incorporation of nanoparticles enhances the hardness of Ni-B coatings [**Kaya et al. 2008; Niksefat and Ghorbani, 2015; Radwan et al. 2015, Taha-Tijerina et al. 2019**]. Initially, nickel-boron ions adhere to the nanoparticle surface which is incorporated into the Ni-B coating bath solution and subsequently attached with the specimen surface. As a result, nickel-boron atoms trap the particles, causing them to be incorporated into the coating. The nano-particles incorporated into the coatings provides resistance against the dislocation resulting an enhancement in surface hardness [**Shakoor et al., 2014**]. The addition of the nano-particles also restricts the grain growth leading to a development in density resulting an increase in coating hardness as well as the yield stress of the coated surface [**Yazdani et al., 2018**]. Moreover, the addition of nano-particles into Ni-B matrix and their uniform distribution also led to an improvement

in its hardness for the nano-particles itself being hard [Georgiza et al., 2017]. These are the main mechanisms through which the inclusion of nano-particles augment hardness.

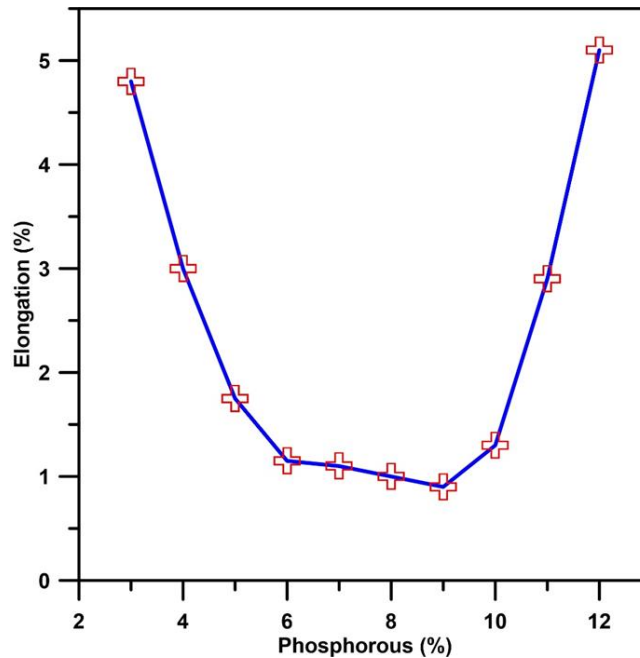


Figure 1.13: Ductility vs Phosphorus Content Plot for Electroless Ni-P Coatings [Duncan, 1996]

1.7.3.3 Ductility and Tensile Strength

Tensile strength and ductility are primarily influenced by the presence of amount of phosphorus in the coatings. **Duncan (1996)** has proposed the relationship between the mechanical properties and the various phases present in the coatings on the basis of Ni-P equilibrium phase diagram. It is noted that β and γ phases exist along with the α -Ni phase. The β phase constitutes a solid solution of 4.5 wt. % phosphorus in nickel, exhibiting a crystalline nature. Conversely, the γ phase is amorphous with approximately 11% to 15% phosphorus. These phases are metastable and tend to decompose into Ni_3P and α -nickel upon heat treatment [Duncan, 1996]. The same is also reported by **Kreye et al. 1986**. The **Figure 1.13** elaborates the significance of phosphorus content on the ductility of the coatings as reported by **Duncan, 1996**. The **Figure 1.13** also indicates that the coatings with low or high phosphorous content usually are ductile in nature relative to the coatings with mid phosphorous content. The mid-phosphorous content

coatings contain a mixture of α and β phases besides the high stress [Duncan, 1996]. The high stress along with two metastable phases leads to reduction in ductility of the mid-phosphorous coatings.

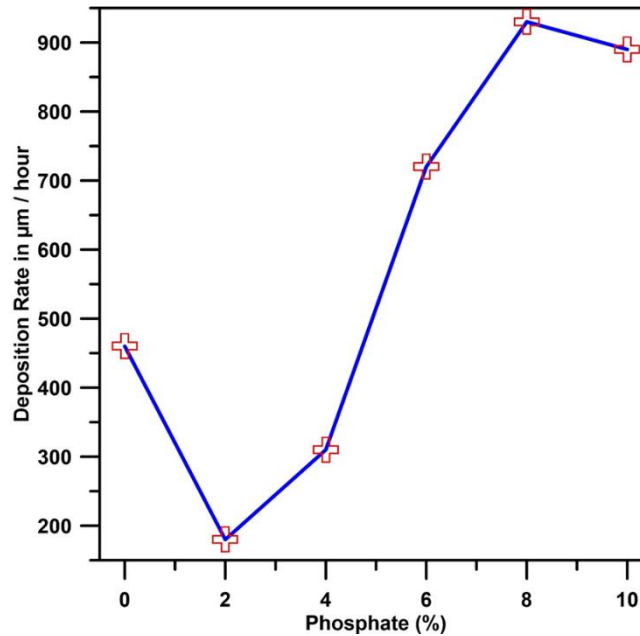


Figure 1.14: Tensile Strength vs Phosphorus Content Plot for Electroless Ni-P Coatings [Duncan, 1996]

Figure 1.14 illustrates the relationship between tensile strength and phosphorus content in coatings. **Duncan (1996)** has also reported a higher tensile strength for the coatings with medium and high phosphorus contents. The coatings usually contain β -phase solid solutions at lower concentrations of phosphorous. However, with an increase in phosphorus content, the proportion of the amorphous phase increases with the formation of γ phase. This transition leads to development of a stressed microstructure resulting an initial increase in tensile strength. However, the tensile strength decreases with the phase transformation into fully amorphous.

1.7.4 Tribological Test

Wear is nothing but a gradual material removal or damage or deformation of solid surfaces due to the relative motion of one surface over another. It can result from various

wear mechanisms which is known as modes of wear. The specific combination of these mechanisms depends on the surface contact conditions. Common wear mechanisms include adhesive, abrasive, fatigue, corrosive, fretting, erosion, and chemical wear. In real-world scenarios, it's typical for multiple wear mechanisms to act simultaneously. It is found that there is a correlation between surface hardness and wear resistance of coatings like wear rate decreases with increased surface hardness. Hence, electroless nickel (EN) coatings usually exhibit excellent wear resistance and abrasion resistance due to their high hardness. Numerous researchers have confirmed the superior wear resistance of EN coatings [Gawne and Ma, 1988; Barker, 1993; Baudrand and Bengston, 1995; Berkh et al. 1996]. Additionally, the incorporation of tungsten with binary EN coatings has been found to enhance their wear resistance due to increased surface hardness of ternary alloy coatings. The surface hardness and wear resistance are even comparable to hard chromium and high alloy materials [Nemane et al. 2022]. The surface hardness of any material serves as an indicator of its resistance to wear. There are several other factors like surface texture and applied stress, also play significant roles in deciding wear resistance of any surface [Madah et al. 2015]. The wear resistance of any electroless nickel-based coatings is influenced by factors such as composition, surface morphology, surface roughness and the type of heat treatment, heat treatment duration etc [Balaraju et al. 2016, Sürdem et al. 2019]. Heat treatment typically enhances the coating's hardness which consequently improves its wear resistance [Balaraju et al. 2016, Sürdem et al. 2019]. Heat treatment may also help to form a rough surface due to coarsening of the grains of the coatings become coarse which potentially may lead to a reduction in its wear resistance [Vitry and Bonin, 2017; Arias et al. 2019]. Study suggests that the as-deposited coatings or the furnace annealed coatings possess higher wear rate compared to the laser irradiated coatings [TsujiKawa et al., 2005]. But the increased hardness may be achieved through appropriate heat treatment methods which makes them preferable for wear-resistant applications. However, it is worth noting that the coatings heat treated at 400°C in an environment of 5% H₂ and 95% Ar, the Taber wear index drastically dropped to 13 for electroless Ni-B coatings [Kanta et al., 2010]. For applications requiring high wear resistance, such as sliding surfaces or flow through pipes, deposition of electroless Ni-B coatings over aluminium substrates may prove to be more effective

than plated steel [Kanta et al., 2009]. Vitry et al. (2008) carried out scratch test which demonstrates strong adhesion between electroless Ni-B coating and aluminum alloy substrate. It is reported by Srinivasan et al. (2010b) that the electroless Ni-B coatings possess columnar structure which is suitable for tribological behaviours and it is believed to be the main reason for their high wear resistance. This type of columnar structure aids in holding lubricant even during adhesive type wear. It is observed that electroless nickel-based coatings generally exhibit abrasive type or adhesive type or combination both type of wear mechanism. Due to the high solubility of nickel and iron with each other, adhesive wear mechanism typically dominates the deterioration of as-deposited Ni-B coatings from the counter surface material. It is observed that some tailored coatings demonstrate superior wear behavior compared to the substrate material upon incorporation of particles with electroless nickel which is very common. Incorporation of tungsten with electroless Ni-P coatings has been shown to enhance their wear resistance possibly due to strengthening of nickel matrix in a solid solution [Palaniappa and Seshadri, 2008]. Nickel atoms present in electroless nickel-phosphorous deposits are drawn towards iron atoms present in the counter disc. This attraction leads to wear and gradual removal of the coating material. In certain cases, oxide particles adhere to the interface between the coated pin and the counter disc, resulting in a negative wear depth curve [Palaniappa and Seshadri, 2008]. Additionally, the accumulation of oxides at the interface serves as a lubricant, effectively decreasing the COF value for the heat-treated coatings [Palaniappa and Seshadri, 2008].

Additionally, the addition of ZrO_2 with electroless Ni-P-W coatings is seen to enhance the wear resistance of the coatings as reported by Gay et al., 2007. Studies have shown that the abrasion resistance of steel may be improved upon incorporation of tungsten carbide (WC) as reinforcement with electroless Ni-P matrix to form Ni-P-WC [Liu et al. 2007; Luo et al. 2015]. The enhanced abrasion resistance observed in Ni-P-WC composite coatings may be attributed to the supportive role of the nickel matrix. This matrix effectively holds the tungsten carbide (WC) particles within its structure [Liu et al. 2007; Luo et al. 2015]. This structural arrangement enables the electroless coating to endure excessive damage caused by the shearing action of the sliding counterpart. Various other soft and hard particulates like alumina (Al_2O_3) [Alirezaei et al. 2005],

boron carbide (B_4C) [Araghi and Paydar, 2010], and silicon carbide (SiC) [Sarret et al. 2006], have been demonstrated as particle inclusions in these types of coatings. The EN coatings heat treated above $400^\circ C$ has a detrimental effect on wear resistance of the coatings as seen to be reported by several researchers [Novák et al. 2010; Gilley, K.L. et al. 2012; Goettems et al. 2017; Mukhopadhyay et al. 2018f]. This phenomenon arises from the formation of intermetallic phases resulting a reduction in adhesion between the coating and the substrate. Novák et al. (2010) investigated wear tracks and identified the abrasion type wear mechanism to dominate. The study further reveals the delamination of coatings heat treated above $450^\circ C$ due to formation of excessive intermetallic phases [Pal et al. 2011; Domínguez-Ríos et al. 2012; Pancrecious et al. 2018]. The study also suggests that the incorporation of Al_2O_3 with Ni-P matrix reduced flaking and improved the wear resistance compared to as-deposited Ni-P coatings [Alirezai et al. 2005]. There exists a reciprocal correlation between the volume percentage of B_4C particles and the wear resistance demonstrated by Ni-P- B_4C coatings as reported by Ebrahimian-Hosseiniabadi et al. (2006). The wear resistance of Ni-P- B_4C composite coatings enhanced with addition of B_4C particles upto 25% volume percentage and the wear resistance decreases drastically upon further rise in B_4C particle percentage [Araghi et al. 2010]. This reduction in wear resistance of the Ni-P- B_4C coatings is attributed to the presence of particles within the matrix and effective support to retain them [Araghi et al. 2010]. The inclusion of SiO_2 nanoparticles aids in impeding the dislocation movements within the composite coatings, facilitating the accompanying crystallization of an amorphous Ni-P matrix at elevated temperatures [Sadreddini et al. 2014; Li et al. 2017]. A study also reported an improvement in specific wear rate of Ni-P- TiO_2 due to incorporation of 4 g/l nano- TiO_2 compared to as-deposited Ni-P coatings [Makkar et al. 2014].

1.7.5 Corrosion Resistance Test

EN coatings serves as a protective layer over substrate by shielding the substrate material from environmental damage. In their deposited form, these coatings usually possess amorphous phase in its as-deposited condition and exhibit high resistance against corrosion [Anik et al. 2008, Wan et al. 2016]. The amorphous phase structure and

absence of grain boundaries contribute to their excellent anti-corrosive properties of the coatings [Anik et al. 2008, Wan et al. 2016]. However, it is seen that the corrosion resistance of electroless coatings reduces due to a microstructural change in the coatings from amorphous to crystalline upon heat treatment [Anik et al. 2008, Wan et al. 2016]. Tomlinson and Carroll (1990) investigated and reported the relationship among surface roughness, coating thickness, and corrosion resistance of the coatings. The study also suggests that the corrosion resistance increased with coating thickness for a given substrate roughness.

1.7.6 Nanocomposite Coatings

The electroless coatings are also developed with the addition of various particles of micro or nano size to deposit composite coatings. The various composite coatings may be developed with the use of reinforcement of several types of particles like SiC, WC, diamond, TiC, Cr₃C₂, Al₂O₃, SiO₂, Cr₂O₃, TiO₂, ZrO₂, CeO₂, YSZ, Fe₃O₄, K₂Ti₆O₁₃, Si₃N₄, MoS₂, PTFE, BN, Talc, B₄C, CaF₂, polymer, CNT and graphite [Liu et al. 2007; Matsubara et al. 2007; Yu et al. 2011; Afroukhteh et al. 2012a, Afroukhteh et al. 2012b; Ashassi-sorkhabi and Es, 2013; Sharma and Singh, 2013; Ma et al. 2014; Hsu et al. 2015; Islam et al. 2015; Luo et al. 2015; Murty et al. 2015; Soleimani et al. 2015; Wang et al. 2015; Wu et al. 2015; Ardakani et al. 2017; Dadkhah and Ansari, 2016; Sharma and Sharma, 2016; Shi et al. 2016; Farrokhzad, 2017; Li et al. 2017; Sadreddini et al. 2017; Xie, 2017]. It is reported in many literatures that the addition of these nano-particles as reinforcement has improved the surface hardness of the coated specimens besides an enhancement in the wear resistance of the nano-composite coatings [Xu et al. 2005; Bigdeli and Allahkaram, 2009; Ranganatha et al. 2012; Karthikeyan and Ramamoorthy, 2014; Sadreddini and Afshar, 2014]. Makkar et al. (2014) studied the impact of TiO₂ addition with electroless Ni-P matrix and demonstrated an enhancement in wear resistance behaviour of TiO₂ reinforced nano-composite compared to as-deposited Ni-P [Wu et al. 2015]. The Table 1.5 represents a comparative report on specific wear rate of as-deposited Ni-P coatings and TiO₂ reinforced nano-composite coatings at different applied loads and sliding speeds. The study indicates a reduction in

specific wear rate of TiO₂ reinforced composite coatings by 30% approximately which confirms the improvement in wear resistance due to TiO₂ inclusion.

Table 1.3: Comparison of Wear Rates Against Applied Load and Sliding Speed for Ni-P and Ni-P-TiO₂ [Makkar et al. 2014]

Coatings	Load (N)	Specific wear rate (10 ⁻⁶ mm ³ /Nm)	Sliding Velocity (m/s)	Specific wear rate (10 ⁻⁶ mm ³ /Nm)
Ni-P	1.00	7.85	0.10	8.00
	1.50	25.00	0.20	15.00
	2.00	61.78		
Ni-P-TiO ₂	1.00	1.43	0.10	1.50
	1.50	3.93	0.20	4.48
	2.00	18.9		

1.7.7 Lead Free Coatings with the use of Green Bath

The electroless coatings are deposited using a chemical solution which need to be stable during the coating deposition by reduction reaction. The chemical bath contains some metal salts which do not react with each other at room temperature. But the chemical reaction starts at certain temperature and the chemical reaction is expected to continue till the metal ions present in the solution. The metal ions are reduced with the help of a suitable reducing agent. There are few metal salts which helps to stabilize the chemical reaction process so that the chemical bath does not decompose fast. There are a few commonly used stabilizers reported in different literatures [Bonin et al. 2019; Bonin et al. 2020; Agarwal et al. 2024]. The most of the chemical bath solutions to deposit coatings based on nickel-boron uses lead as stabilizers. Lead is a well-known hazardous material and hence banned in many countries. Therefore, it imposes a restriction to develop coating using lead-based stabilizers. However, this electroless coating deposition method cannot be neglected due to its superior tribo-mechanical behaviours. Hence, the researchers are trying to develop lead free coating bath solution or stabilizer free coating bath solution [Bonin and Vitry, 2020; Yunacti et al. 2021; Agarwal et al. 2024]. On the other hand, few more chemicals like bismuth, tin is found to be used as stabilizers in different coating baths which may replace lead as stabilizer [Bonin et al. 2019; Bonin et al. 2020; Agarwal et al. 2024]. Hence, development of eco-friendly production in the field of electroless coating is drawing attention all over the globe [Bonin et al. 2019;

Bonin et al. 2020; Bonin and Vitry, 2020; Yunacti et al. 2021; Banerjee et al. 2022; Agarwal et al. 2024].

Overall, it is seen that the electroless coating has become popular gradually since the time of invention by Brenner and Riddell in 1946 [**Brenner and Riddell 1946**] for its excellent properties. Generally, electroless nickel-phosphorous coating is well known for its mechanical properties and nickel-boron coating is popular for its tribological properties. The use of electroless coatings can be found in industries like automobile, chemical, oil, gas and aerospace for their excellent mechanical, physical and tribological behaviours. Hence, chemically deposited Ni-B coatings were studied by several researchers based on deposition rate, plating thickness, surface morphology and surface texture etc. [**Anik et al. 2008; Kanta et al. 2009; Kanta et al. 2010; Hamid et al. 2010; Bonin et al. 2019; Mohanty et al. 2019; Sukackiene et al. 2020**]. It is seen that the coating characteristics depend on the composition, temperature and pH of the coating bath [**Anik et al. 2008; Bonin et al. 2018; Bonin et al. 2019; Sukackiene et al. 2020, Bonin et al. 2020**]. The behaviour of the coatings is further modified through heat treatment [**Bekish et al. 2010; Pal et al. 2011; Taha-Tijerina et al. 2019**]. It is seen that the surface morphology and phase structure of as-deposited coatings is changed upon heat treatment. The amorphous phase of as-deposited coatings turns crystalline upon heat treatment [**Hamid et al. 2010; Taha-Tijerina et al. 2019**]. Boron content in the coating also depends on sodium borohydride concentration as well as coating bath temperature [**Baskaran et al. 2006; Hamid et al. 2010; Sukackiene et al. 2020**]. The as-deposited coating with low boron content (of about 4 wt. %) possesses crystalline phase structure which becomes a combination of amorphous and crystalline structure with the rise in boron content in the coatings [**Baskaran et al. 2006; Venkatakrishnan and Karthik, 2019**]. It is also seen that the behaviour of coatings also depends on boron concentration. The surface morphology and phase structure found to vary with the coating's chemical composition which leads to a change in coatings behaviours [**Pal et al. 2011; Venkatakrishnan and Karthik, 2019; Sukackiene et al. 2020**]. The study also suggests that the surface hardness and wear resistance of as-deposited coatings increase with boron concentration [**Bekish et al. 2010**] and this improvement in hardness is possible for the homogeneous distribution of boron and amorphous structure. The same is improved

further with heat treatment [Balaraju et al. 2016; Mohanty et al. 2019] and may be attributed with the evolution of various boride phases like Ni_2B , Ni_3B during thermal treatment [Krishnaveni et al. 2005; Anik et al. 2008; Kanta et al. 2009; Hamid et al. 2010; Vitry et al. 2012; Yildiz et al. 2017]. But the corrosion resistance deteriorates after heat treatment [Riddle and Bailer 2005; Anik et al. 2008]. Tribological and mechanical behaviours are also seen to vary with the change in microstructure [Pal and Jayaram 2018]. Amorphous structure of coating shows improved adhesion strength to aluminium substrate which results in an increase in surface hardness besides friction and wear behaviour [Delaunois et al. 2002; Hamid et al. 2010; Vitry et al. 2011]. It is reported that the surface hardness of the as-deposited coatings does not change much with the boron content upto 6 wt. % but the same improves due to increase in boron concentration upto 9 wt. % [Vitry and Bonin, 2017]. It is also found that various alloy coatings are also deposited with addition of different hard particles like Mo, W and investigated based on different coating characteristics [Serin et al. 2015; Serin and Göksenli, 2015; Hosseini et al. 2019; Nemane and Chatterjee, 2020]. Chemically deposited Ni-B-W or Ni-B-Mo coatings exhibit cauliflower like surface morphology which is a common feature of borohydride reduced ENB coatings [Serin et al. 2015; Serin and Göksenli, 2015; Yildiz et al. 2017]. The low boron content coatings show crystalline structure but addition of both tungsten and molybdenum prevents the nucleation leading to formation of amorphous structure [Yildiz et al. 2013; Aydeniz et al. 2013; Yildiz et al. 2017]. The addition of tungsten with electroless Ni-B to form ternary Ni-B-W alloy coating improved the coated surface hardness further [Aydeniz et al. 2013; Yildiz et al. 2013; Mukhopadhyay et al. 2018g; Nemane et al. 2022] but the addition of molybdenum does not improve the surface hardness of Ni-B-Mo coatings [Serin and Göksenli, 2015; Serin et al. 2015; Mukhopadhyay et al. 2018e]. The addition of molybdenum improved the thermal stability of electroless Ni-B-Mo coatings compared to Ni-B coatings [Serin and Göksenli, 2015; Serin et al. 2015; Mukhopadhyay et al. 2018e]. It is also observed that the surface porosity of electroless Ni-B-W coated surface is reduced due to tungsten oxide layer deposition over surface upon heat treatment [Yildiz et al. 2013]. The wear behaviours of Ni-B-W coated surface is also improved after heat treatment. Nano-hardness and elastic modulus of coatings are

determined using loading-unloading curve obtained from nano-indentation based model [Musil et al. 2002; Wei and Lin 2005] which shows good agreement for lower indentation depth with the data obtained from “Korsunsky and Kings” model [Domínguez-Ríos et al. 2012]. Surface hardness and Young’s modulus of electroless Ni-B coatings are seen to increase after heat treatment within the temperatures range of 300°C to 450°C. It is reported that the mechanical properties are observed to increase with heat treatment duration and this increase may be attributed to the dissipation of hard boride phases like Ni₂B, Ni₃B etc during heat treatment [Vitry et al. 2011; Domínguez-Ríos et al. 2012]. Moreover, hardness and Young’s modulus value of coatings are seen to increase further due to incorporation of hard nano-particles like ZrO₂, Al₂O₃ because of grain refinement [Radwan et al. 2015]. The reinforcement of nano-particles reduces the active area for entry of corrosive solution leading to improvement in corrosion behaviour [Radwan et al. 2015]. Surface hardness, corrosion resistance and wear behaviour of as-deposited and heat-treated nano-composite coatings improve with reinforcement of hard nano-particles like TiO₂, ND, alumina etc into Ni-B matrix [Kaya et al. 2008; Niksefat and Ghorbani, 2015; Taha-Tijerina et al. 2019].

1.13 Summary of Literature Review

Electroless nickel (EN) plating is a deposition process by chemical reaction of reducing agent present in the coating bath itself without the use of electricity. It has received widespread attention for industrial applications due to its high hardness, good corrosion resistance, uniformity of coatings, etc. EN coatings can be classified into three main categories, namely pure nickel, alloy, and composite coatings. Several research works have been already carried out to investigate the characteristics of EN Pure coating, binary (Ni-B, Ni-P, etc.), and ternary alloy coatings (Ni-W-P, Ni-Cu-P, etc.). Metallic elements like tungsten (W), Cobalt (Co), molybdenum (Mo) have been incorporated to form binary, ternary, or quaternary alloys coatings to improve the properties like thermal stability, hardness, tribological behavior, and corrosion resistance. Nanoparticles like Al₂O₃, SiO₂, ZrO₂, TiO₂, and SiC are being widely used due to their excellent wear resistance and hardness. TiN may also be an ideal candidate for coating due to its high hardness, chemical resistance, and high melting point. Carbon nanotube (CNT) and

Carbon nanofibers (CNFs) are being used since they possess outstanding electrochemical and mechanical properties including high tensile strength and elastic modulus.

Various EN coatings are observed to deposit with different combinations of bath composition to determine the coating characteristics. The electroless nickel-based alloy coatings are observed to investigate based on coating deposition rate, coating thickness, surface morphology, phase structure, tribological and mechanical behaviours of coatings. The deposition rate and coating thickness are observed to vary with coating bath parameter concentration as well as operating conditions. The surface morphology and phase structure are also observed to depend on coating bath composition. The surface morphology, as well as phase structure ultimately, lead to a change in coating characteristics.

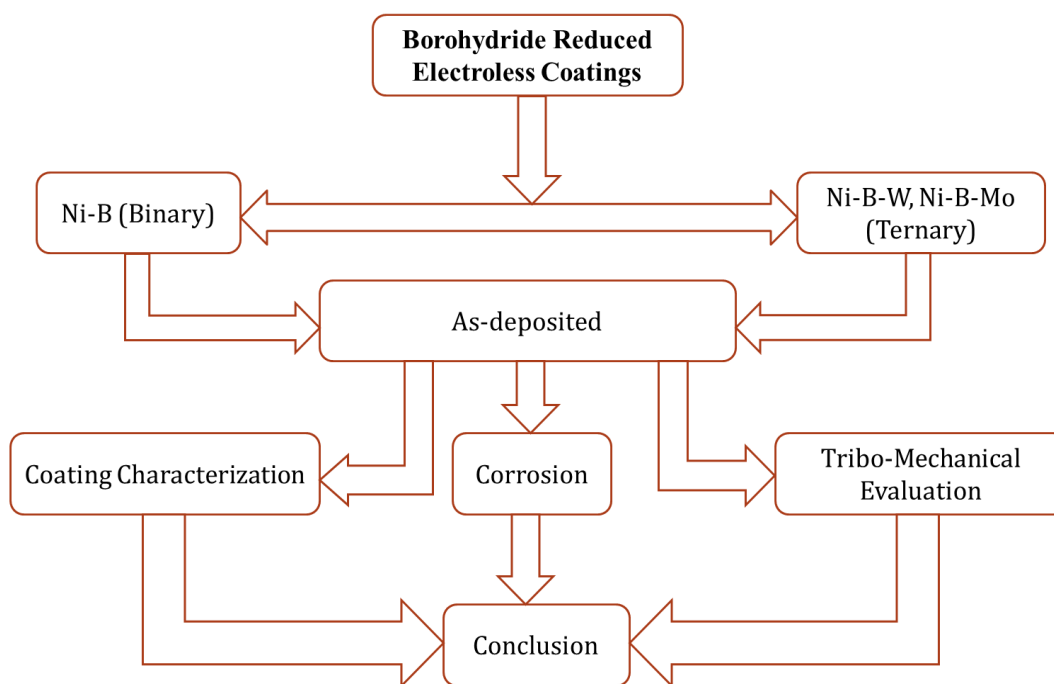


Figure 1.15: Research Work Plan

It was observed from the previous studies that the electroless Ni-B (ENB) coatings deposited with low sodium borohydride in the coating bath exhibit a crystalline structure. The same transformed into an amorphous structure with the rise in sodium borohydride concentration leading to an increase in surface hardness of the coatings. The

surface hardness also improved due to the rise in boron content in the coatings with the increase in sodium borohydride concentration in the coating bath solution. Hence, the variation of the coating bath parameters and concentration may impact the coating composition. The change in coating composition may lead to a change in surface roughness, surface morphology, and phase structure which may ultimately lead to a change in coating characteristics. The proposed work aims to explore the impact of bath parameters on the coating characteristics of different electroless nickel coatings such as Ni-B, Ni-B-W, and Ni-B-Mo.

1.14 Research Work Plan

Based on the literature survey, research objectives and outline of the work are defined. The **Figure 1.15** represents the research work plan.

1.15 Research Objectives

Based on the literature survey following objectives have been derived.

- To prepare borohydride reduced electroless Ni-B, Ni-B-W and Ni-B-Mo coatings.
- To characterize the coatings on the basis of surface morphology, phase structure and elemental analysis using SEM, XRD and EDAX.
- To study the surface roughness and tribological behaviours of the as-deposited coatings.
- To study the surface hardness and elastic modulus of the as-deposited coatings using nano-indentation techniques.
- To study the scratch hardness of the as-deposited coatings using micro-scratch test
- To study the corrosion resistance of the coatings.
- To compare the Ni-B based binary and ternary coatings with different bath compositions.

1.16 Research Work Methodology

The research work decided from the literature survey which is to be carried out under the current investigation. The same is elaborated through the flowchart as mentioned in **Figure 1.15**. The research work methodology is also explained through the **Figure 1.16**.

The flowchart displayed in **Figure 1.16**, elaborates the coating deposition to coating characterisation process. The coatings are then tested for different coating characteristics.

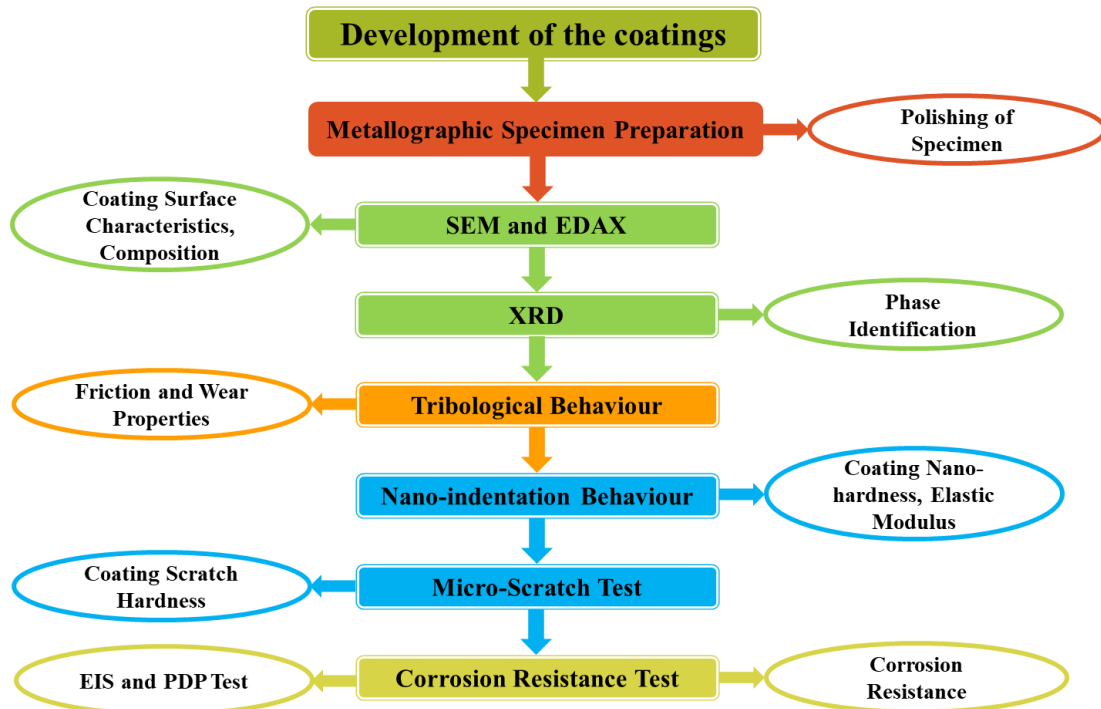


Figure 1.16: Research Methodology to be Followed

1.17 Closure

The literature survey elaborates the current state of the research work on electroless nickel-boron based coatings. The literature survey also presents the importance of electroless Ni-B coatings in industrial applications. However, there are lot of questions regarding the variation in tribo-mechanical behaviour of electroless nickel-boron based coatings is yet to be answered completely. What may be the impact of variation in coating bath composition on mechanical and tribological behaviour of coatings? How the variation in coating bath composition may impact the corrosion behaviour of nickel-boron based coatings? An attempt has been made to answer these questions in the following chapters which is the outcome of the current study.

This page is intentionally left blank

Chapter 2: Materials and Methods

Outline: 2.1 Introduction, 2.2 Sample Preparation, 2.3 Bath Composition and Coating Deposition, 2.4 Coating Characterisation, 2.4.1 Coating Thickness, 2.4.2 Surface Morphology, 2.4.3 Chemical Composition, 2.4.4 Phase Structure, 2.5 Physical and Mechanical Behaviours, 2.5.1 Surface Roughness, 2.5.2 Nanoindentation Test, 2.5.3 Micro-Scratch Test, 2.6 Tribological Test, 2.7 Corrosion Resistance Test, 2.7.1 Potentiodynamic Polarisation, 2.7.2 Electrochemical Impedance Spectroscopy, 2.8 Closure

2.1 Introduction

The current chapter elaborates the fundamental aspects of sample preparation and coating deposition process for different coatings. This chapter also contains the coating bath composition to deposit coated layer of Ni-B, Ni-B-W and Ni-B-Mo coatings. The chapter further elaborates the characterisation techniques used for characterisation of coatings. The detailed test procedure to understand the variation in tribo-mechanical behaviours and corrosion resistance behaviour is also elaborated in this chapter. Different test parameters and procedures are also discussed in the following sections.

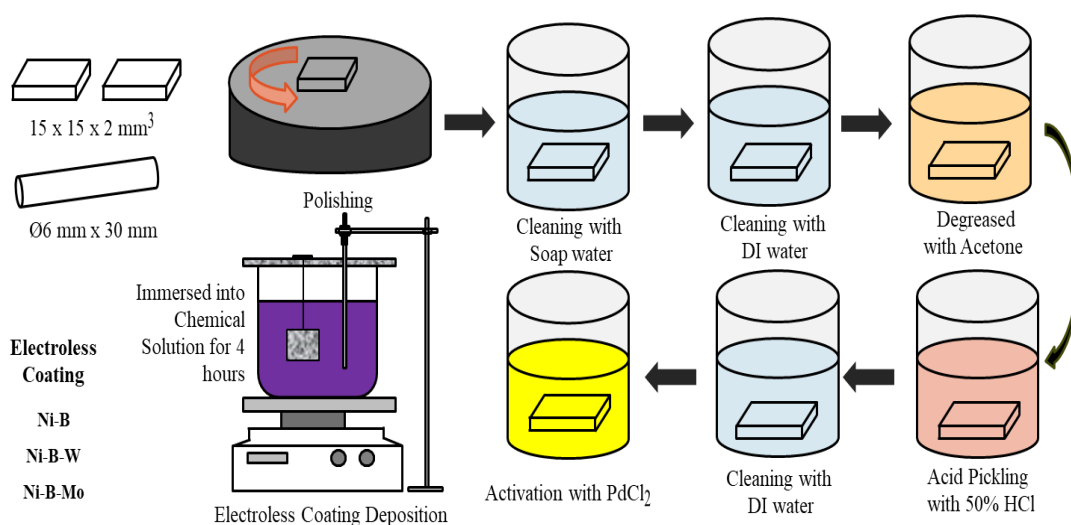


Figure 2.1: Flowchart of Sample Preparation

2.2 Sample Preparation

For coating deposition, AISI 1040 steel is used as substrate material. Samples with dimensions of 15 mm × 15 mm × 2 mm were used for basic characterization and mechanical tests. The samples with dimensions of 6 mm diameter x 30 mm long dimension were used for tribological tests. AISI 1040 steel contains 0.32-0.43 wt.% C, 0.10-0.25 wt.% Si, 0.68-0.85 wt.% Mn, 0.03 wt.% S, 0.06 wt.% P and the remainder is Fe. The samples were prepared and the surfaces were ground to achieve smooth surface finish with an average surface roughness value of 0.285 μm (Ra). The electroless nickel (EN) coatings are known to follow the substrate's surface profile. The specimens with homogeneous surface texture were chosen for the EN coatings. The specimens were washed properly with soap water and degreased by dipping them into acetone followed by rinsing with deionized water. The specimens were again rinsed with deionized water after the acid pickling treatment in 50% HCl solution. This treatment ensures the smooth and defect free surface of the specimens without any rust or oxide layers. Then the specimens were dried and used for the coating deposition. The same process is elaborated through the process flowchart displayed in **Figure 2.1**.

2.3 Bath Composition and Coating Deposition

The electroless borohydride reduced alloy coatings (Ni-B, Ni-B-W, Ni-B-Mo) were deposited over steel substrates. The specimens with smooth and uniform surface are selected for the coating deposition. The steel substrate possesses catalytically active surface. Hence, the coatings may be deposited over the steel substrates straightway through chemical deposition process. However, the specimens are dipped into lukewarm PdCl_2 to accelerate the deposition process further. The steel substrates were dipped into the coating bath solution for about 4 h. Double coating baths were used by replacing 200 ml coating bath with another one after 2 h to ensure significant coating thickness. The specimens are removed from the coating bath solution after four hours and are rinsed with deionized water. The coating bath load is maintained within the range of 28.5 to 31.1 cm^2/L . No mechanical or ultrasonic agitation is used during the coating deposition process. Alternatively, bath replenishment is chosen so that the coating bath stability and deposition rate is not hampered as well as the deposition of diffused layer does not

take place due to the reduction of reactive species. The detailed coating procedure is also explained through the flowchart given in the **Figure 2.2**.

Coating Deposition on Steel Substrate of size 15x15x2 mm³ and ϕ 6x30 mm³

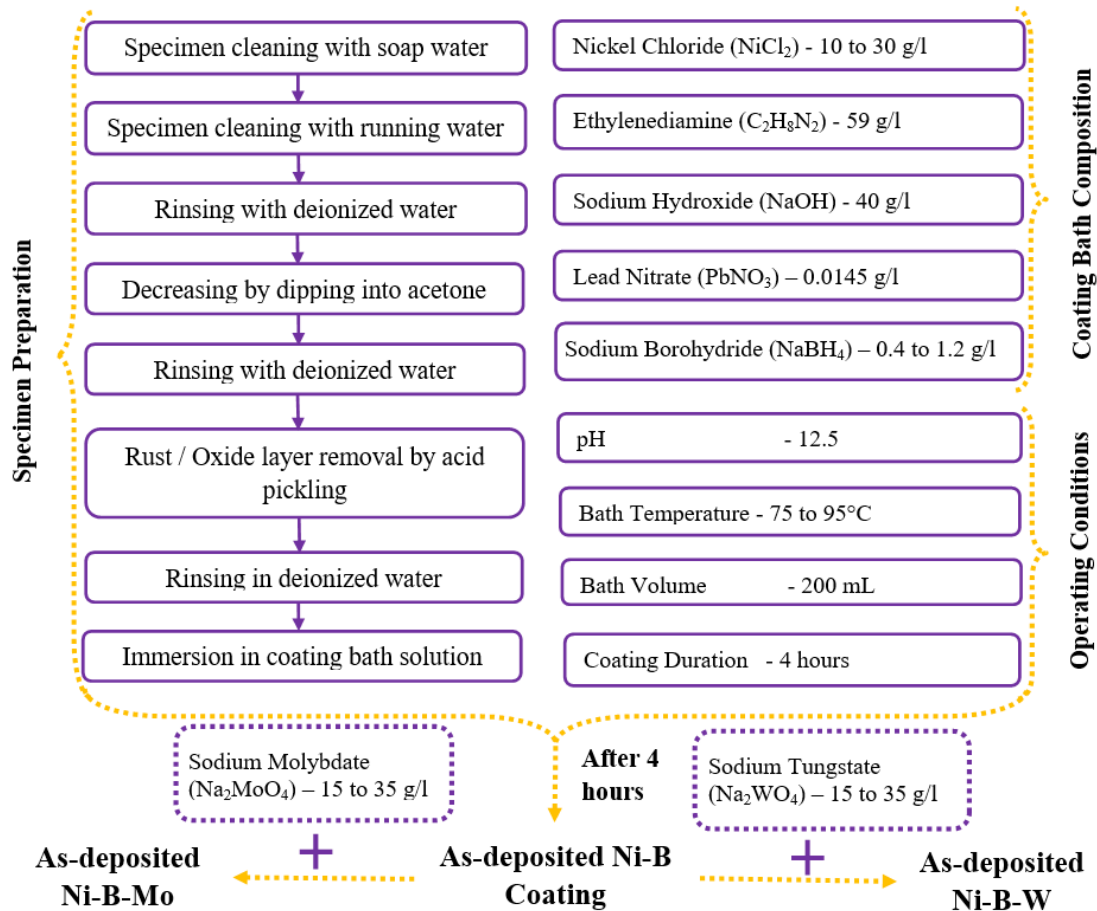


Figure 2.2: Flowchart of Coating Deposition Process

The coating bath contains nickel chloride (NiCl_2) as source of nickel ions and sodium borohydride (NaBH_4) is the source of boron ions in the solution. The sodium borohydride also acts as reducing agent. Suitable amount of ethylenediamine ($\text{C}_2\text{H}_8\text{N}_2$), sodium hydroxide (NaOH) and lead nitrate (PbNO_3) were also used as complexing agent, buffer and stabilizer, respectively. Electronic heater cum stirrer was used to maintain the necessary temperature of the coating bath while the bath pH was monitored using a digital pH meter and maintained at about 12.5. The coating bath temperature is controlled with the help of the electronic heater which is displayed in **Figure 2.3**. The

coatings are deposited by varying each parameter individually with temperature and keeping the other parameters constant at their mid-level values. The working range of the chemicals with their level of concentrations used for coating deposition are mentioned in the **Table 2.1**.

Table 2.1: Coating Bath Parameters and Their Level of Concentrations

Elements	Purpose	Level 1	Level 2	Level 3	Level 4	Level 5
NiCl ₂ in g/l	Source of Ni ion	10	15	20	25	30
NaBH ₄ in g/l	Reducing Agent Source of B ion	0.40	0.60	0.80	1.00	1.20
Na ₂ WO ₄ in g/l	Source of W ion	15	20	25	30	35
Na ₂ MoO ₄ in g/l	Source of Mo ion	15	20	25	30	35
Temperature (°C)	Operating condition	75	80	85	90	95
C ₂ H ₈ N ₂ in g/l	Complexing Agent	59				
NaOH in g/l	Buffer	40				
PbNO ₃ in g/l	Stabilizer	0.0145				

The chemical used during the coating deposition process is supplied from Merck Life Science Private limited. The substrates were cleaned with acetone (Merck, 99%) and made rust-free using HCl acid (Merck, 37%) solution. The chemicals present in the coatings bath are Nickel (II) Chloride Hexahydrate (Merck, 98%), Sodium Hydroxide Pellets (Merck, 97%), Sodium Borohydride (Merck, 95%), Sodium Tungstate Dihydrate (Merck, 99%), Sodium Molybdate Dihydrate (Merck, 99%), Lead (II) nitrate purified (Merck, 99%), Ethylenediamine (Merck, 99%).

The chemical required for specific coatings are mixed by adding them sequentially in appropriate proportionate to get the final chemical solution. All the chemical salts remain present in the solution but do not react with each other at room temperatures. The chemical bath prepared in this process is also known as autocatalytic bath which is used to deposit coatings. This coating deposition method do not use any electricity unlike electrodeposition method rather it uses chemical reduction reaction to

deposit coatings. The electroless coating bath solution contains a reducing agent which extracts the metal ions. The same metal ions then deposit over the substrate surface. The substrates used for coating deposition process must possess a catalytically active surface or the surface is activated if do not possess catalytically active surface. Sometimes, some catalysts are also used to accelerate the coating deposition process.

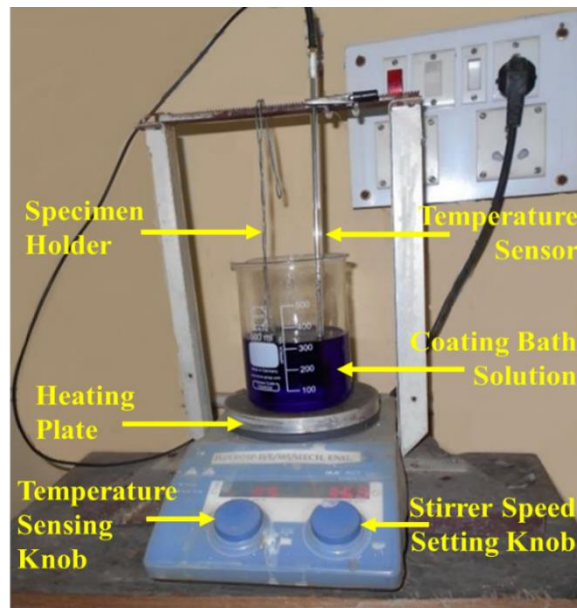


Figure 2.3: Coating Deposition Set up

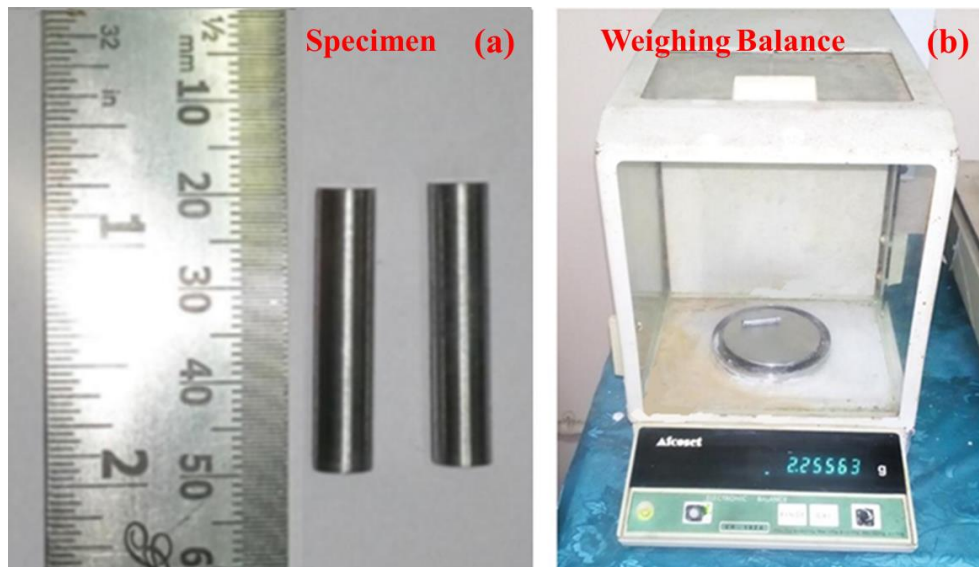


Figure 2.4: (a) Prepared Cylindrical Specimen and (b) Weighing Balance

2.4 Coating Characterisation

2.4.1 Coating Thickness

The coatings are developed over steel substrates with different compositions. The coatings are known to follow substrate surface and possess a uniform thickness. The prepared samples of 6 mm diameter and 30 mm lengths are shown in **Figure 2.4(a)**. The coatings are also developed over samples of size 15 mm x 15 mm x 2 mm. The weight of the samples is measured before and after the coating deposition process. The mass gain of the samples indicates the deposition of coatings. The thickness of the coated layers is also calculated from the mass gain and a constant coating density. The mass of the specimens is measured by a sensitive electronic balance Afcoset ER-182 A which is shown in **Figure 2.4(b)**. The coated square shaped and cylindrical samples are displayed in **Figure 2.5**.

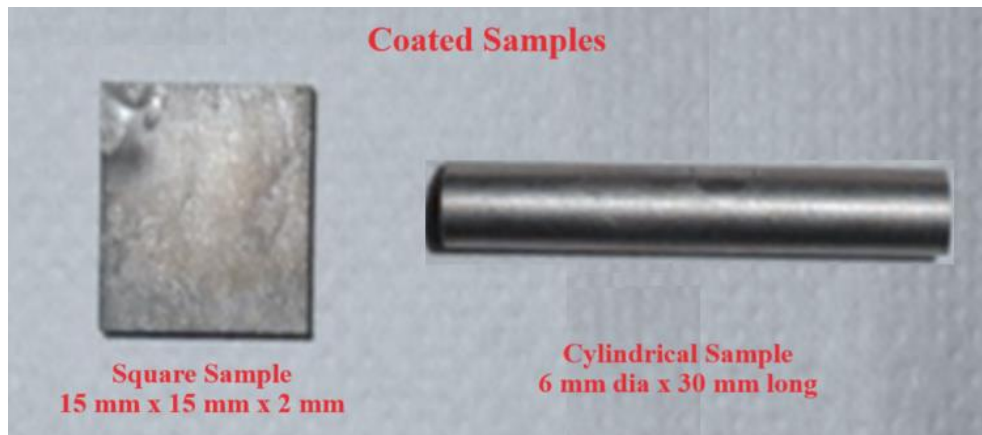


Figure 2.5: Coated Substrates

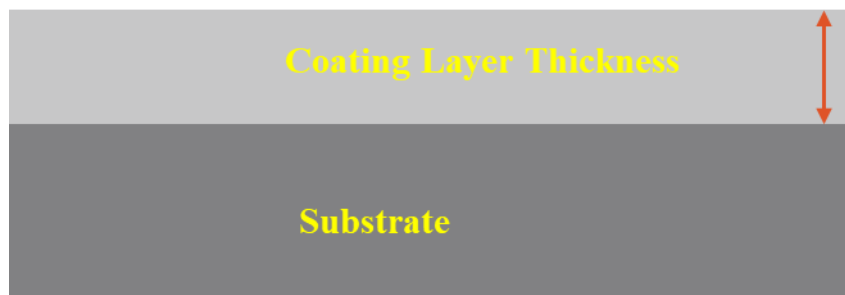


Figure 2.6: Schematic Diagram of Coated Layer Thickness

The electroless Ni-B coatings which contains 5% boron is seen to possess a density of 8.25 gm/cm^3 [Vitry et al. 2022]. Hence, a constant density of 8.25 gm/cm^3 is considered to estimate the coating thickness. So, considering a constant density and uniform coating thickness, initial estimation of coating thickness is done from the mass gain.



Figure 2.7: SEM, S3400N, HITACHI

The same coating thickness is further measured using scanning electron microscopy (SEM) with different magnifications. The specimens are cross cut to expose the coated layer thickness. The same coated layer is examined under SEM to measure the coated layer thickness. A schematic diagram of coating thickness is displayed in **Figure 2.6** where the substrate and the coated layer may be observed clearly.

2.4.2 Surface Morphology

The coated surfaces are further observed under SEM to examine the surface morphology. The coatings are examined using Scanning Electron Microscope (SEM, S3400N, HITACHI) with secondary electron detector. The SEM set up is displayed in

Figure 2.7. The cross cut coated specimens are examined under SEM not only just to measure the coated layer thickness but also to understand the coating deposition process. The coating deposition mechanism ultimately leads to the development of final surface morphology of the coatings. The coated surface is investigated for the understanding of the surface formed during coating deposition process at different condition which ultimately may lead to modifications in coating behaviours.



Figure 2.8: FESEM, SIGMA, CARL ZEISS

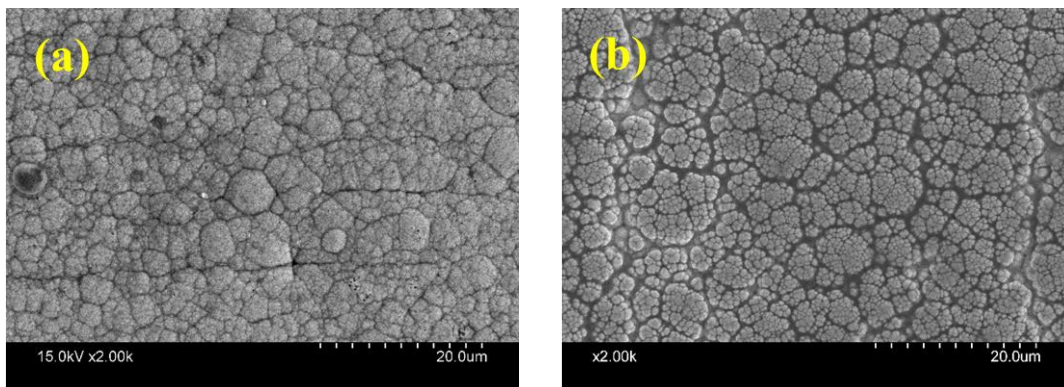


Figure 2.9: SEM Image of Coated Surface Morphology, (a) SEM Image and (b) FESEM Image

Figure 2.8 shows a FESEM (Field Emission Scanning Electron Microscope) set up which is also used to determine the coating thickness as well as surface morphology of the coatings. The SEM set up contains a beam of electrons which is directed towards the

specimen surface and it generates signals in the form of secondary / backscattered electrons or characteristic X-rays. The signals actually represent the surface structures and hence the signals are received by detectors to generate images of the same surface structure on a computer screen. The FESEM machine are equipped with a field emission guns (FEGs) attachment which provides high resolution images. **Figure 2.9** (representative) represents the SEM images obtained from SEM and FESEM machines.

2.4.3 Chemical Composition

The deposition of coated layer is confirmed through scanning electron microscope. The next important step is to investigate the chemical composition of the coating and the phase structure of the coatings obtained with different coating bath compositions and operating conditions. The chemical composition study is to ensure the presence of all the key elements in the coatings which is expected to deposit. The concentration of those key elements and their distribution over the coated surface also plays an important role to decide the material properties and performance to certain extent. Energy Dispersive X-ray Spectroscopy (EDAX / EDS / EDX) is very common and popular technique in this regard. The chemical composition was determined at a low energy level of 10-15 KeV using EDAX. The EDAX setup carries a super ultrathin window for the effective transmission of low-energy x-rays. The system is calibrated with Si. While the ENB coating EDAX spectrum was compared with a standard boron sample spectrum to determine the boron content.

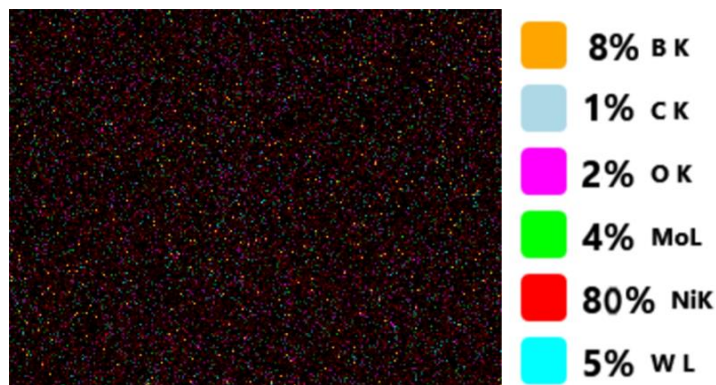


Figure 2.10: Representative EDAX Mapping Image of Coated Surface

The FESEM set up displayed in **Figure 2.8** contains additional attachment with it which has a field emission guns (FEGs) which enables it in the detection of different elements present in a material. Generally, it is difficult to detect light elements (atomic number < 9) under most of the SEM machines. The FESEM is capable of detecting light elements. Moreover, the FESEM is better suited for EDAX mapping of elements or analysis of composition through energy dispersive spectroscopy (EDS) attachment. It uses the energy of X-rays produced due to the electron beam directed towards the material surface and it allows the identification of elements. The representative EDAX mapping image of the coated surfaces are displayed in **Figure 2.10** which shows the distribution different elements on coated surfaces. On the other hand, the **Figure 2.11** show a representative EDAX spectrum of coated surface. Different peaks corresponding to different elements present in the EDAX spectrum confirms their presence in the coatings.

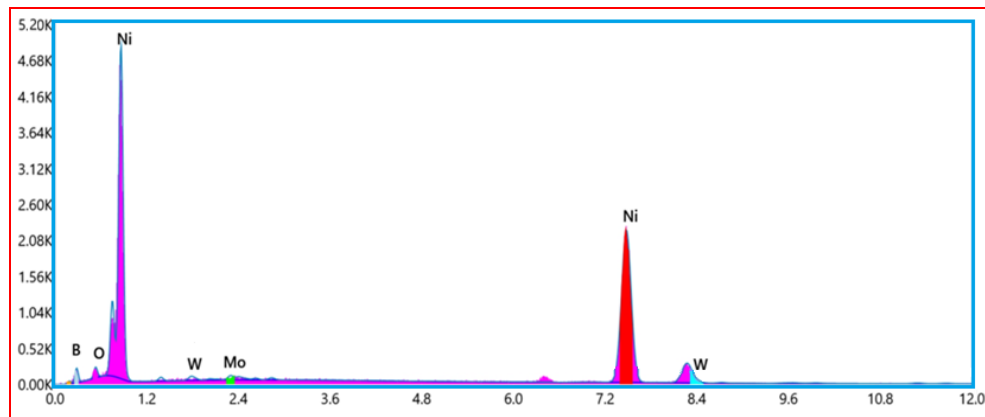


Figure 2.11: Representative EDAX Spectrum of Coatings

These are useful to quickly determine the relation between material structure and the properties. In the field of material research microscopic techniques are at the forefront wherein newer combinations of material properties are examined and developed. Test samples are carefully prepared by standard metallography. Different tools like optical microscope, scanning electron microscope, X-ray diffraction, Raman spectroscopy, atomic force microscopy etc. are available for characterisation purpose. The objective of the present microstructural study is to examine the distribution of particles, grain structure, and identification of phase elements in the as-deposited coated surfaces.



Figure 2.12: X-ray Diffraction (XRD) Instrument (D8ADVANCED, BRUKER, USA)

2.4.4 Phase Structure

XRD is a non-destructive method. The fundamental principle behind X-ray diffraction (XRD) is based on the constructive interference of monochromatic X-rays with crystalline material. These X-rays are generated by a cathode ray tube, filtered to ensure monochromaticity, collimated to focus them, and then directed towards the sample. When the incident rays strike the sample under conditions satisfying Bragg's Law ($n = 2d \sin\theta$), they produce constructive interference and a diffracted ray. As per Bragg's Law, the lattice spacing and diffraction angle in a crystalline sample are directly proportional to the wavelength of the electromagnetic radiation used for diffraction. Detection and analysis of the diffracted X-rays are necessary. By scanning the sample across a range of 2θ angles, which exposes the material to all possible diffraction directions of the lattice. The diffraction peaks can be observed and converted to d-spacings for identification. The **Figure 2.12** shows the XRD instrument

(D8ADVANCED, BRUKER, USA) used for XRD analysis. The phase structures of the as-deposited coatings were determined using the diffractometer which is equipped with Cu-K α radiation source with a scanning rate of 0.02°/s within the range of $2\theta_1$ to $2\theta_2$ of 20° to 90°. The characteristics of XRD plots can rapidly determine whether a specific phase is crystalline or amorphous. Crystalline phases are identified by sharp, well-defined diffraction peaks. Whereas amorphous phases exhibit broad, diffuse peaks. This distinction is fundamental in analyzing the structural properties of materials using X-ray diffraction techniques. A representative XRD pattern obtained from the instrument is displayed in **Figure 2.13**.

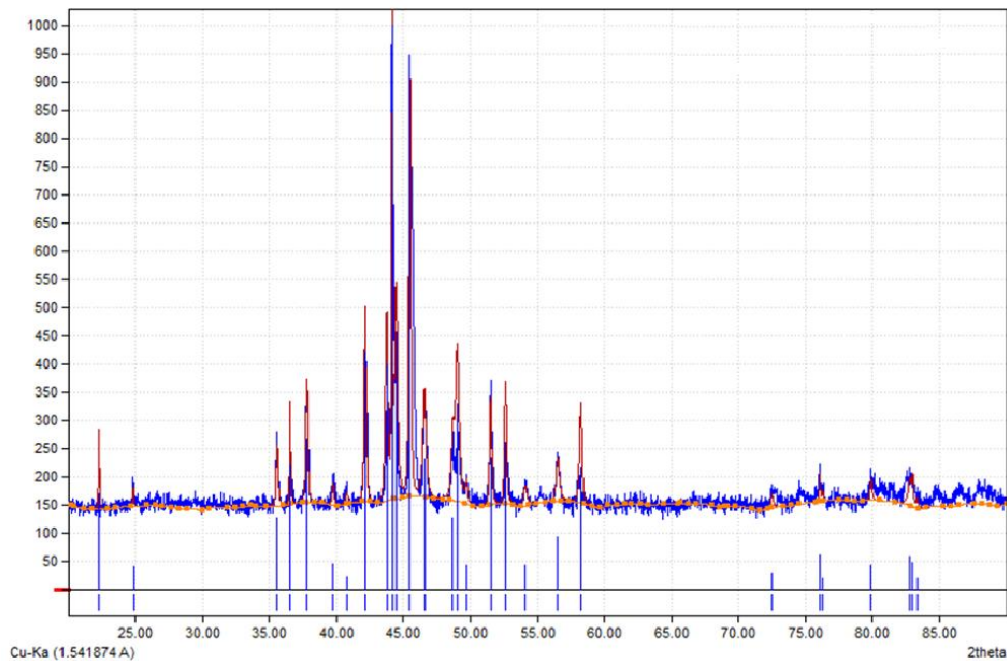


Figure 2.13: Representative XRD Spectrum of Coatings

2.5 Physical and Mechanical Behaviours

2.5.1 Surface Roughness

The geometric parameters are crucial to a coating. Its surface roughness, significantly impacts its mechanical integrity. Thus, precise measurement of roughness is essential for coating evaluation. The contact method, employing a stylus traversing the surface, is utilized to measure the surface roughness of the electroless nickel coatings. A

Talysurf profilometer (Surtronic 3+, Taylor Hobson, UK) is employed for measuring the required roughness parameters. The surface roughness tester employed under current study is displayed in **Figure 2.14**. After the deposition of electroless Ni-B coating over AISI 1040 steel substrates, the surface roughness of the coatings is also measured with another stylus based profilometer (MGW SURFACE ROUGHNESS TESTER SRT-1) for few specimens. The set up is equipped with a diamond stylus having a tip radius of 5 μm . The measurements were taken for a sampling length of 4 mm.



Figure 2.14: Surface Roughness Tester (Surtronic 3+, Taylor Hobson)

Measurements typically start from the extreme outward position, with the measuring stroke determined by the traverse length, which is usually five times the cut-off length by default. The surface roughness measurements are conducted with a Gaussian filter and 4 mm sampling length, while the stylus traverse speed is maintained at 1 mm/s. Measurements on coated samples are repeated at least three times in different orientations, and the average of the three values is recorded finally. The average roughness serves as the response variable for the conducted studies. The measured profile from the Talysurf is digitized and processed through the advanced surface finish analysis software Talyprofile for evaluating the roughness parameters considered in the present work.

2.5.2 Nanoindentation Test

Nanoindentation has gained popularity as a method for measuring properties at the nano/micro-scale, such as creep resistance, hardness, fracture toughness, and elastic modulus, particularly for thin films and coatings. Unlike traditional methods, nanoindentation calculates the contact area indirectly from the penetration depth without the need for imaging the indent. This makes it a versatile and efficient technique for characterizing material properties at small scales. The test set up may be used to conduct the indentation test in two basic methods. One is indentation depth-based method and the other one is applied load-based method. In depth-based method, the indentation is carried out for a fixed depth of indentation and the applied load varies depending upon the material property. The higher the load required, higher the indentation hardness. On the other hand, the applied load-based method is carried out for a fixed load and the indentation depth may vary depending upon the material property. The higher is the indentation hardness if the indentation depth is less.

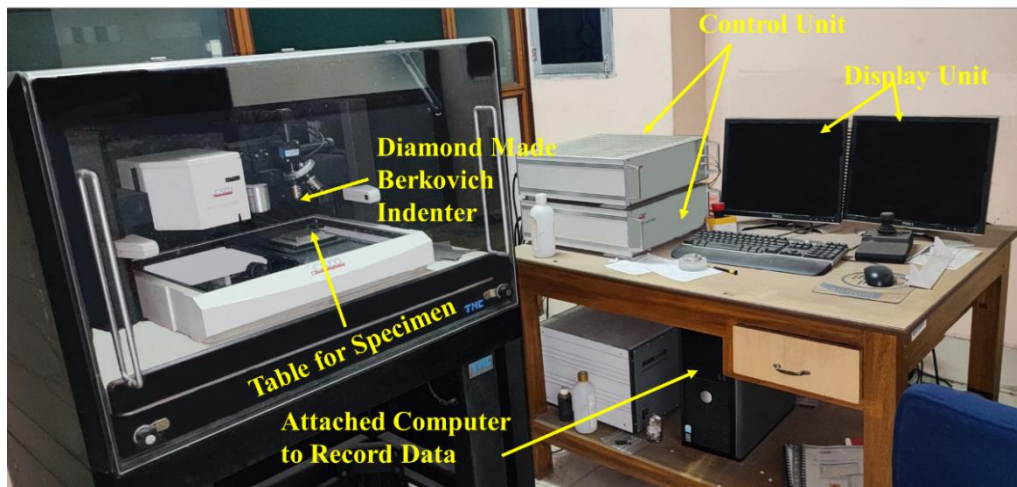


Figure 2.15: Nano-indentation Test Setup (NHT-1, CSM)

Nano-indentation behaviour of the electroless nickel-boron based coated samples is tested with the help of a nano-indentation tester (NHT-1, CSM) which is displayed in **Figure 2.15**. The test set up is equipped with a triangular based pyramid shaped Berkovich indenter. All the nano-indentation tests are conducted for a maximum indentation depth of 500 nanometre. A uniform loading unloading rate of 40 mN/min and

a pause time of 2 seconds are used to carry out the tests. The surface hardness and elastic modulus are determined from the loading unloading curve obtained from the data recorded in the computer attached with the nano-indentation test set up. The mechanical properties of the coatings can be determined from the data obtained from nano-indentation test (Hysitron, Nano-indenter) using Oliver and Pharr method [Domínguez-Ríos et al. 2012]. The nano-indentation tests are conducted with the help of indentation depth-based method [Vitry et al. 2008] for a maximum indentation depth of 500 nanometre. To avoid the substrate effect on the mechanical properties of the coatings, the maximum indentation depth of indentation is maintained less than one-tenth of minimum coating thickness [Pal et al. 2018]. All the nano-indentation tests are carried out for three times. The average values of those three test results of nano-hardness are calculated and reported.

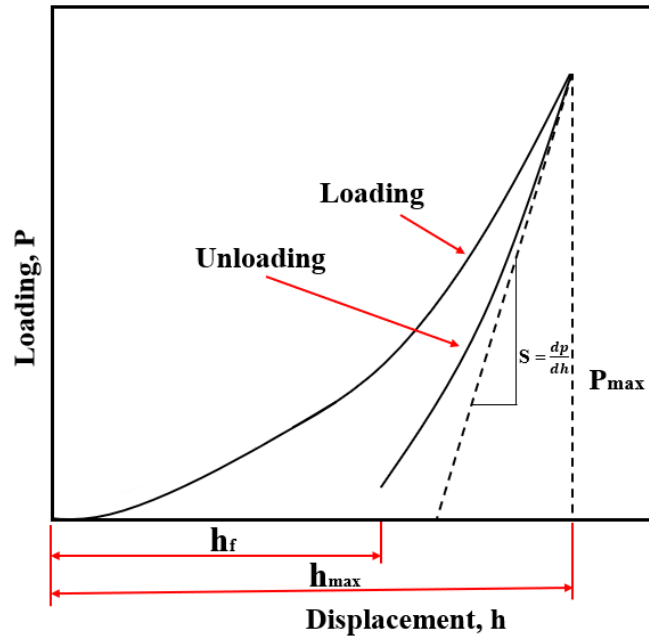


Figure 2.16: A Typical Loading-unloading Curve

The data generated during the nano-indentation test is recorded in a computer attached with the set up. The loading unloading curve obtained using the recorded data is displayed in **Figure 2.16**. The loading unloading curve is used to calculate the elastic modulus. The calculation of the elastic modulus in nanoindentation follows the Oliver

and Pharr method, which relies on generating a load-displacement curve. This curve provides insight into the elastic modulus of the specimen. The analysis method, proposed by **Oliver and Pharr in 1992**, utilizes the specimen's elastic unloading response to determine the tip-sample contact size during unloading. The stiffness of the elastic contact is determined based on Hertz' theory, providing a robust framework for understanding material properties at small scales.

The stiffness of contact is determined from the **Eq. 2.2**,

$$S = \frac{dP}{dh} \quad (2.2)$$

The effective elastic modulus value is determined from **Eq. 2.3**,

$$E_e = \left(\frac{\sqrt{\pi}}{2} \right) \left(\frac{S}{\sqrt{A_c}} \right) \quad (2.3)$$

Where, $E_e = 1/[(1 - \nu_{sample}^2)/E_{sample} + (1 - \nu_{indenter}^2)/E_{indenter}]$, from this equation the term $(1 - \nu_{sample}^2)/E_{sample}$ may be obtained as the indenter properties are known and the E_e is calculated from the **Eq. 2.3**.

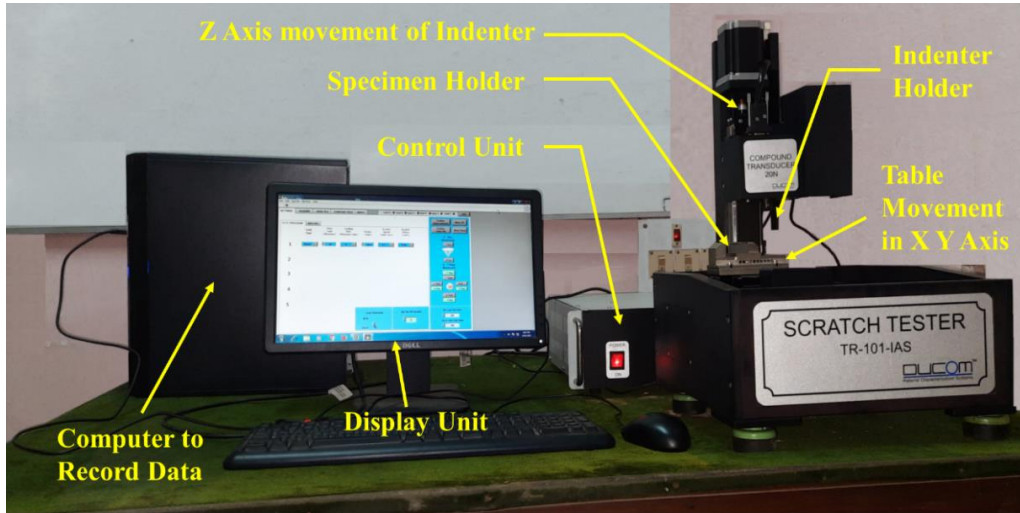


Figure 2.17: Micro-Scratch Tester (TR-101-IAS, DUCOM, India)

2.5.3 Micro-Scratch Test

The scratch tester is used for the micro-scratch tests. The test setup comprises of various components necessary for the testing process as depicted in **Figure 2.19**. Scratch

hardness is measured using a micro-scratch test set up (TR-101-IAS, DUCOM, India) as per ASTM G171-03 standard. The test setup is provided with a diamond made Rockwell C type indenter and the indenter tip radius is 200 μm . The **Figure 2.18** shows the scratch test process with the help of a conical shaped diamond indenter. The test set up contains a moveable table on which the specimen is fixed and the test specimen is moved with the table as required. The indentation load of 20N is applied with the help of a transducer. The scratch test is carried out on the coated surface at 5 different locations parallel to each other. The scratch width of each scratch is measured at different locations as shown in **Figure 2.19**.

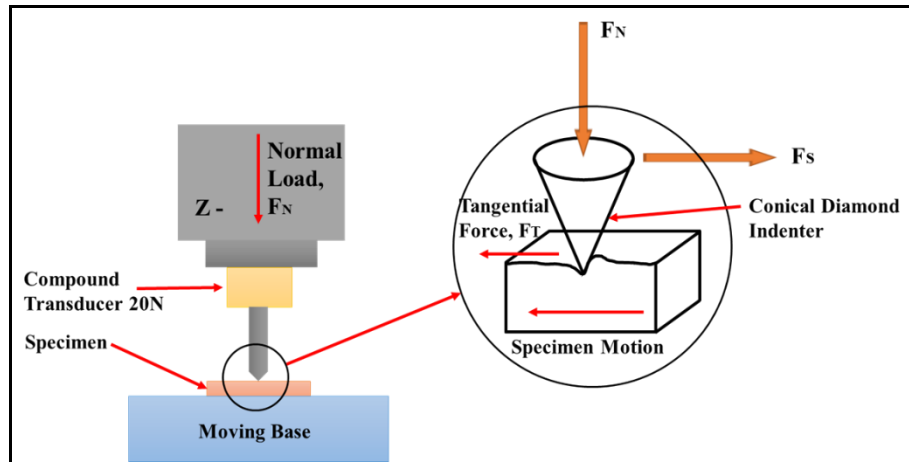


Figure 2.18: Schematic Diagram of Scratch Test Process

The tests are conducted against an applied load of 20N and the scratch length is kept as 5 mm. The scratch velocity is kept constant at 0.1 mm/sec. Scratch marks made on the coated surface are captured using the scratch tester's integrated image acquisition system. The acquisition system is equipped with a camera boasting a resolution of 5 megapixels. To facilitate input and visualization of test parameters, the scratch tester is linked to a computer via the "Winducom 2010" software. This software serves as a platform for managing and analyzing the scratch test data. The scratch width is measured at 10 different locations and the average of those values is used to calculate the scratch hardness. To ascertain the scar widths and calculate the scratch hardness (in GPa), the "Scar View 2016" software was employed. Following the guidelines outlined in ASTM

G171-03, the scratch hardness is determined based on the applied load and the average width of the scratch. This standardized approach ensures consistency and accuracy in the evaluation of scratch resistance. The following **Eq. 2.4** is used to calculate the scratch hardness:

$$HS_p = 24.98 \frac{N}{X^2} \text{ GPa} \quad (2.4)$$

Where HS_p is scratch hardness, N is applied load in gm and X is scratch width in μm .

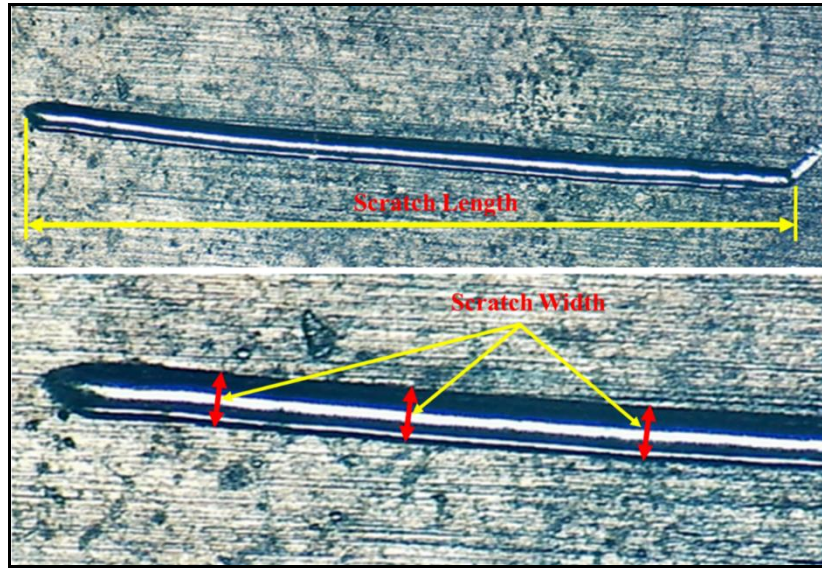


Figure 2.19: Typical Image of Scratch Width

2.6 Tribological Test

The tribological behaviour of the coatings is investigated using a pin-on-disc tribotester (TR-20LE-CHM-400, DUCOM, India) under dry condition. The schematic diagram of the test set up is displayed in **Figure 2.20**. The coated pin samples are used as specimen for the tribo test. A circular disc of 115 mm diameter and 8 mm thick is used as counter surface. The circular disc is made of EN31 (58-68 HRC) steel. The specimens are kept fixed at a position and the counter surface is allowed rotate to provide sliding action. The pin sample is allowed to slide for a sliding distance of 514 m with a sliding velocity of 42.86 cm/sec at a track diameter of 60 mm against an applied load of 40N. The

computer attached to the tribotester is used to control the parameters and record the frictional force between the pin sample and the rotating disc.

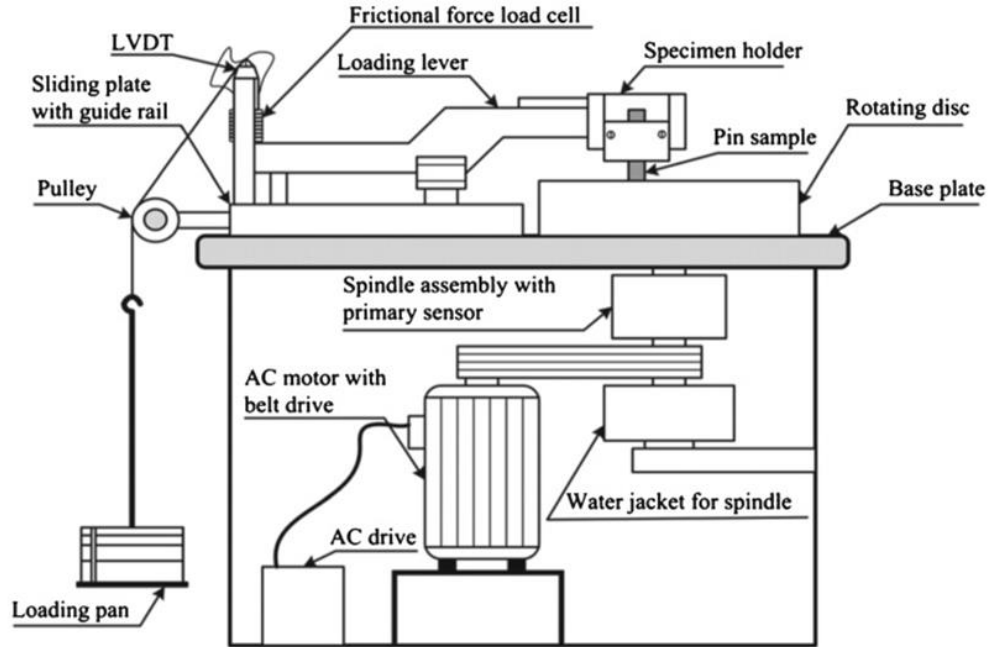


Figure 2.20: Schematic Diagram of Pin-on-disk Tribo-tester

The wear rate is measured from the mass loss of the samples by measuring the mass before and after the test using a precision weighing balance with 0.01 mg precision. The specific wear rate (W_s in kg/N.m) is determined using the **Eq. 2.5**,

$$W_s = \frac{M}{L.W} \quad (2.5)$$

Where M is the wear mass, L is sliding distance and W is the applied load. Sliding distance is calculated from the track diameter and the total revolution turned by the pin.

The tribological test set up used in this current work is displayed in **Figure 2.21**. The tests are carried out as per ASTM G99-05 standard. The pin specimens are attached vertically at one end of loading lever against a rotating counter disc, made of EN31. The hardness of the counter surface is significantly higher compared to specimen. Constant load is applied through the loading pan at the end of loading lever which is operated manually. The test parameters like speed, test duration is controlled through specialized

software. The software also displays the real time variation in friction coefficient with sliding duration. The same real time data is recorded in the attached computer and it is used for further analysis.



Figure 2.21: Pin-on-disk Tribotester (TR-20LE-CHM-400, DUCOM, India)

2.7 Corrosion Resistance Test

The corrosion behaviour of the coatings is investigated through Electrochemical Impedance Spectroscopy (EIS) and Potentiodynamic Polarisation (PDP) test methods. A three-electrode based potentiostat (Gill AC, ACM Instruments, UK) was employed for this purpose. The corrosion resistance behaviour of the coated specimens was tested against 3.5% sodium chloride (NaCl) solution as a corrosive medium. Only 1 cm² area of the samples was exposed to the corrosive environment. A reference electrode (saturated calomel electrode) was used to estimate the potential difference. An auxiliary electrode was used to allow the applied current flow to the solution. Initially, open circuit potential (OCP) was provided a settling time of 15 min. The coated substrates were used to act as working electrode (WE), while a platinum electrode and saturated calomel electrode were employed to serve as an auxiliary electrode (AE) and reference electrode (RE), respectively. The potentiostat with electrochemical cell is displayed in **Figure 2.22**. The potentiostat set up was used to carry out PDP and EIS test to investigate the corrosion resistance of the as-deposited samples at normal room temperature of about 27°C. The

saturated calomel electrode was used as the reference electrode to measure the accurate potential difference. A platinum electrode (auxiliary electrode) makes the way of applied current flow to the solution. A dedicated software installed in the computer was used to collect the data and analyse. Double layered capacitance (C_{dl}) and charge transfer resistance (R_{ct}) values were determined by fitting a semicircle with the Nyquist plot using the software installed in the accompanying computer. The corrosion current density (i_{corr}) and the corrosion potential (E_{corr}) of the electroless as-deposited coatings were obtained using Tafel extrapolation method.

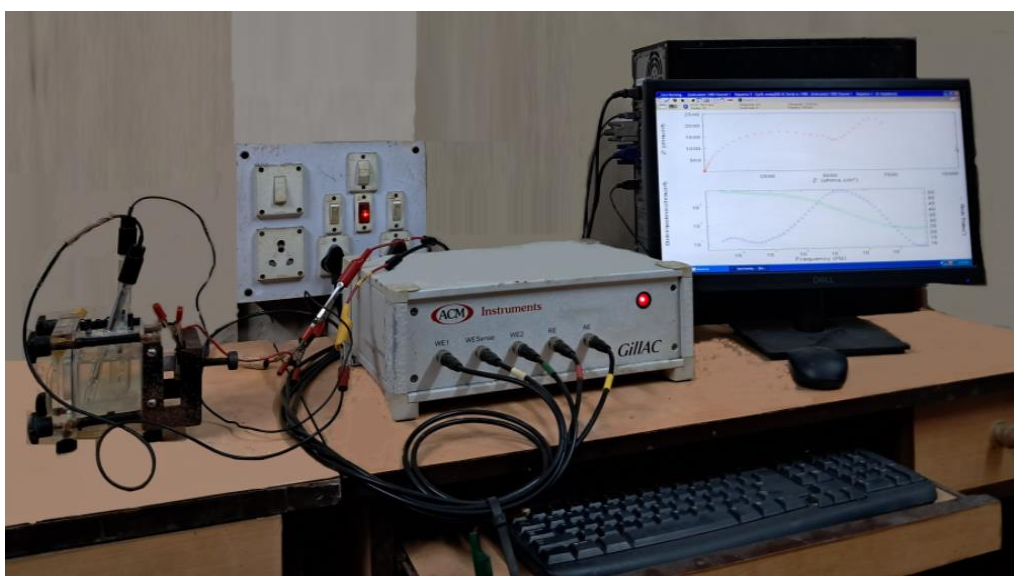


Figure 2.22: Electrochemical Corrosion Test Setup (3 Electrode Potentiostat)

2.7.1 Potentiodynamic Polarization

Polarization is a technique in electrochemistry to study the metal electrode behaviour against corrosive medium by adjusting the electrode's potential from its natural state and measuring the resulting current. If a metal isn't connected to any external circuit, then its potential is called Open Circuit Potential (OCP). This OCP represents the metal's equilibrium state and helps to determine its corrosion potential, dissolution potential, or equilibrium potential. An increase in the corrosion potential typically suggests the formation of protective films on the metal surface. These films act as barriers, shielding the metal from further corrosion. Conversely, a decrease in corrosion potential indicates

the breakdown or removal of these protective films, leaving the metal more vulnerable to corrosion. Therefore, monitoring changes in corrosion potential over time provides valuable insights into the stability and effectiveness of these protective films in corrosive environments.

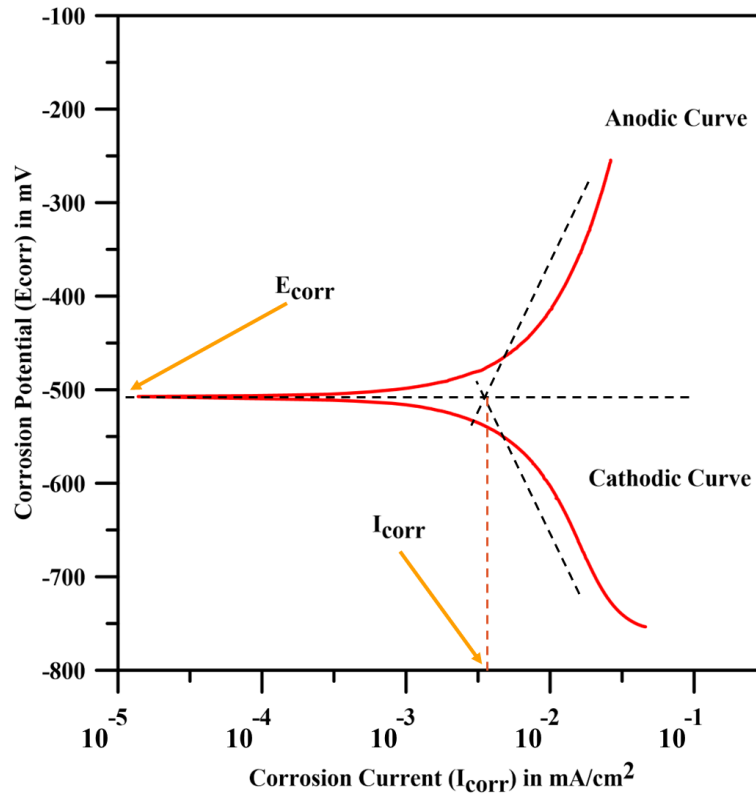


Figure 2.23: Typical Tafel Plot

During anodic polarization, the potential of the working electrode shifts positively, making it the anode and causing the removal of electrons from it. This results in the oxidation of metal ions on the electrode surface, leading to corrosion. The current passing through the electrode during anodic polarization is directly proportional to the rate of metal ion oxidation. Conversely, cathodic polarization occurs when the potential of the working electrode shifts negatively, turning it into the cathode and supplying electrons to it. This leads to the reduction of metal ions on the electrode surface, potentially forming a protective film that reduces the corrosion rate. The current flowing through the electrode during cathodic polarization is directly proportional to the rate of

metal ion reduction. The data recorded from the Polarization test is used to obtain the Tafel plot. Tafel plot is obtained by using the corrosion potential along Y axis and logarithmic value of corrosion current along X axis. It provides important information about the corrosion resistance of substrate material. The informations like corrosion rate, corrosion current density (I_{corr}) and the corrosion potential (E_{corr}) may be obtained from this Tafel plot. **Figure 2.23** represents a typical Tafel plot which contains an anodic and a cathodic part. The linear segment of the plot is known as Tafel region. It is visual illustration of the correlation between electrode potential and the logarithm of the related current density during the electrochemical reactions. It emerges elevated overvoltage and points out the step that controls the electrochemical reaction rate. This method is widely acknowledged as a quick and precise technique for assessing the corrosion rate of materials. The Tafel extrapolation method's ability to offer continuous monitoring of exceedingly low corrosion rates makes it suitable across diverse applications which includes the prediction and mitigation of corrosion in both industrial and natural environments. The accuracy of this method may depend on various factors like temperature, electrode geometry, and solution composition etc. Hence, it may not provide the results compared to some other methods.

2.7.2 Electrochemical Impedance Spectroscopy

Electrochemical impedance spectroscopy (EIS) or Impedance Spectroscopy is a non-destructive method. It serves as a technique for analyzing the dynamic behaviour like corrosion performance of electrochemical systems. It involves measuring electrical impedance of the system across various frequencies. EIS offers insights of the system resistance, capacitance, and inductance. These parameters may be further utilized to calculate the corrosion rate and inhibition level. The EIS also offer some important data which is useful for controlling the electrochemical process through optimization and this facility makes the system suitable for the use in materials science, corrosion engineering, and electrochemistry. In EIS, the electrode impedance vs frequency plot is used to analyse the behavior of electrical circuits. A small voltage signal supplied with the help of auxiliary electrode. The same is applied to the substrate surface through the corrosive solution. The response is received in the reference electrode to make a comparison. The

Randle's circuit, commonly employed as equivalent electrical circuit diagram for ideal and non-ideal behaviours is presented in **Figure 2.24**.

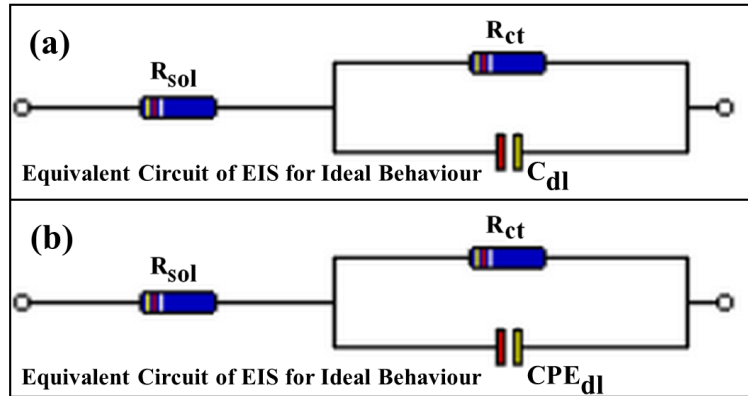


Figure 2.24: Randle's Circuit Obtained from Gill AC Instrument for (a) Ideal Behaviour and (b) Non-ideal Behaviour

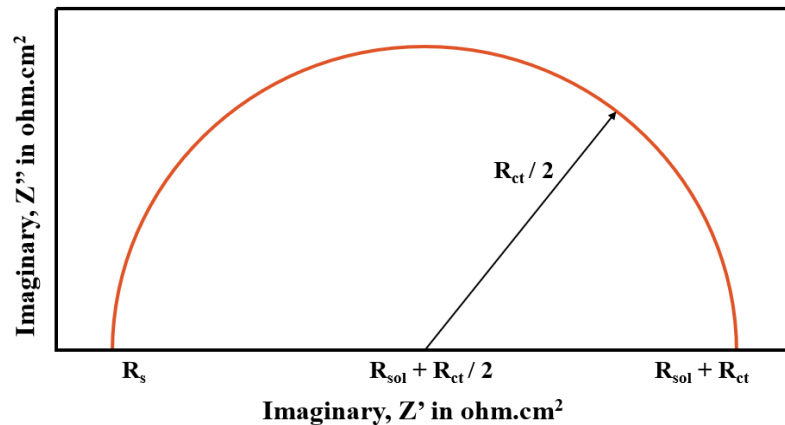


Figure 2.25: Typical Nyquist Plot

It is frequently utilized in electrochemistry to analyse electrochemical systems. In **Figure 2.24**, R_{sol} is the corrosive solution resistance in-between substrate surface / working electrode and reference electrode, and R_{ct} is the charge transfer resistance. The double layer capacitance is represented as C_{dl} used in equivalent circuit diagram for ideal behaviour. While, CPE_{dl} is the double layer capacitance for non-ideal behaviour. The data recorded during EIS test is used to obtain nyquist plot. The installed software in the attached computer uses the data collected during the test to plot the Nyquist plot

considering imaginary impedance on the y-axis and real impedance on the x-axis. **Figure 2.25** displays a typical Nyquist plot. The EIS test is carried out within the frequency range of 10^{-3} Hz to 10^5 Hz. The impedance is estimated from the measurements of the phase angle and induced current magnitude. The data generated and recorded during the EIS test with the help of potentiostat and frequency response analyzer may be stored in the attached computer for detailed analysis. A scanning speed of 1mV/s is used during the test.

2.8 Closure

This chapter contains the detailed elaboration of the specimen preparation, coating deposition, mechanical and tribological test procedures used in the current study. The chapter starts with the specimen preparation details, electroless coating deposition process with compositions. The chapter explains the coating characterisation like different characterisation techniques with the specification of the instruments and the process to interpret the test results. The basic material characterization techniques used under current study are XRD, SEM and EDAX. It is followed by nano-indentation behaviour, scratch test, corrosion test and tribological test. The tests are important to understand the tribo-mechanical behaviours of the coatings and may be correlated with the characterisation results. Finally, these tests are also helpful to compare the different materials developed in the current study.

This page is intentionally left blank

Chapter 3: Electroless Ni-B Alloy Coatings

Outline: 3.1. Introduction, 3.2 Experimental Details, 3.3 Coating Characterisation, 3.3.1 Coating Thickness, 3.3.2 Surface Morphology, 3.3.3 Chemical Composition, 3.3.3 Phase Structure, 3.4 Physical and Mechanical Behaviours, 3.4.1 Surface Roughness, 3.4.2 Nano-indentation Test, 3.4.3 Micro-Scratch Test, 3.5 Tribological Test, 3.6 Corrosion Resistance Test, 3.7 Closure

3.1 Introduction

The electroless coatings are deposited through chemical deposition process. Generally, sodium borohydride or dimethylaminborane (DMAB) is used to develop nickel-boron alloy coatings. Electroless nickel-boron coating is for its tribological properties. The behaviour of the chemically deposited nickel-boron coatings usually depends on the surface morphology, phase structure and coating composition. The surface morphology, phase structure and coating composition further depends on coating bath composition and coating bath operating conditions like bath temperature and pH. A little change in these may change the coating surface morphology, phase structure and coating composition resulting a change coating behaviour. The current chapter is focused on the analysis of the influence of the coating bath parameters on the different coating characteristics and it is extensively discussed in the following sections.

3.2 Experimental Details

Two different types of specimens are utilized to deposit coatings. The elements required for coating deposition are arranged. The coating bath elements are mixed in proper proportionate to prepare the coating bath solution. The sodium borohydride, nickel chloride and coating bath temperature is varied at five different levels. The nickel chloride is varied from 10 to 30 g/l. While, sodium borohydride and coating bath temperature is varied within the range of 0.4 to 1.2 g/l and 75 to 95 °C, respectively. The other coating bath elements are kept constant at their specified values. The low-level concentration (LLC) indicates the coating bath which contains 10 g/l NiCl_2 , 0.40 g/l

NaBH₄ and coating bath temperature is maintained at 75°C. The mid-level (MLC) concentration is meant for 20 g/l NiCl₂, 0.80 g/l NaBH₄ and 85°C while high level (HLC) concentration contains 30 g/l NiCl₂, 1.20 g/l NaBH₄ and 95°C coating bath temperature. From now on, the different concentration levels will be called as LLC, MLC and HLC. But for the trend analysis, the coatings are deposited by varying the one parameter at a time and rest are kept constant at their mid-level values. So, the coatings are deposited for 4 hours. The coated cylindrical specimens are cross cut to expose the coating layer thickness and the same is utilized to measure the coating thickness using SEM. The chemical composition of the coatings is examined through EDAX. The phase structure of the coatings is studied using X-ray Diffraction (XRD). The surface roughness of the coatings is examined using a stylus based profilometer. The indentation hardness of the coated surface and elastic modulus is determined using nanoindentation depth-based techniques. Whereas, the scratch hardness of the coated surface is determined using a micro-scratch tester against a constant applied load of 20N. The measured scratch width is utilized to calculate the scratch hardness and the same is reported in this report. The tribological tests are carried out to investigate the variation trend for friction and wear with different coating bath parameter concentrations. A three-electrode based potentiostat is also used to determine the corrosion resistance behaviour of the coatings against 3.5% NaCl solution. The detailed test procedure and methodology is elaborated in chapter 2.

3.3 Coating Characterisation

3.3.1 Coating Thickness

The coatings deposited with various composition are characterized based on coating thickness, surface morphology, elemental analysis and phase structure. The cross section of the coatings is determined using SEM as shown in **Figure 3.1**. The rise in coating thickness with the bath parameter concentration increase can be observed from **Figure 3.1**. Lowest thickness of 8.714 µm is achieved for the low level concentrations while coatings obtained at mid-level and high-level concentration exhibit a minimum thickness of 21.96 µm and 30.60 µm, respectively. The increase in coating thickness is an indication of increase in deposition rate with the rise in level of parameters as the coating

deposited for all the combination is for equal time duration i.e., 4 hrs. The deposition rate increases as NaBH_4 concentration increases in coating bath solution [Vitry et al. 2012] as well as increase in coating bath temperature. The increase in deposition rate with borohydride concentration can be attributed due to the increase in reduction rate with reducing agent [Vitry et al. 2012; Sukackiene et al. 2020].

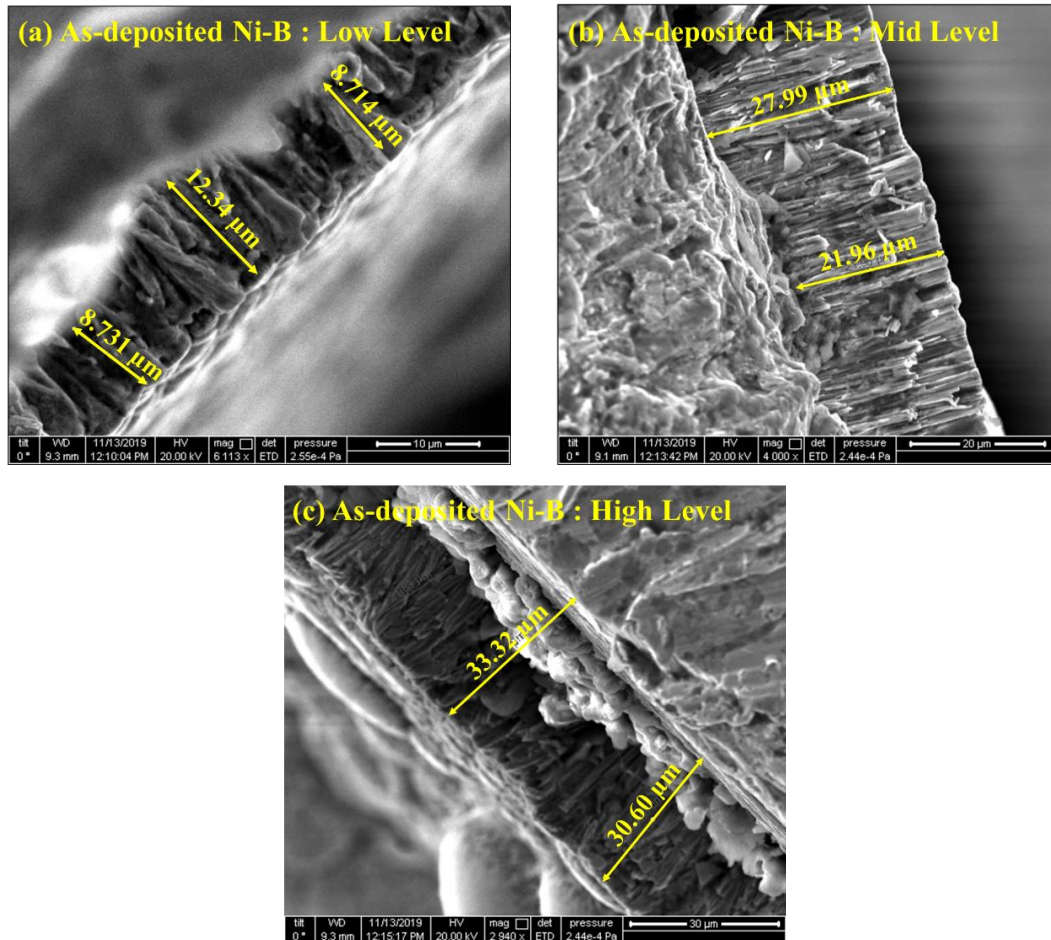
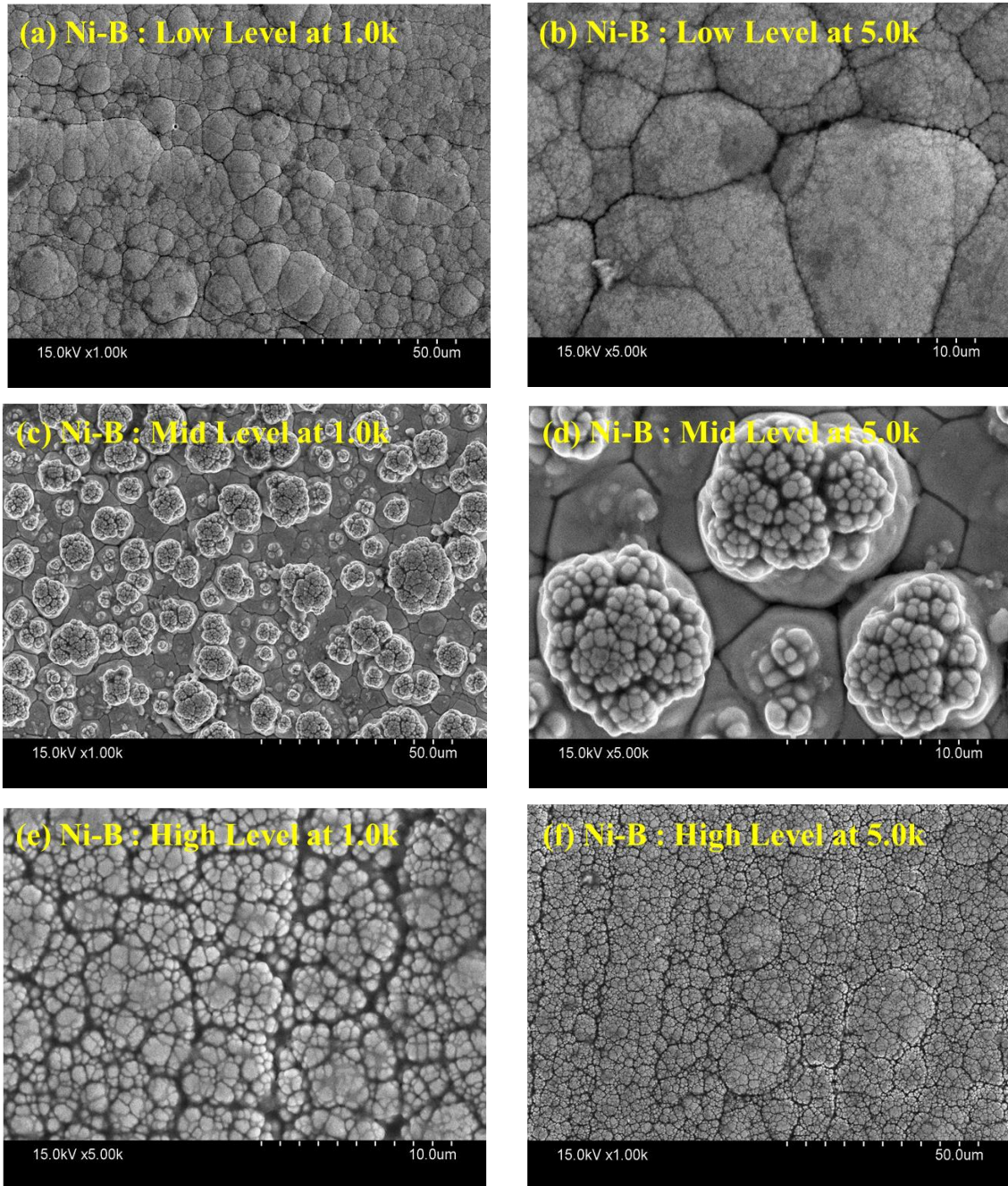


Figure 3.1: SEM Image of Coating Thickness of As-deposited Ni-B Coatings Obtained at (a) Low Level, (b) Mid-Level and (c) High Level Concentrations

3.3.2 Surface Morphology

All the as-deposited coating surface is bright and smooth for the coatings obtained below sodium borohydride concentration of 1.0 g/l but the same turns out to be grey coloured appearance and the surface also becomes a bit rough compared to the other

combinations when the borohydride concentration increased to 1.20 g/l [Vitry et al. 2012]. The surface morphology of the as-deposited coatings is displayed in **Figure 3.2**.



**Figure 3.2: SEM Image of Surface Morphology of As-deposited Ni-B Coatings
Obtained at (a)-(b) Low Level, (c)-(d) Mid-Level and (e)-(f) High Level
Concentrations**

From **Figure 3.2**, it can be seen that the low, mid and high; all three level coatings possess cauliflower like surface morphology for sodium borohydride concentration of 0.40 g/l to 1.20 g/l, nickel chloride range of 15 g/l to 35 g/l and operating temperature range of 75°C to 95°C [Delaunois et al. 2000; Krishnaveni et al. 2005; Baskaran et al. 2006; Vitry et al. 2008; Bülbül et al. 2013; Madah et al. 2015; Wan et al. 2016; Yazdani et al. 2018; Bonin et al. 2019, Sukackiene et al. 2020]. Besides, it also shows a homogeneous distribution of nodules throughout the coated surface [Delaunois et al. 2000; Krishnaveni et al. 2005; Baskaran et al. 2006; Vitry et al. 2008; Bülbül et al. 2013; Wan et al. 2016]. Cauliflower like surface morphology is famous for tribological applications as it decreases coefficient of friction between the mating surfaces by reducing the actual surface contact area between two surfaces [Baskaran et al. 2006]. Nodule size of as-deposited ENB coating increases with the level of parameters which can be attributed due to increased nodule size with sodium borohydride concentration and surface becomes compact [Baskaran et al. 2006]. This might help in improving the tribological behaviour of coatings.

3.3.3 Chemical Composition

The EDAX mapping of the as-deposited coating of various compositions has been displayed in **Figure 3.3**. **Figure 3.3(a)** shows the presence of nickel in the coatings while **Figure 3(b)** shows the presence of boron in the coating for low level concentration of coating bath elements. Similarly, **Figure 3.3(c)-(d)** and **Figure 3.3(e)-(f)** represent the presence of nickel and boron for medium and high level concentration of coating bath elements, respectively. From **Figure 3.3**, it can be observed that the intensity of green colour in the figure decreases with the increase in coating bath parameter concentration which is an indication of decrease in nickel percentage but at the same time the yellow colour intensity increases with coating bath parameter concentration which is an indication of rise in boron content. The elemental analysis of the coatings has been carried out through EDAX [Kaya et al. 2008; Bülbül et al. 2013; Dellasega et al. 2017]. The EDAX spectrum of the as-deposited coatings has been displayed in **Figure 3.4**. From **Figure 3.4**, it is clearly evident that the boron content increases with the increase in coating bath composition [Sürdem et al. 2019]. The boron contents in the coatings are

3.30-3.90% for low level, 6.30-7.10% and 8.30-9.70% for mid and high-level coatings while nickel concentration is 93.30-95.10%, 88.90-90.50% and 86.20-89.30% for low, mid and high-level concentration, respectively.

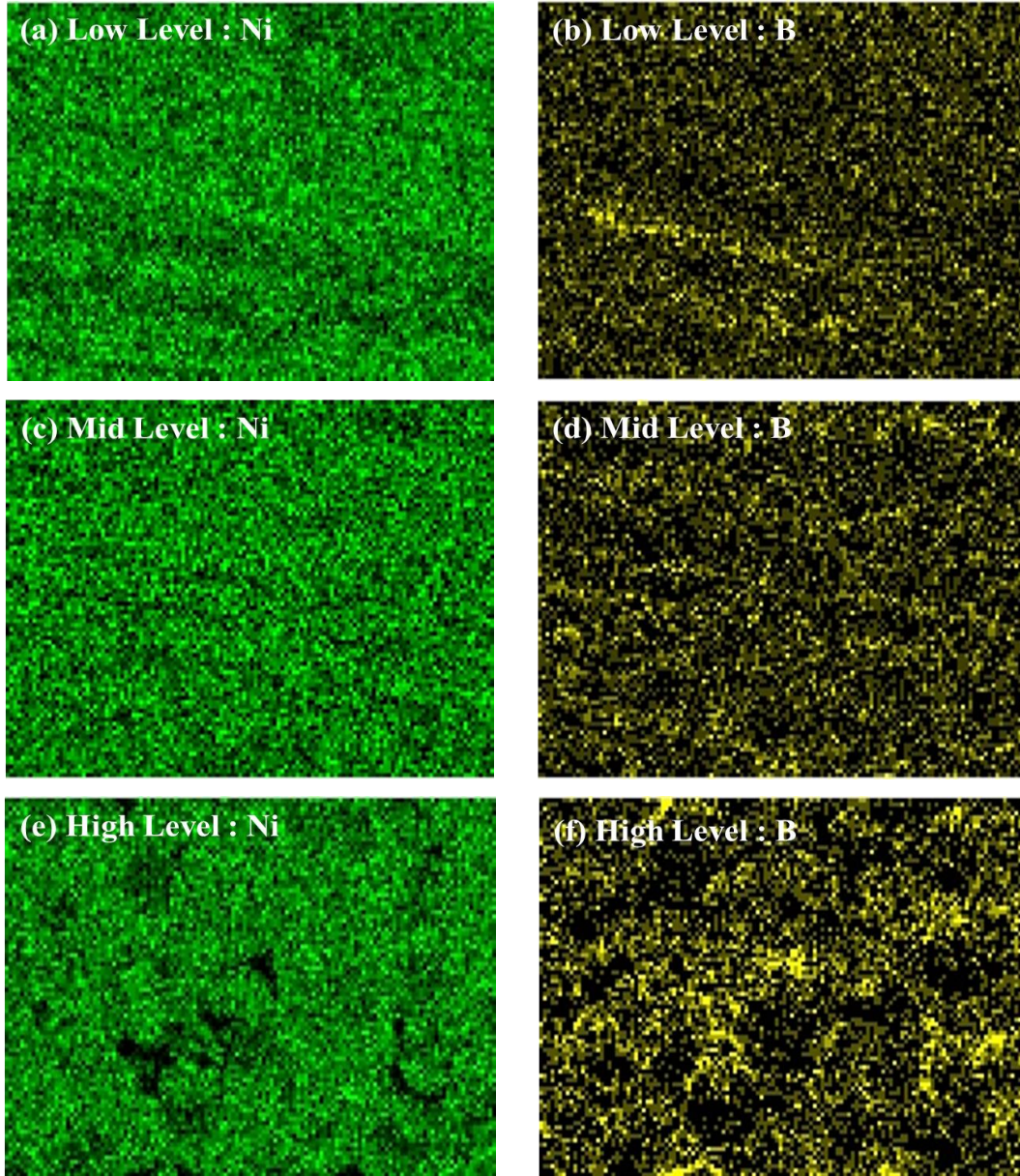


Figure 3.3: EDAX Mapping Images of As-deposited Ni-B Coatings Obtained at (a)-(b) Low Level, (c)-(d) Mid-Level and (e)-(f) High Level Concentrations

Similar trend of increase in boron concentration is observed in previous works [Sürdem et al. 2019]. The increase in boron concentration may be attributed due to the

increase in reduction rate as the amount of borohydride increased in the coating bath [Sürdem et al. 2019]. On the other hand, nickel concentration decreases though the nickel chloride concentration increased. The decrease in nickel concentration is possibly due to rise in boron concentration where the increase in boron acts as dominant one. The existence of oxygen as well as carbon is observed but the concentration is very low. Therefore, it can be neglected as this negligible amount of oxygen and carbon might have accumulated from the external sources.

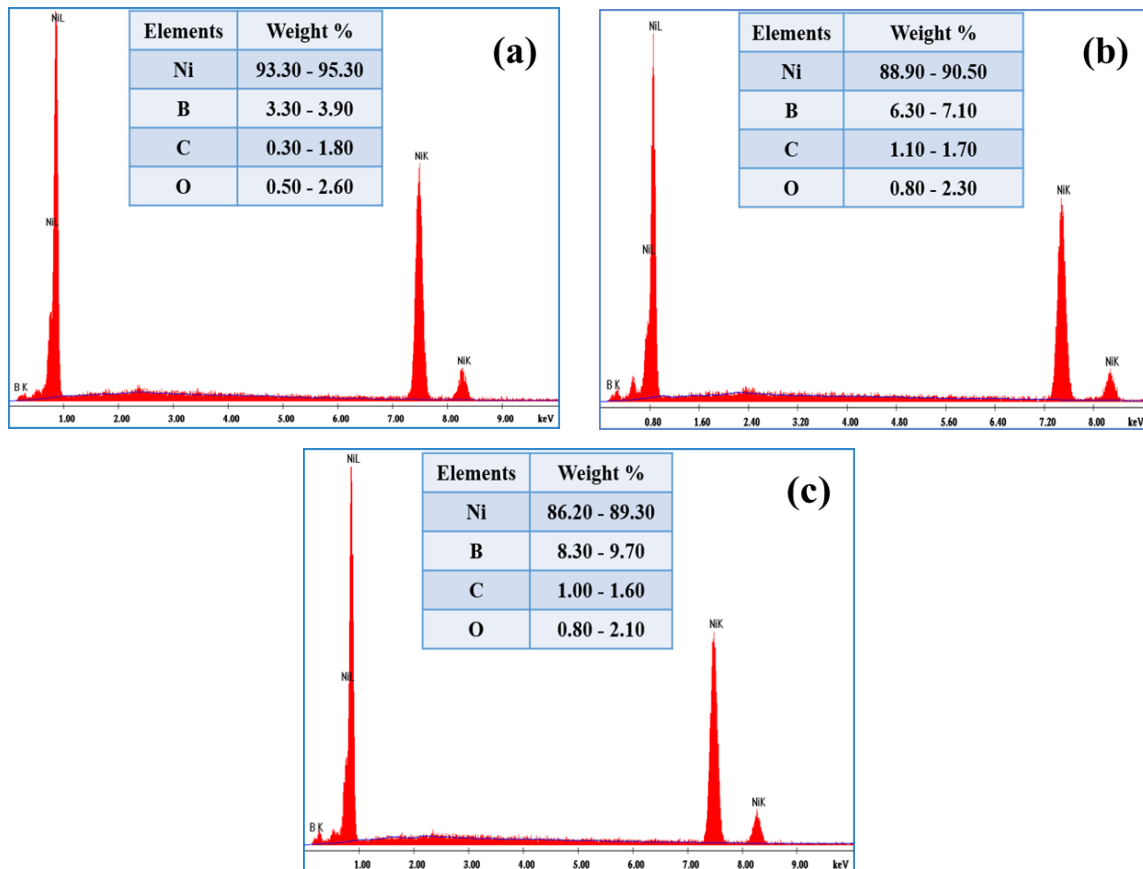


Figure 3.4: EDAX Spectrum of As-deposited Electroless Ni-B Coatings Obtained at (a) Low Level, (b) Mid-Level and (c) High Level Concentrations

3.3.4 Phase Structure

The XRD patterns of the as-deposited ENB coatings for low, mid and high-level bath composition are displayed in **Figure 3.5**. The low-level coating possesses a broad peak at about 53° [Jappes et al. 2005; Anik et al. 2008; Vitry et al. 2014; Vitry and

Bonin 2017; Sürdem et al. 2019]. The presence of hump in a XRD pattern indicates the presence of amorphous phase while the presence of sharp peaks indicates the presence of crystalline phase [**Sürdem et al. 2019, Vitry and Bonin 2017**]. The presence of both together is the indication of coexistence of amorphous-crystalline phase [**Bülbül et al. 2013, Sürdem et al. 2019, Vitry and Bonin 2017, Yildiz et al. 2017**]. Hence, the XRD pattern of the coatings obtained at LLC indicates the coexistence of amorphous and nano-crystalline phase structure [**Vitry et al. 2008; Bülbül et al. 2013; Yildiz et al. 2017; Vitry and Bonin 2017; Sürdem et al. 2019**].

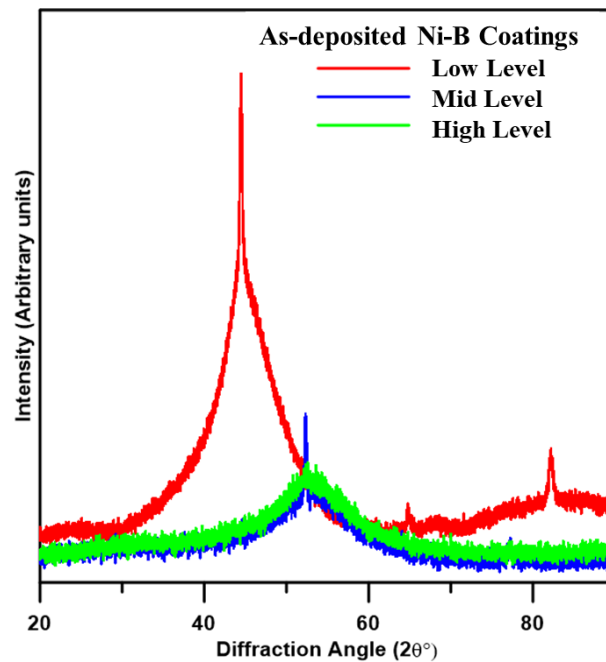


Figure 3.5: XRD Patterns of As-deposited Ni-B Coatings

The same broad peak diminishes for the mid-level and high-level concentration coatings which means that the phase structure of the coatings transformed into amorphous structure. The rise in borohydride concentration in as-deposited coating leads to transformation of crystalline to amorphous phase structure [**Sürdem et al. 2019**]. It is observed in previous studies that the coating with boron content less than 4 wt.% exhibits crystalline phase [**Bekish et al. 2010, Baskaran et al. 2006, Venkatakrishnan and Karthik 2019**]. The same phase gradually transforms into amorphous phase with the increase in boron content [**Baskaran et al. 2006, Venkatakrishnan and Karthik 2019**].

Hence, the transformation of phase structure from amorphous-crystalline to amorphous phase under the current study may be correlated with the increase in boron content which is confirmed from EDAX results.

3.4 Physical and Mechanical Behaviours

3.4.1 Surface Roughness

The variation of average surface roughness (Ra) value obtained with respect to varying coating bath temperature, nickel chloride and sodium borohydride concentration are displayed in **Figure 3.6**. **Figure 3.6(a)** represents the variation of average surface roughness with respect to coating bath temperature and sodium borohydride concentration which shows an increasing trend of average surface roughness with coating bath temperature as well as borohydride concentration. The chemical reaction starts at around 70°C which gradually increases upon increasing temperature upto around 90°C [Baskaran et al. 2006; Hamid et al. 2010].

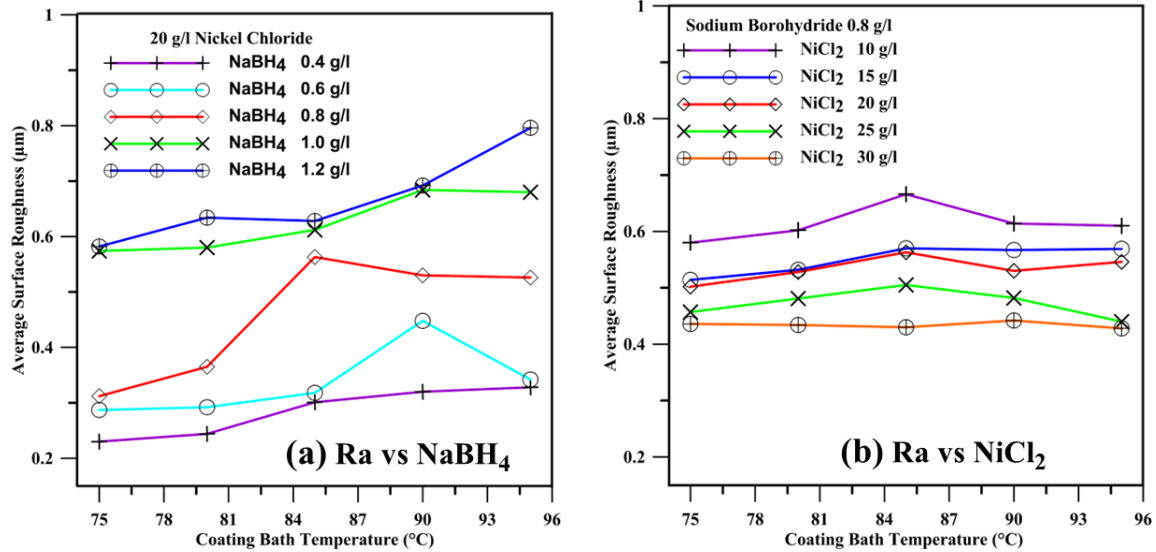


Figure 3.6: Average Surface Roughness Plot with Varying Temperature and (a) Sodium Borohydride and (b) Nickel Chloride Concentrations

Further increase in temperature does not impact the chemical reaction much. This increase in average surface roughness might be due to the increase in reduction rate

[Kanta et al. 2009; Vitry et al. 2012; Vitry et al. 2012; Bülbül et al. 2013; Madah et al. 2015; Wan et al. 2016]. Further increase in temperature does not change surface roughness for significant amount. But the surface roughness values are seemed to decrease at 0.4 g/l and 0.6 g/l concentration of sodium borohydride compared to substrate ($R_a = 0.285 \mu\text{m}$) which increased upon further increase in sodium borohydride concentration upto 1.2 g/l. The surface smoothening action can be attributed with the lower reduction rate upto 0.6 g/l borohydride concentration [Vitry et al. 2012] and the increase in surface roughness is due to the high reduction rate at higher borohydride concentration [Vitry et al. 2012; Sürdem et al. 2019]. Figure 3.6(b) shows that the surface roughness is found to decrease as the nickel chloride concentration in the coating bath solution increases. For any concentration of borohydride, average roughness increases upto 85°C which is possibly due to the increase in chemical reaction after 70°C [Hamid et al. 2010]. Upon increasing the temperature further does not change the chemical reaction much but higher concentration of nickel chloride smoothen the surface. Hence, the coated surface becomes smoother with the rise in nickel chloride concentration.

3.4.2 Nano-Indentation Test

Figure 3.7 shows the indentation depth vs applied load plot for various level of coating bath parameters, where it can be seen that the coating obtained at low level of bath parameter concentration requires minimum amount of load for same indentation. The high level of bath parameter concentration coatings requires maximum load. Therefore, this can be concluded that the hardness of the coatings increased as the bath parameter concentration increases. As-deposited coating hardness increases with boron content in the coating [Lekka et al. 2018; Sürdem et al. 2019]. The boron content in coatings increases with increase in borohydride concentration [Lekka et al. 2018; Sürdem et al. 2019]. The increase in borohydride concentration as well as nickel chloride may be the reason of this increase. Electroless Ni-B coating layer over steel substrate improves the surface hardness of underlying steel [Kaya et al. 2008]. The nano-hardness test results have been displayed in the Figure 3.8 with the variation of temperature, nickel chloride and sodium borohydride. Figure 3.8(a) shows the increasing

trend of surface hardness with sodium borohydride as boron content increases with NaBH_4 in the coatings [Anik et al. 2008; Bonin and Vitry 2016; Vitry and Bonin 2017; Lekka et al. 2018; Sürdem et al. 2019].

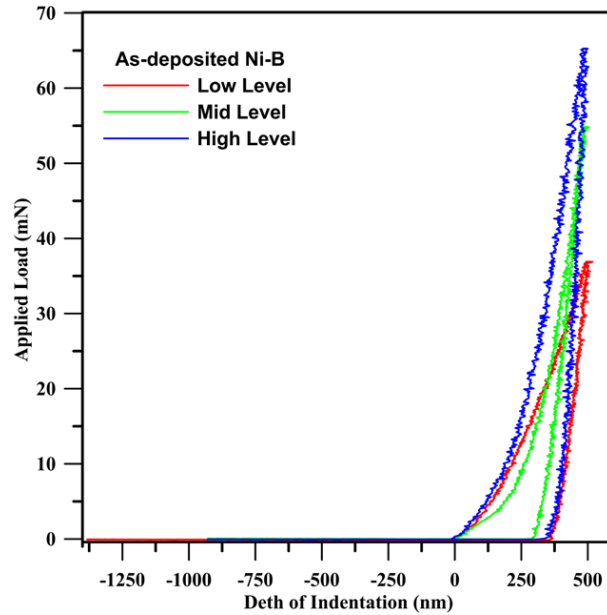


Figure 3.7: Depth of Indentation vs Applied Load Plot

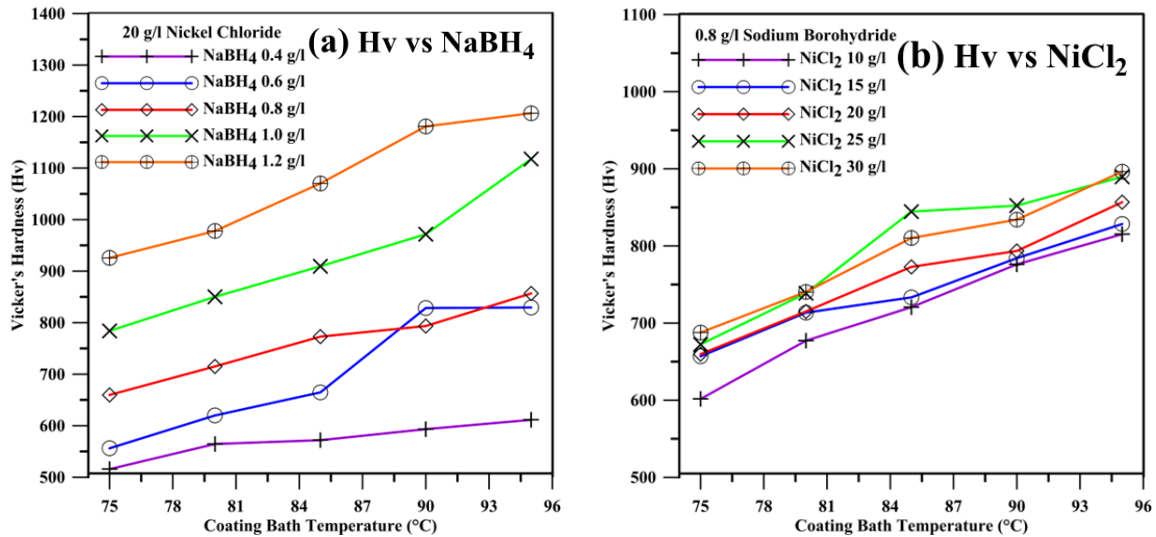


Figure 3.8: Hardness Plot with Varying Temperature and (a) Sodium Borohydride and (b) Nickel Chloride Concentrations

The hardness is also found to increase as coating bath temperature increases which might be due to the increase in chemical reaction with temperature rise. The chemical reaction increases with the increase in coating bath temperature which may lead to an increase in boron content in the coating [Bonin and Vitry 2016; Lekka et al. 2018; Sürdem et al. 2019]. The surface hardness was observed to be a function of boron content. Hence, the increased boron content with temperature may leads to an increase in surface hardness [Anik et al. 2008; Bonin and Vitry 2016; Lekka et al. 2018; Sürdem et al. 2019]. The surface hardness variation plot with respect to temperature and nickel chloride displayed in **Figure 3.8(b)** also shows an increasing trend with nickel chloride content and temperature of coating bath solution. The surface hardness of nickel boron found to vary with boron content and grain size of as-deposited coatings [Bonin and Vitry 2016; Lekka et al. 2018]. The boron content as well as grain size of coatings increases with the increase in NaBH₄ concentration in the coating bath [Bonin and Vitry 2016; Lekka et al. 2018; Sürdem et al. 2019]. This might be a possible reason of increase in nano-hardness of the as-deposited coatings. The increase in nickel chloride might have increased the nickel content slightly and the combination of nickel and boron might be a possible reason for the increase in surface hardness with nickel chloride concentration though this change is less compared to the variation of borohydride.

The elastic modulus of the as-deposited coatings was determined and represented in **Figure 3.9**. **Figure 3.9(a)** represents the fluctuation of elastic modulus with temperature and borohydride concentration. **Figure 3.9(b)** represents the fluctuation of elastic modulus with temperature and nickel chloride. The elastic modulus of nickel-boron coatings is found to be the independent one to hardness [Vitry et al. 2008]. But, the elastic modulus of coating is also seen to depend on grain size [Zhou et al. 2003]. The elastic modulus of the as-deposited coatings is observed to increase with the sodium borohydride as well as nickel chloride concentration but it does not follow any specific trend with temperature variation. While the grain size of the coatings is found to increase with sodium borohydride concentration. Therefore, the increase in elastic modulus may be attributed with the increase in grain size of the as-deposited Ni-B coatings. Elastic modulus of the coatings is found to increase with NaBH₄ concentration due to rise in boron content in the coating in previous works which agrees well with the current

increasing trend of elastic modulus. The lower elastic modulus shows less wear compared to higher elastic modulus [Vitry et al. 2008]. The coatings at low level concentration shows less wear besides low elastic modulus in this current study which also agrees well with the previous works [Vitry et al. 2008].

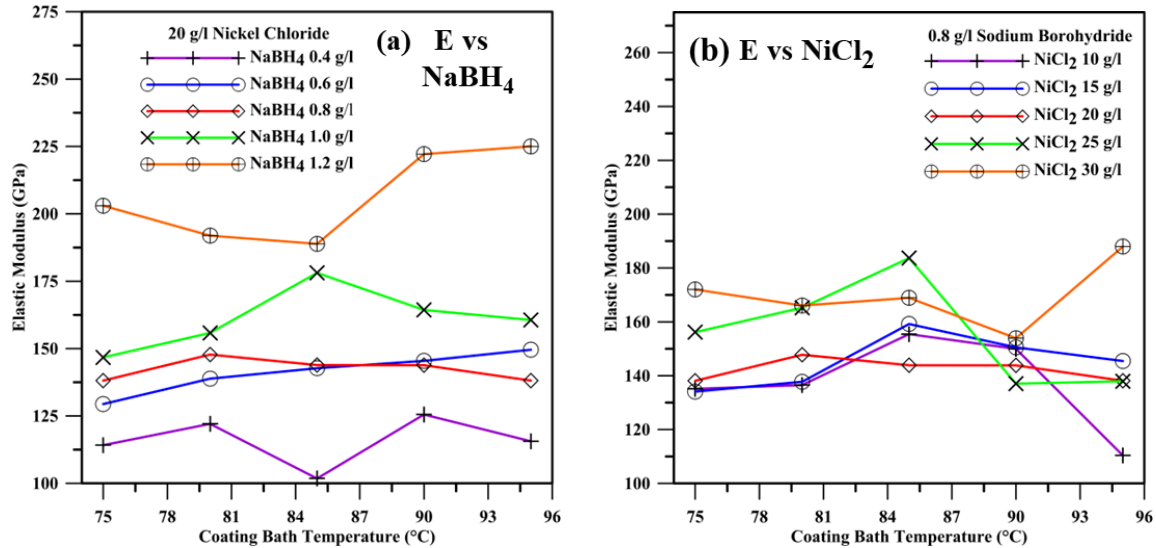


Figure 3.9: Elastic Modulus Plot with Varying Temperature and (a) Sodium Borohydride and (b) Nickel Chloride

3.4.3 Micro-Scratch Test

The scratch hardness of the coating was determined using the micro-scratch test and displayed in the **Figure 3.10**. From **Figure 3.10(a)**, it can clearly be observed that the scratch hardness value increased with the NaBH₄ concentration as well as coating bath temperature. Similar, trend may also be observed with the variation of nickel chloride and coating bath temperature. The scratch hardness is observed to increase with boron concentration. The boron concentration in the as-deposited coatings increases with the increase in sodium borohydride [Vitry and Bonin. 2017; Lekka et al. 2018; Sürdem et al. 2019]. The rise in boron content in the coating with sodium borohydride concentration might be the possible reason of this increase in scratch hardness [Anik et al. 2008; Sürdem et al. 2019]. Whereas, increase in reduction rate leads to an increase in boron content which further leads to an increase in scratch hardness as well as surface hardness

of the as-deposited coatings. Deposition of nickel with boron in the as-deposited coatings with the increase in nickel chloride might have increased nano-hardness as well as scratch hardness of the coatings. The coexistence of nickel and boron like hard particle in the Ni-B matrix might be a possible reason for the increase in surface hardness and scratch hardness.

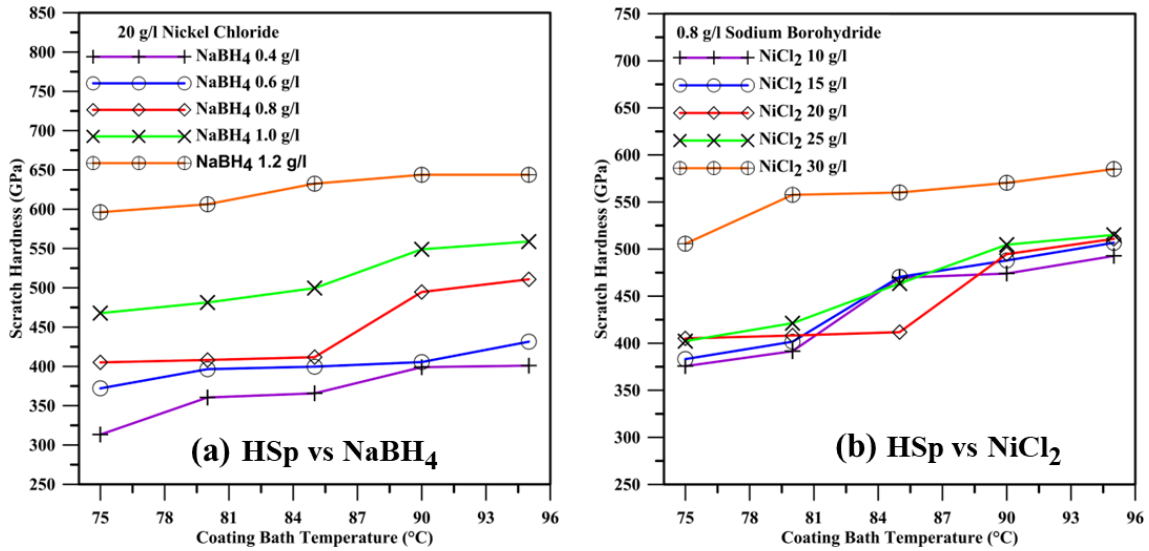


Figure 3.10: Scratch-Hardness Plot with Varying Temperature and (a) Sodium Borohydride and (b) Nickel Chloride Concentrations

3.5 Tribological Test

Figure 3.11 displays the variation of COF value with sliding duration which shows that COF value increased from low-level to mid-level. This increase in COF from low-level to mid-level might be due to increased sodium borohydride concentration as it increases surface roughness. The reduction rate during coating deposition is found to increase with borohydride concentration which may lead to high surface roughness [Vitry et al. 2012; Sürdem et al. 2019]. In contrary to the rise in surface roughness with borohydride concentration, the COF value decreased slightly at high level compared to mid-level but remained higher than low-level values. This decrease from mid-level to high-level is possibly due to increase in grain size with high boron content. The roughness peaks may have been grinded and smoothened the surface leading to reduction

in friction coefficient at high level concentration. Similar trend may also be observed in previous works [Madah et al. 2015].

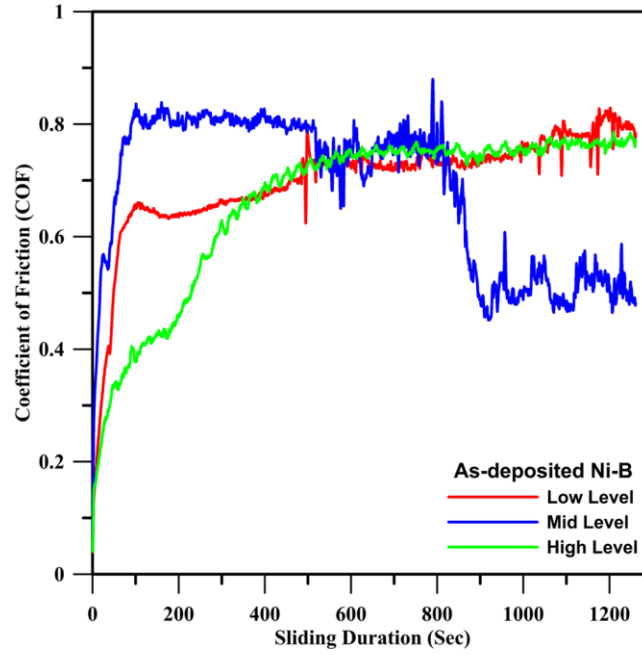


Figure 3.11: Coefficient of Friction (COF) vs Sliding Duration Plot

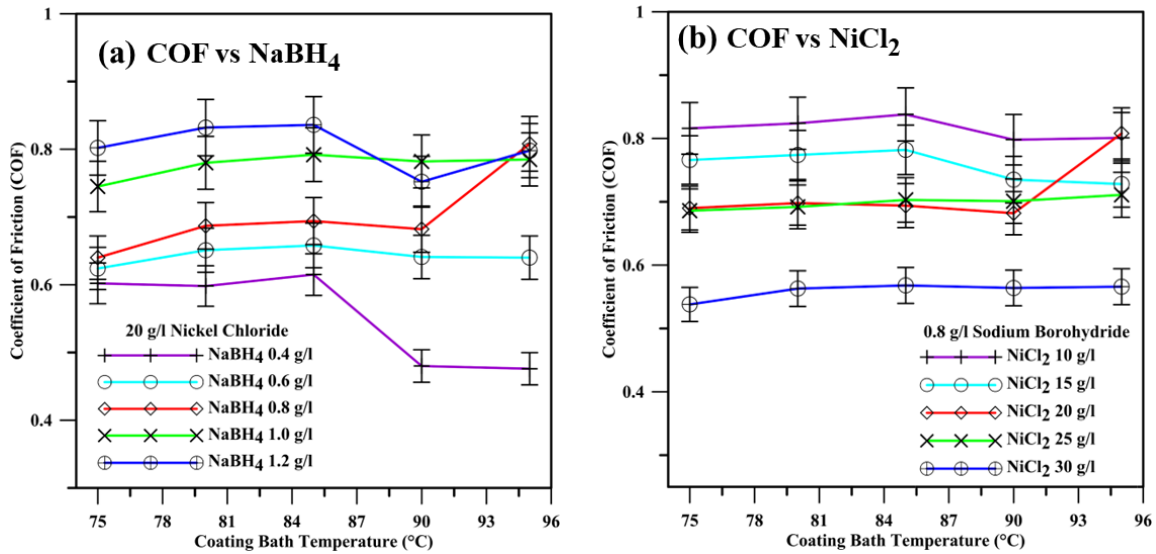


Figure 3.12: Average Coefficient of Friction (COF) Plot with Varying Temperature and (a) Sodium Borohydride and (b) Nickel Chloride

The as-deposited Ni-B coatings, as observed possess an average COF value of 0.69 in previous work [Yazdani et al. 2018]. The COF value of the as-deposited coatings in this current study was observed to follow the similar trend [Yazdani et al. 2018]. **Figure 3.12(a)** presents the variation of COF values against coating bath temperature and sodium borohydride concentration. From **Figure 3.12(a)** clearly displays that the friction gradually increased with the rise in NaBH_4 content in the coating bath. The boron concentration increased with the increase in coating bath concentration level as sodium borohydride concentration increased with bath parameter level. The higher borohydride concentration increases the boron concentration as well as reduction rate during coating deposition [Madah et al. 2015; Vitry and Bonin. 2017]. Hence, the surface roughness increases with the increased reduction rate due to rise in NaBH_4 content which further leads to an increase in friction coefficient [Bülbül et al. 2013; Madah et al. 2015; Wan et al. 2016]. This increase in COF values agrees well with the rise in average surface roughness which also increases with sodium borohydride concentration. **Figure 3.12(b)** shows the variation of COF values with respect to coating bath temperature and nickel chloride concentration where it can be clearly seen that the friction coefficient gradually decreased with the rise in nickel chloride concentration in the coating bath. On the other hand, the COF value does not change significantly with coating bath temperature. The surface roughness of the as-deposited coatings was also observed to decrease with increase in nickel chloride concentration which agrees well with the improvement in friction behaviour due to the smoothening of surfaces with increased nickel chloride concentration. The increase in nickel chloride smoothenes the surface, which leads to a decrease in friction coefficient value. But the friction coefficient does change significantly with temperature variation.

Figure 3.13 represents the specific wear rate plot with the variation of coating bath parameters. From **Figure 3.13(a)**, the specific wear rate of the as-deposited coatings is found to increase with the increase in NaBH_4 but the same decreased with the rise in coating bath temperature. The surface roughness increases with sodium borohydride. Crushing and grinding of the roughness peaks during sliding leads to an increase in specific wear rate [Vitry and Bonin 2017]. On the other hand, the reduction rate increases with the increase in coating bath temperature. The increase in reduction rate

makes the coated surface rough which again increases the specific wear rate by breaking the asperities and grinding the wear debris into the worn-out surface [Madah et al. 2015; Vitry and Bonin 2017]. On the other hand, **Figure 3.13(b)** shows an increasing trend of specific wear rate with nickel chloride which might be due to the increase in Ni concentration in the coating and reduction in boron content. But for both cases, it was found to decrease the specific wear rate as the temperature rises. As discussed earlier that the chemical reaction for coating deposition starts at around 70°C and it increases with the temperature upto 90°C but it does not change much upon further increase upto 95°C. Hence, the chemical reaction rate increases with temperature which confirms the increase in nickel and boron content at higher temperature. This might be the reason of reduction in specific wear rate. On the other hand, the surface also becomes dense and compact at higher level of concentration this can also leads to an improvement in wear behaviour of as-plated coatings.

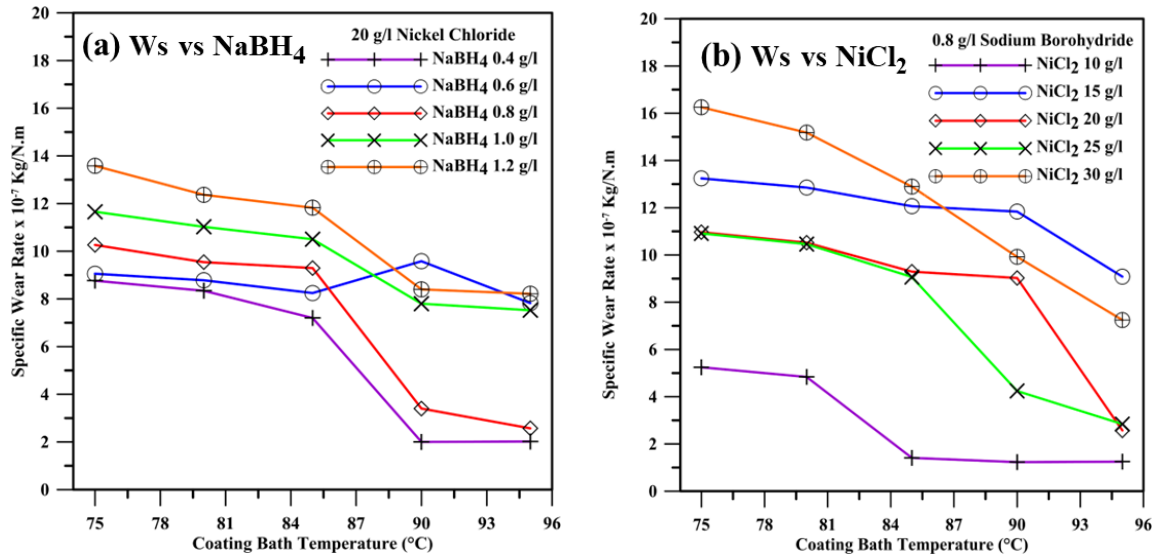
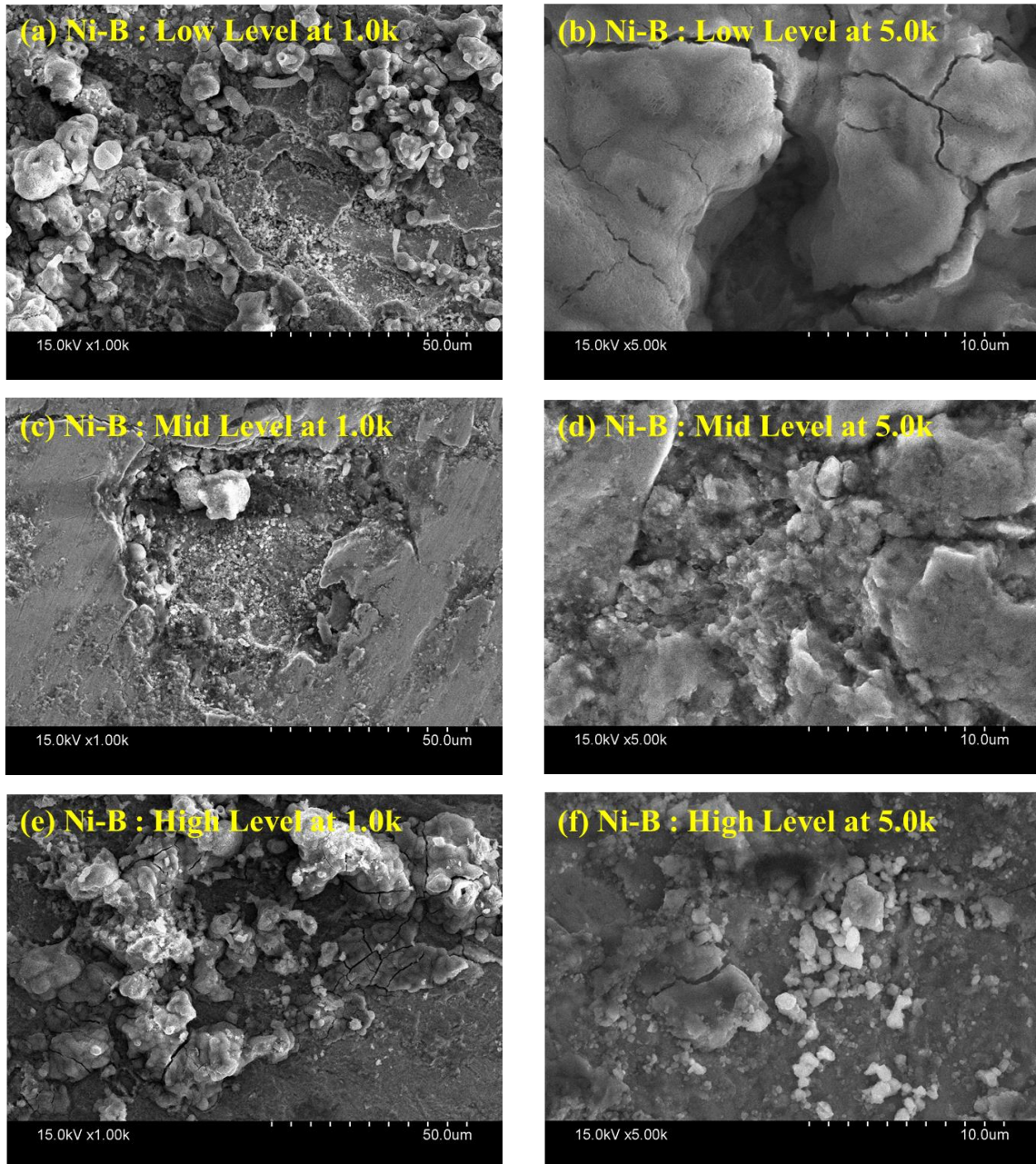


Figure 3.13: Specific Wear Rate Plot with Varying Temperature and (a) Sodium Borohydride and (b) Nickel Chloride

The wear mechanism of the as-deposited coatings has been analysed with the help of the SEM images of worn-out surfaces displayed in **Figure 3.14**. **Figure 3.14(a)-(b)** shows the worn-out surfaces of as-deposited coating at low level concentrations which

shows the wear debris present in the wear track. Some pits and prows are formed as well [Krishnaveni et al. 2005; Madah et al. 2015; Mukhopadhyay et al. 2018].



**Figure 3.14. SEM Image of Worn-out Surface of As-deposited Ni-B Coatings
Obtained at (a)-(b) Low Level, (c)-(d) Mid-Level and (e)-(f) High Level
Concentrations**

The magnified view of the worn-out surface also shows some crack formation. This is an indication of coexistence of delamination wear as well as adhesive wear mechanism [Madah et al. 2015]. The coating layers might have delaminated due to repeated loading during sliding [Madah et al. 2015]. Figure 3.14(c)-(d) also shows the presence of wear debris as well as patches. The similar type of wear mechanism can also be seen in Figure 3.14(e)-(f) where the rough surface peaks have been grinded severely. The grinding of rough asperities might have increased the specific wear rate of the coating with sodium borohydride concentration [Madah et al. 2015]. The surface roughness increases with sodium borohydride which leads to an increase in roughness peaks. Those roughness peaks are crushed and grinded during the sliding test. The grinded debris must have been trapped in between the two-mating surface which might have formed grooves along the sliding direction. This delaminated wear debris might be the reason of crack formation.

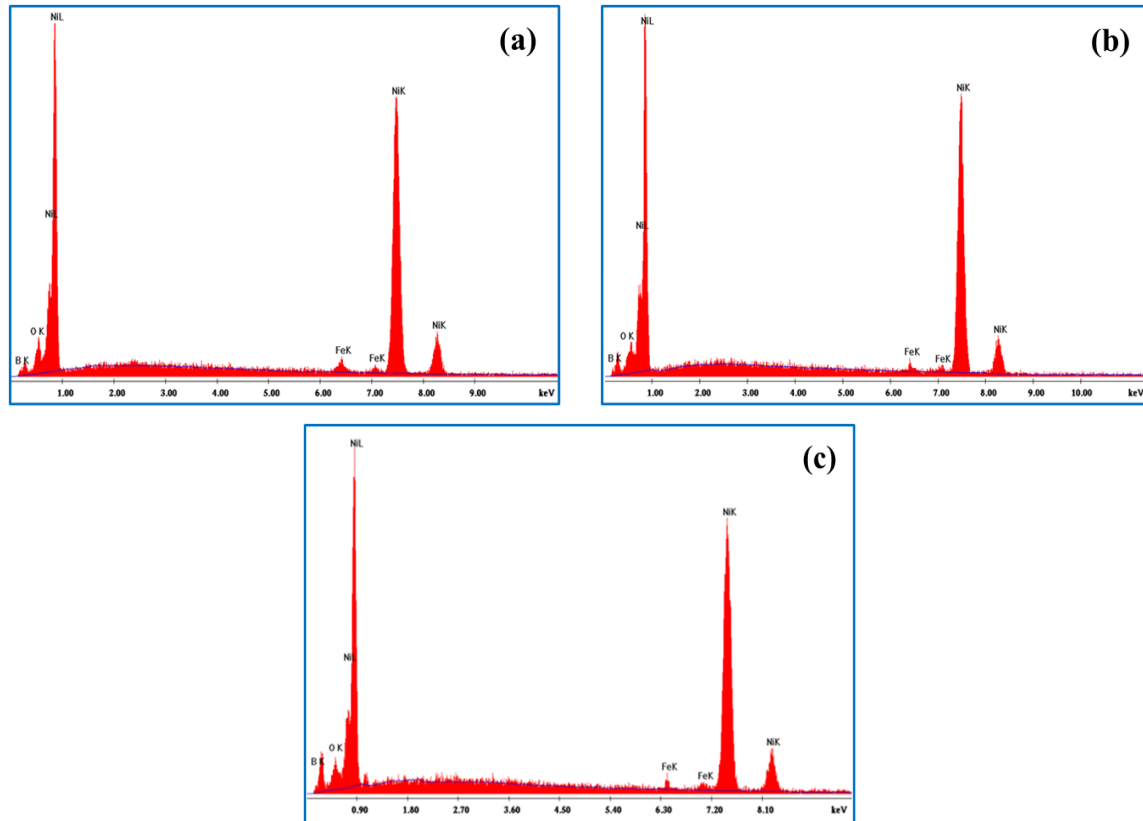


Figure 3.15: EDAX Spectrum of Worn-out Surfaces of As-deposited Ni-B Coatings Obtained at (a) Low Level, (b) Mid-Level and (c) High Level

The worn-out surfaces further investigated for chemical composition with the help of EDAX which confirms the presence of Ni, B, C and O displayed in **Figure 3.15**. Although the concentrations of C and O in the wear debris were found to be very less which confirms that the wear depth have not reached upto substrate. This trend can also be seen in previous research work [Madah et al. 2015]. Moreover, the substrate deformation was not observed as well. Hence, the C present in the wear debris is an indication of adhesive type of wear [Madah et al. 2015].

3.6 Corrosion Resistance Test

The corrosion tests are carried out using EIS and PDP tests. The charge transfer resistance (R_{ct}) and double layer capacitance (C_{dl}) value may be obtained by fitting a circle with the nyquist plot obtained from the EIS test. On the other hand, the tafel plot obtained from PDP test and it may be used to obtained the corrosion potential (E_{corr}) and corrosion current density (i_{corr}) values. The Nyquist plot obtained from EIS test and the tafel plot obtained from PDP test are displayed in **Figure 3.16**. The corrosion resistance of uncoated steel substrate improves after electroless Ni-B coatings [Bülbül et al. 2013].

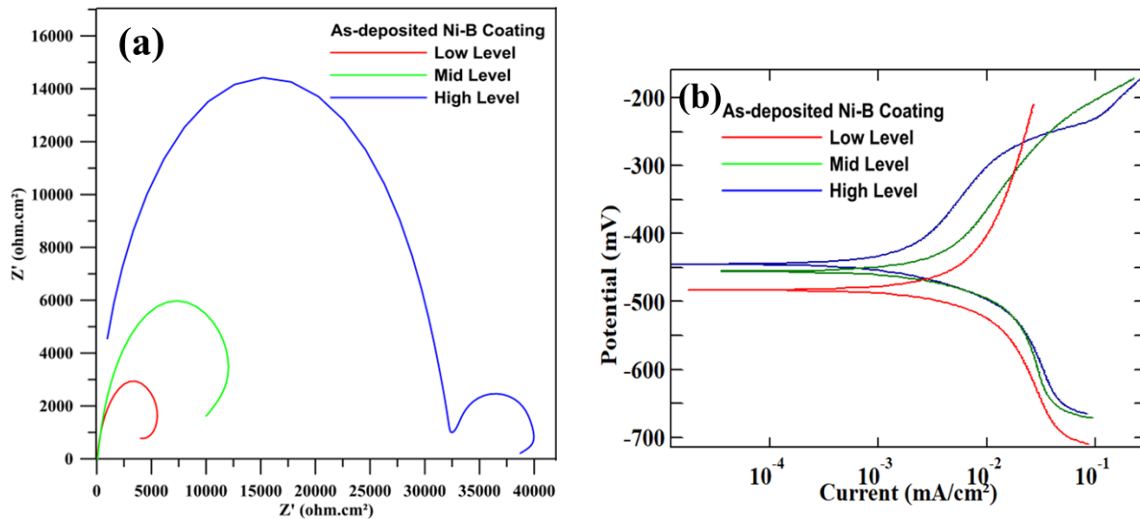


Figure 3.16: EIS and PDP Test Plot for As-deposited Ni-B Coatings, (a) Nyquist Plot and (b) Tafel Plot

The big semi-circle loop indicates the higher corrosion resistance of coatings [Kanta et al. 2009; Mukhopadhyay et al. 2019] while the less negative corrosion potential obtained from the Tafel plot indicates the better corrosion resistance of coatings [Anik et al. 2008; Kanta et al. 2009; Mukhopadhyay et al 2017]. The semi-circular loop of nyquist plot is seen to become bigger with increased coating bath concentration level as displayed in **Figure 16(a)**. This rise in corrosion potential is an indication of improvement in corrosion resistance as the borohydride concentration rises in coating bath solution [Vitry and Bonin 2017]. The tafel plot is displayed in Figure 16(b) which also shows that the coating obtained at high level of coating bath concentration possess lowest negative value of corrosion potential i.e. the highest corrosion resistance. Therefore, both EIS and PDP test results show the similar trend of corrosion resistance. The change in corrosion resistance may be observed to change with the change in surface morphology and phase structure [Kanta et al. 2009]. The corrosion resistance of coatings is also seen to depend on coating composition especially boron content. The addition of boron leads to an improvement of corrosion resistance of coatings [Vitry and Bonin, 2017]. Hence, the increase in boron content with sodium borohydride can be attributed as the reason for increase in corrosion resistance with coating bath concentration levels. On the other hand, the concentration of nickel might have been increased with nickel chloride in the coating bath which may be a possible reason of increase in corrosion potential. The increase nickel might have smoothened the surface by filling the pores and denying the corrosive medium to penetrate through the surface. The chemical reaction rate increases with temperature which leads to an increase in Ni concentration or boron in the coating which may be another possible reason for increase in corrosion resistance with coating bath concentration level.

The SEM images of the corroded surface of as-deposited coating with different coating bath composition are displayed in **Figure 3.17**. From **Figure 3.17(a)**, the corrosion compound accumulation above the surface can be observed which is an indication of corrosion attack by the corrosive solution. But in **Figure 3.17(b)**, the coated surface is found to be less effected and the effect is in outer layer only. The damaged surfaces of low borohydride concentration coatings under corrosive action are the

indication of lower corrosion resistance compared to coatings obtained at high concentration.

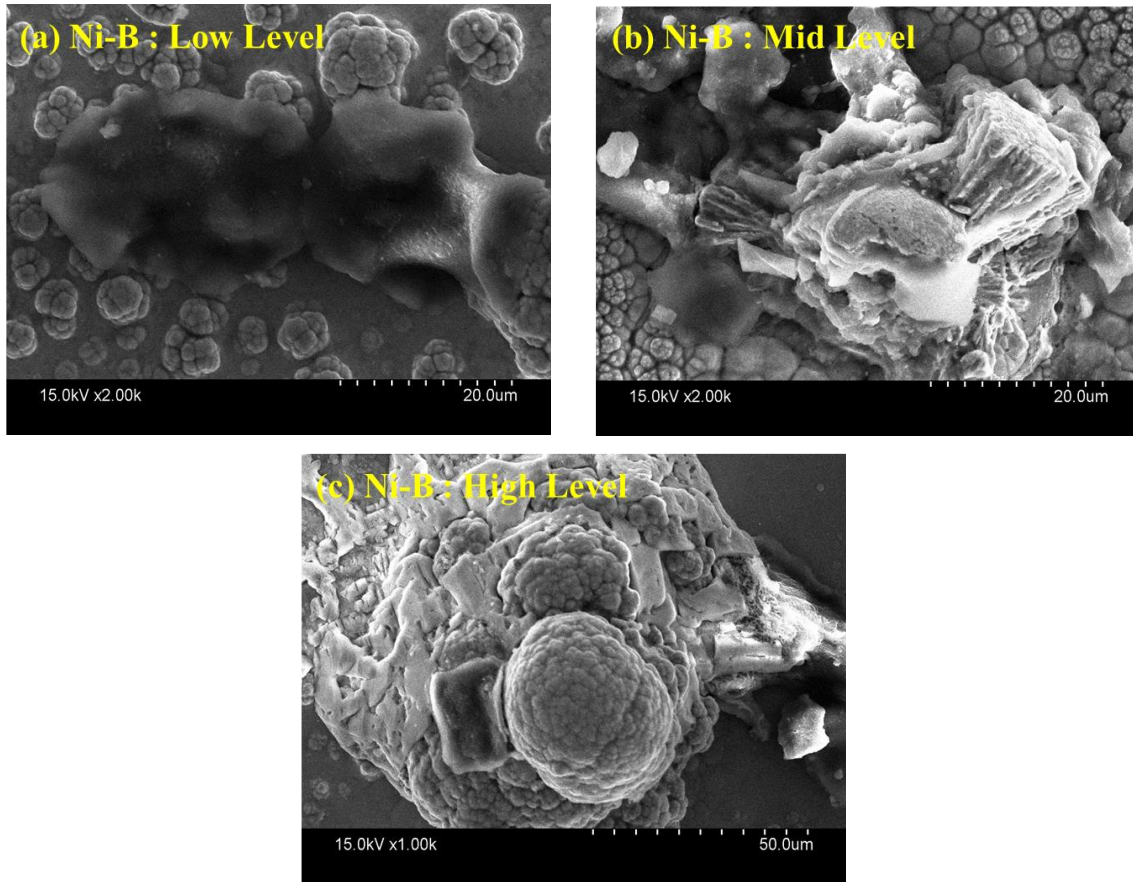
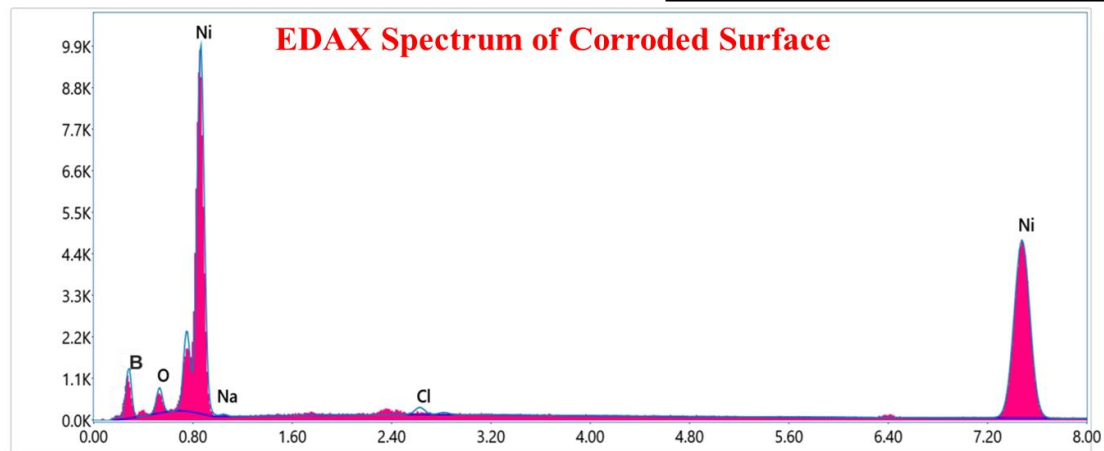
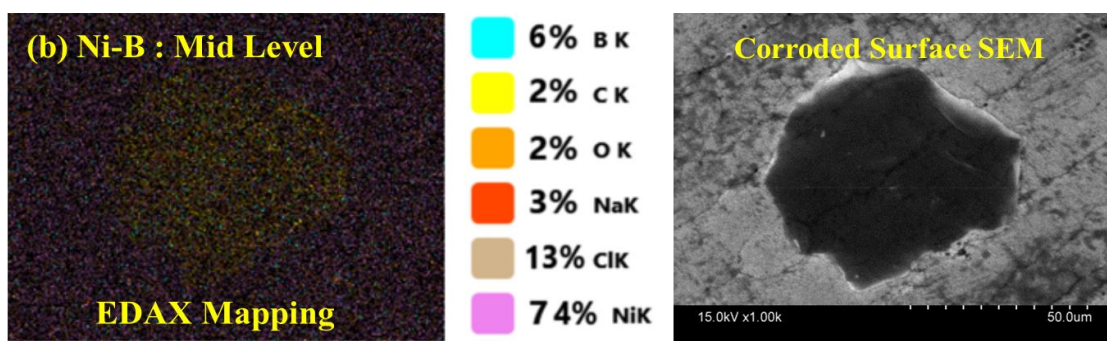
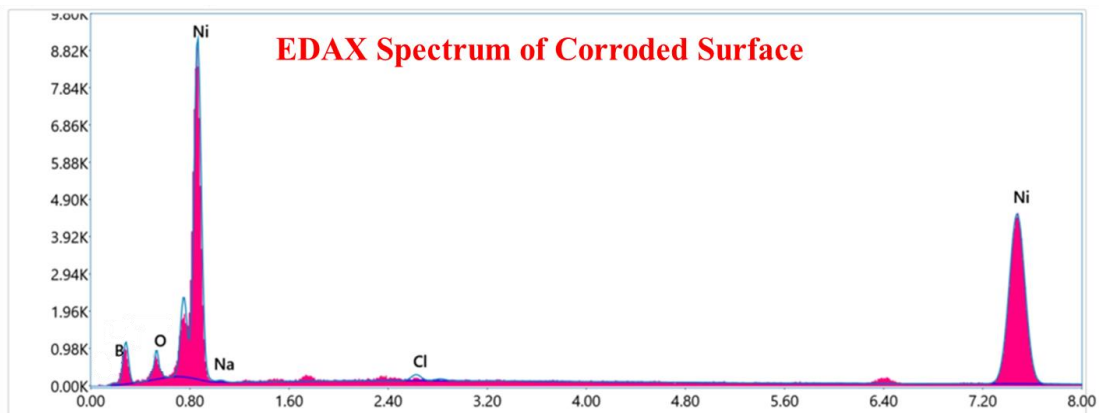
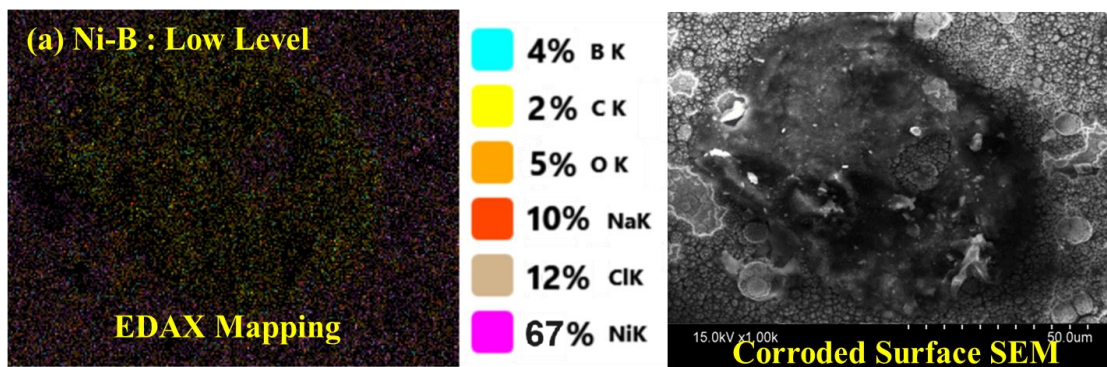


Figure 3.17: SEM Image of Corroded Surface of As-deposited Ni-B Coatings Obtained at (a) Low Level, (b) Mid-Level and (c) High Level Concentrations

Hence, it may be said that the coatings obtained at high level concentration of parameters observed to be better than medium and lowest concentration level. The surface roughness as-deposited coatings increase with the rise in borohydride concentration which is supposed to decrease the corrosion resistance. In contrary to surface roughness, corrosion resistance increases with increase in boron concentration. On the other hand, pores present in the rough surface might have been filled with nickel grains due to high concentration of nickel which might have increased the corrosion resistance. Therefore, the above discussion confirms that overall corrosion resistance of the as-deposited coating improves as the bath parameter concentration level increases.

Whereas **Figure 3.17(c)** shows the coated surface to be least effected by the corrosive medium and a spongy type appearance over the surface only. Corrosion resistance changes with surface and structural modification of the coated surface [**Yazdani and Mahboubi 2019**]. The corrosion resistance is found to decrease while phase structure transforms from amorphous to nano-crystalline structure [**Anik et al. 2008; Hamid et al. 2010; Bülbül et al. 2013**]. The surface gaps between the nodules allow electrolyte penetration. The corrosion resistance of amorphous structure is better than nanocrystalline structure. The better corrosion resistance of high boron content as-deposited coatings can be attributed for its amorphous structure [**Anik et al. 2008**] and presence of higher concentration of boron.

The corroded surfaces are further investigated using EDAX for the compositional analysis. The EDAX results of the corroded surfaces of electroless Ni-B coatings are displayed in **Figure 3.18**. The EDAX mapping and spectrum, both show presence of Ni, B, C, O, Na and Cl, i.e. the main coating bath elements and the corrosive medium elements may also be observed. The peaks of Na and Cl in the EDAX spectrum are because of the electrolyte used in the test, whereas, C as well as O are also present at negligible amount. Generally, the grain boundaries of coated surface are the corrosion attack zone. Those helps the corrosive solution to penetrate through it. The corrosion byproducts are observed on the corroded surface displayed in **Figure 3.17** which may be correlated with the presence of Na and Cl peaks in the EDAX spectrum. The presence of Cl ion in the corroded surface confirms the corrosive action. The SEM images showed some sediments on the corroded surface which are just the insoluble byproducts of corrosive action. It also confirms the corrosive action but for not all samples. The presence of Na and Cl ion is not significant in all cases as seen in the EDAX results. This suggest that the electrolytes penetrated only till the top layer of the coatings as the substrate composition elements are not observed in EDAX results. Hence, the coated layers are found to prevent the corrosive solution to reach till the substrate surface in most cases.



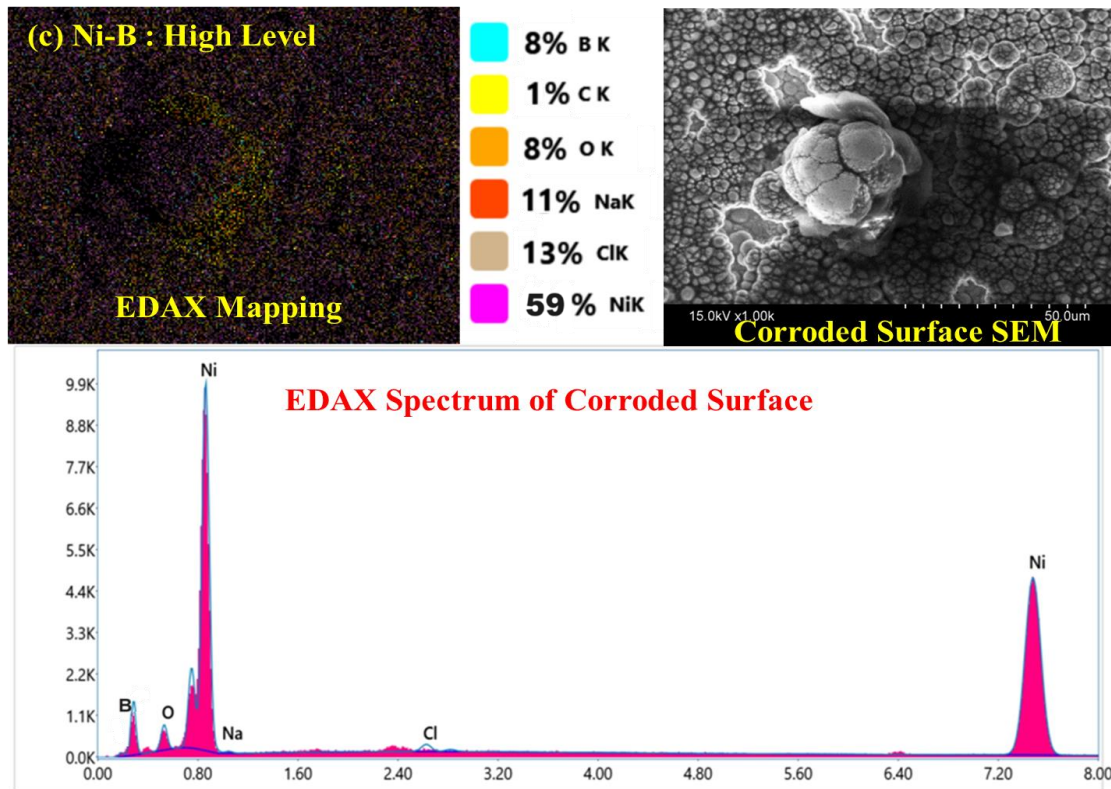


Figure 3.18: EDAX Results of Corroded Surfaces of As-deposited Ni-B Coatings Obtained at (a) Low Level, (b) Mid-Level and (c) High Level Concentrations

3.7 Closure

The nickel-boron alloy coatings are deposited with varying bath composition within a certain range to study the significance of the coating bath parameters on coating characteristics:

- The surface morphology of the as-deposited coatings is found to be cauliflower like appearance while the grain size of the as-deposited coatings is seen to increase with coating bath concentrations due to increase in sodium borohydride concentration.
- The phase structure of as-deposited Ni-B coatings are seen to depend on boron content. Amorphous and nano-crystalline structure are found to co-exists in as-deposited coatings obtained from low borohydride content coating bath solution which transforms into amorphous structure upon increase in borohydride

concentration. This change in phase structure can be attributed with the increase in boron content with NaBH_4 .

- The boron content in the coating is increased with reduction rate due to increase in NaBH_4 concentration and coating bath temperature. The reduction rate increases with rise in NaBH_4 concentration as well as coating bath temperature.
- The increase in boron content due to rise in reduction rate leads to an increase in surface roughness whereas the same is found to decrease with increase in nickel chloride and temperature as the nickel might have smoothened the coated surface.
- The increased surface roughness leads to a rise in COF value and the specific wear rate increases due to grinding and crushing of roughness peaks during sliding of pin sample over the counter surface.
- The increase in boron content with sodium borohydride also leads to an increase in surface hardness and scratch hardness. This improvement of surface hardness as well as scratch hardness is possibly due to rise in boron content.
- The increase in bath parameter concentration leads to an improvement in corrosion resistance of as-deposited coatings. The increased boron concentration in the coating might have transformed the phase structure from mixture of nano-crystalline and amorphous to amorphous structure which also might have improved the corrosion resistance of coatings

Chapter 4: Electroless Ni-B-W Alloy Coatings

Outline: 4.1. Introduction, 4.2 Experimental Details, 4.3 Coating Characterisation, 4.3.1 Coating Thickness, 4.3.2 Surface Morphology, 4.3.3 Chemical Composition, 4.3.4 Phase Structure, 4.4 Physical and Mechanical Behaviours, 4.4.1 Surface Roughness, 4.4.2 Nano-indentation Test, 4.4.3 Micro-Scratch Test, 4.5 Tribological Test, 4.6 Corrosion Resistance Test, 4.7 Closure

4.1 Introduction

The electroless coatings are generally applied over any substrate to provide some protection or modify the surface behaviour of base metal. The electroless coatings find its wide applicability in chemical, electrical and aerospace industries for its excellent tribo-mechanical behaviours. The borohydride reduced polly alloy coatings are deposited to enhance various coating behaviours. The addition of different elements with nickel may lead to modification in the coating behaviours. The coating bath parameters and their concentrations play an important role to decide the coating characteristics of electroless Ni-B coatings. Hence, the addition of tungsten with electroless Ni-B is also expected to change the coating characteristics. This chapter contains the effect of different coating bath elements and their concentrations on electroless Ni-B-W coating characteristics.

4.2 Experimental Details

The electroless Ni-B-W coatings are developed using chemical reaction over AISI 1040 steel substrates as explained in Chapter 2. The same procedure as of electroless Ni-B coatings is used for the current ternary alloy (Ni-B-W) coating deposition as well. Only sodium tungstate is incorporated with the Ni-B alloy coating composition as source of tungsten. The sodium tungstate concentration is varied within the range of 15 g/l to 35 g/l. The coatings are deposited through chemical deposition method. The steel substrates used is having a catalytically active surface. Still, those are dipped into lukewarm PdCl_2 just before dipping them into coating bath solution to accelerate the deposition process further. No ultrasonic or mechanical agitation is used. The bath loading is maintained

from 28.5 to 31.1 cm² /L. All major key elements of the coating bath are varied at 5 different levels. Low Level Concentration (LLC) of coating bath contains 10 g/l of NiCl₂, 0.4 g/l of BaBH₄, 15 g/l of Na₂WO₄ and 75 °C coating bath temperature. So, from now on the Low-Level Concentration will be called as LLC. While, Mid-Level Concentration (20 g/l of NiCl₂, 0.8 g/l of BaBH₄, 25 g/l of Na₂WO₄ and 85 °C coating bath temperature) and High-Level Concentration (30 g/l of NiCl₂, 1.2 g/l of BaBH₄, 35 g/l of Na₂WO₄ and 95 °C coating bath temperature) will be called as MLC and HLC, respectively.

The coating characterisations are done on these three levels of concentrations only. While the tribo-mechanical behaviour of the coatings is carried out with varying bath parameter individually to understand the correlation. All the tests are carried out as per the test procedure elaborated in chapter 2.

4.3 Coating Characterisation

4.3.1 Coating Thickness

The Ni-B-W alloy coated substrates are initially examined for coating thickness, surface morphology, chemical composition and phase structure. The coating layer thickness is measured using SEM and the results were displayed in **Figure 4**. The minimum coating thickness of 14.61 µm is observed at LLC as displayed in **Figure 4.1(a)**. The minimum coating thickness values of 26.33 µm and 31.32 µm are achieved for MLC and HLC as presented in **Figure 4.1(b)** and **Figure 4.1(c)**, respectively. The coated layer thickness is observed to rise with increased concentration level. This rise in coating thickness indicates the enhancement of deposition rate with coating bath parameter concentration level as the time duration is constant at 4 h. The plating rate is improved with higher borohydride concentration [Vitry et al. 2012]. The improvement in deposition rate against NaBH₄ content may be because of the improvement in reduction rate with NaBH₄ concentration [Vitry et al. 2012]. It is observed to possess a bright and smooth surface for the coatings deposited at 0.80 g/l NaBH₄. The same coatings become grey coloured as well as become slightly rough relative to the other combinations when deposited at 1.10 g/l NaBH₄ concentration [Vitry et al. 2012]. Similarly, the Ni-B-W coated specimens also own a bright and smooth surface till mid-level concentration. The same coated layer is seen to turn into grey coloured appearance and get slightly rough at

high level concentration of coatings.

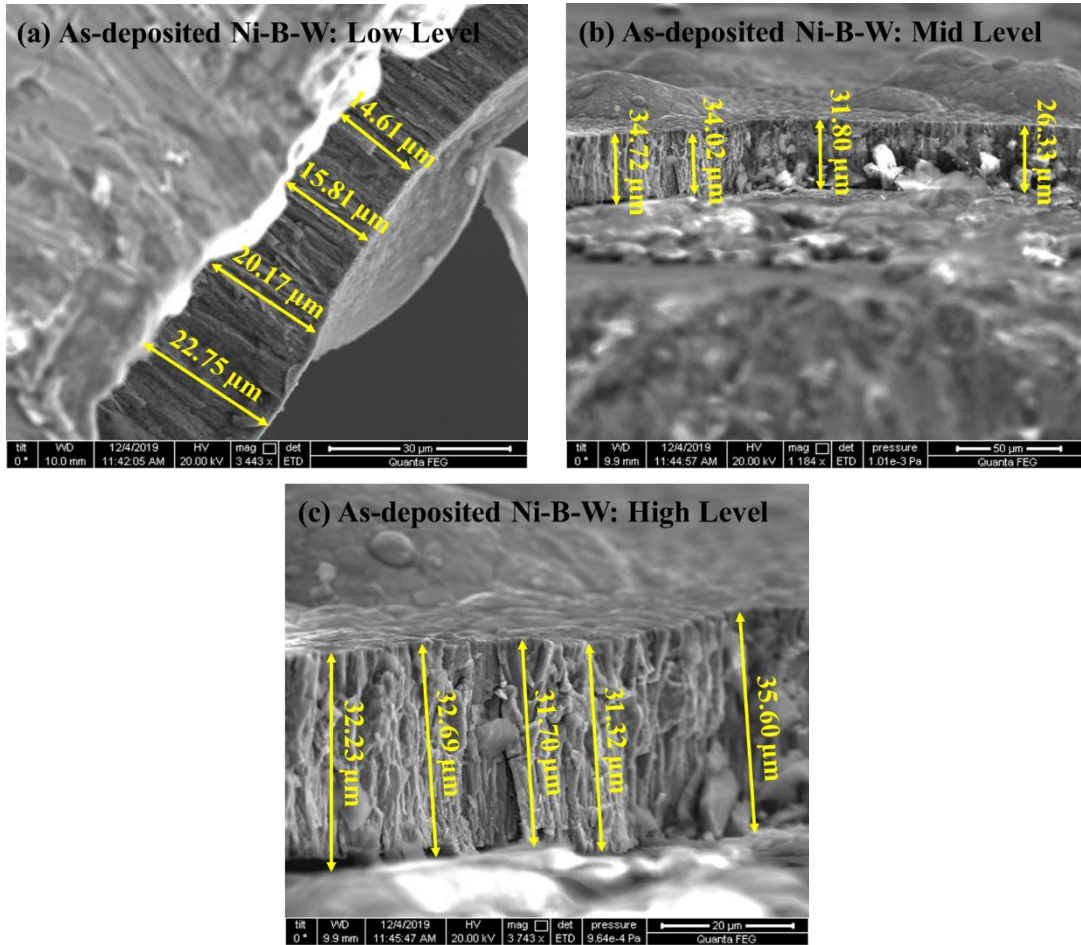


Figure 4.1: SEM Image of Coating Thickness of As-deposited Ni-B Coatings Obtained at (a) Low Level, (b) Mid-Level and (c) High Level Concentrations

4.3.2 Surface Morphology

The surface morphology of Ni-B-W coated surface is displayed in **Figure 4.2** which shows that the low, mid and high; all three-level coatings possess closely packed nodular surface morphology [Hosseini et al. 2019; Nemanee and Chatterjee, 2020] within the working range of parameters. This type of dense nodular surface morphology is found to be associated with cauliflower-like surface morphology which usually can be found in EN coatings [Balaraju et al. 2016; Vitry and Bonin, 2017; Hosseini et al. 2019; Nemanee and Chatterjee, 2020].

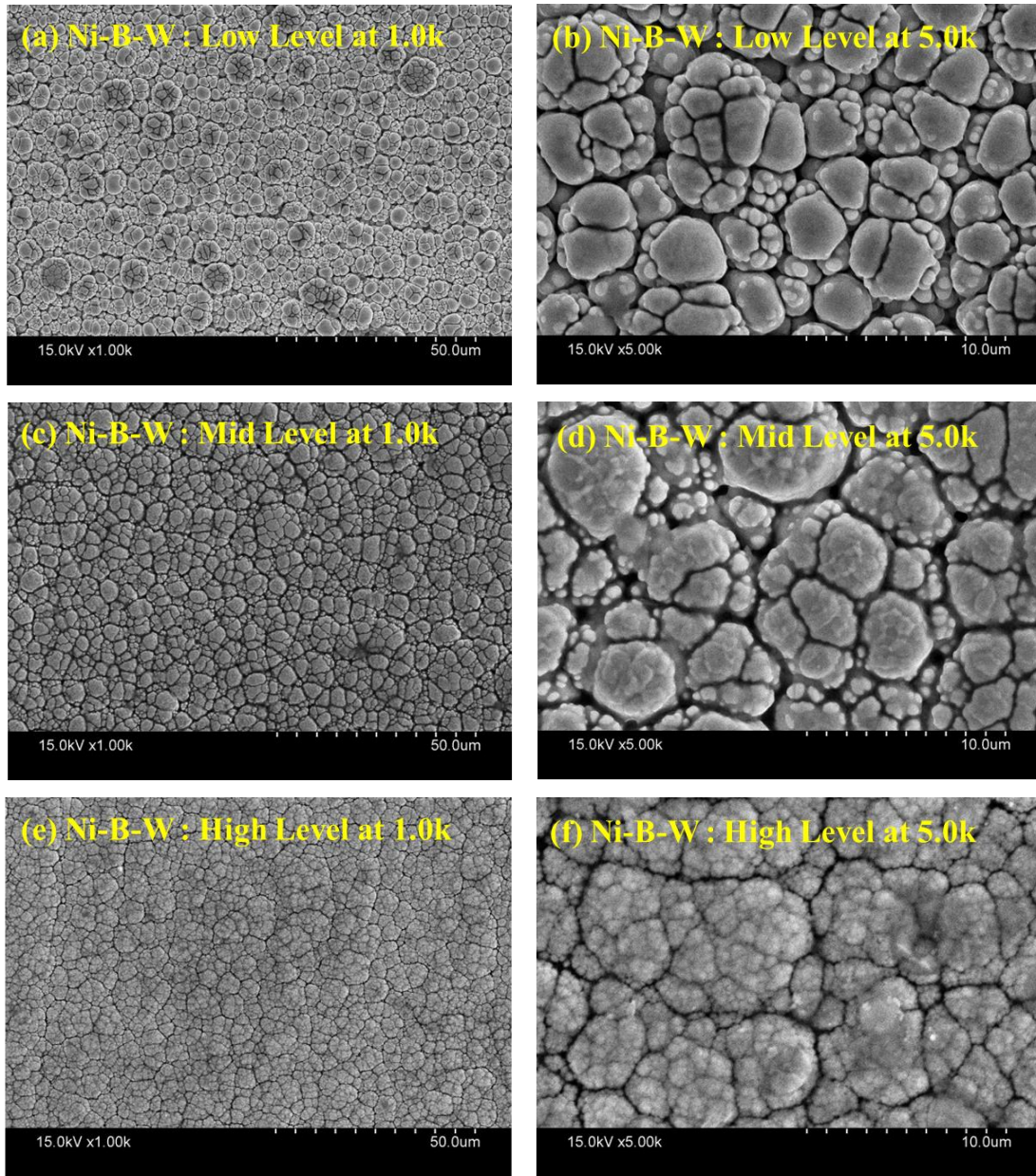


Figure 4.2: SEM Image of Surface Morphology for As-deposited Ni-B-W Coating Obtained at (a) Low Level, (b) Mid-Level and (c) High Level Concentrations

Columnar growth may also be observed in the cross-cut SEM image displayed through **Figure 4.1** which is an obvious feature of borohydride reduced EN coatings [Balaraju et al. 2016; Vitry and Bonin, 2017; Mukhopadhyay et al. 2017; Hosseini et al. 2019]. This type of columnar growth and cauliflower-like surface morphology cause a decrement in friction coefficient of the as-deposited coated specimens due to reduction in

the actual contact area in between mating surfaces [Hosseini et al. 2019]. The nano-grain nucleation occurs at multiple nucleation points at isolation zones preferably at surface crests and valleys of rough surface. The same progresses along the lateral direction to form smooth continuous film through columnar growth and finally leads to cauliflower-like surface morphology [Vitry et al. 2010; Hosseini et al. 2019]. The nodular surface is seemed to become more compact leading to cauliflower-like morphology with the increase in level of concentration.

4.3.3 Chemical Composition

The EDAX mapping results of Ni-B-W coated surface at different bath parameter concentrations is presented in **Figure 4.3**. The green colour presented in **Figure 4.3(a)** represents the existence and distribution of Ni on the coated surface, while yellow colour and purple colour shown in **Figure 4.3(b)** and **Figure 4.3(c)**, represent the existence and distribution of boron and tungsten, respectively at LLC. Similarly, **Figure 4.3(d)-(f)** and **Figure 4.3(g)-(i)** represent the existence of nickel (Ni), boron (B) and tungsten (W) on coated surface obtained at MLC and HLC, respectively. The intensity of green colour decreased with the coating bath composition level which indicates reduction of nickel content in the as-deposited coatings. Similarly, yellow and purple colour indicate the presence of boron and tungsten on the coated surface, where it is observed that the boron content initially increased from low level to mid-level but the same decreased at high level of coating composition. Similarly, tungsten content is also seen to increase with level of concentration which can be a reason for reduction in boron content at high level of concentration. The EDAX spectrums of the Ni-B-W coated specimens are displayed in **Figure 4.4**. Usual trend of borohydride reduced electroless coating is to increase the boron concentration with bath parameter concentrations [Sürdem et al. 2019]. But the rate of increase in boron content lowered slightly though boron content increased with the rise of concentration level from low level to mid-level for Ni-B-W coatings. It possesses $90.50 \pm 0.60\%$ nickel, $3.90 \pm 0.30\%$ boron and $2.80 \pm 0.20\%$ tungsten at low level of concentration. The mid-level and high-level concentrations Ni-B-W coatings contain $88.40 \pm 0.50\%$ and $86.30 \pm 0.70\%$ Ni, $5.70 \pm 0.30\%$ and $5.30 \pm 0.30\%$ B, $3.30 \pm 0.40\%$ and $4.20 \pm 0.30\%$ W, respectively. Therefore, nickel concentration is reduced as the bath

concentration level increased but the tungsten is seen to increase [Mukhopadhyay et al. 2018g].

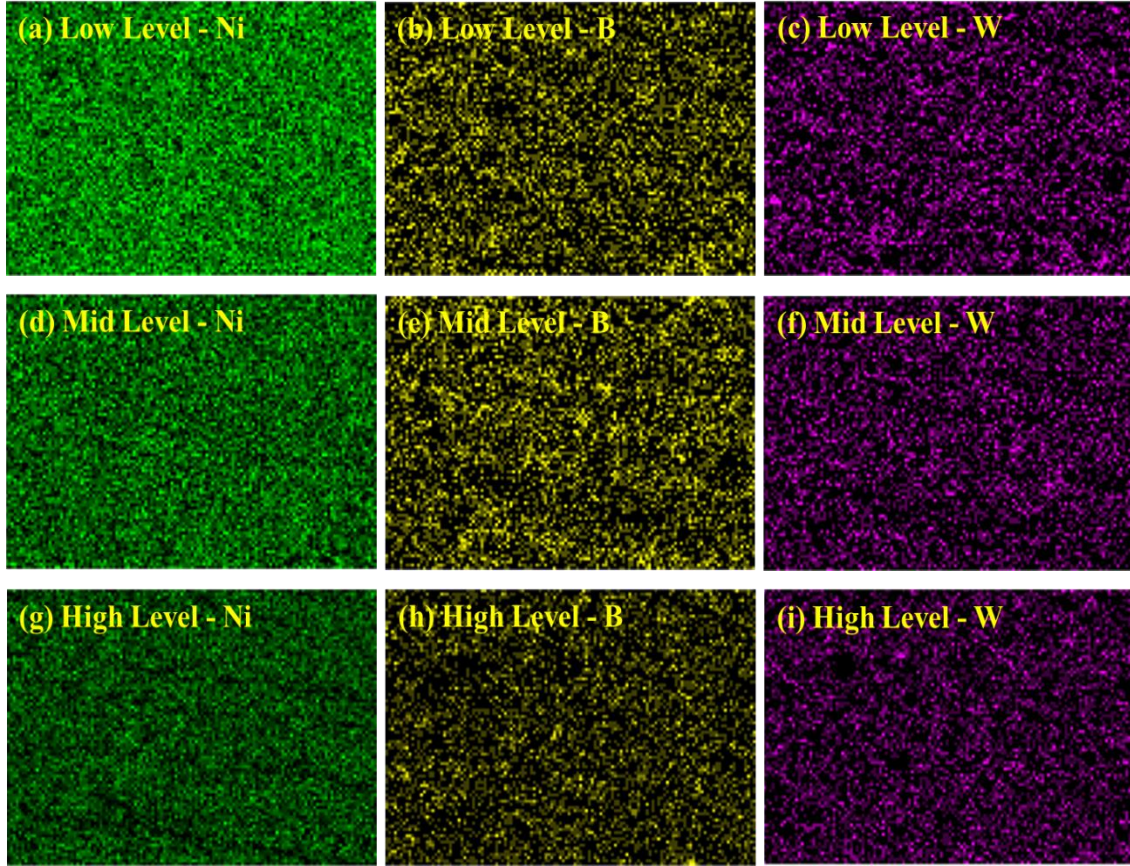


Figure 4.3: EDAX Mapping Images of As-deposited Ni-B Coatings Obtained at (a)-(c) Low Level, (d)-(f) Mid-Level and (g)-(i) High Level Concentrations

The boron concentration is increased initially from low to mid-level concentration and then slight reduction can be observed upon further rise in concentration level till high level though it is very negligible. This reduction in boron content may be due to the co-deposition of tungsten with boron [Mukhopadhyay et al. 2018c]. The tungsten concentration is observed to rise due to increase in bath parameter level from low to high. The rise in tungsten content on coating layers due to higher concentration of sodium tungstate in the solution might have decreased the boron concentration [Mukhopadhyay et al. 2018g]. While, the boron content for coatings obtained with mid or high-level concentration remained more than the low-level concentration. Ni content in the coatings

is reduced against the rise in NiCl_2 concentration. This reduction in Ni content may be because of the rise in boron and tungsten content in the coatings [Mukhopadhyay et al. 2018g]. The presence of O and Fe can also be seen at negligible amount. Therefore, this negligible amount of O and Fe may be overlooked because these might have gathered from any extraneous origin.

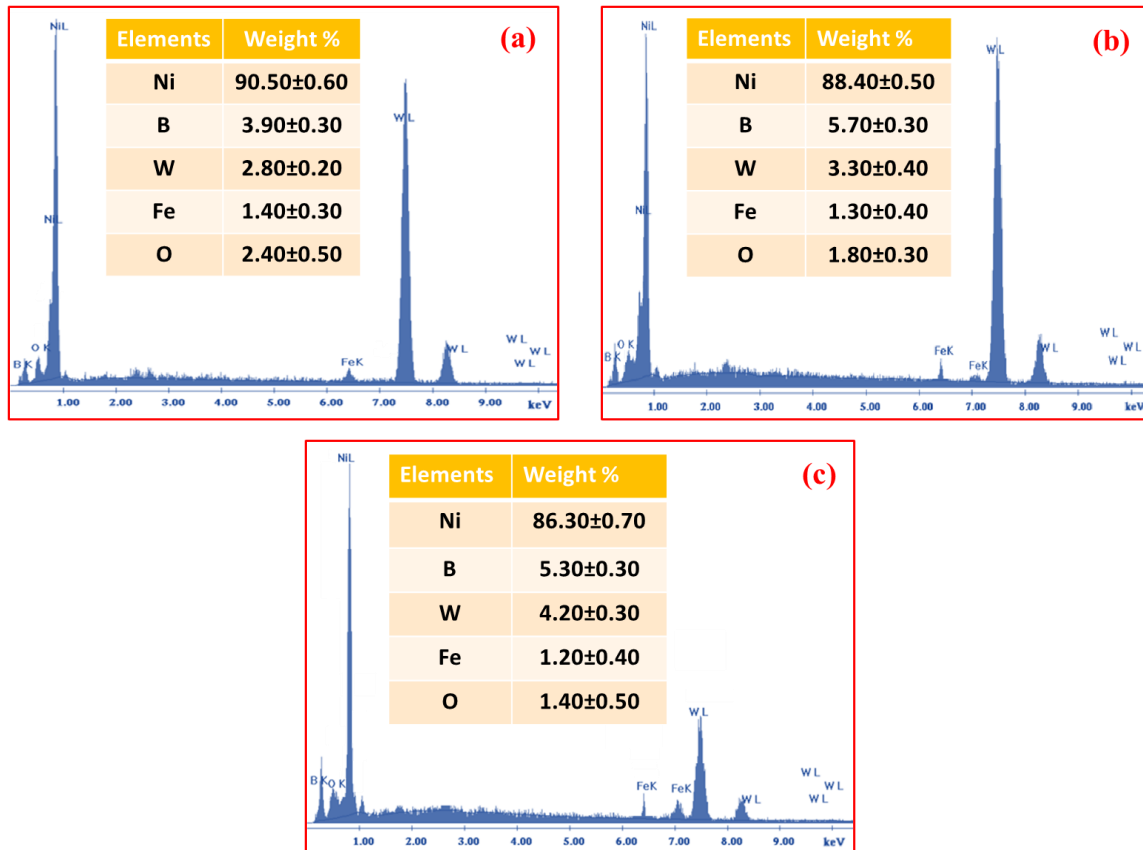


Figure 4.4: EDAX Spectrum of As-deposited Electroless Ni-B-W Coatings Obtained at (a) Low Level, (b) Mid-Level and (c) High Level Concentration

4.3.4 Phase Structure

The XRD patterns at different level of concentration are displayed in **Figure 4.5** where the Ni-B-W coated specimens obtained with low level exhibit a peak at 44.5° while the same can be observed at 52.3° for mid and high levels. The XRD pattern of low level comprises of a hump with a crystallinity peak where the hump signifies the presence of amorphous phase and the sharp peak represents the crystalline phase of coatings [Vitry

and Bonin, 2017; Sürdem et al. 2019]. Therefore, coexistence of hump with broad peak is the indication of bearing the amorphous-crystalline phase together in coatings [Bülbül et al. 2013; Yildiz et al. 2017; Vitry and Bonin, 2017; Sürdem et al. 2019] which resembles with the current study. Three peaks observed at 44.5° , 64.8° and 82.5° for coating obtained at low level of concentrations. The peak at 44.5° corresponds to Ni which is superimposed with Fe phase. The other two peaks observed at 64.8° and 82.5° are also corresponds to Fe phase. The similar results can also be observed in previous studies [Correa et al. 2013; Agrawal and Mukhopadhyay, 2022]. The coatings with more than 6.5% boron usually prevents nucleation of nickel phases which leads to formation of amorphous phases in electroless coating process [Vitry et al. 2010; Correa et al. 2013; Mukhopadhyay et al. 2017; Mukhopadhyay et al. 2018h; Agrawal and Mukhopadhyay, 2022]. On the other hand, the presence of tungsten promotes amorphous phase formation [Vitry et al. 2010; Correa et al. 2013; Mukhopadhyay et al. 2017; Mukhopadhyay et al. 2018h; Agrawal and Mukhopadhyay, 2022].

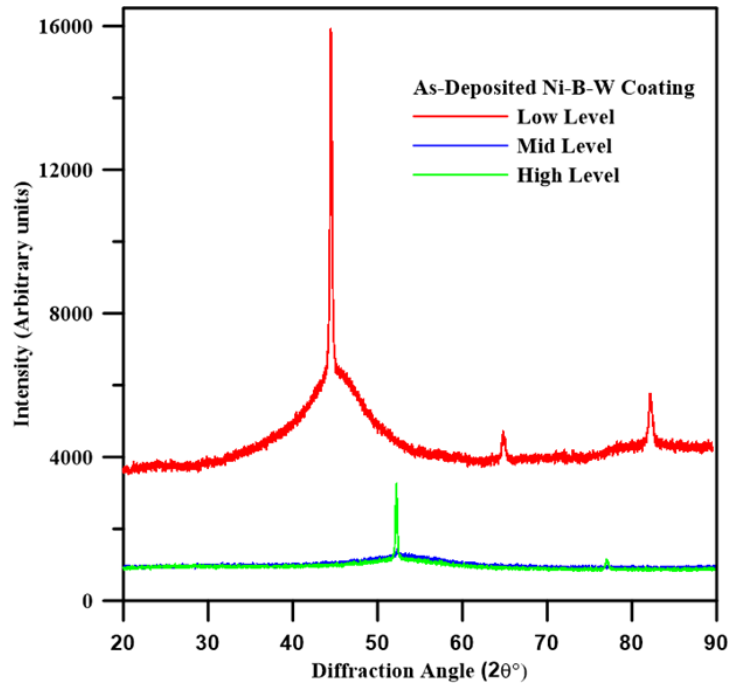


Figure 4.5: XRD Patterns of As-deposited Ni-B-W Coatings

Ni-B-W coatings at low level contain only $3.90 \pm 0.30\%$ boron and $2.80 \pm 0.20\%$ tungsten where low boron might be the reason for crystalline phase and tungsten can be

the reason for amorphous phase. The crystalline peak is found to diminish at mid-level of concentration which confirms the transformation of amorphous phase from amorphous-crystalline phase. The increase in boron content from low- to mid-level concentration might lead to formation of amorphous phase structure. Similar phase structure can also be observed in previous work [Yildiz et al. 2017]. The crystalline peak is again found to increase slightly at high level of concentration but the hump remained. Two sharp peaks appear at 52.3° and 77.09° for the coating obtained at high level of concentrations. The peak appears at 52.3° is found to be crystalline phase of Ni and Fe. The other peak at 77.09° is also of Fe. This indicates again the coexistence of amorphous-crystalline phases. Therefore, coexistence of crystalline peak with a hump confirms the coexistence of these phases at high level of concentration. The peak of Fe is observed in XRD spectrum which supports the EDAX analysis report where existence of Fe also can be found. Similar results may be observed in previous studies [Correa et al. 2013; Agrawal and Mukhopadhyay, 2022]. The XRD and EDAX methods for obtaining phase and elements are straight forward. The results depend on the coating thickness as well as surface roughness. The rough surface of the coated layers may be the possible reasons for the Fe peaks in the XRD and EDAX results which are in well agreement with previous studies [Correa et al. 2013; Agrawal and Mukhopadhyay, 2022].

4.4 Physical and Mechanical Behaviours

4.4.1 Surface Roughness

The surface roughness (centre line average, R_a) of as-deposited Ni-B-W alloy coatings is found to be less relative to substrate ($R_a = 0.285 \mu\text{m}$) at LLC which is $R_a = 0.189 \mu\text{m}$. The reduction rate of borohydride reduced electroless coatings remain low at lower level of concentration due to low borohydride concentration which may be the possible reason for this decrease in surface roughness [Vitry et al. 2012]. The surface roughness is also found to increase further at mid-level ($R_a = 0.515 \mu\text{m}$) and high level ($R_a=0.808 \mu\text{m}$) of concentrations compared to low level concentration as well as substrate. The borohydride content in the solution rises as the concentration level increased which increased the reduction rate [Vitry et al. 2012; Sürdem et al. 2019].

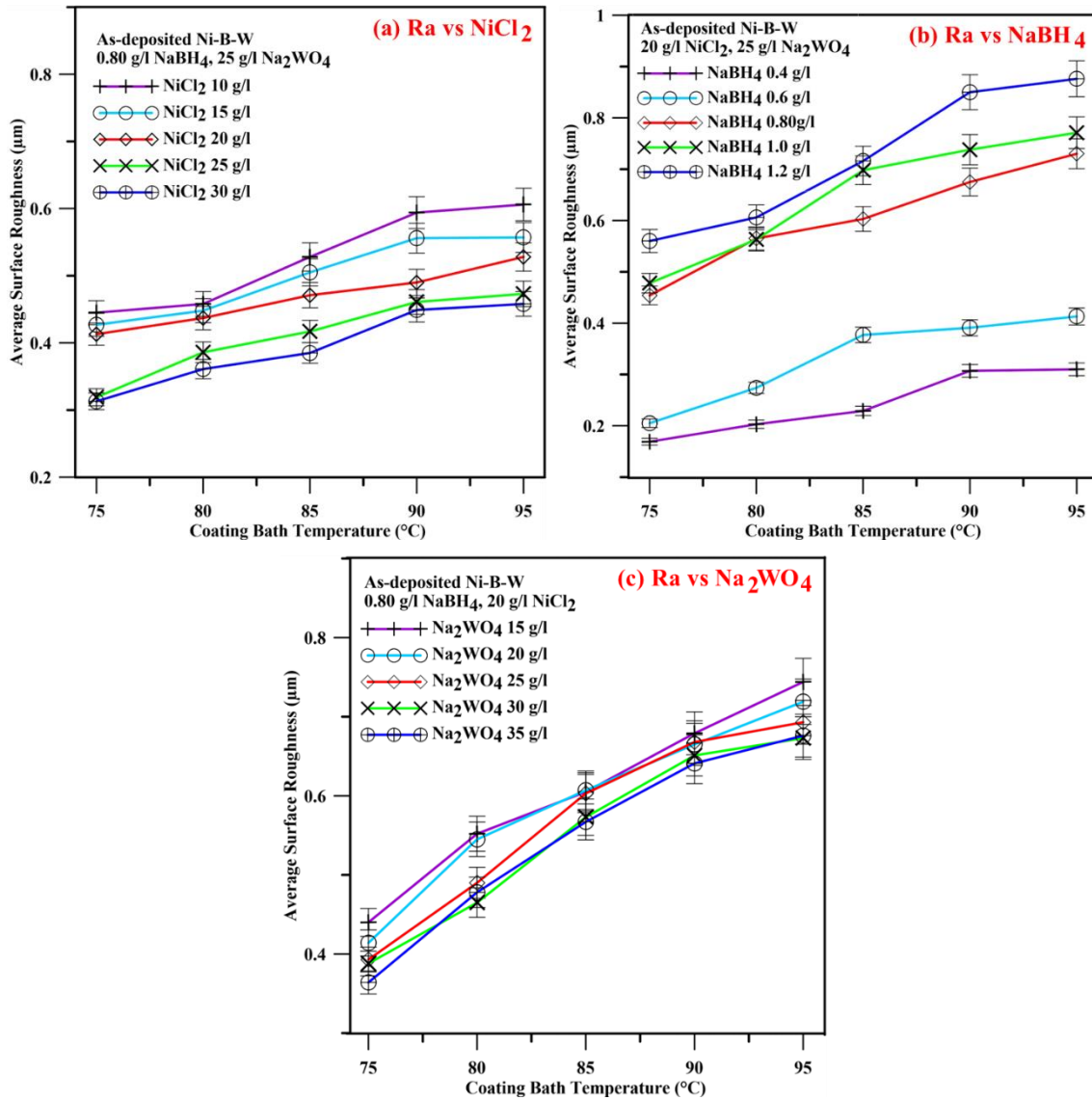


Figure 4.6: Average Surface Roughness Plot with Varying Temperature and (a) Nickel Chloride, (b) Sodium Borohydride and (c) Sodium Tungstate Concentrations

The higher reduction rate leads to random deposition of hard particles leading to rough surface [Vitry et al. 2012; Bülbül et al. 2013; Madah et al. 2015; Wan et al. 2016]. The surface roughness increased from lower to higher level of concentration possibly because of this higher reduction rate. **Figure 4.6(b)** also showing the same trend that the surface roughness increased with sodium borohydride concentration as well as coating bath temperature. The rise in bath temperature accelerates the reduction and hence the surface roughness increases. In contrary, from **Figure 4.6(a)**, the surface

roughness was observed to reduce with the increase in nickel chloride concentration due to possibly smoothening of surface. The surface roughness does not vary much with the variation of sodium tungstate concentration in the coating bath solution as shown in **Figure 4.6(c)**. But the same surface becomes rougher with the increase in bath temperature which is possibly due to the higher reduction rate. The reduction is found to increase with temperature which acted as the dominating one.

4.4.2 Nano-indentation Test

The loading unloading curve is presented in **Figure 4.7** where the applied load is plotted against indentation depth. It represents the applied loads required for same indentation depth for coatings deposited with different level of concentrations. The higher value of applied load indicates the higher surface hardness of coatings and vice-versa. It can be seen from **Figure 4.7** that the highest applied load is required for the same indentation of coatings obtained with high level of coating bath concentration followed by mid-level and low level. This indicates the rise in surface hardness with coating bath concentration level.

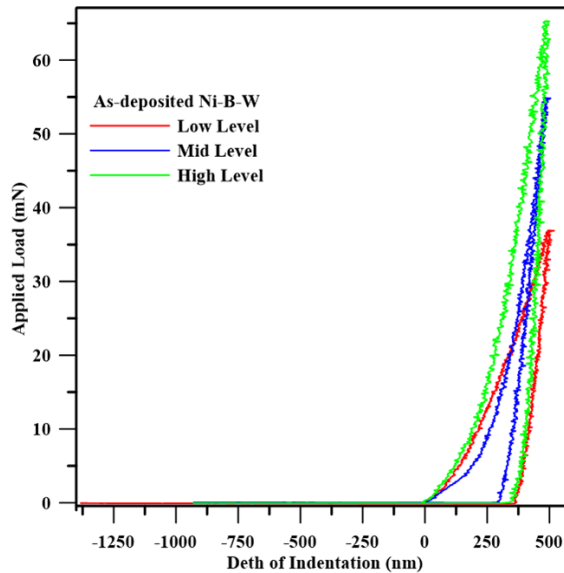


Figure 4.7: Depth of Indentation vs Applied Load Plot

The surface hardness of ENB coated specimens were seen to increase with the rise

in boron on coated surface [Lekka et al. 2018; Sürdem et al. 2019]. The boron content was further seen to rise in the coatings due to increase in borohydride concentration [Lekka et al. 2018; Sürdem et al. 2019]. The elemental analysis result also shows a rise in boron content in Ni-B-W coated specimens till mid-level concentration which resembles with the previous trend of increasing surface hardness trend [Sürdem et al. 2019]. Boron content was found to decrease slightly at high level because of rise in tungsten content in the coated layers [Yildiz et al. 2017]. Therefore, the improvement in surface hardness at high level can be attributed with the addition of hard tungsten particle. The variation of nano-hardness property of Ni-B-W coatings against various coating bath parameter concentration and bath temperature is displayed in **Figure 4.8**. The variation of surface hardness with nickel chloride is presented in **Figure 4.8(a)** which represents an improvement in nano-hardness value with an increase in NiCl_2 ions in the coating bath solution. The elemental analysis result represents a reduction in Ni content in the coated layers, other elements like boron and tungsten increased even at high level of NiCl_2 . It confirms that the boron and tungsten content in the coatings dominates to control the Ni-B-W coating characteristics. It may be the reason for the improvement in surface hardness even with the increase in NiCl_2 concentration. The surface hardness value is also observed to improve with the bath temperature. The ion reduction rate is low at low bath temperature and it accelerates with coating bath temperature rise which did stable at around 90°C . Therefore, the boron and tungsten content also increased at higher temperatures of coating bath which in turn leads to the improvement in nano-hardness value of the coatings. The variation of nano-hardness against NiBH_4 concentration is presented in **Figure 4.8(b)**. **Figure 4.8(b)** represents a rising trend of nano-hardness value with sodium borohydride. The hardness value is found to improve with NiBH_4 concentration because of the rise in boron content on coated surface [Bonin and Vitry, 2016; Vitry and Bonin, 2017; Lekka et al. 2018; Sürdem et al. 2019]. The elemental analysis also shows a rise in boron content in as-deposited coatings till mid-level of concentration with NiBH_4 rise. Hence the elemental analysis result agrees well with the surface hardness trend. The presence of tungsten in the coated layer further improves the surface hardness. The co-existence of boron and tungsten improved the surface hardness.

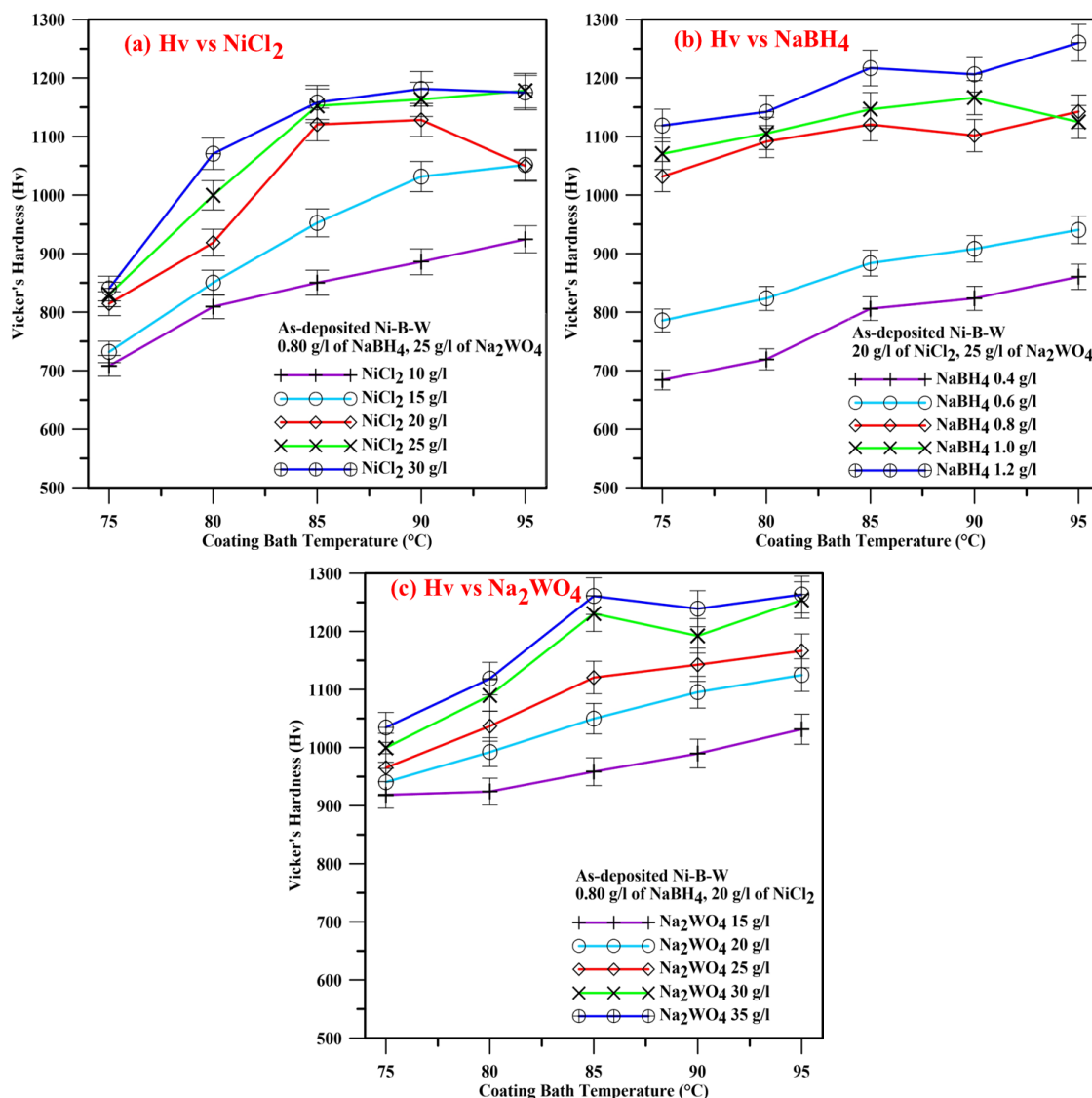


Figure 4.8: Hardness Plot with Varying Temperature and (a) Nickel Chloride, (b) Sodium Borohydride, and (c) Sodium Tungstate Concentrations

The hardness is also found to increase with bath temperature. The chemical reaction rate begins near 70°C which accelerates upon coating bath temperature rise till a certain limit. This leads to a rise in chemical composition of coatings specially the boron content which ultimately helps in the improvement of surface hardness [Bonin and Vitry, 2016; Lekka et al. 2018]. The nano-hardness variation with sodium tungstate is presented in **Figure 4.8(c)**. The improvement in nano-hardness behaviour of Ni-B-W coated specimens was seen to improve due to increase in sodium tungstate concentration though the improvement is not very much. The tungsten content in the coated layers

increased slightly leading to increase in nano-hardness as well. Hence, the improvement of nano-hardness with sodium tungstate is possibly due to the rise of tungsten in the coatings. The nano-hardness is also improved with coating bath temperature but no specific trend can be observed, rather an overall improvement may be observed. This improvement is possibly because of the acceleration of reduction reaction in the coating bath solution with temperature rise and the corresponding modification in chemical composition of coatings.

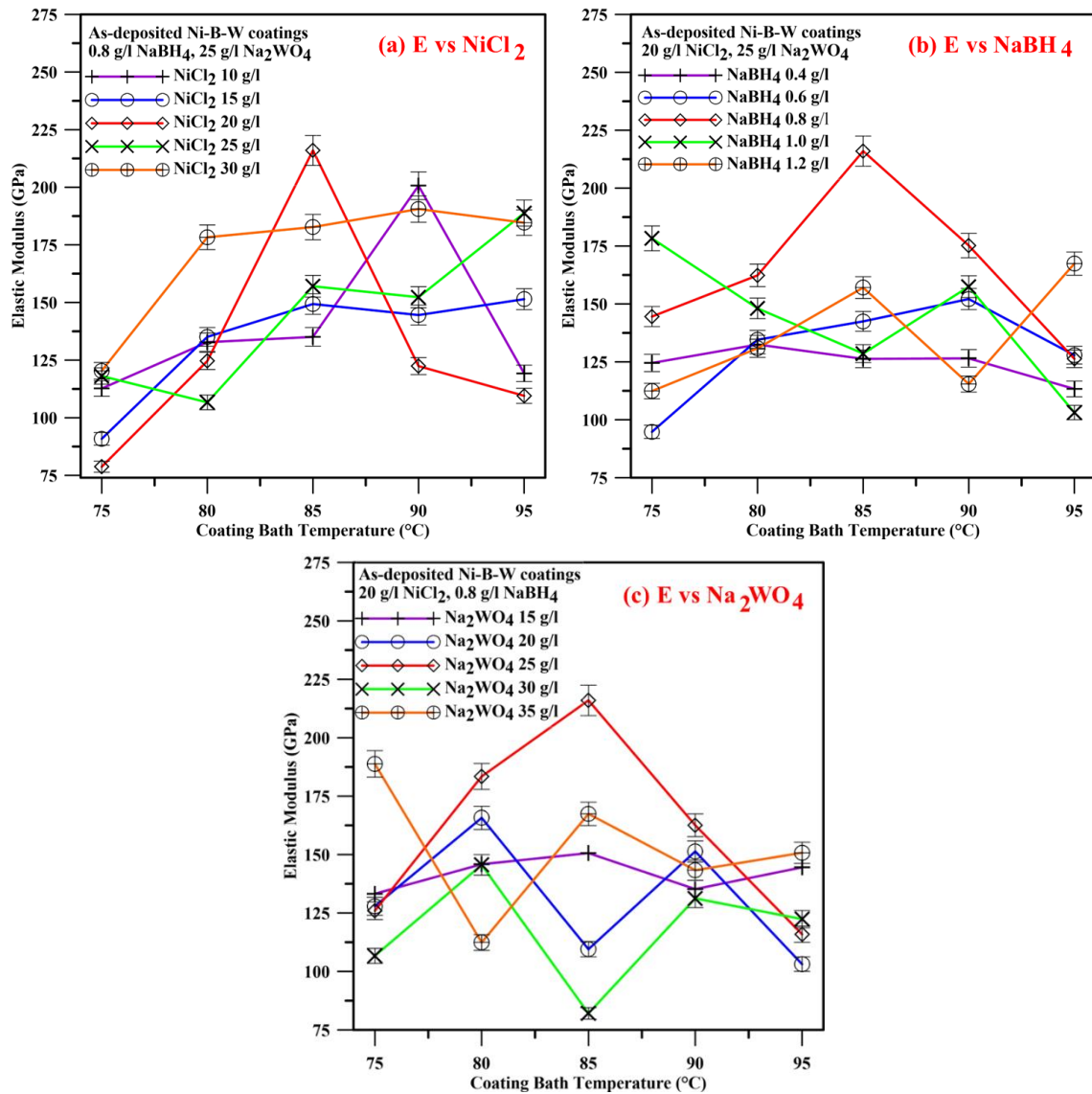


Figure 4.9: Elastic Modulus Plot with Varying Temperature and (a) Nickel Chloride, (b) Sodium Borohydride, and (c) Sodium Tungstate Concentrations

The plots for elastic modulus with the variation of bath composition as well as temperature are represented in **Figure 4.9**. It was seen that elastic modulus of coatings does not depend on surface hardness [Sürdem et al. 2019]. But it was observed to vary the elastic modulus with grain size. Further, the grain size of borohydride reduced ENB coatings was observed to rise due to increase in NaBH_4 concentration. This rise of grain size of ENB coatings due to increased boron content might have led to an increase in elastic modulus of ENB coatings. The borohydride content in the coating bath solution prevents Ni nucleation and promotes amorphous phase formation [Nemane and Chatterjee, 2020]. The rise of NiCl_2 in the solution lead to increase in Ni ions which may produce multiple nucleation points at isolated zones, preferably at roughness peaks or valleys of the substrate and the coating growth progresses in the lateral directions to form a smooth film with columnar structure [Nemane and Chatterjee, 2020; Nemane et al. 2022]. The compact surface of crystalline coatings may lead to higher surface hardness but the elastic modulus does not vary with this. The variations in elastic modulus with NiCl_2 , NaBH_4 and Na_2WO_4 concentration are presented in **Figure 4.9(a)**, **Figure 4.9(b)** and **Figure 4.9(c)**, respectively, which do not follow any specific trend. The coatings with lower elastic modulus are found to possess better wear resistance relative to higher elastic modulus [Sürdem et al. 2019]. But any specific trend with bath concentration variation and bath temperature cannot be observed in this current study.

4.4.3 Micro-Scratch Test

The scratch hardness of Ni-B-W coated specimens was measured using micro-scratch test and the average of the measured values are plotted to analyse the variation of scratch hardness with coating bath parameters and operating conditions. The variations of scratch hardness plots against nickel chloride, sodium borohydride, sodium tungstate and bath temperature are presented in **Figure 4.10**. The scratch hardness value is observed to improve with Nickel chloride, sodium borohydride, sodium tungstate as well as bath temperature. This improvement in scratch hardness as well as nano-hardness may be observed due to the surface hardening with the incorporation of boron and tungsten in the coatings [Nemane and Chatterjee, 2020].

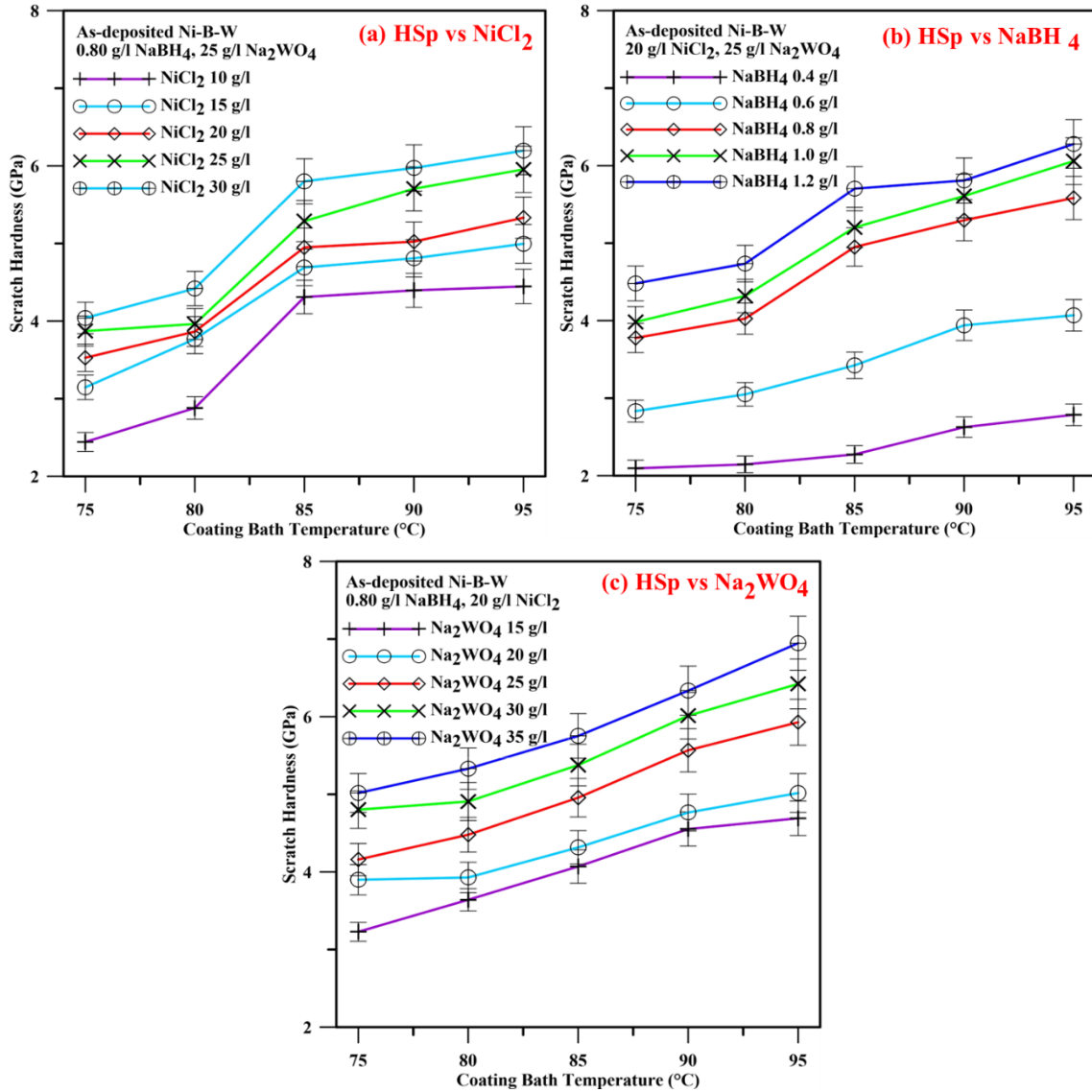


Figure 4.10: Scratch-Hardness Plot with Varying Temperature with (a) Nickel Chloride, (b) Sodium Borohydride, and (c) Sodium Tungstate Concentrations

The acceleration of reduction reaction in the coating bath with the temperature rise leads to a rise in boron content and tungsten content which ultimately improve the nano-hardness and scratch hardness. It was also observed to increase the scratch hardness with addition of sodium tungstate in the bath solution possibly due to the solid solution strengthening with the addition of tungsten in the Ni-B matrix [Nemane and Chatterjee, 2020]. The SEM images displayed in Figure 4.2 also show that the surface becomes more compact with bath parameter concentration level which may also be a probable

cause for the improvement in nano-hardness as well as scratch hardness. The elemental analysis (**Figure 4.3 and Figure 4.4**), surface morphology and the experimental results are in well agreement with each other in the current study.

4.5 Tribological Test

The variation of COF value during the whole sliding duration of tribo-test is displayed in **Figure 4.11**. It depicts that the COF value raised drastically initially during the sliding till reached to its maximum and then it became stable after some time. The surface roughness peaks are broken and grinded in the sliding surface which makes the surface smooth leading to decrease in friction coefficient value. This trend can be observed throughout the working range of the coating bath parameters from low to high level of concentrations. But overall, the friction coefficient plot at higher level is seen to be higher than low- and mid-level of concentrations. The surface roughness value increases with NiBH_4 concentration which may cause a rise in friction coefficient till mid-level of concentrations. The friction coefficient was higher even though the boron content decreased slightly at high level of concentration. This is possibly because of the incorporation of hard particles in Ni-B matrix. The broken roughness peaks containing tungsten like hard particles may have increased the friction coefficient.

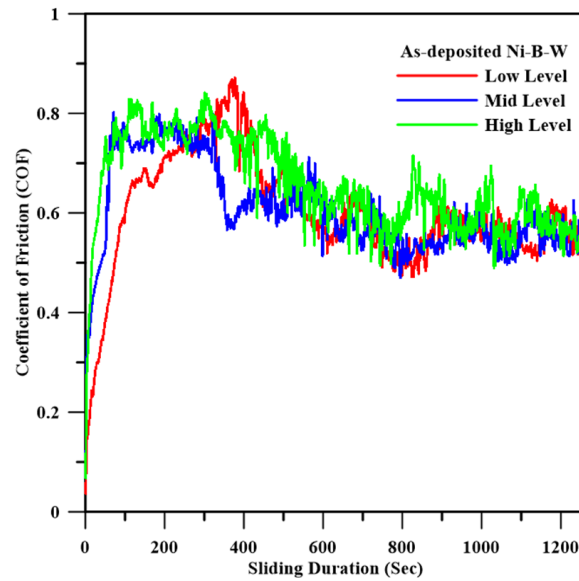


Figure 4.11: Coefficient of Friction (COF) vs Sliding Duration Plot

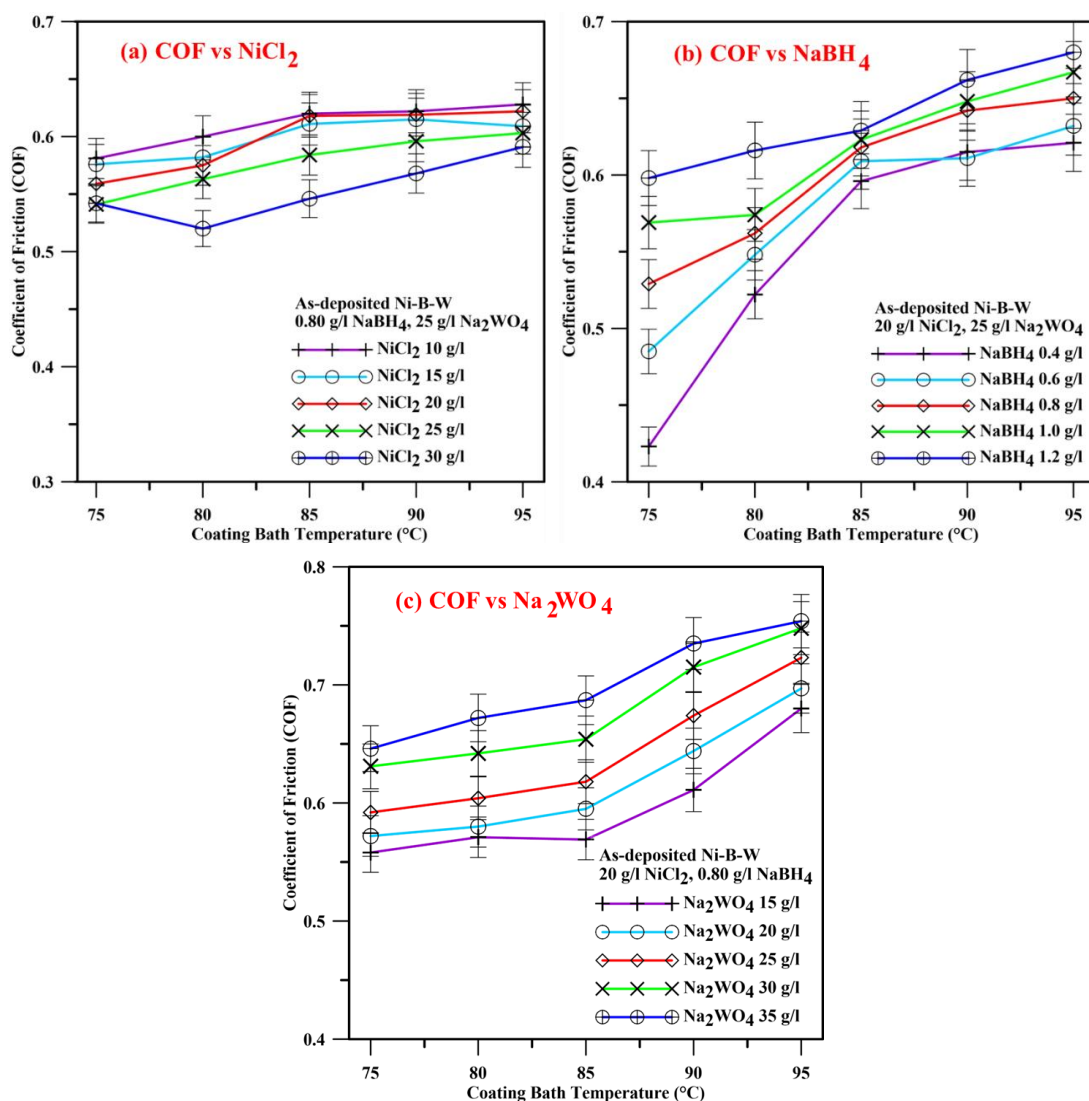


Figure 4.12: Average Coefficient of Friction (COF) Plot with Varying Temperature with (a) Nickel Chloride, (b) Sodium Borohydride and (c) Sodium Tungstate Concentrations

The friction coefficient (COF) variation against nickel chloride, sodium borohydride, sodium tungstate and coating bath temperature is displayed through **Figure 4.12**. A decreasing trend of friction coefficient value with the increase of nickel chloride concentration can be observed from **Figure 4.12(a)**. The friction coefficient is found to increase with coating bath temperature but it remained lower at higher concentration of nickel chloride compared to other concentrations. The presence of nickel chloride may have smoothened the coated surface resulting in decrease of surface roughness value

which ultimately reduces the friction coefficient. The variation in average COF value with sodium borohydride is presented in **Figure 4.12(b)**. The COF is seen to rise with NiBH_4 concentration while the same further rises with bath temperature. The higher concentration of NiBH_4 in the coating solution accelerates the reduction reaction rate leading to random deposition of metal ions over substrate surface which makes the surface rough [Bülbül et al. 2013; Wan et al. 2016; Madah et al. 2015]. The reduction reaction also accelerates with coating bath temperature up to a certain level which also makes the surface rough. The rough coated surface ultimately increases the COF value. The variation in COF value against sodium tungstate concentration and coating bath temperature is presented in **Figure 4.12(c)**. The figure shows a considerable increase in friction coefficient with sodium tungstate and coating bath temperature. This rise in friction coefficient may be correlated with the rising trend of surface roughness with sodium tungstate concentration rise.

The specific wear rate (Ws) of the Ni-B-W coated specimens was determined from mass loss and the values are presented in **Figure 4.13**. The variations of Ws value with NiCl_2 are presented in **Figure 4.13(a)** which represents a rising trend against NiCl_2 till mid-level of concentration. But the same is seen to decrease with further rise in NiCl_2 . The initial increase with NiCl_2 follows the trend of surface roughness variation till the mid-level concentration due to rough surface. In contrary to the surface roughness of coatings, specific wear rate is reduced against the increase in NiCl_2 concentration. The roughness peaks of the coatings at higher nickel chloride concentration are grinded over the surface and filled the roughness valleys of rough surface. The grinding of roughness peaks and smoothening the surface trigger the reduction in Ws value. Moreover, the grinded debris under the sliding surface acts as load bearing surfaces leading to reduction in Ws value. The variation of Ws with NaBH_4 is presented in **Figure 4.13(b)**. In **Figure 4.13(b)**, the Ws value is observed to rise against the rise in sodium borohydride till 1.0 g/l while the same is found to reduce upon further rise in NiBH_4 till 1.2 g/l. The same is found to increase further upon rise in coating bath temperature but no specific trend can be found. The Ra value rises against NiBH_4 and Ws value rises because of crushing the roughness peaks [Vitry and Bonin, 2017].

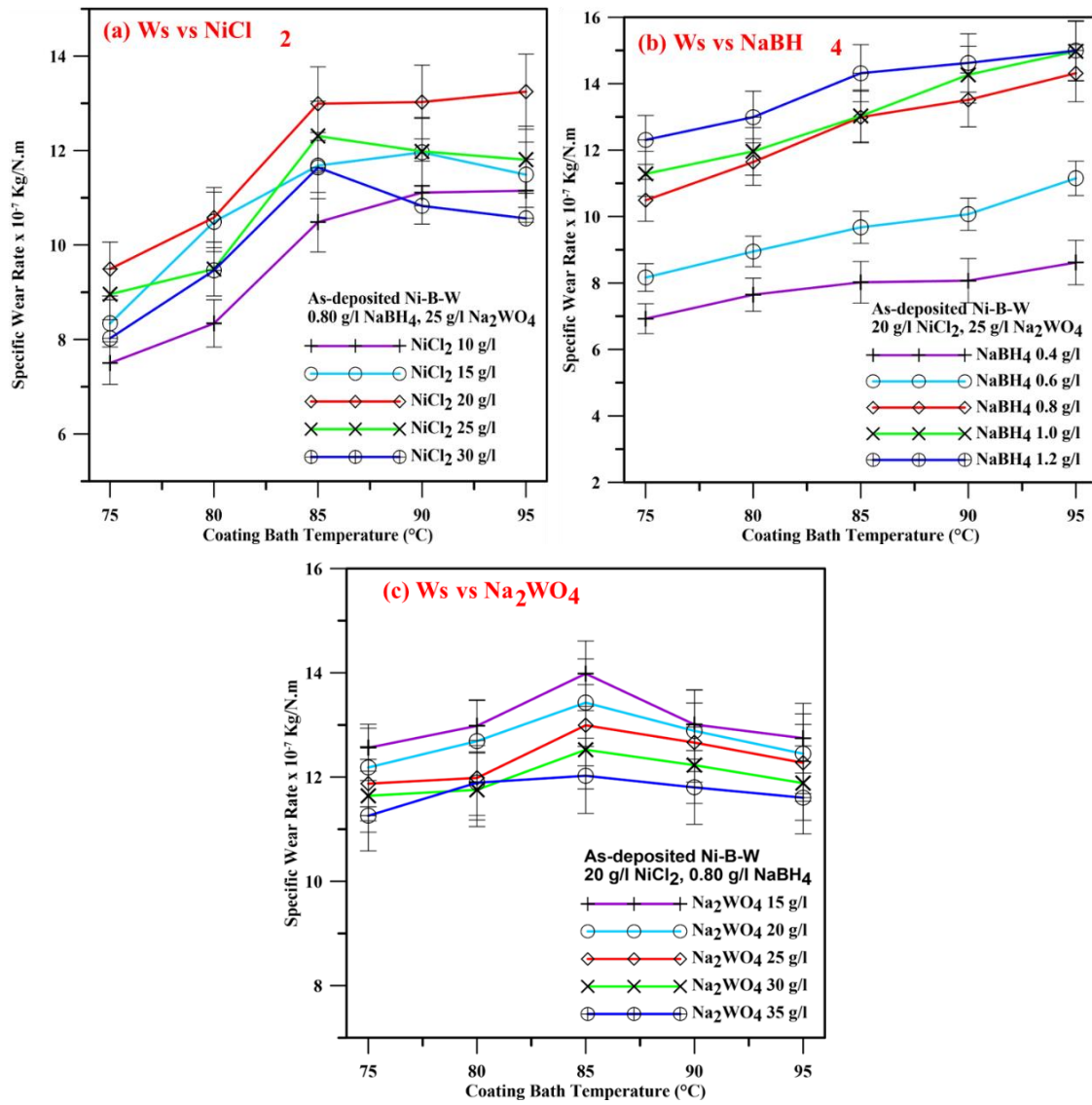


Figure 4.13: Specific Wear Rate Plot with Varying Temperature with (a) Nickel Chloride, (b) Sodium Borohydride, and (c) Sodium Tungstate Concentrations

The temperature rise in the coating bath accelerates the chemical reaction which increases surface roughness and this triggers the rise in Ws value [Vitry and Bonin, 2017]. The increased amount of borohydride in the solution increases boron content in the as-deposited coating which makes the surface hard. The hard surface may further lead to an enhancement in wear resistance or decrease in specific wear rate at the highest concentration of sodium borohydride. The specific wear rate variation against sodium tungstate concentration is displayed in **Figure 4.13(c)**. The figure shows a decreasing trend of specific wear rate against sodium tungstate content in the coating bath. This trend

is in contrary to the surface roughness trend. The tungsten content on coated surface rises against Na_2WO_4 concentration rise which improves the surface hardness of the coatings. It may be a possible cause of the reduction in specific wear rate with sodium tungstate concentration rise in the coating bath solution. The specific wear rate was not seen to vary considerably against coating bath temperature.

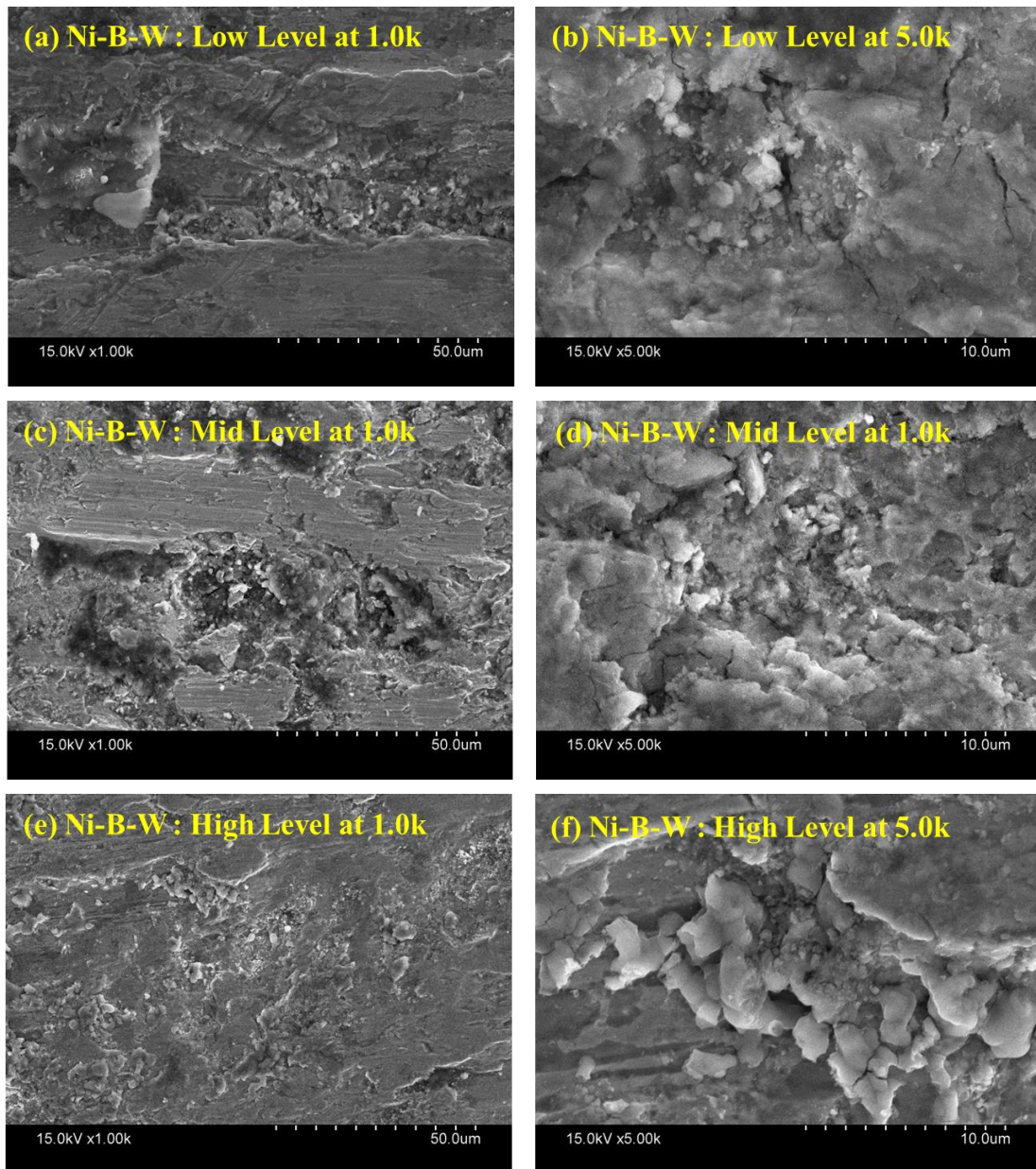


Figure 4.14: SEM Image of Worn-out Surface of As-deposited Ni-B-W Coatings Obtained at (a) Low Level, (b) Mid-Level and (c) High Level Concentrations

Surface morphology investigation of worn-out surfaces through SEM image is presented in **Figure 4.14**. It is clearly evident from **Figure 4.14** that the roughness peaks are crushed and grinded during the sliding test. The SEM image indicates the presence of wear debris on the worn-out surface. The presence of wear debris in the worn-out surface indicates the adhesive type of wear mechanism. It may be observed very often for borohydride reduced electroless coatings [Madah et al. 2015; Arias et al. 2019]. The surface can also be seen to possess some grooves formed during the repetitive sliding over the surface. Accumulation of grinded debris on the wear track may lead to smoothening of the surface leading to reduction in friction coefficient.

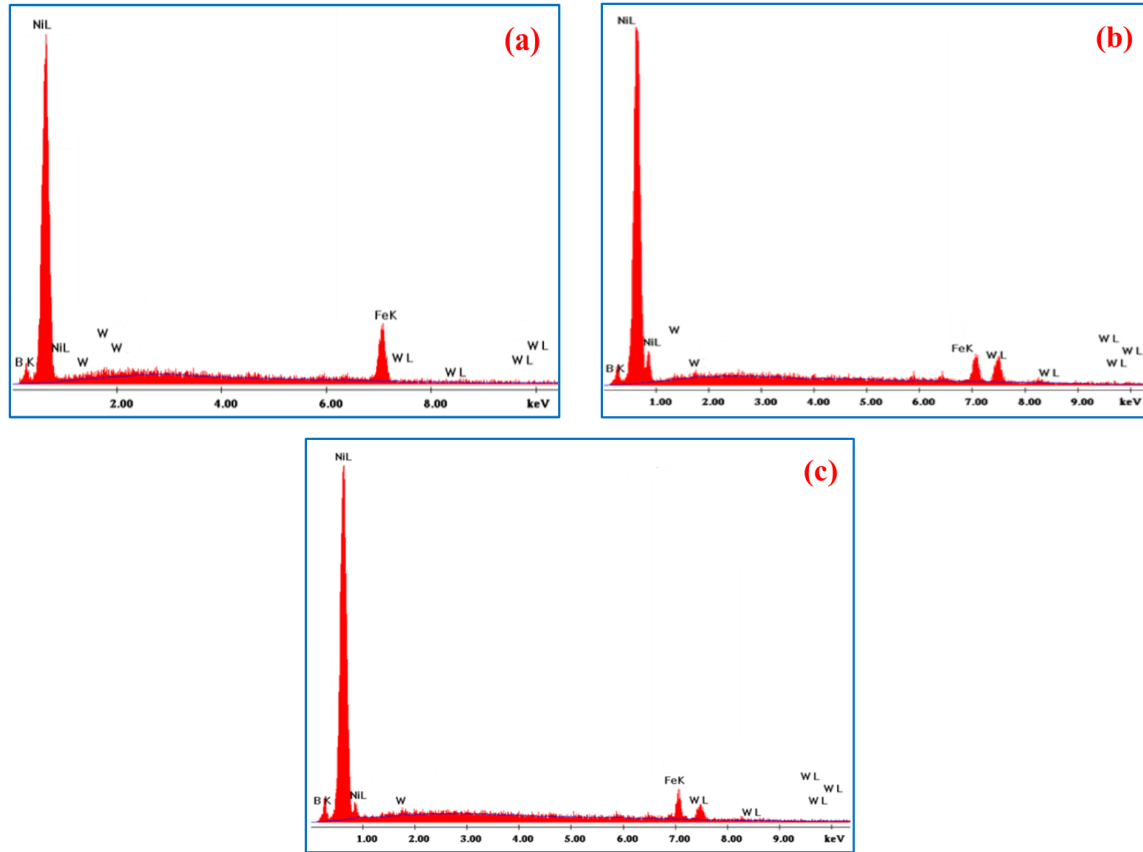


Figure 4.15: EDAX Spectrum of Worn-out Surfaces of As-deposited Ni-B Coatings Obtained at (a) Low Level, (b) Mid-Level and (c) High Level Concentrations

The presence of coarse debris may make the surface rough leading to increase in friction coefficient [Madah et al. 2015; Mukhopadhyay et al. 2018b; Mukhopadhyay

et al. 2018g] which also may act as load bearing surfaces and ultimately leading to reduction in specific wear rate. From **Figure 4.14(a)**, **Figure 4.14(b)** and **Figure 4.14(c)**, it may be observed that the surface obtained with high level of concentration exhibits less damage than the low- and mid-level coatings. The images also show that the less amount of debris is present on worn out surfaces of the coatings deposited with high level of concentration. The presence of higher tungsten particles improved the surface hardness and leading to improvement in wear resistance and hence this reduces surface damage.

The worn-out surfaces were further investigated through elemental analysis using EDAX. **Figure 4.15(a)-(c)** represents the presence of different elements in the worn-out surfaces. **Figure 4.15** confirms that nickel, boron, tungsten, iron and oxygen are present on worn-out surfaces. But the amount of iron and oxygen are found to be present on worn out surface at very less amount which indicates the coated layer have not been removed during sliding [Madah et al. 2015]. Moreover, the substrate deformation was not also seen after sliding test. Therefore, the presence of these small amount of iron and oxygen in the worn-out surface is a sign of adhesive type wear mechanism [Madah et al. 2015].

4.6 Corrosion Resistance Test

The nyquist plot and tafel plot is generated using the software provided with the test setup. The tafel plot is obtained from the PDP test and the nyquist plot is obtained from the EIS test. The software uses the data collected in the computer to generate the nyquist plot considering imaginary impedance on the y-axis and real impedance on the x-axis. The bigger semicircle of nyquist plot represents the better corrosion performance of coatings [Miri et al. 2013; Mukhopadhyay et al. 2018c] and lower negative value of corrosion current potential (E_{corr}) acquired using tafel plot indicates the improvement in corrosion performance of the coated layers [Anik et al. 2008; Kanta et al. 2009; Kanta et al. 2010]. The performance of coated layers against corrosion is also found to depend on its morphology and phase structure [Kanta et al. 2009; Kanta et al. 2010]. An increment in R_{ct} value obtained from nyquist plot indicates the improvement in corrosion performance [Anik et al. 2008; Kanta et al. 2009; Kanta et al. 2010]. Corrosion resistance of coatings is found to depend on various factors like surface porosity, microstructure, heterogeneities, columnar growth, phase structure etc. [Yildiz et al.

2013]. The ENB coated layers are found to prevent the steel substrate against corrosion [Bülbül et al. 2013]. **Figure 4.16(a)** represent the tafel plots obtained at different level of concentrations. The nyquist plot of the same coatings are displayed in **Figure 4.16(b)**. It may be found from the **Figure 4.16(a)** that the negative E_{corr} value is decreased with coating bath concentration till mid-level. The semi-circle loop in the **Figure 4.16(b)** also becomes bigger with coating bath concentration till mid-level. Therefore, the corrosion resistance of Ni-B-W coated specimens is increased. The boron concentration is raised with $NaBH_4$ concentration which ultimately improved the corrosion resistance of Ni-B-W coated layers [Vitry et al. 2012]. Generally, the rougher surface is suitable for the corrosive medium to penetrate.

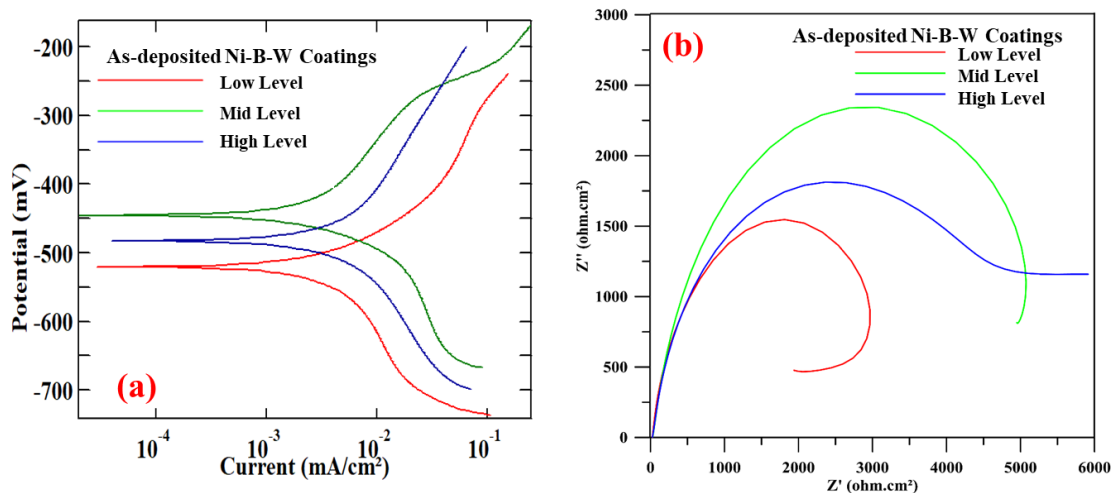


Figure 4.16: EIS and PDP Test Plot for As-deposited Ni-B-W Coatings, (a) Tafel Plot and (b) Nyquist Plot

The surface roughness of Ni-B-W coated surface is seen to increase with sodium borohydride concentration but decreased with nickel chloride and sodium tungstate concentration. Moreover, boron content at high level concentration also decreased slightly. The amorphous-crystalline phase of as-deposited Ni-B-W coatings gets transformed into amorphous phase with increased bath concentration level. The amorphous phase is familiar for better corrosion behaviour compared to crystalline phase [Anik et al. 2008]. The increase in boron content, amorphous phase may be the reason for increase in corrosion resistance of as-deposited Ni-B-W coatings till mid-level

concentration. While a reduction in boron content and increase in surface roughness may be correlated with the decreased in corrosion resistance at high level concentrations.

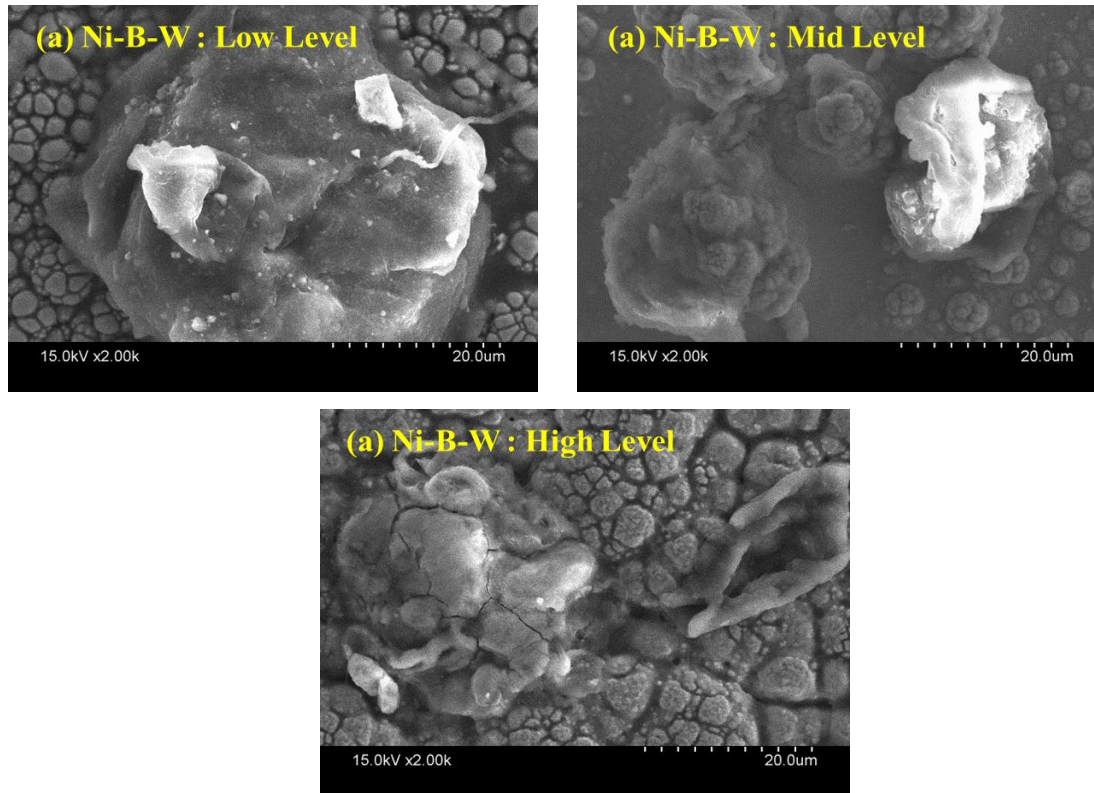
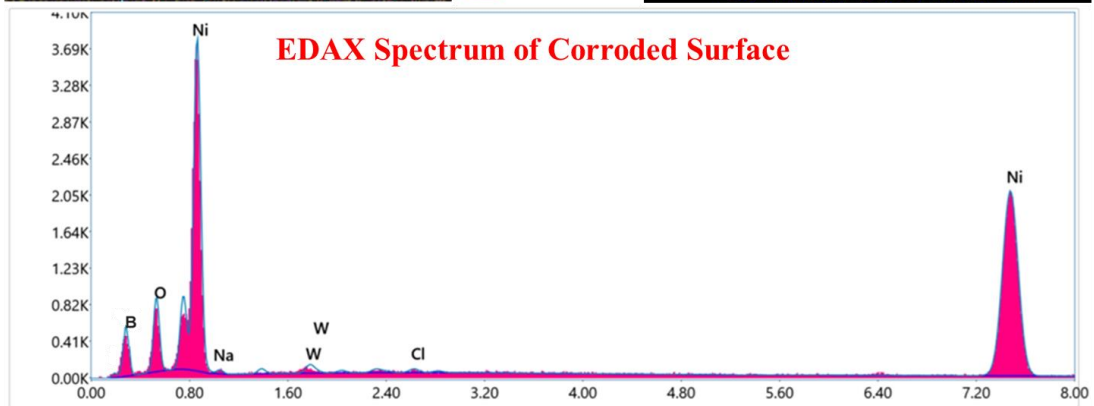
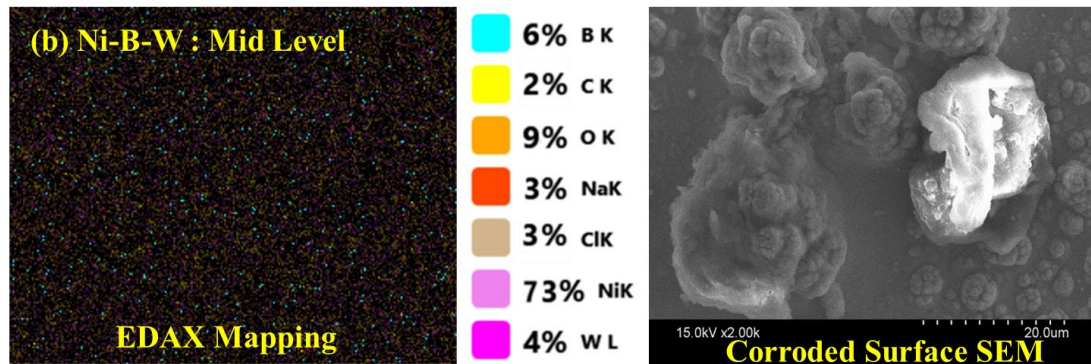
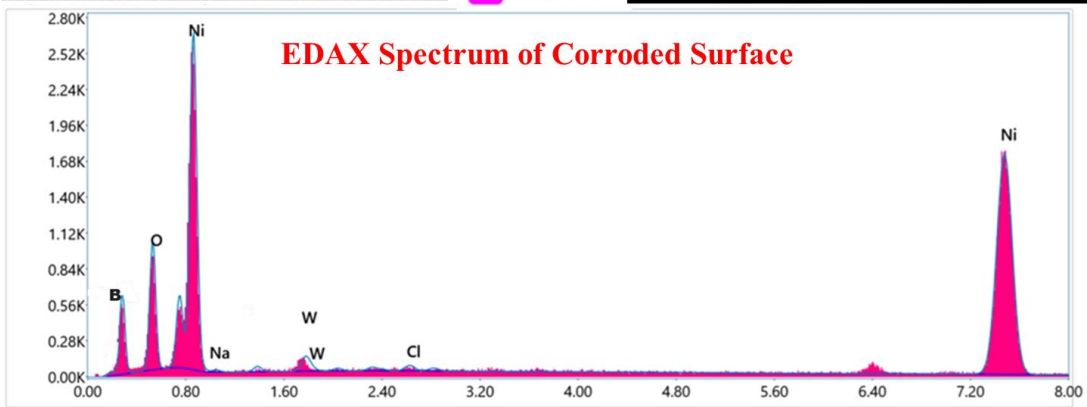
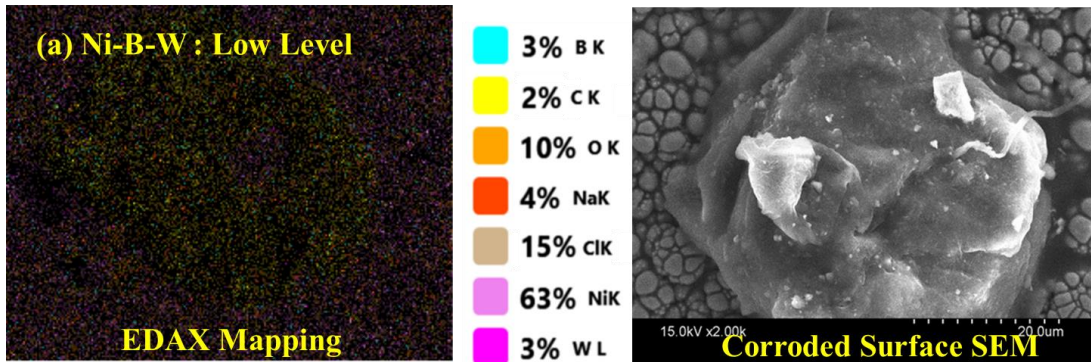


Figure 4.17: SEM Image of Corroded Surface of As-deposited Ni-B-W Coatings Obtained at (a) Low Level, (b) Mid-Level and (c) High Level Concentrations

The substrate underwent corrosion test are further analysed through SEM. The SEM images of the corroded substrates obtained at various concentrations are displayed in **Figure 4.17**. The corroded surfaces at low and high levels are observed to possess corrosion byproducts deposited over the substrate surface. The accumulation of the corrosion byproducts over the substrate confirms the corrosion attack of the corrosive electrolytes. The SEM images of Ni-B-W coated surfaces displayed in **Figure 4.17** and obtained at low level concentration are found to be mostly affected by the corrosion attack. The coated surface obtained at mid-level concentration is seen to be least effected by corrosive medium. This result agrees well with the EIS and PDP test results. The corrosion attacks are possibly remained till the outer layers only and only some localised corrosion attacks occurred by the electrolytes which might have penetrated through grain

boundaries [Serin et al. 2015; Mukhopadhyay et al. 2018c].



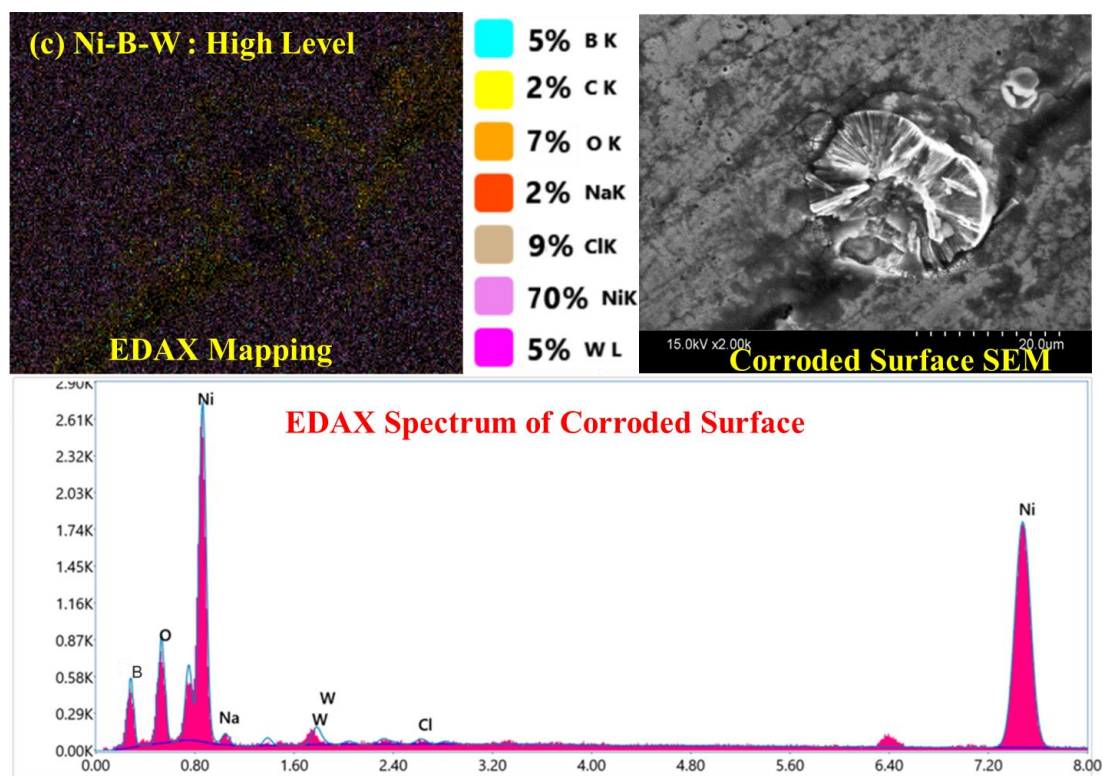


Figure 4.18: EDAX Results of Corroded Surfaces of As-deposited Ni-B-W Coatings Obtained at (a) Low Level, (b) Mid-Level and (c) High Level Concentrations

The corroded surfaces are further studied under EDAX for the chemical composition of the byproducts deposited over the corroded surface. The EDAX results obtained for the Ni-B-W coatings deposited at different concentrations are displayed in **Figure 4.18**. The EDAX mapping results show the elements present in the corroded surface. The EDAX spectrums also show the peaks corresponding to Ni, B, W, C, O, Na and Cl, i.e. the main coating bath elements and the corrosive medium elements may also be observed. The presence of these peaks confirms their presence. The presence of Na and Cl may be due to the NaCl solution used as electrolyte during the test. The presence of C and O are the indication of the corrosive medium to reach till substrate surface. But the negligible amount of C and O may come from some external source as well. The nyquist plot displayed in **Figure 4.16(b)** shows a single semi-circular loop which indicates that the corrosive medium failed to penetrate through the coatings. Generally, the grain boundaries of coated surface are the corrosion attack zone. Those helps the corrosive solution to penetrate through it. The corrosion byproducts are observed on the

corroded surface displayed in **Figure 4.17** which may be correlated with the presence of Na and Cl peaks in the EDAX spectrum. The presence of Cl ion in the corroded surface confirms the corrosive action. It also confirms the corrosive action but for not all samples. The presence of Na and Cl ion is not significant in all cases as seen in the EDAX results. The single loop in nyquist plot, insignificant amount of C and O, corroded surface SEM indicates that the electrolytes penetrated only till the top layer of the coatings.

4.7 Closure

The electroless ternary coatings (Ni-B-W) are deposited with different bath parameter concentrations to study the importance of the bath parameter concentrations on tribo-mechanical behaviours of coatings. The investigation results are as follows:

- As-deposited coatings are found to possess compact and uniform surface morphology with closely packed nodular surface within the working range. The coating thickness is observed to increase with bath level concentration from 14.61 to 31.32 μm .
- The boron content is found to increase from 3.9 to 5.3 wt.% while tungsten content increases from 2.8 to 4.2 wt.% which leads to an increase in surface hardness measured with nano-indentation technique and scratch hardness measured from micro-scratch test.
- The surface roughness of the Ni-B-W coated surface is observed to become 0.185 μm at low concentration of NiBH_4 which is smoother than the substrate having surface roughness of 0.285 μm . The same surface becomes rougher with the increase in NiBH_4 concentration. The addition of sodium tungstate makes the rougher than substrate but it does not vary much with the its variation.
- COF of the Ni-B-W coated layer slightly decreases from 0.628 to 0.520 with NiCl_2 concentration in the solution which agrees well with the surface roughness trend. The increasing trend of surface roughness with NaBH_4 leads to an increase in COF value from 0.423 to 0.680 within the working range. The COF value also increases slightly from 0.558 to 0.754 with Na_2WO_4 concentration.

Chapter 5: Electroless Ni-B-Mo Alloy Coatings

Outline: 5.1 Introduction, 5.2 Experimental Details, 5.3 Coating Characterisation, 5.3.1 Coating Thickness, 5.3.2 Surface Morphology, 5.3.3 Chemical Composition, 5.3.4 Phase Structure, 5.4 Physical and Mechanical Behaviours, 5.4.1 Surface Roughness, 5.4.2 Nano-indentation Test, 5.4.3 Micro-Scratch Test, 5.5 Tribological Test, 5.6 Corrosion Resistance Test, 5.7 Closure

5.1 Introduction

Chemical deposition or electroless coating method is well known to improve the surface behaviour of base metal which helps to achieve required properties in materials to use in different applications. Electroless nickel-boron (ENB) coating possesses good tribological behaviour. Borohydride reduced binary alloy coatings are also used to enhance the hardness of steel specimen. The characteristics of coatings vary with their chemical composition, surface morphology, and phase structure. These features may be altered as per the requirement by controlling the deposition process, chemical composition, and coating bath operating conditions. Addition of any other metal with binary coatings may further alter the coating characteristics. The variation in concentration of bath elements may also alter the surface morphology, phase structure and chemical composition of coatings which ultimately may impact the coating behaviours. The variation in coatings characteristics due to addition of molybdenum with Ni-B and variation in coating bath composition is elaborated in this chapter.

5.2 Experimental Details

The electroless Ni-B-Mo coatings were developed using chemical reaction over AISI 1040 steel substrates as explained in Chapter 2. The same procedure was used for the current ternary alloy (Ni-B-Mo) coating deposition as well. Only sodium molybdate was incorporated with the Ni-B alloy coating composition as source of molybdenum. The sodium molybdate concentration is varied within the range of 15 g/l to 35 g/l. The coatings are deposited through chemical deposition method. The steel substrates used is

having a catalytically active surface. Still, those are dipped into lukewarm PdCl_2 just before dipping them into coating bath solution to accelerate the deposition process further. All major key elements of the coating bath are varied at 5 different levels. Low Level Concentration (LLC) of coating bath contains 10 g/l of NiCl_2 , 0.4 g/l of BaBH_4 , 15 g/l of Na_2MoO_4 and 75 °C coating bath temperature. So, from now on the Low-Level Concentration will be called as LLC. While, Mid-Level Concentration (20 g/l of NiCl_2 , 0.8 g/l of BaBH_4 , 25 g/l of Na_2MoO_4 and 85 °C coating bath temperature) and High-Level Concentration (30 g/l of NiCl_2 , 1.2 g/l of BaBH_4 , 35 g/l of Na_2MoO_4 and 95 °C coating bath temperature) will be called as MLC and HLC, respectively.

The coating characterizations are done these three level on concentrations only. While the tribo-mechanical behaviour of the coatings is carried out with varying bath parameter individually to understand the correlation. All the test are carried out as per the test procedure elaborated in chapter 2.

5.3 Coating Characterisation

5.3.1 Coating Thickness

The cross-cut coating thickness is measured using SEM which is displayed in **Figure 5.1**. The minimum coating thickness value is 9.964 μm at LLC of coating bath concentration. The minimum coating thickness value of 27.39 μm and 41.57 μm may also be observed for MLC and HLC of coating bath, respectively. This indicates that coating thickness increases due to higher bath parameter concentration which confirms the improvement in plating rate with increased bath parameters concentration. The plating rate is known to improve due to rise in sodium borohydride concentration [Vitry et al. 2012]. This improvement may be correlated with the improvement in reduction rate with borohydride [Vitry et al. 2012]. The increase in coating bath temperature may also lead to an increase in reduction rate.

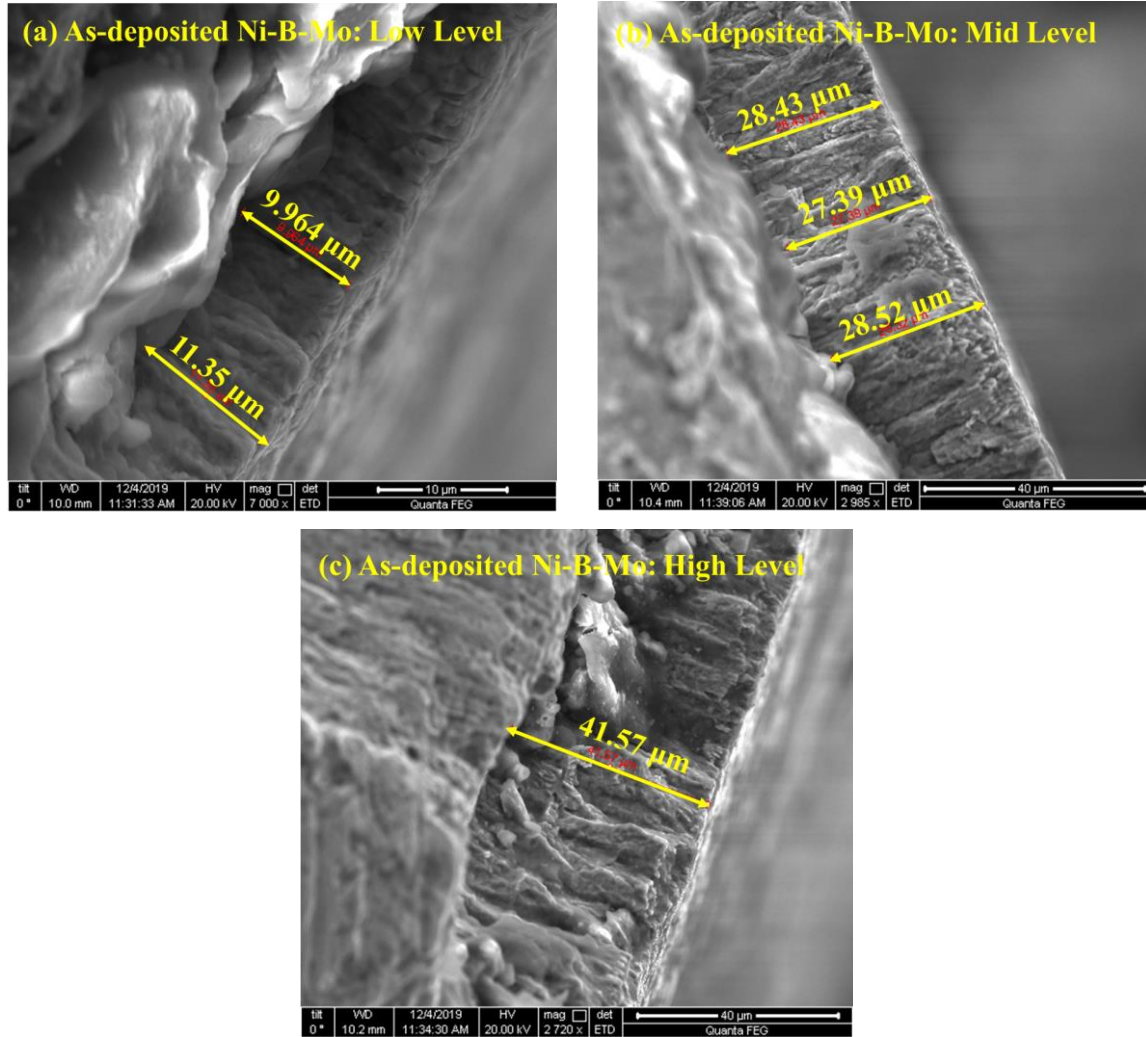


Figure 5.1: SEM Image of Coating Thickness of As-deposited Ni-B Coatings Obtained at (a) Low Level, (b) Mid-Level and (c) High Level Concentrations

5.3.2 Surface Morphology

The surface morphology of the untreated Ni-B-Mo coatings can be observed in **Figure 5.2** which shows that the coatings obtained from low, mid and high concentrations possess cauliflower like surface morphology within the working range of sodium borohydride, nickel chloride, sodium molybdate and operating temperature. This type of dense nodular surface morphology is found to be associated with cauliflower like surface morphology which usually can be found in EN coatings [Balaraju et al. 2016; Vitry and Bonin, 2017; Mukhopadhyay et al. 2018]. Columnar growth may be observed in the cross-cut SEM image displayed in **Figure 5.1** which is an obvious feature

of borohydride reduced EN coatings [Balaraju et al. 2016; Vitry and Bonin, 2017; Mukhopadhyay et al. 2018]. Figure 5.2 exhibits dense, homogeneous and cauliflower like surface morphology.

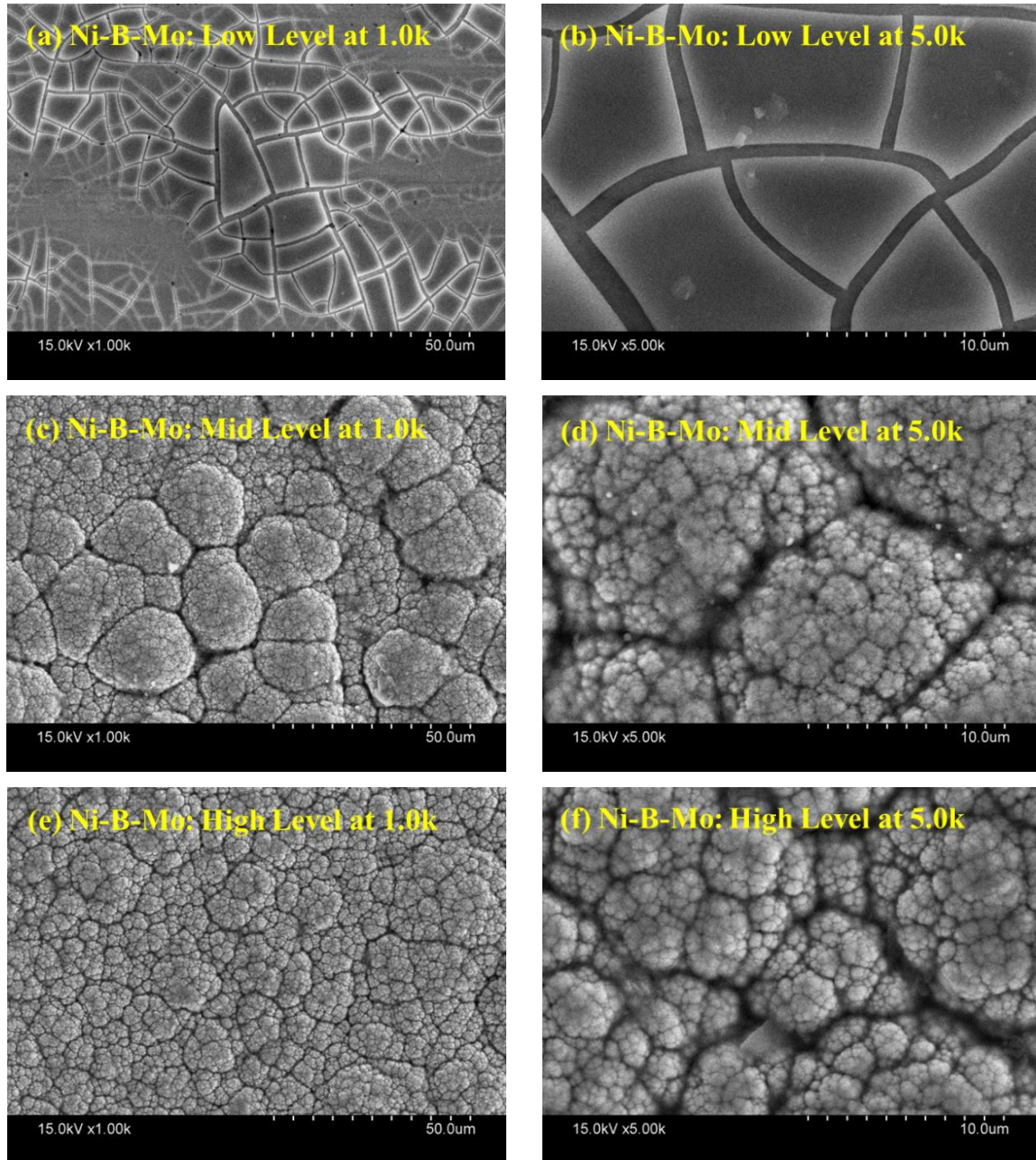


Figure 5.2: SEM Image of Surface Morphology for As-deposited Ni-B-Mo Coatings Obtained at (a)-(b) Low Level, (c)-(d) Mid-Level and (e)-(f) High Level Concentrations

The columnar growth during the initial stages of coating deposition leads to formation of cauliflower like surface morphology which ultimately helps in decrease of COF value of the as-deposited coatings with the reduction in actual contact area in between mating surfaces [Mukhopadhyay et al. 2018]. The nano-grain nucleation occurs at multiple nucleation points at isolation zones preferably at surface peaks and valleys which further progresses along the lateral direction to form smooth continuous film through columnar growth leading to cauliflower like surface morphology [Vitry et al. 2010; Nemane and Chatterjee, 2020]. The nodular surface seems to become more compact leading to cauliflower like morphology with the increase in level of concentration.

5.3.3 Chemical Composition

The elemental investigation of the untreated Ni-B-Mo coated specimens was carried out through EDAX. **Figure 5.3** displays the presence of different key elements on the coated surface obtained with different level of bath composition. The green, yellow and magenta colours displayed in **Figure 5.3** indicate the presence of nickel, boron and molybdenum, respectively. The variation in intensity of these colours as proportional to variation in concentration of the elements onto coated surface. The increase in intensity of green colour due to increase in bath composition level indicates the increase in Ni content on the coated surface. Similarly, yellow and purple colours indicate the existence of boron and molybdenum on the coated surface, respectively where it may be observed that the boron content initially increases significantly from low level to mid-level and the same increases further with negligible amount at high level of coating composition. Molybdenum content is seen to increase uniformly with level of concentration which might have dominated the rise of boron at high level of concentration.

The EDAX spectrum of Ni-B-Mo coated specimens is displayed in **Figure 5.4**. Coated surface shows the peaks of Ni, B and Mo which reassert the presence of these elements onto coated surface. The boron found on coated surface is about $3.70 \pm 0.40\%$, $5.60 \pm 0.50\%$ and $5.90 \pm 0.60\%$ at low, mid and high-level, respectively. The amount of nickel is found to be $90.30 \pm 0.60\%$, $88.50 \pm 0.80\%$ and $86.10 \pm 0.90\%$ for low, mid and high-level, respectively.

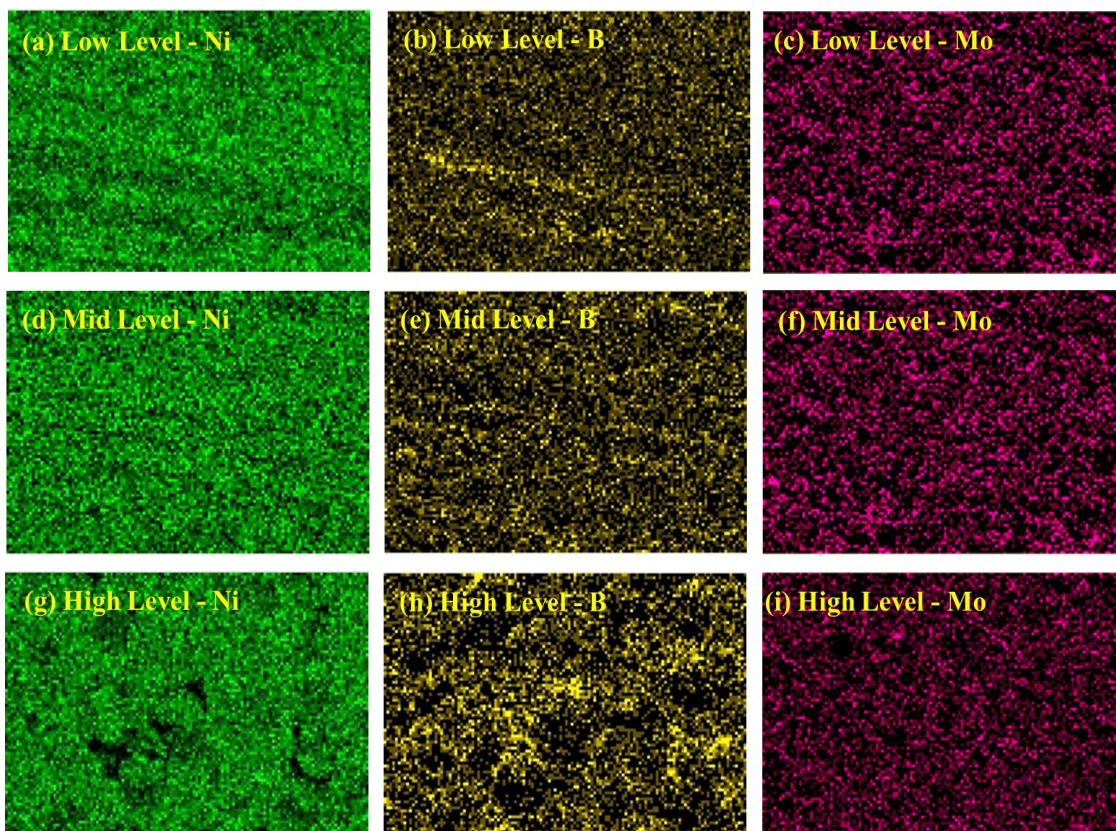


Figure 5.3: EDAX Mapping Images of As-deposited Ni-B-Mo Coatings Obtained at (a)-(c) Low Level, (d)-(f) Mid-Level and (g)-(i) High Level Concentrations

Concentrations of molybdenum in the coating are found to be $3.20 \pm 0.30\%$, $4.10 \pm 0.30\%$ and $4.70 \pm 0.40\%$ for low, mid and high level of concentrations, respectively. The increase in boron content on the coated surface may be associated with the increase in reduction reaction due to rise in borohydride concentration though the same is found to be less in Ni-B-Mo coated surface relative to Ni-B coated surface, possibly because of the co-deposition of molybdenum. **Figure 5.4** shows a rise in boron content because of the increase in bath parameter concentration. In the contrary, Ni content is observed to reduce even though NiCl_2 concentration is high. The reduction in Ni content may be attributed with the increase in boron and molybdenum content on coated surface. The presence of O and Fe can also be found at a very less amount in Ni-B-Mo coated specimens. The presence of O and Fe at negligible amount may be ignored which may have gathered from some other sources.

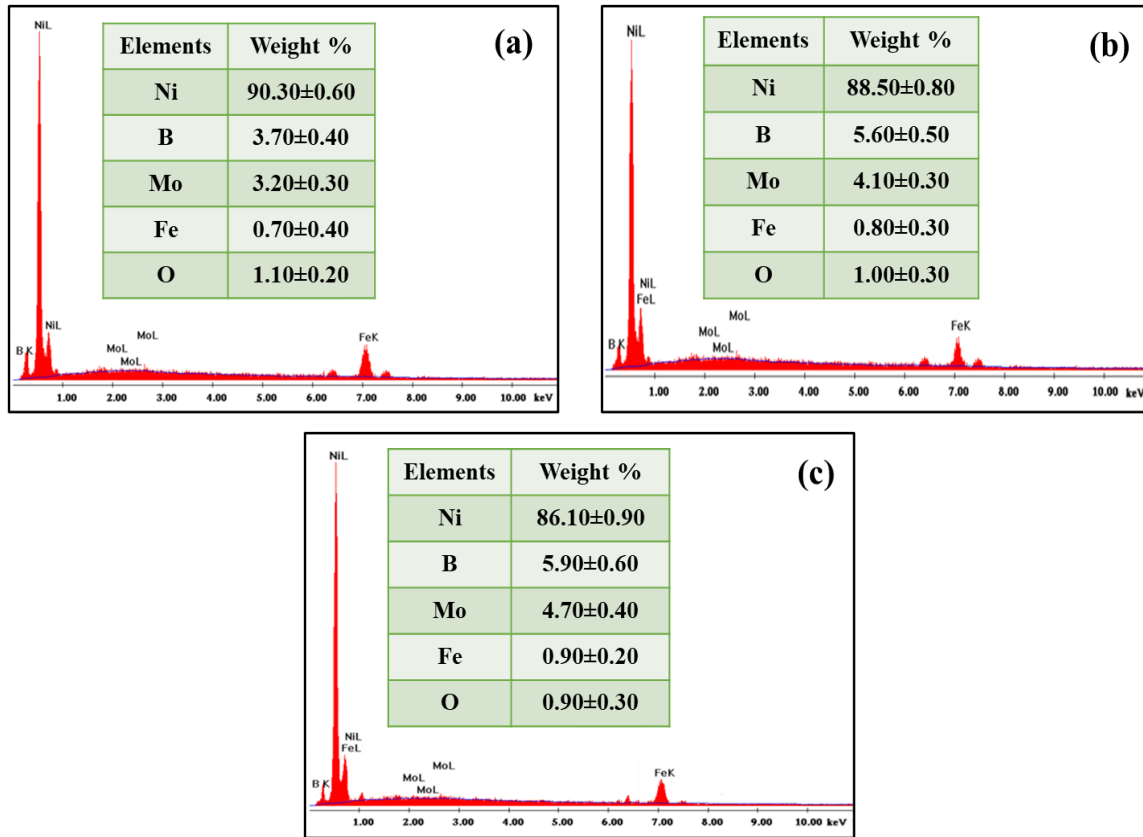


Figure 5.4: EDAX Spectrum of As-deposited Electroless Ni-B-Mo Coatings Obtained at (a) Low Level, (b) Mid-Level and (c) High Level Concentrations

5.3.4 Phase Structure

Figure 5.5 shows the XRD pattern at various level of bath parameter concentration. The XRD pattern comprises of a hump with a crystallinity peak where the hump denotes amorphous phase of coatings and the peak denotes the crystalline phase of coatings. The coexistence of hump with broad peak is the indication of their co-existence in the coatings. The coated specimens obtained with low level possesses a small hump with a peak which confirms the presence of amorphous-crystalline phase together for untreated Ni-B-Mo coatings [Serin et al. 2015; Serin and Göksenli, 2015; Mukhopadhyay et al. 2018; Mukhopadhyay et al. 2019]. The coatings with more than 6.5% boron usually prevent nucleation of nickel phases which lead to formation of amorphous phase in electroless coating process [Mukhopadhyay et al. 2018]. The Ni-B-Mo coatings at low level contains only $3.70 \pm 0.40\%$ boron and $3.20 \pm 0.30\%$

molybdenum where low boron might be the reason for crystalline phase and presence of molybdenum (Mo) has promoted the formation of amorphous phase. The peaks of boron and molybdenum in the EDAX spectrum show their existence in the coatings which may be attributed for the coexistence of amorphous and crystalline structure at low level of concentration. The crystalline peak is diminished at mid-level of concentration which confirms the transformation of amorphous-crystalline into amorphous phase. The sharp peak again is found to decrease and the broadening of hump is noticed at high level of concentration. The broadening of hump is an indication of amorphous phase which is possibly due to higher concentration of Mo while the sharpening and rise of crystalline peak is due to the reduction in boron content. The presence of Mo in the coatings prevents the nucleation of nickel ions leading to amorphous phase formation [Mukhopadhyay et al. 2018; Mukhopadhyay et al. 2019]. The sharp peak observed at around 45° for the coatings obtained from low level concentration is nothing but the crystalline peak of Ni (111) [Serin et al. 2015; Serin and Göksenli, 2015; Mukhopadhyay et al. 2018]. The sharp peaks found for the coatings at mid and high level of concentration at around 53° are due to the crystalline phase of Ni (200) [Serin et al. 2015; Serin and Göksenli, 2015; Mukhopadhyay et al. 2018]. The EDAX results presented in **Figure 5.4** show the increase in molybdenum content on the coated surface which prevents the nucleation of nickel leading to formation of amorphous phase. The decrease in intensity of crystalline peak in XRD results shown in **Figure 5.5** also indicates the same phase transformation trend. Hence, both EDAX and XRD results confirm the phase transformation from amorphous-nanocrystalline to amorphous phase formation. diminished at mid-level of concentration which confirms the transformation of amorphous-crystalline into amorphous phase. The sharp peak again is found to decrease and the broadening of hump is noticed at high level of concentration. The broadening of hump is an indication of amorphous phase which is possibly due to higher concentration of Mo while the sharpening and rise of crystalline peak is due to the reduction in boron content. The presence of Mo in the coatings prevents the nucleation of nickel ions leading to amorphous phase formation [Mukhopadhyay et al. 2018; Mukhopadhyay et al. 2019]. The sharp peak observed at around 45° for the coatings obtained from low level concentration is nothing but the crystalline peak of Ni (111) [Serin et al. 2015; Serin

and Göksenli, 2015; Mukhopadhyay et al. 2018]. The sharp peaks found for the coatings at mid and high level of concentration at around 53° are due to the crystalline phase of Ni (200) [Serin et al. 2015; Serin and Göksenli, 2015; Mukhopadhyay et al. 2018]. The EDAX results presented in Figure 5.4 show the increase in molybdenum content on the coated surface which prevents the nucleation of nickel leading to formation of amorphous phase. The decrease in intensity of crystalline peak in XRD results shown in Figure 5.5 also indicates the same phase transformation trend. Hence, both EDAX and XRD results confirm the phase transformation from amorphous-nanocrystalline to amorphous phase formation.

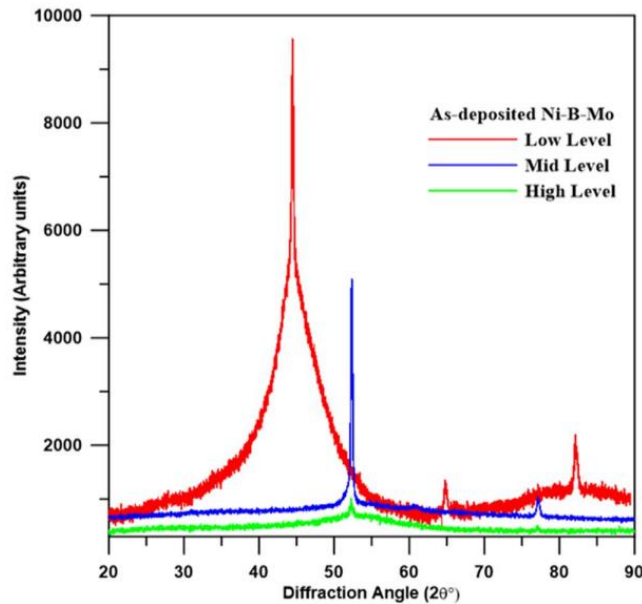


Figure 5.5: XRD Patterns of As-deposited Ni-B-Mo Coatings

5.4 Physical and Mechanical Behaviours

5.4.1 Surface Roughness

The Ni-B-Mo coatings were deposited over steel substrate having average R_a value of $0.28\ \mu\text{m}$. The coatings obtained with low, medium and high bath concentrations possess a surface roughness value of $0.30\ \mu\text{m}$, $0.57\ \mu\text{m}$ and $1.05\ \mu\text{m}$, respectively. The results indicate a rise in R_a value because of the rise in bath level. The variation of R_a value against the variation of coating bath temperature, NiCl_2 , NaBH_4 and Na_2MoO_4

concentration is presented in **Figure 5.6**. The change in Ra value with temperature as well as NiCl_2 concentration, is presented in **Figure 5.6(a)**. It increases with the NiCl_2 concentration slightly till 25 g/l but the same decreases suddenly at 30 g/l NiCl_2 concentration. The roughness is further observed to increase slightly with the rise in coating bath temperature initially and it decreases slightly upon further rise in temperature. The coating bath reduction reaction starts at around 70 °C and hence the deposition of various elements remains low leading to comparatively lower surface roughness but it is more than the substrate. The roughness is observed to rise further due to rise in temperature till 90 °C [**Hamid et al. 2010**]. The higher reduction rate causes the random deposition of elements leading to rise in surface roughness [**Bülbül et al. 2013; Wan et al. 2016; Bonin et al. 2018; Madah et al. 2015**]. From **Figure 5.6(b)**, an increase in the surface roughness value with the increase in NaBH_4 concentration till 1.2 g/l may be observed. The presence of NaBH_4 helps in reduction reaction and the rise in its concentration accelerates the reduction reaction leading to haphazard deposition of metal ions on the surface leading to higher surface roughness. It is also seen to increase slightly upon increase in coating bath temperature but with insignificant amount [**Sürdem et al. 2019; Vitry et al. 2012**]. **Figure 5.6(c)** shows the surface roughness plot against bath temperature and sodium molybdate concentration. The roughness value is observed to rise with increased sodium molybdate concentration in the solution which increases further with bath temperature, but this increase is not very much. The reduction reaction accelerates as temperature rises which leads to higher boron content and rougher surface. Moreover, the addition of molybdenum ion aids in the creation of cracks due to high stress growth leading to coarse surface morphology [**Mukhopadhyay et al. 2018; Mukhopadhyay et al. 2019**]. This coarse surface morphology can be attributed for the high Ra value of coatings in as-deposited conditions. The addition of molybdenum into Ni-B matrix leads to coarse grained surface morphology with crack formation leading to higher surface roughness. The SEM images displayed in **Figure 5.2** also show some coarse grain surface morphology with visible cracks. Hence, the surface morphology results are in well agreement with the surface roughness results.

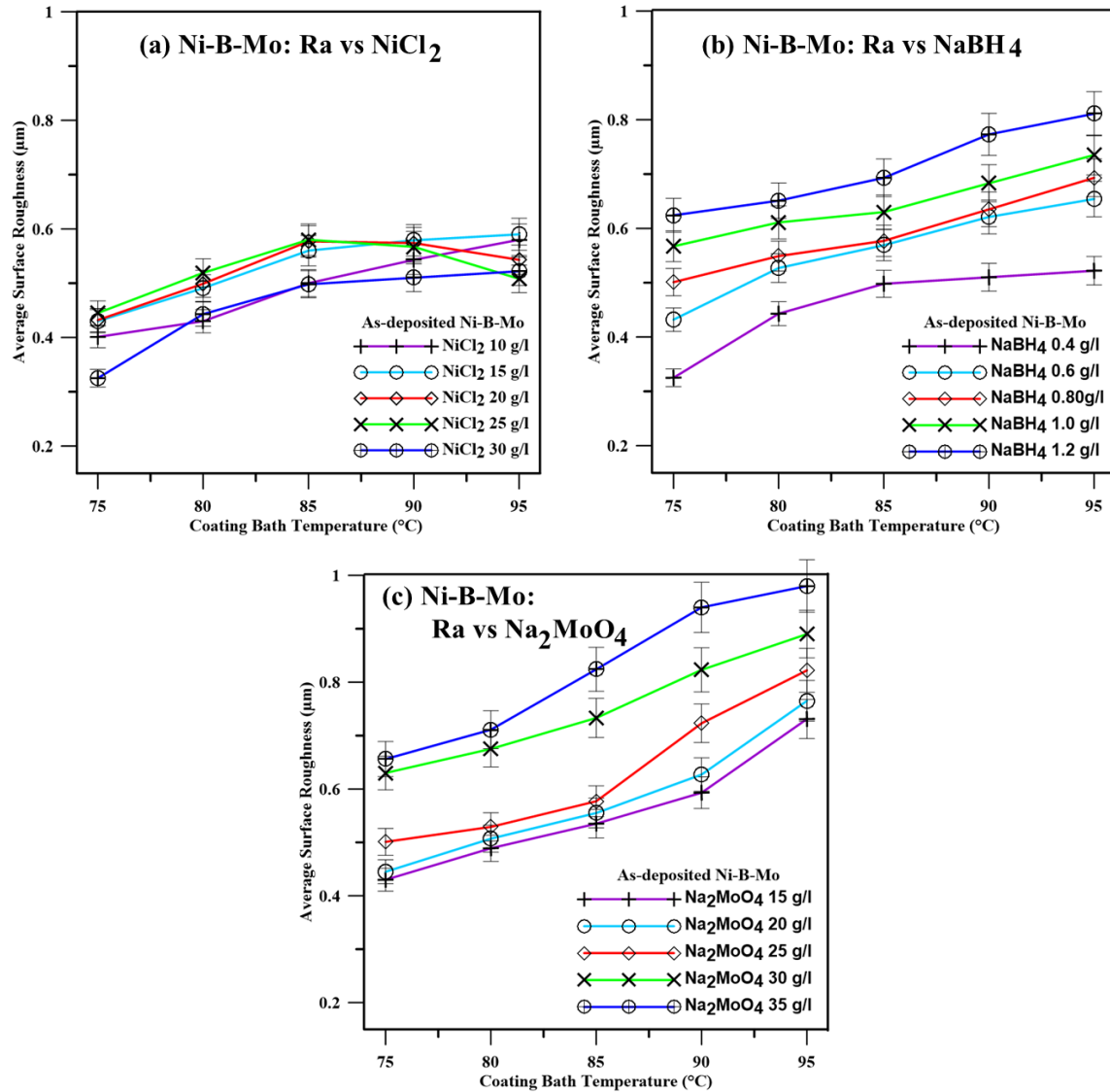


Figure 5.6: Average Surface Roughness Plot with Varying Temperature and (a) Sodium Borohydride, (b) Nickel Chloride and (c) Sodium Molybdate Concentrations

5.4.2 Nano-Indentation Test

The surface hardness of the Ni-B-Mo coated layers were observed through nano-indentation technique. The variation of applied load against indentation depth for different coating bath concentration level is presented in **Figure 5.7**. It represents that the coatings deposited with low coating bath level require minimum applied load. On the other hand, the coated layer with high level of concentration needs the highest applied

load, which confirms the improvement in coated surface hardness due to rise in level of concentration. The amount of boron present on coated surface is seen to increase with NaBH_4 concentration leading to improvement in surface hardness [Sürdem et al. 2019; Lekka et al. 2018].

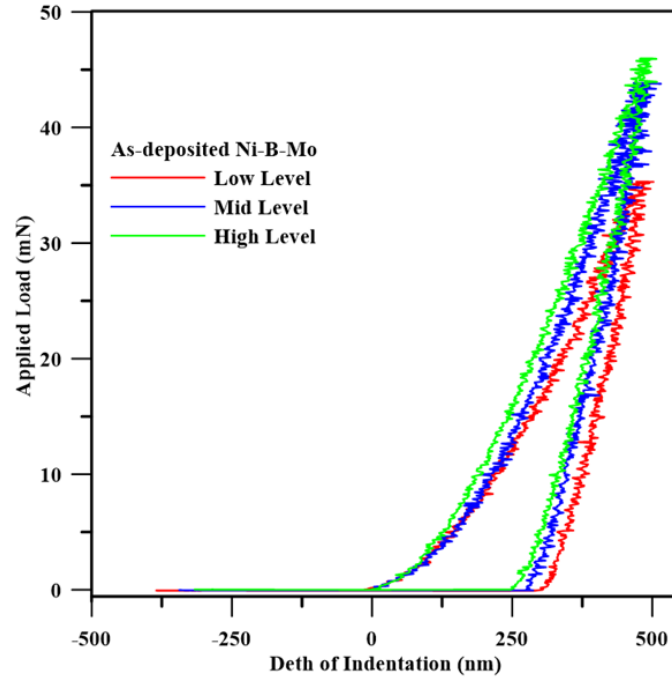


Figure 5.7: Depth of Indentation vs Applied Load Plot

The Ni ions into the coated surface also might have increased because of the rise in NiCl_2 concentration which might have improved the surface hardness further. The ENB coated specimens are observed to possess higher surface hardness than steel substrate [Sürdem et al. 2019]. The variation of surface hardness against bath temperature, NiCl_2 , NaBH_4 and Na_2MoO_4 concentrations are presented through **Figure 5.8**. The variation of surface hardness against NiCl_2 concentration and coating bath temperature is presented in **Figure 5.8(a)**. It is observed from **Figure 5.8(a)** that the surface hardness value increases gradually with NiCl_2 and bath temperature. The surface hardness (H_v) values are found to increase from 533 to 729 with the increase in NiCl_2 concentration within the working range. The rise in NiCl_2 content might have increased the nickel content in the coated layer. The coated layer might have become more compact

and smoother due to higher nickel content leading to improved surface hardness. The variation of nano-hardness with sodium borohydride concentration and bath temperature is presented in **Figure 5.8(b)**. The boron content in the ENB coatings is found to increase with NaBH_4 concentration [Sürdem et al. 2019; Lekka et al. 2018]. The surface hardness of ENB coated specimens is known to improve due to rise in boron content. The improvement in nano-hardness (H_v) value may be observed from 504 to 971 with the increase in sodium borohydride concentration in the coating bath solution from 0.4 g/l to 1.2 g/l. This increasing trend of surface hardness may be observed possibly due to the increase of boron content with sodium borohydride [Sürdem et al. 2019; Mukhopadhyay et al. 2018; Lekka et al. 2018; Bonin and Vitry, 2016]. The same is further observed to improve a little with bath temperature. The coating bath chemical reaction usually starts around 70°C and it accelerates further with temperature rise. Therefore, the boron content might have improved with the increase in reduction rate due to rise in coating bath temperature leading to improvement in hardness of Ni-B-Mo coated surface [Lekka et al. 2018; Bonin and Vitry, 2016]. The variation of surface hardness with sodium molybdate concentration is displayed in **Figure 5.8(c)**. It shows a reduction in surface hardness due to sodium molybdate concentration rise. The nano-hardness (H_v) value is observed to vary from 869 to 556. The surface hardness is seen to be a function of coating composition and grain size [Lekka et al. 2018; Bonin and Vitry, 2016]. The boron content in ENB coated specimens is found to improve with NaBH_4 concentration rise formation but the presence of Mo promotes the amorphous phase formation [Wan et al. 2016]. The surface hardness of amorphous phase is observed to be better relative to crystalline phase which can be attributed for the improvement in hardness of Ni-B-Mo coated surface with sodium borohydride because of the increase in boron content onto coated surface [Mukhopadhyay et al. 2018; Mukhopadhyay et al. 2019]. The untreated Ni-B-Mo coated surface is found to agglomerate Ni leading to clusters formation [Mukhopadhyay et al. 2018; Mukhopadhyay et al. 2019] which agrees well with the current study. There is not much difference in boron content on Ni-B-Mo coated surface compared to Ni-B coatings. But a decrease in Ni concentration in the Ni-B-Mo coated surface may be observed with the addition of molybdenum into Ni-B matrix. The untreated Ni-B-Mo coated surface is seen

to exhibit coarse grained and cracked surface morphology leading to lower surface hardness value.

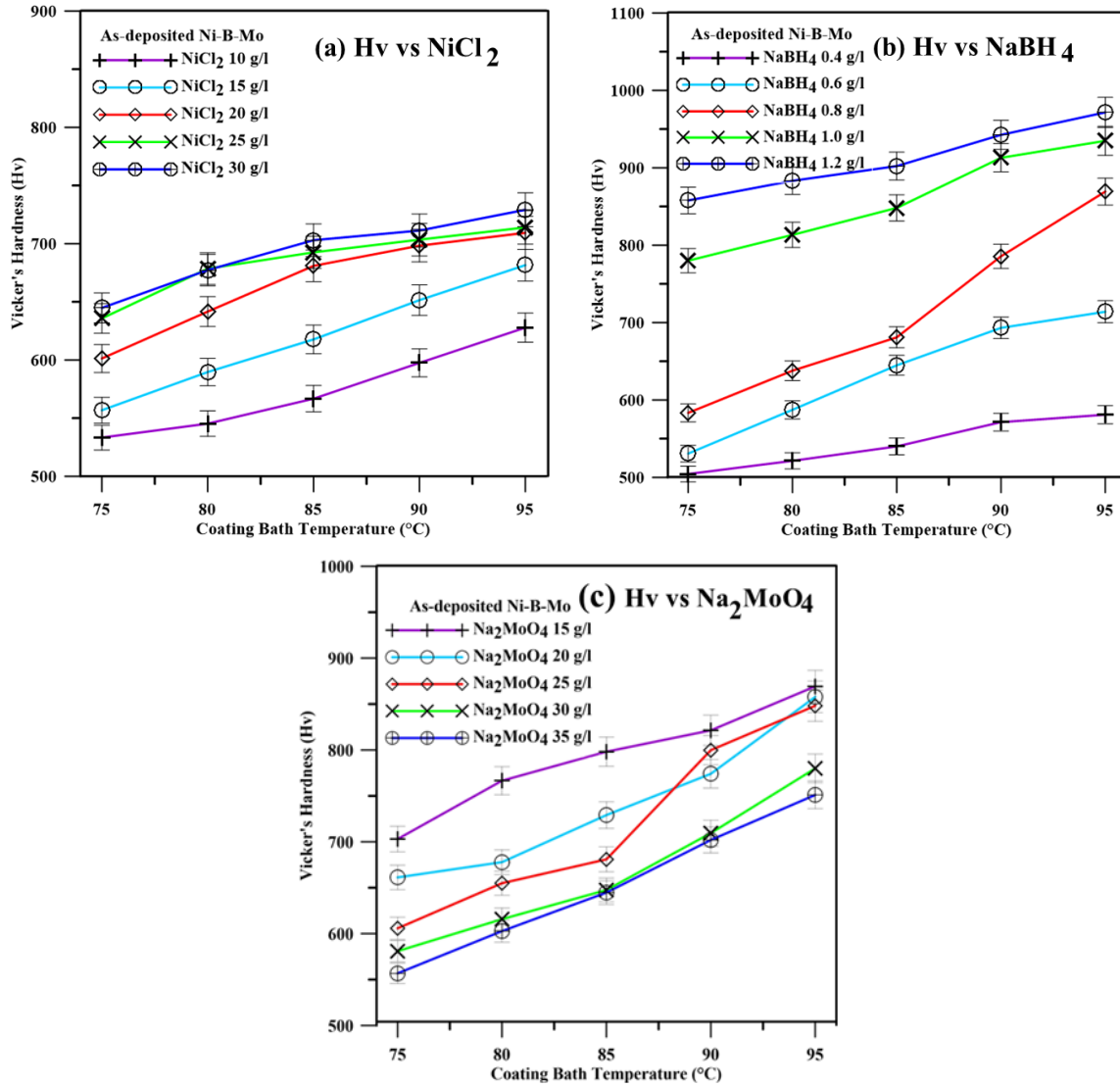


Figure 5.8: Hardness Plot with Varying Temperature and (a) Sodium Borohydride, (b) Nickel Chloride and (c) Sodium Molybdate Concentrations

The increase in Mo content in the coated surface encourages the formation of amorphous phase which is supposed to increase the surface hardness but Mo content rise accelerates the coarse grained and cracked surface morphology ultimately leading to deterioration of nano-hardness of Ni-B-Mo coating with sodium molybdate concentration [Sürdem et al. 2019; Bonin and Vitry, 2016]. But the same for Ni-B-Mo coatings does

not improve with molybdenum concentration rise. The incorporation of molybdenum into Ni-B matrix makes surface rough leading to decrease in surface hardness of Ni-B-Mo coated surface. The untreated Ni-B-Mo coated specimens possess an amorphous-nano-crystalline phase structure at lower concentration of bath parameters. The lower concentration of borohydride and presence of sodium molybdate lead to a decrease in concentration of boron which promotes the crystalline phase formation but the presence of Mo promotes the amorphous phase formation [Wan et al. 2016]. The surface hardness of amorphous phase is observed to be better relative to crystalline phase which can be attributed for the improvement in hardness of Ni-B-Mo coated surface with sodium borohydride because of the increase in boron content onto coated surface [Mukhopadhyay et al. 2018; Mukhopadhyay et al. 2019]. The untreated Ni-B-Mo coated surface is found to agglomerate Ni leading to clusters formation [Mukhopadhyay et al. 2018; Mukhopadhyay et al. 2019] which agrees well with the current study. There is not much difference in boron content on Ni-B-Mo coated surface compared to Ni-B coatings. But a decrease in Ni concentration in the Ni-B-Mo coated surface may be observed with the addition of molybdenum into Ni-B matrix. The untreated Ni-B-Mo coated surface is seen to exhibit coarse grained and cracked surface morphology leading to lower surface hardness value. The increase in Mo content in the coated surface encourages the formation of amorphous phase which is supposed to increase the surface hardness but Mo content rise accelerates the coarse grained and cracked surface morphology ultimately leading to deterioration of nano-hardness of Ni-B-Mo coating with sodium molybdate concentration.

The elastic modulus of the as-deposited coatings was determined and represented in **Figure 5.9**. **Figure 5.9(a)** shows the variation of elastic modulus with temperature and nickel chloride concentration. **Figure 5.9(b)** represents the variation of elastic modulus with temperature and sodium borohydride. The variation of elastic modulus with bath temperature and sodium molybdate concentration is presented in **Figure 5.9(c)**. The obtained elastic modulus of the coated layers is observed to vary from 83 GPa to 197 GPa. But this variation in elastic modulus value of electroless coatings does not follow the surface hardness variation trend [Sürdem et al. 2019]. The elastic modulus was observed to be a function of grain size. The grain size of ENB coatings is observed to

increase with sodium borohydride concentration in the coating bath solution leading to increase in elastic modulus value.

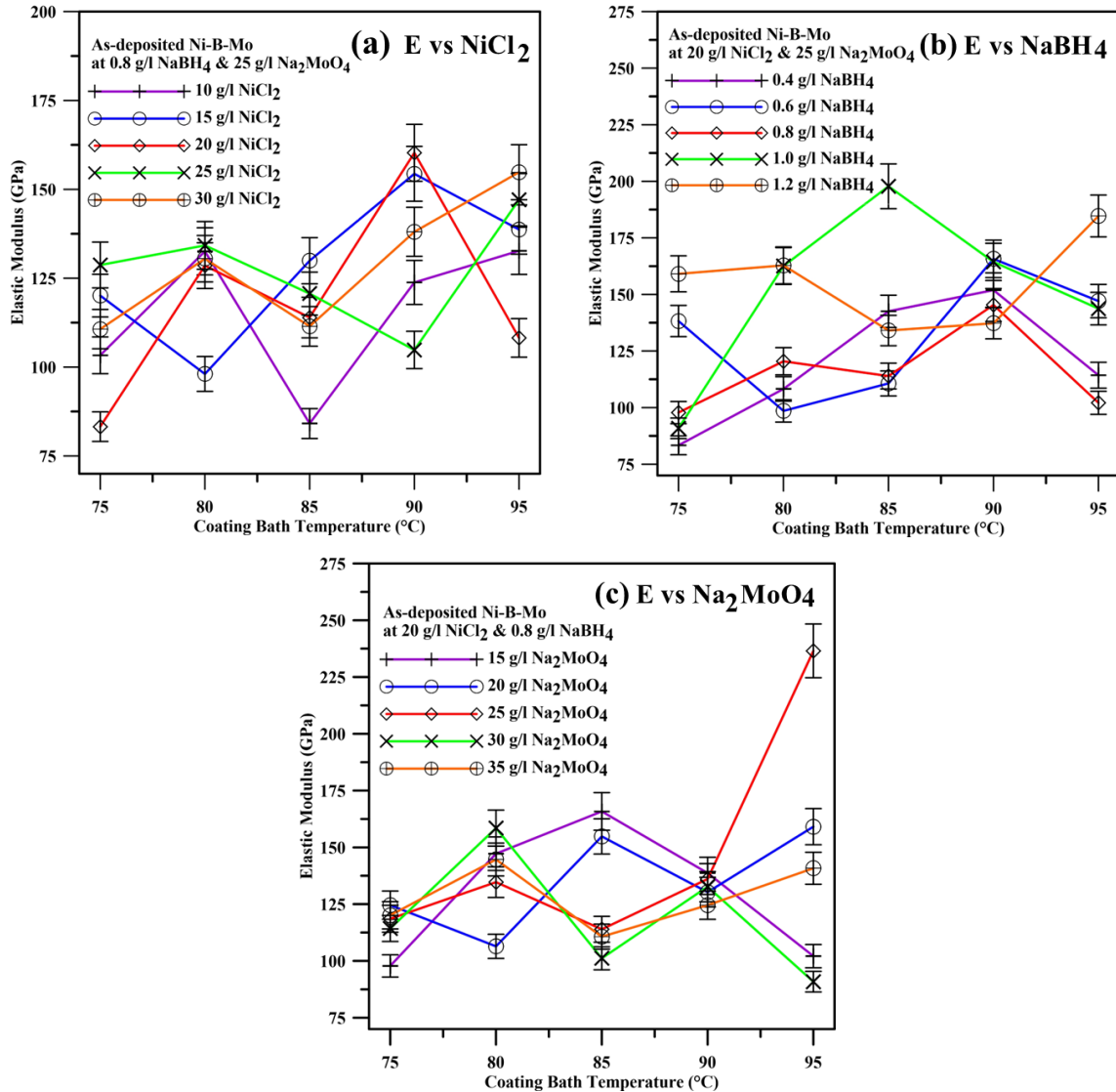


Figure 5.9: Elastic Modulus Plot with Varying Temperature and (a) Sodium Borohydride, (b) Nickel Chloride and (c) Sodium Molybdate Concentrations

The presence of boron ions in the coating bath solution prevents Ni nucleation and promotes amorphous phase formation [Nemane and Chatterjee, 2020]. The increase of NiCl₂ in the coating bath solution increases the Ni ions which creates multiple nucleation points at isolated zones. Those isolated zones are preferably at roughness peaks or valleys of the substrate. This leads the coating growth in the lateral directions to

form a smooth film with columnar structure [Nemane and Chatterjee, 2020; Nemane et al. 2022]. The compact surface of crystalline coatings may lead to higher surface hardness but the elastic modulus does not vary with it. Therefore, the elastic modulus variation trend displayed in **Figure 5.9** does not follow any specific trend. The coatings with lower elastic modulus are found to possess better wear resistance relative to higher elastic modulus [Sürdem et al. 2019]. But any specific trend with bath concentration variation and bath temperature cannot be observed in this current study.

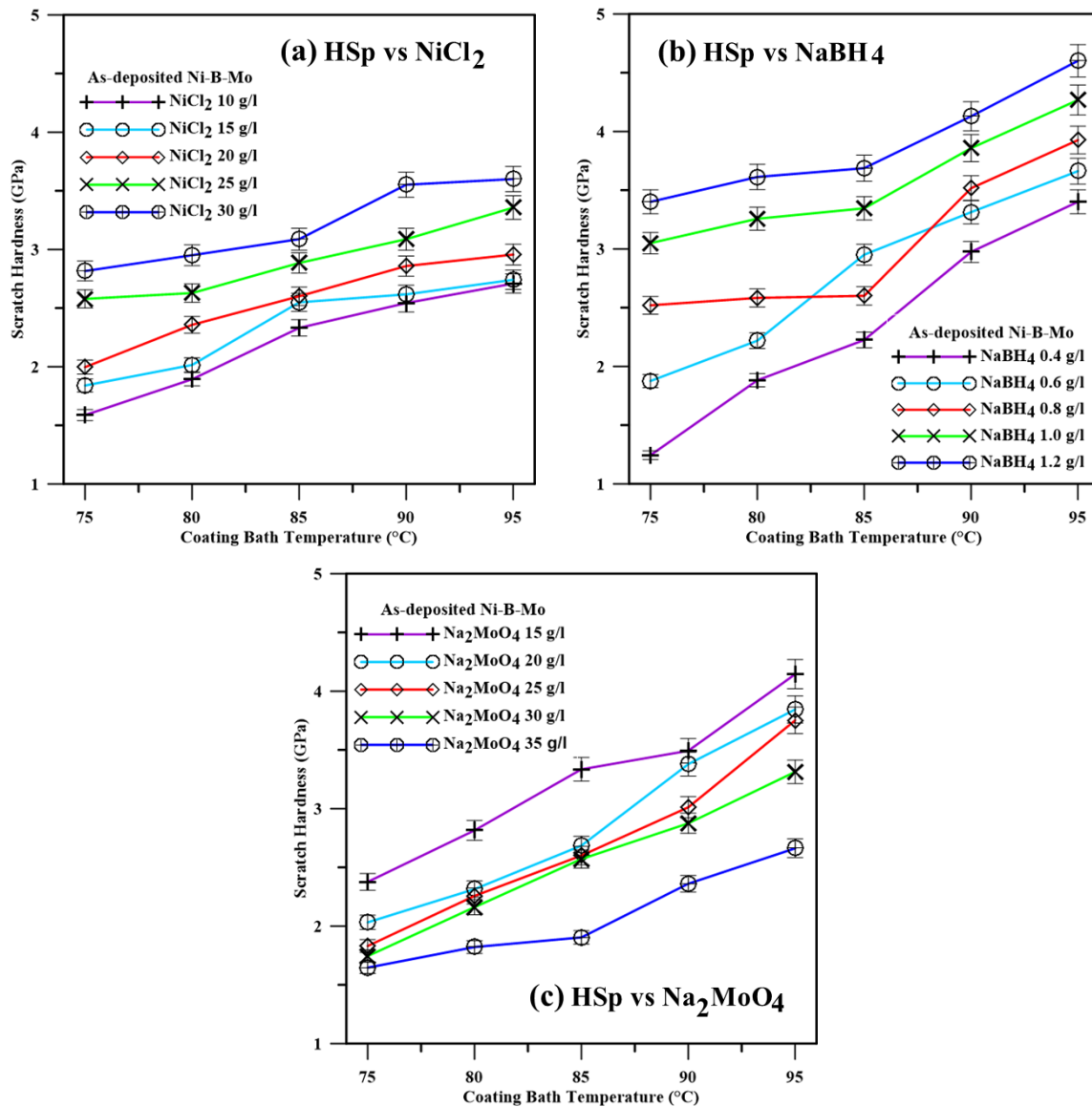


Figure 5.10: Scratch-Hardness Plot with Varying Temperature and (a) Sodium Borohydride, (b) Nickel Chloride and (c) Sodium Molybdate Concentrations

5.4.3 Micro-Scratch Test

The variation of scratch hardness of the coatings is presented in **Figure 5.10**. **Figures 5.10(a)** and **5.10(b)** represent an improvement in scratch hardness with NiCl_2 , NaBH_4 and bath temperature. The increase of scratch hardness is relatively lower for nickel chloride than the sodium borohydride. The amount of boron content on coated surface becomes higher with NaBH_4 concentration which might have led to an improvement in scratch hardness as well [Sürdem et al. 2019] possibly due to higher boron content. The enhanced reduction rate with bath temperature also may improve the boron content onto coated surface ultimately leading to an improvement in scratch hardness further. The incorporation of Mo into Ni-B matrix does not reduce the boron content onto coated surface but addition of molybdenum creates coarse grained with cracked surface morphology leading to decrease the scratch hardness with Na_2MoO_4 concentration.

5.5 Tribological Test

The surface roughness of the as-deposited Ni-B-Mo coated specimen varies with bath parameter concentrations. The friction coefficients of those surfaces also vary with sliding distance or time during the test. The variation of the friction coefficient (COF) against sliding duration at various level of concentration is presented in **Figure 5.11**. It may be noticed from the plot that the friction coefficient at all levels increases drastically at the beginning of the sliding and then it is settled down after some time and varies within a small range. The plot also shows that the friction coefficient plot at mid-level is above the plot obtained at low level concentration. The plots at mid-level and high-level concentration remain almost similar where in certain section the high-level plot remains above mid-level and in certain sections of the mid-level curve remains higher. These variations are possibly because of the presence of wear debris in-between the two mating surfaces. The rise in friction coefficient may be associated with the rise in surface roughness value of the coated specimens due to the higher molybdenum concentration which makes the surface coarse grained and crack formation in certain cases. The rough surface has the tendency to break the asperity peaks. The grinding of asperity peaks and the debris formed at the beginning of the sliding test comes on the wear track and

increases the COF value. After some time, the grinded wear debris entrapped in-between the mating surfaces and acts as load bearing elements leading to reduction in friction. The sliding friction transforms into rolling friction and hence the friction coefficient reduces. The SEM images of surface morphology also agree with this tribological test behaviour.

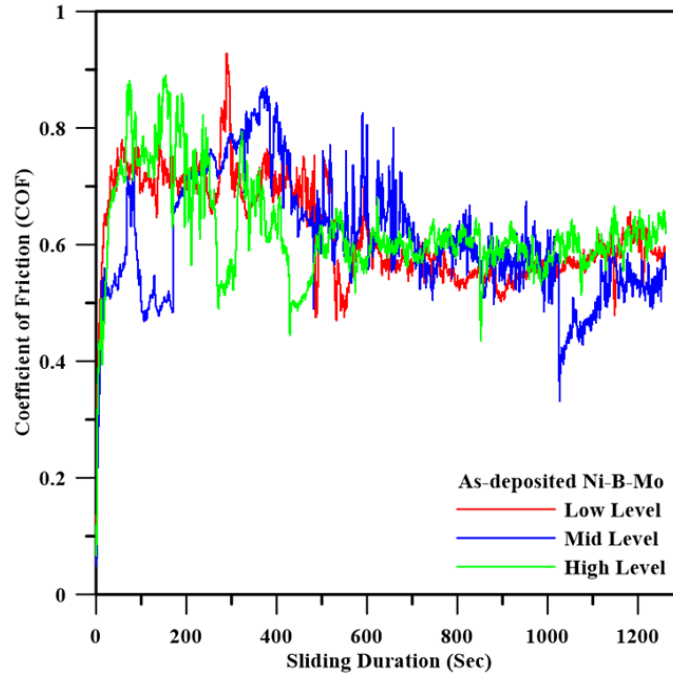


Figure 5.11: Coefficient of Friction (COF) vs Sliding Duration Plot

The average friction coefficient (COF) value is plotted against the variation of NiCl_2 , NaBH_4 , and Na_2MoO_4 concentration and presented in **Figure 5.12**. A decreasing trend of COF value with increasing concentration of nickel chloride may be observed from **Figure 5.12(a)**, while COF value increases slightly with temperature. The COF value is found to decrease from 0.73 to 0.47 due to smoothening of surface with increase in NiCl_2 concentration. The borohydride reduced electroless coatings generally form columnar structure due to the nuclei formation near the substrate [Barati and Hadavi, 2020]. These columnar structures lead to formation of cauliflower like surface morphologies which are helpful in reduction of friction coefficient due to reduction in actual contact area [Vitry et al. 2010; Nemane et al. 2022]. But the presence of molybdenum prevents the nuclei formation and leading to amorphous surface morphology. The increase in Ni ion in the coating solution is expected to accelerate the

nucleation and smoothen the surface but the presence of molybdenum prevents the nuclei formation and leads to a rough and coarse-grained surface [Mukhopadhyay et al. 2021]. Here, the presence of Mo might have suppressed the impact of NiCl_2 concentration rise and by increasing the surface roughness ultimately increases the COF value. The change in friction behaviour against sodium borohydride concentration and bath temperature is presented in **Figure 5.12(b)**.

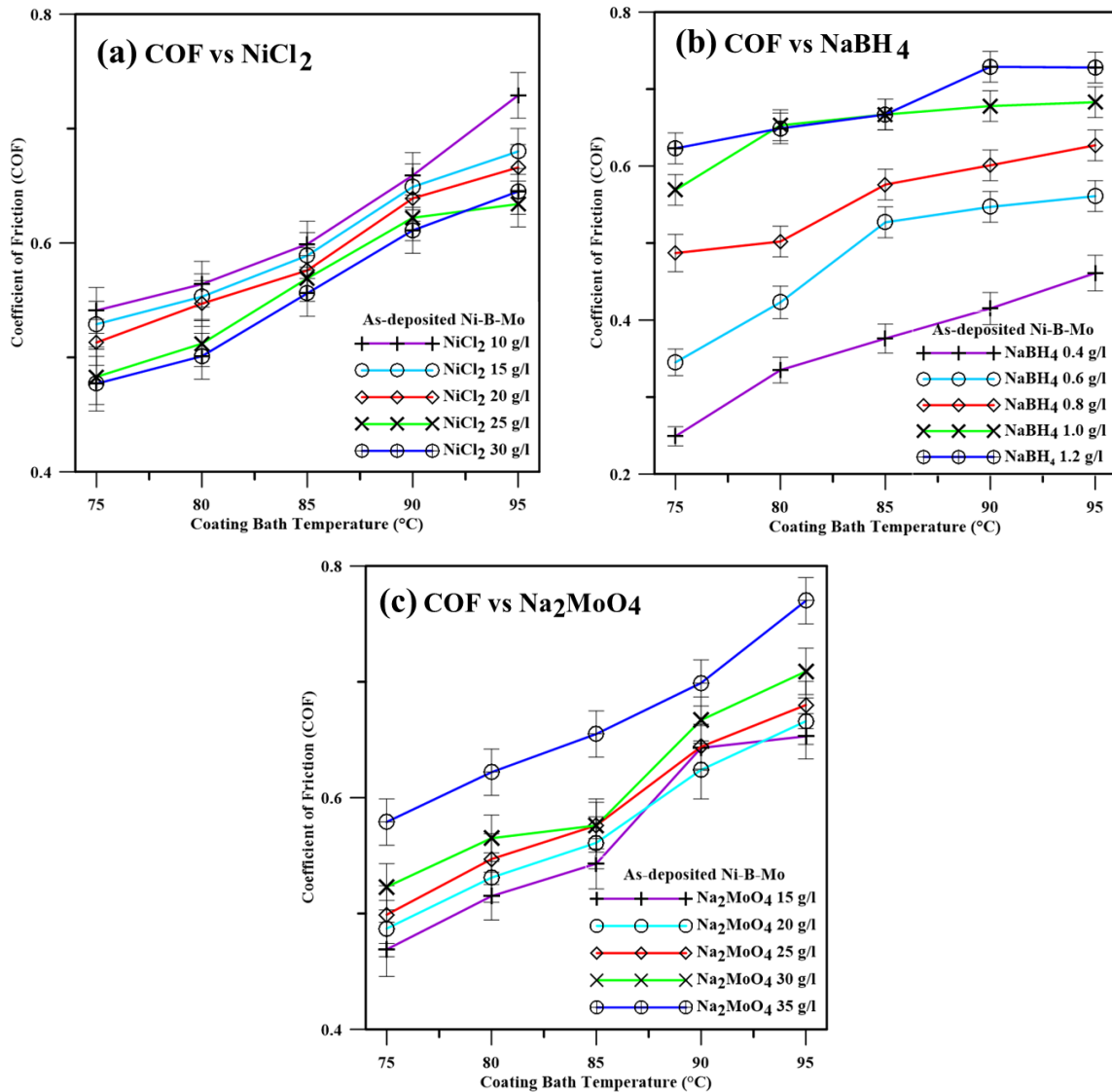


Figure 5.12: Average Coefficient of Friction (COF) Plot with Varying Temperature and (a) Sodium Borohydride, (b) Nickel Chloride and (c) Sodium Molybdate Concentrations

The deposition rate improves due to the increase in reduction rate with the rise of NaBH_4 concentration in the coating bath solution [Bülbül et al. 2013; Wan et al. 2016; Madah et al. 2015; Barati and Hadavi, 2020]. The rise of surface roughness value may increase the friction coefficient of the coatings [Bülbül et al. 2013; Wan et al. 2016; Madah et al. 2015]. The COF value is found to increase from 0.25 to 0.73 with the increase in NaBH_4 concentration. The reduction rate rises with borohydride concentrations leading to rougher surface. The presence of molybdenum in the coating bath accelerates the formation of rough and coarse-grained surface. Sometimes cracks may also be observed for Ni-B-Mo coatings [Mukhopadhyay et al. 2018; Mukhopadhyay et al. 2019; Mukhopadhyay et al. 2021]. Hence, the COF value of the coated specimens is observed to rise with NaBH_4 concentration. **Figure 5.12(c)**, represents the variation of average friction coefficient (COF) value against Na_2MoO_4 . The friction coefficient represents a rising trend with sodium molybdate and coating bath temperature. The presence of sodium molybdate concentration aids formation of rough and coarse-grained surface structure with cracks due to high stress growth [Mukhopadhyay et al. 2018; Mukhopadhyay et al. 2019]. The coarse-grained surface morphology is the reason for high surface roughness ultimately leading to higher friction coefficient of Ni-B-Mo coatings. The COF value increases from 0.47 to 0.77 with sodium molybdate concentration in the coating bath solution. The surface roughness trend completely agrees with the current trend of friction coefficient.

The variation of specific wear rate with different parameters is presented in **Figure 5.13**. The specific wear rate is seen to increase initially with NiCl_2 till mid-level but then it decreases as shown in **Figure 5.13(a)**. The wear rate usually decreases against the improvement in surface hardness [Madah et al. 2015]. The hard surface improves the wear resistance behaviour of coatings but crushing and grinding of roughness peaks may lead to a rise in wear rate of the same coatings. The surface roughness variation with the NiCl_2 concentration agrees well with the variation of wear rate which may also be attributed with the reduction in boron concentration due to the rise in NiCl_2 concentration. The surface becomes smoother with the NiCl_2 concentration rise leading to lesser asperity peaks and hence the lower mass loss is obtained. Moreover, the increase in hardness with NiCl_2 concentration as seen from **Figure 5.8(a)**, might have also promoted

the reduction in wear rate. **Figure 5.13(b)** represents a rising trend of wear rate of coatings because of the increase in sodium borohydride. The specific wear rate also increases with coating bath temperature without any specific trend. The increased boron content in the coatings due to increased NaBH_4 concentration enhances the surface hardness and roughness.

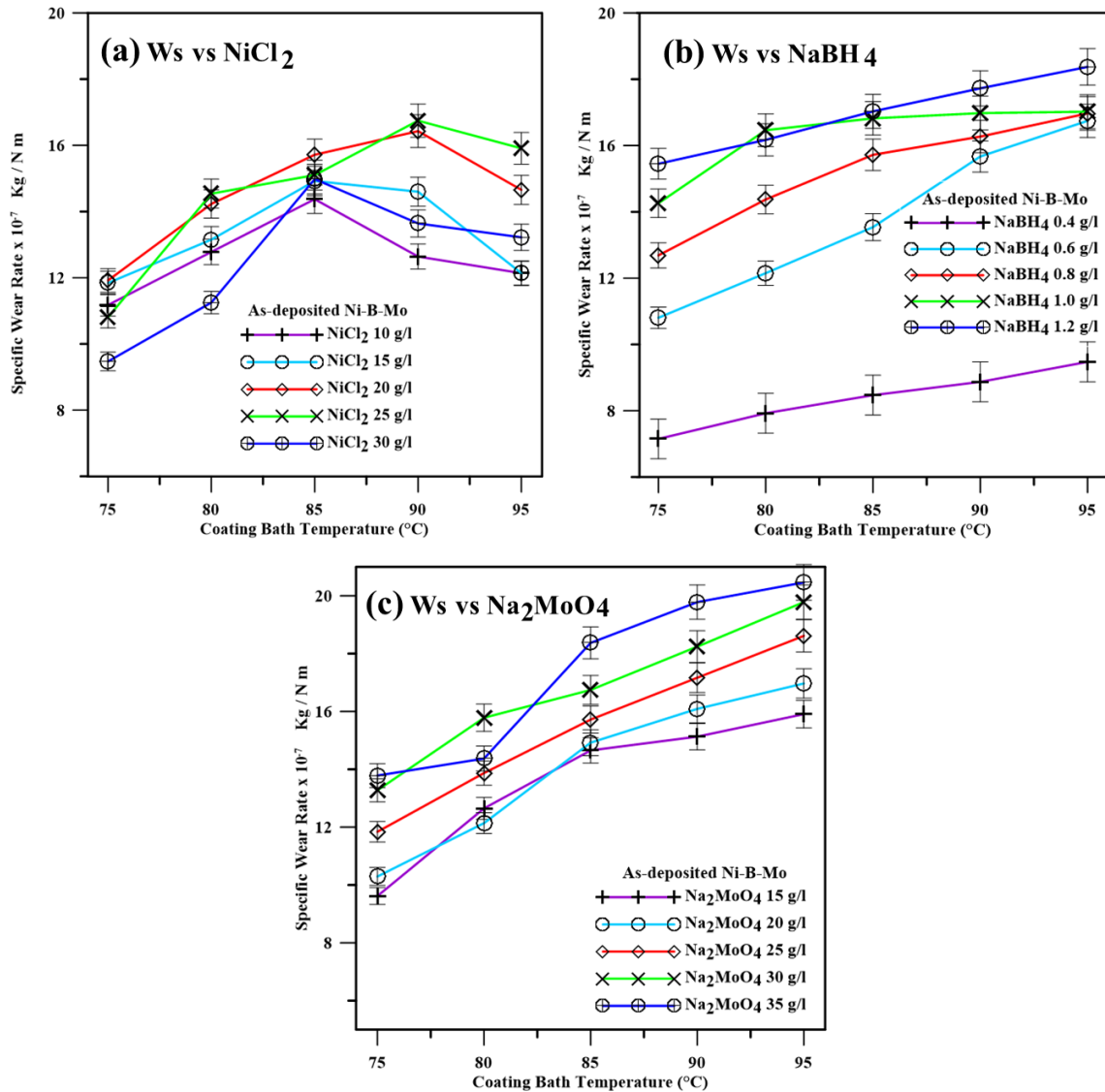


Figure 5.13: Specific Wear Rate Plot with Varying Temperature and (a) Sodium Borohydride, (b) Nickel Chloride and (c) Sodium Molybdate Concentrations

The increased concentration of sodium borohydride increases the reduction rate ultimately leading to increase in surface roughness value [Vitry and Bonin, 2017]. The

increasing trend of surface roughness with sodium borohydride concentration may be observed from **Figure 5.6(b)**. The increased surface roughness is the indication of higher roughness asperity peaks. Those roughness asperity peaks of the surfaces are crushed and grinded during the sliding leading to rise in wear rate [Vitry and Bonin, 2017]. The rise of temperature in the coating bath improves the reduction rate leading to rough surface and this results in deterioration of wear resistance [Vitry and Bonin, 2017]. The increased amount of sodium borohydride concentration leads to improvement in surface hardness. But the breaking of asperity peaks dominates the wear rate. It is also observed to increase the roughness value with increased amount of sodium molybdate concentration. The roughness value further increases due to increase in bath temperature. The reduction rate is also increased due to coating bath temperature rise leading to higher boron and hence the rougher surface is achieved. Moreover, the addition of molybdenum ion aids in the creation of cracks due to high stress growth leading to coarse surface morphology [Balaraju et al. 2014; Mukhopadhyay et al. 2017; Mukhopadhyay et al. 2018]. This coarse surface morphology can be attributed for the high average surface roughness of Ni-B-Mo coated specimens. The coarse morphology containing roughness peaks may be the possible reason for higher wear rate. The addition of sodium borohydride and sodium molybdate promotes the rough surface formation which increases the overall wear rate of the Ni-B-Mo coated specimens.

The SEM images of the worn-out surfaces are displayed in **Figure 5.14** to study the wear mechanism of as-deposited Ni-B-Mo coatings. The broken nodules smearing onto wear track can be observed at low and mid-level of concentration as well as deep crater can also be seen which is displayed in **Figure 5.14(a)-(d)**. Wear grooves formation due to wear cutting and deposition of wear debris on the worn-out surface can be observed which confirms the adhesive type wear mechanism [Mukhopadhyay et al. 2017]. The cutting and delamination of coating layer occurs due to strain hardened debris at higher loads for Ni-B-Mo coatings [Mukhopadhyay et al. 2018; Mukhopadhyay et al. 2019; Mukhopadhyay et al. 2018] which also leads to high wear rate. The wear debris may also be found in the wear grooves. The breaking of asperity peaks and accumulation of wear debris are observed for whole working range leading to rough

surface appearance with deep grooves leading to high wear rate of as-deposited coatings [Mukhopadhyay et al. 2019].

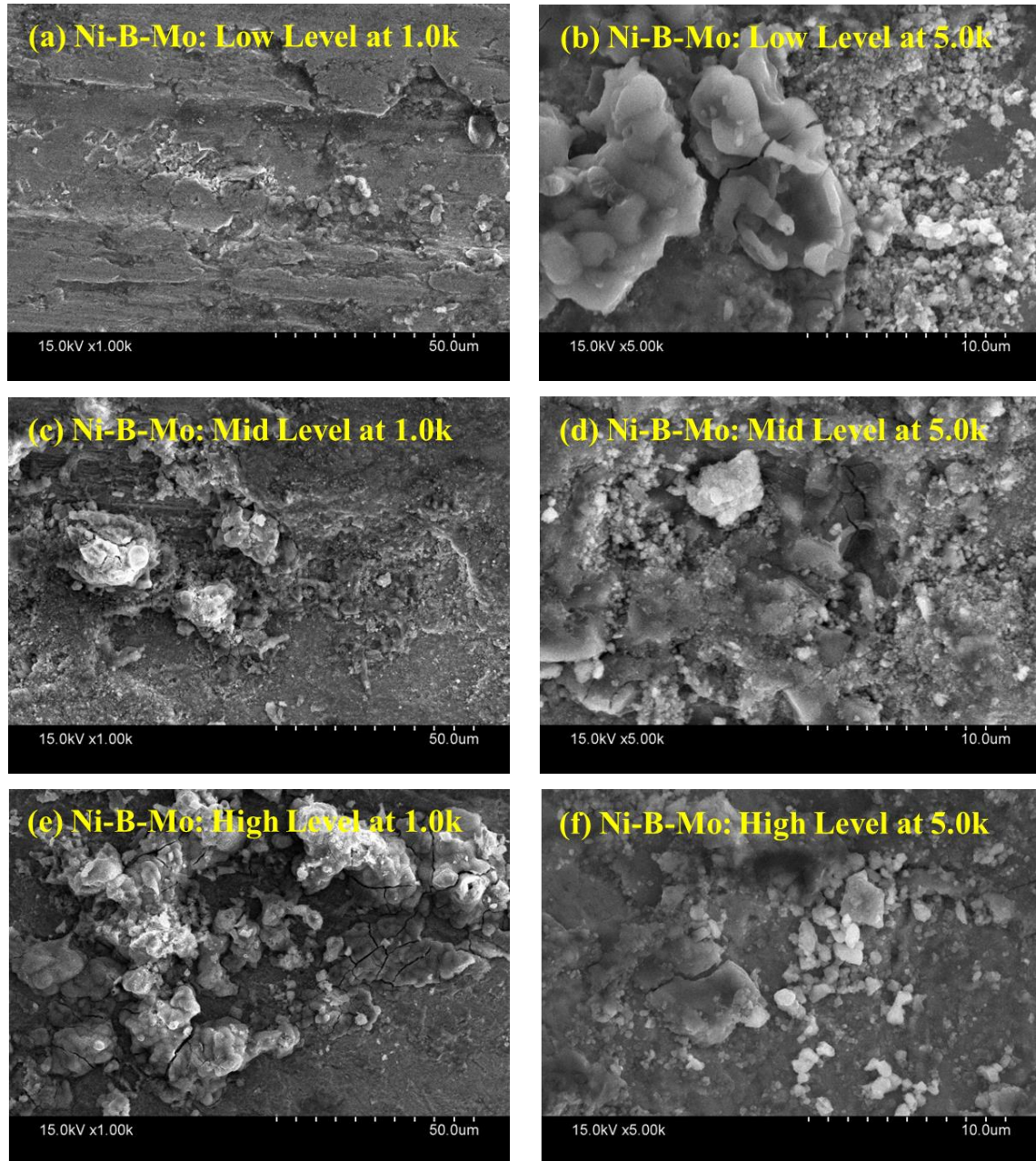


Figure 5.14: SEM Image of Worn-out Surface of As-deposited Ni-B-Mo Coatings Obtained at (a) Low Level, (b) Mid-Level and (c) High Level Concentrations

Figures 5.14(e)-(f) shows some crack formation at high level of concentration. This indicates that the wear mechanism is a mixture of delamination and adhesive wear

[Madah et al. 2015]. The continuous loading unloading during tribo test may lead to delamination of coated layers [Madah et al. 2015]. Figure 5.14 also displays the existence of wear debris and patches in the wear track. The grinding of rough asperities may have raised the wear rate of the coated specimens with sodium borohydride and sodium molybdate concentration [Madah et al. 2015]. The roughness value increases due to the increase in NaBH_4 as well as sodium molybdate concentration leading to rise in roughness peaks. Those roughness peaks are crushed and grinded leading to increase in wear rate and make the surface smooth resulting a decrease in COF value. The wear debris might be entrapped onto sliding surfaces leading to grooves formation along the sliding direction, whereas the debris formed due to delamination may be the cause of crack formation.

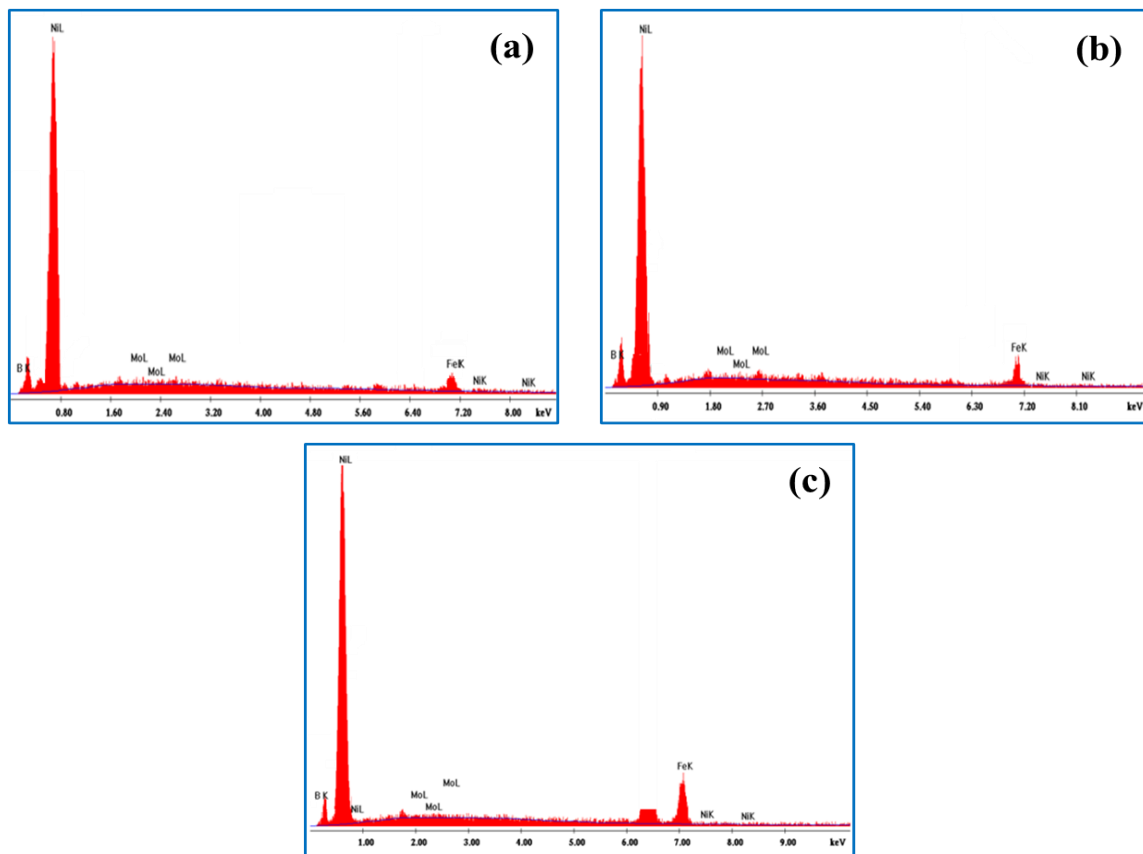


Figure 5.15: EDAX Spectrum of Worn-out Surfaces of As-deposited Ni-B-Mo Coatings Obtained at (a) Low Level, (b) Mid-Level and (c) High Level Concentration

Further, investigations have been carried out on the worn-out surfaces through chemical analysis using EDAX. The EDAX spectrum presented in **Figure 5.15** shows the peaks for Ni, B, Mo, Fe and O. Fe and O may be observed on EDAX result besides the principal elements in worn out surfaces though the amount was seen to be negligible. This confirms that the wear depth is not reached upto substrate [**Mukhopadhyay et al. 2019; Madah et al. 2015**]. Hence, Fe observed in the worn out EDAX result of wear debris may be due to adhesive type of wear [**Madah et al. 2015**] whereas presence of O in the coatings may have come from some external sources.

5.6 Corrosion Resistance Test

The corrosion resistance test is carried out using electrochemical impedance Spectroscopy (EIS) and potentiodynamic Polarisation (PDP) test with the help of a three-electrode based potentiostat. The data obtained from the tests are utilised to generate the tafel plot and nyquist plot using the software provided with the test setup. The tafel plot is obtained from the PDP test and the nyquist plot is obtained from the EIS test. The software generated the nyquist plot considering imaginary impedance on the y-axis and real impedance on the x-axis which provides a semi-circular loop. The bigger semicircle of nyquist plot represents the better corrosion performance of coatings [**Miri et al. 2021; Mukhopadhyay et al. 2018**]. The tafel plot is generated considering the corrosion potential along y-axis and corrosion current along x-axis. The lower negative value of corrosion current potential (E_{corr}) acquired using tafel plot indicates the improvement in corrosion performance of the coated layers [**Anik et al. 2008; Kanta et al. 2010; Kanta et al. 2009**]. The performance of coated layers against corrosion is also found to depend on its morphology and phase structure [**Kanta et al. 2010; Kanta et al. 2009**]. An increment in R_{ct} value obtained from nyquist plot indicates the improvement in corrosion performance [**Anik et al. 2008; Kanta et al. 2010; Kanta et al. 2009**]. Corrosion resistance of coatings is found to depend on various factors like surface porosity, microstructure, heterogeneities, columnar growth, phase structure etc. [**Yildiz et al. 2013**]. The electroless Ni-B coatings are observed to prevent the steel substrate against corrosion [**Bülbül et al. 2013**].

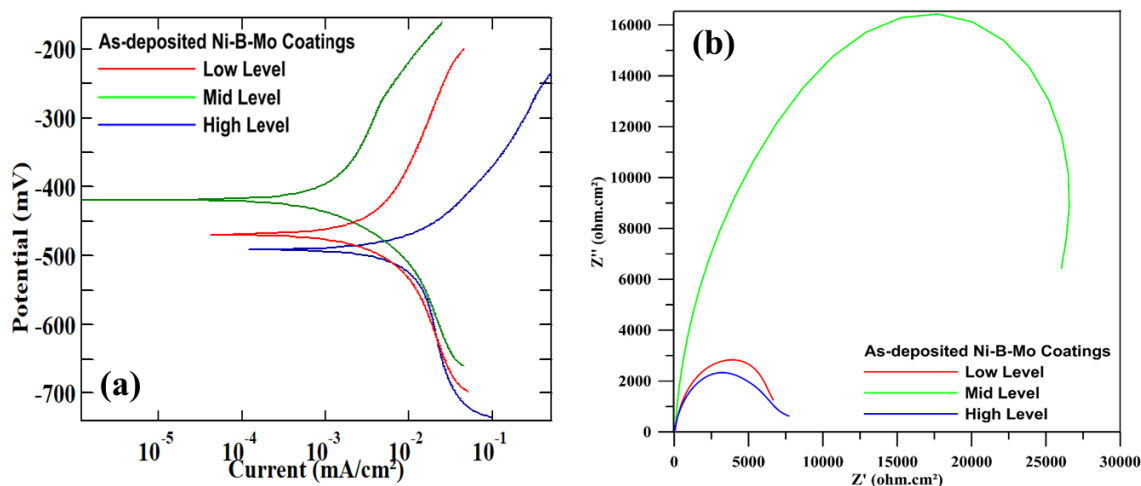


Figure 5.16: EIS and PDP Test Plot for As-deposited Ni-B Coatings, (a) Tafel Plot and (b) Nyquist Plot

Figure 5.16(a) represent the tafel plots for as-deposited electroless Ni-B-Mo coatings obtained for different coating bath concentration levels. The nyquist plot of the same coatings are displayed in **Figure 5.16(b)**. It may be found from **Figure 5.16(a)** that the negative E_{corr} value is decreased with coating bath concentration till mid-level which means the corrosion resistance is increased with bath concentration upto mid-level concentrations. On the other hand, the semi-circle loop in **Figure 5.16(b)** also becomes bigger with coating bath concentration level and this is also indication of increase in corrosion resistance from low to mid-level concentration. Both the tafel plot and nyquist also indicates a reduction in corrosion resistance upon further rise in coating bath concentration. The boron content in the Ni-B-Mo coated surface increased with NaBH_4 concentration and the increased boron content is usually leads to an improvement in corrosion resistance of borohydride reduced coatings [Vitry et al. 2012]. The surface roughness value of the Ni-B-Mo coated specimens is raised with borohydride concentration. Generally, the rougher surface favours the electrocyte to penetrate through coatings. The as-deposited Ni-B-Mo coatings obtained at low level concentration possesses cracked surface morphology which may act as active site for corrosive solution to penetrate through it. The as-deposited Ni-B-MO coated surface becomes rough with the addition of Mo in the borohydride reduced electroless coatings which is known to deteriorate the corrosion resistance of coatings [Dominguez-Rios et al. 2012]. On the

other hand, higher boron content prevent usually improves the corrosion resistance by preventing the corrosive solution to penetrate through surface cracks or grain boundaries. Therefore, the increased corrosion resistance at mid-level concentration may be correlated with the increased boron content. Similar trend of higher corrosion resistance is reported in previous studies [Serin et al. 2015; Niksefat et al. 2015; Georgiza et al. 2017]. While, the lowest corrosion resistance of Ni-B-Mo coatings at low level of concentrations may be correlated with its cracked surface morphology. But the corrosion resistance of Ni-B-Mo coated specimens at high level concentration might have decreased due to the rise in Mo content and rough surface morphology.

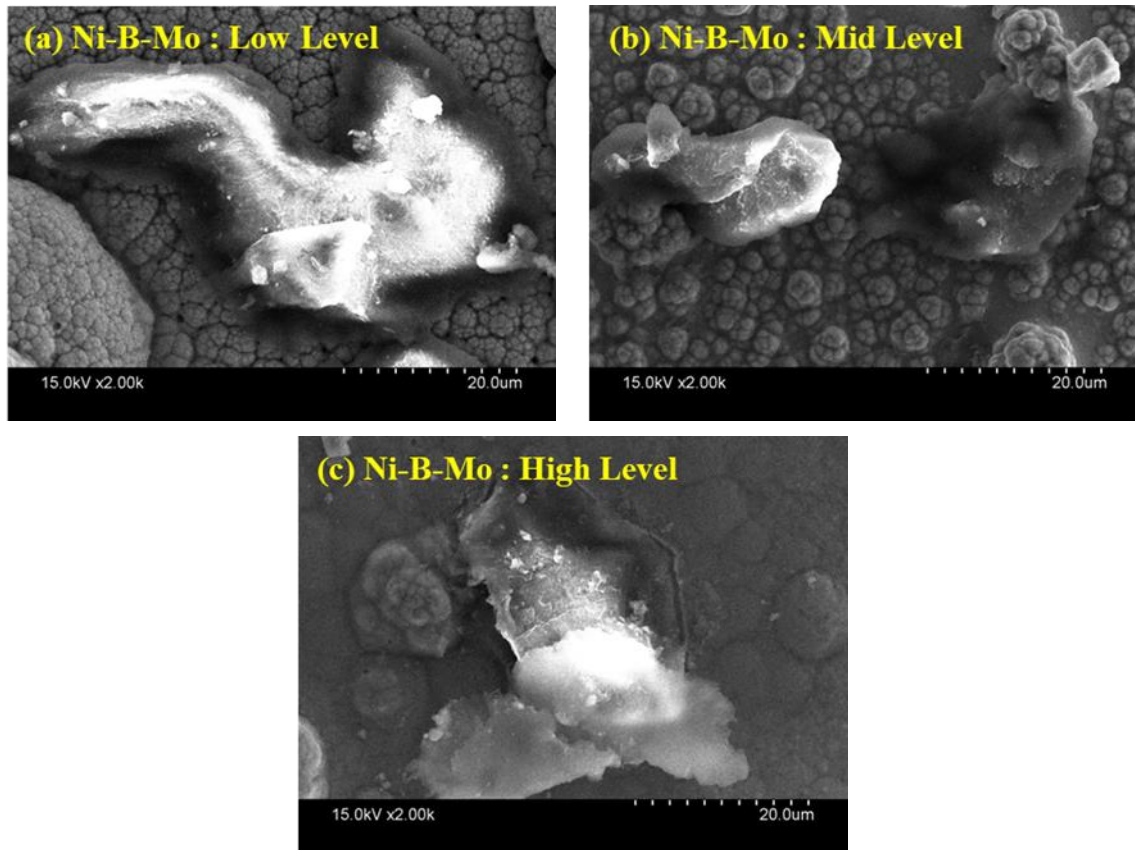
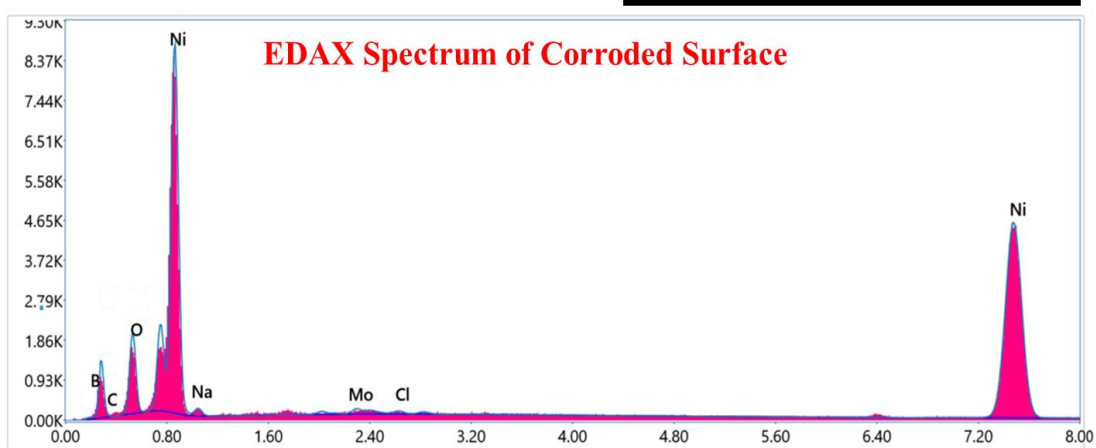
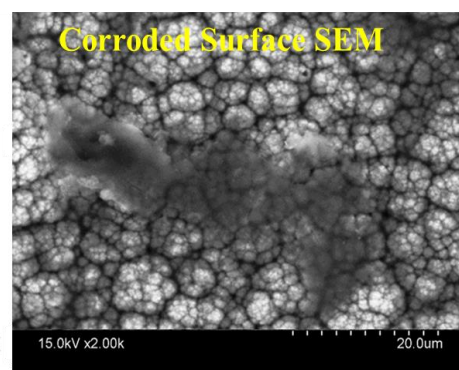
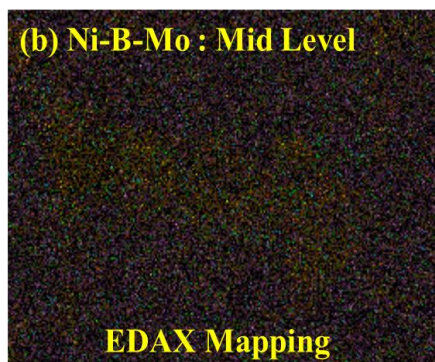
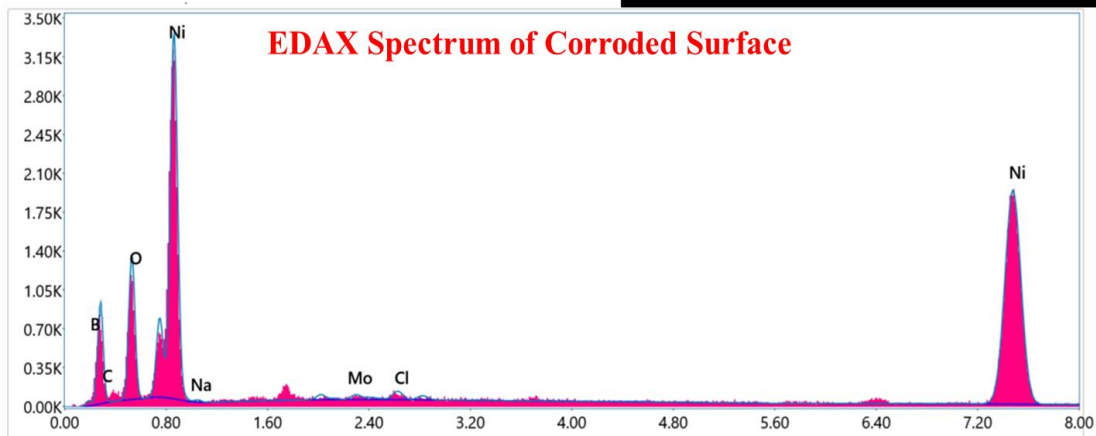
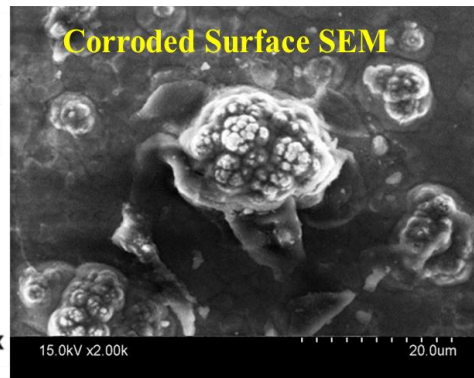
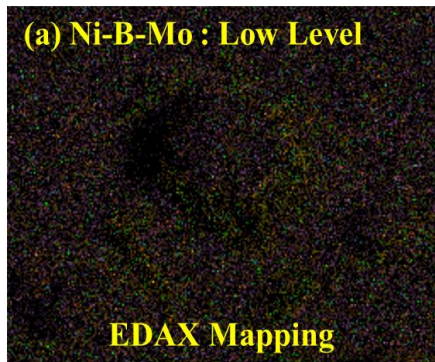


Figure 5.17: SEM Image of Corroded Surface of As-deposited Ni-B-Mo Coatings Obtained at (a) Low Level, (b) Mid-Level and (c) High Level Concentrations

The corroded surfaces of as-deposited Ni-B-Mo coatings are further analysed through SEM. The SEM images of the corroded surfaces are displayed in **Figure 5.17**. The as-deposited Ni-B-Mo coated surfaces underwent corrosion test are seen to possess

corrosion byproducts deposited over the substrate surface. The accumulation of the corrosion byproducts over the substrate surface is indication of corrosion attack by the corrosive medium. **Figure 5.17(b)** shows the corroded surface of as-deposited Ni-B-Mo coatings deposited at mid-level concentration is least effected. The same coatings obtained at high concentrations underwent corrosion attack is seen to possess corrosion byproducts over the substrate surface as well as some corrosion crack as displayed in **Figure 5.17(c)**. Hence, the corrosion resistance of as-deposited Ni-B-Mo coatings obtained at high level of concentrations is lowest compared to other two. The corrosion performance of electroless coatings is seen to vary with phase structure and surface morphology [Mukhopadhyay et al. 2018; Yazdani et al. 2019]. The nano-crystalline phases are seen to be more corrosion sensitive compared to amorphous phase [Bülbül et al. 2013; Anik et al. 2008; Hamid et al. 2010]. The phase structure of the borohydride reduced coatings also transformed from amorphous-nano-crystalline to amorphous phase structure. It may be another cause of this improvement against corrosion resistance.

The as-deposited Ni-B-Mo coatings underwent corrosion test are further investigated using EDAX for chemical composition. The EDAX results of the corroded surface is displayed in **Figure 5.18**. The EDAX results shows that the corroded surface contains the elements like Ni, B, Mo, C, O, Na, and Cl which confirms the presence of corrosive medium elements besides the major coating bath elements. The presence of Na and Cl in the EDAX results may be correlated with the presence of corrosion byproducts observed over the substrate surface. The corroded surface EDAX result also confirms the presence of C and O but the amount is not very significant. The nyquist plot displayed in **Figure 5.16(b)** contains a single semi-circular loop. The single loop is the confirmation that the corrosive medium is failed to penetrate through coatings and reach to substrate. This means the corrosion attack remained limited till the top layer of the coatings only as the substrate composition elements are not observed in EDAX results. Hence, it may be concluded that the corrosion test results agree well with the characterisation results and the Ni-B-Mo coatings succeeded to prevent the corrosive solution to reach till the substrate surface.



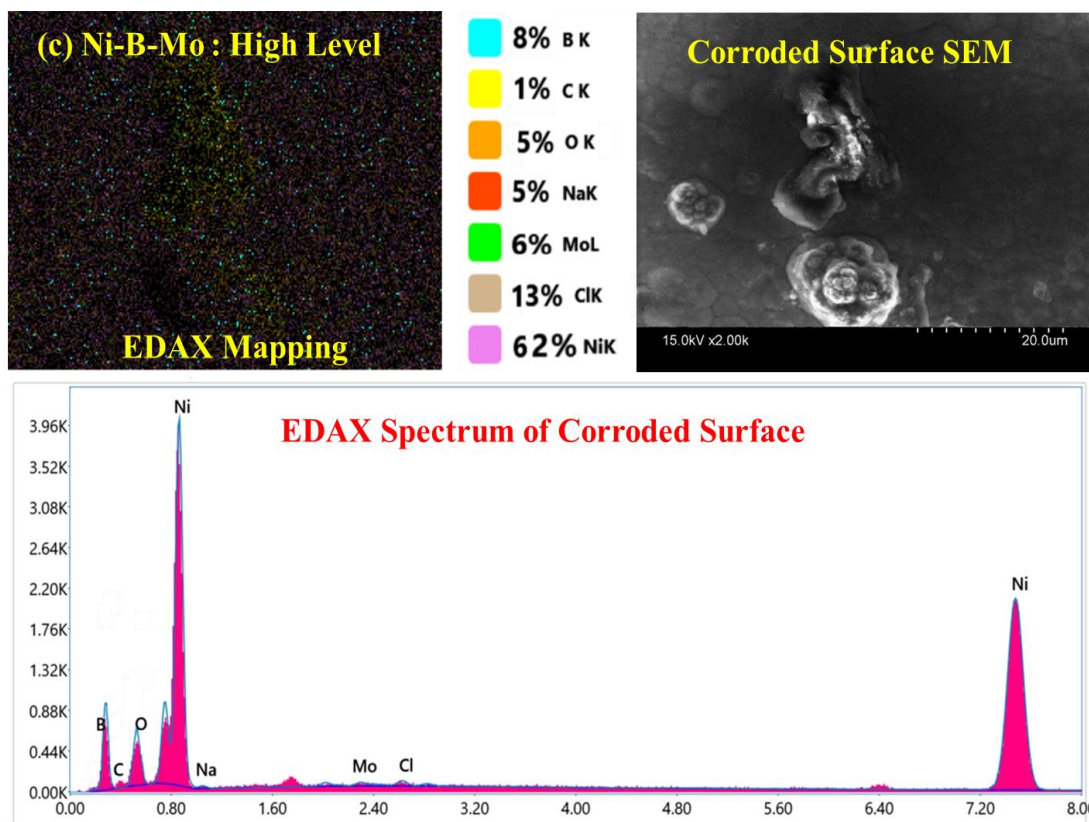


Figure 5.18: SEM Image of Corroded Surface of As-deposited Ni-B-Mo Coatings Obtained at (a) Low Level, (b) Mid-Level and (c) High Level Concentrations

5.7 Closure

The electroless Ni-B-Mo alloy coatings were developed with different concentrations of different coating bath parameters to investigate the significance of those parameters on coating behaviours. The observations are summarized as follows:

- The coating thickness is observed to increase due to the increase in reduction rate with bath level. The coatings possess a cauliflower like surface morphology like other borohydride reduced electroless coatings. The increased concentration of molybdenum does not impact the boron content while the Mo content rose with concentration level.
- The average surface roughness of the coated specimens does not change much with the variation of NiCl_2 . It increases with the increase in sodium borohydride concentration as the reduction rate increases with sodium borohydride

concentration. The increase in molybdenum concentration accelerates the rough and coarse grain surface formation which results in high roughness value.

- The surface hardness of the coated specimens is observed to improve with nickel chloride because of compact and smoothening of surface while the same increases due to higher boron content in the coated specimens with the higher concentration of sodium borohydride. But the surface hardness decreases with the increased molybdenum concentration due to rough and coarse-grained surface morphology. Similar, trend may also be observed for scratch hardness.
- The addition of molybdenum accelerates the formation of rough and coarse grain surface morphology but the COF value is observed to reduce due to rise in NiCl_2 possibly because of smoothening of surface. The COF value increases with the rise in NaBH_4 and molybdenum concentration in the coatings following the surface roughness trend. The wear rate is also observed to rise with sodium borohydride and sodium molybdate concentration.

Chapter 6: Comparison of Electroless Ni-B, Ni-B-W and Ni-B-Mo Alloy Coatings

Outline: 6.1. Introduction, 6.2 Experimental Details, 6.3 Coating Characterisation, 6.3.1 Coating Thickness, 6.3.2 Surface Morphology, 6.3.3 Chemical Composition, 6.3.4 Phase Structure, 6.4 Physical and Mechanical Behaviours, 6.4.1 Surface Roughness, 6.4.2 Nano-indentation Test, 6.4.4 Micro-Scratch Test, 6.5 Tribological Test, 6.6 Corrosion Resistance Test, 6.7 Closure

6.1 Introduction

The current chapter describes the fundamental aspects of borohydride reduced electroless coatings deposited with different elements like tungsten (W), molybdenum (Mo) to form a coating layer of Ni-B, Ni-B-W and Ni-B-Mo coatings. The chapter further elaborates the impact of different coating bath elements and their concentration on the characteristics of the coatings. This chapter also makes a comparative study among different category of coatings developed with different compositions.

Table 6.1: Coating Bath Composition and Concentrations

Elements	Purpose	Low Level Concentration (LLC)	Mid Level Concentration (MLC)	High Level Concentration (HLC)
Nickel Chloride (NiCl ₂) in g/l	Source of Ni ion	10	20	30
Sodium Borohydride (NaBH ₄) in g/l	Reducing agent	0.40	0.80	1.20
	Source of B ion			
Sodium Molybdate (Na ₂ MoO ₄) in g/l	Source of Mo ion	15	25	35
Sodium Tungstate (Na ₂ WO ₄) in g/l	Source of W ion	15	25	35
Coating bath temperature (°C)	Operating condition	75	85	95
Ethylenediamine (C ₂ H ₈ N ₂) in gm/l	Complexing agent		59	
Sodium Hydroxide (NaOH) in gm/l	Buffer		40	
Lead Nitrate (Pb(NO ₃) ₂) in gm/l	Stabilizer		0.0145	

6.2 Experimental Details

The NaBH₄ based binary (Ni-B) and ternary (Ni-B-W, Ni-B-Mo) coated specimens are developed over AISI 1040 steel substrates. The coated substrates of square

shape of size 15 mm × 15 mm × 2 mm are used for characterisation purpose and cylindrical shape of size 6 mm dia × 30 mm long are used for tribo test. The coating bath compositions are provided in **Table 6.1**.

Table 6.2: Coating Types and Bath Elements

Coating Type	Coded Name	Coating Bath Elements
As-deposited Ni-B	NB	NiCl ₂ , NaBH ₄ , C ₂ H ₈ N ₂ , NaOH, Pb(NO ₃) ₂
As-deposited Ni-B-W	NBW	NiCl ₂ , NaBH ₄ , C ₂ H ₈ N ₂ , NaOH, Pb(NO ₃) ₂ , Na ₂ WO ₄
As-deposited Ni-B-Mo	NBM	NiCl ₂ , NaBH ₄ , C ₂ H ₈ N ₂ , NaOH, Pb(NO ₃) ₂ , Na ₂ MoO ₄

Table 6.3: Coating Characterization Techniques

Test Parameters	Equipment used	Specifications	Equipment Parameters
Surface Roughness (Ra)	Talysurf, Surtronic 3+, Taylor Hobson, Leicester, UK	Diamond tipped stylus of 5µm tip radius	Sampling length of 3 mm
Surface Morphology	Scanning Electron Microscopy (SEM) - S3400N, HITACHI	equipped with a secondary electron detector	Energy level of 10-15 KeV, Magnification of 500X to 5000X
Cross Cut Thickness (µm)	Scanning Electron Microscopy (SEM) - S3400N, HITACHI	equipped with a secondary electron detector	Energy level of 10-15 KeV, Magnification of 500X to 5000X
Phase Structure	X-ray Diffraction (XRD)	Set up uses Cu-Kα radiation	Diffraction angle range of 20° to 90° and with 0.02°/sec scanning rate
Elemental Analysis	Energy Dispersive X-Ray Analysis (EDAX) with	The set-up is equipped with a Horiba X-ray detector and having super ultrathin window for effective transmission of low energy x-rays which can detect boron	Very low energy of 10 KeV

The detailed coating development process (substrate pretreatment, coating bath solution preparation, coating bath loading, coating bath operating condition), characterisation techniques (SEM for surface morphology, EDAX for composition, XRD for phase structure) and test methods (surface roughness, nano-indentation test, scratch test, tribological test, corrosion test) are elaborated in details in chapter 2. The coating bath elements and their concentrations are given in **Table 6.1**. The summary of the

different types of coatings are presented in **Table 6.2**. Different characterisation techniques are briefed in **Table 6.3**.

6.3 Coating Characterisation

6.3.1 Coating Thickness

The electroless coating deposition is carried out using steel substrates. The coatings are deposited for 4 hours for all the substrates. The mass gain of the coated substrates is calculated from the weight of the substrates before and after the deposition process. The mass gain of the substrates is the indication of coating deposition. Therefore, the as-deposited coating thickness is calculated from the mass gain, constant coating density, substrate surface area and assuming a uniform coated layer thickness. It is previously documented that electroless Ni-B coatings containing 5 wt.% boron typically has a density of approximately 8.25 gm/cm^3 [Vitry et al. 2022]. The coated layer thickness is further measured with the help of SEM and those are displayed in **Figure 6.1**. The minimum coated layer thickness is achieved for all variants at their lowest concentrations. The calculated coating thickness and measured thickness from SEM are in well agreement. Hence, the minimum coating thickness of the coated layers are presented only for the brevity. The minimum thicknesses are $13.42 \text{ }\mu\text{m}$, $10.14 \text{ }\mu\text{m}$ and $13.65 \text{ }\mu\text{m}$ of NB, NBW and NBM coatings, respectively. The minimum coating thickness obtained at each level for each variant of coatings are represented with the help of a comparative coating thickness plot shown in **Figure 6.1(d)**. The comparative plot shows that the coating thickness of each variant is increased with the increased level of concentrations while each coating is deposited for same time duration of 4 h. The sodium borohydride remains present in the coating bath solution acts as reducing agent [Bülbül et al. 2013; Miri et al. 2021]. The reducing agent extracts the metal ions from the metal salts present in the solution. Those metal ions deposit over the substrate to make a coating layer. Hence, the increased concentration of reducing agent in the coating bath leads to a rise in metal ion extraction rate [Sürdem, et al. 2019; Vitry et al. 2012]. The more metal ions lead to more metal ion deposition over the substrate. The more metal ion deposition i.e., the increased deposition rate leads to an increase in coating thickness.

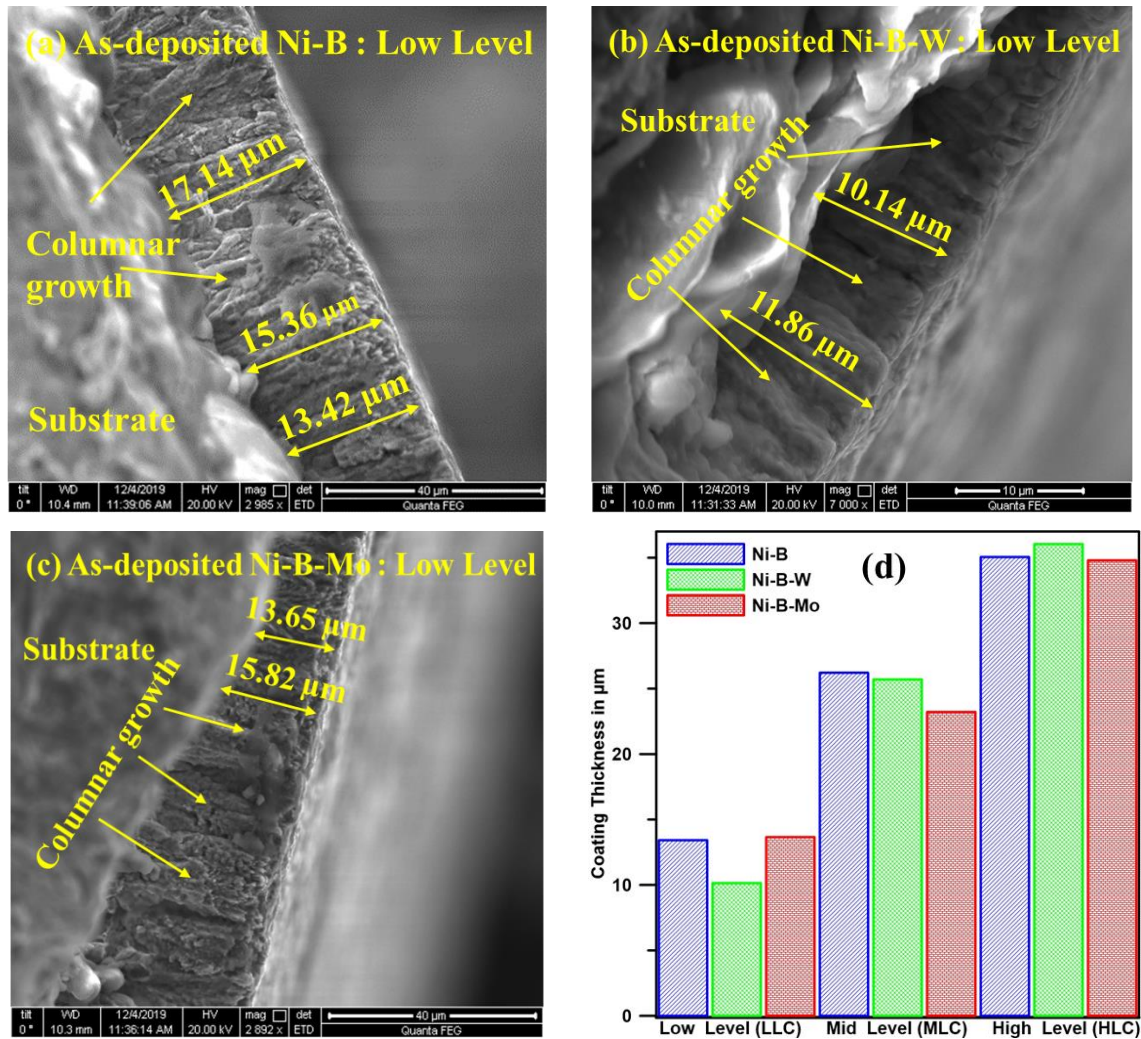


Figure 6.1: As-deposited Coating Thickness of (a) Ni-B, (b) Ni-B-W, (c) Ni-B-Mo and (d) Comparative Plot

The chemical reaction or metal ion extraction process starts at around 70°C [Vitry et al. 2022] and it increases with temperature upto a certain temperature. Hence, the reduction process may get faster with the increased coating bath temperature as well. It also leads to a higher deposition rate resulting increased coating thickness. Therefore, the higher concentration of reducing agent and higher coating bath temperature may be the possible reason for the increased coating thickness with coating level of concentration.

6.3.2 Surface Morphology

The coated surfaces are further examined through the SEM to understand the morphology. The obtained SEM images for Low, Mid and High level are displayed in **Figure 6.2**, **Figure 6.3** and **Figure 6.4**, respectively. All the coated surfaces under investigation are seen to exhibit morphology similar to cauliflower with homogeneous distribution of nodules [Mukhopadhyay et al. 2018; Nemane et al. 2022; Agrawal and Mukhopadhyay, 2022]. **Figure 6.1** also shows the columnar growth of coatings to form cauliflower like morphology [Vitry et al. 2022; Mukhopadhyay et al. 2018; Mukhopadhyay et al. 2018; Bonin and Vitry, 2016; Lekka et al. 2018].

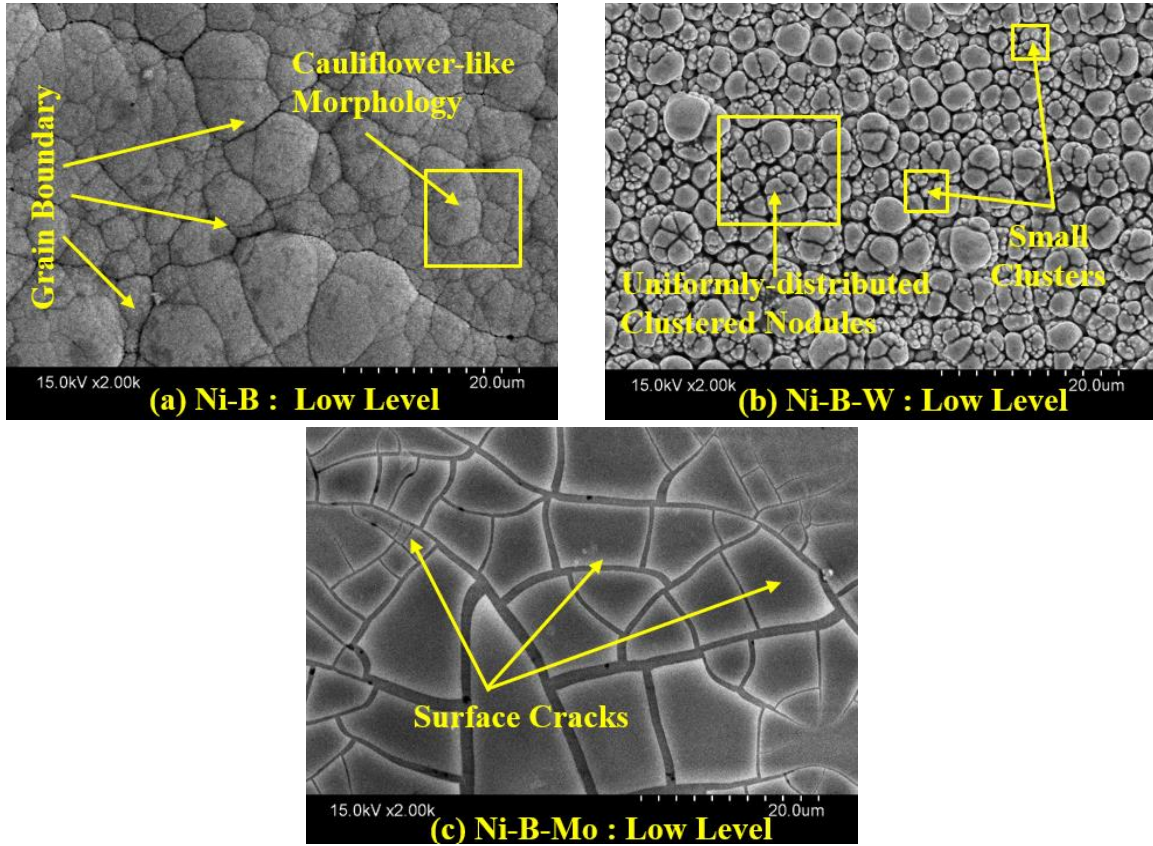


Figure 6.2: Surface Morphology of Electroless Coatings Obtained at Low Level of Concentrations (a) Ni-B, (b) Ni-B-W, and (c) Ni-B-Mo

The cauliflower like morphology is well-known for their self-lubrication behavior due to reduction in the real contact area leading to reduction of COF value [Vitry et al. 2022; Vitry, 2016; Lekka et al. 2018]. The specimens covered with electroless Ni-B coatings appear dense, and the nodules seem to enlarge with the bath level, likely due to

increased NaBH_4 concentration [Sürdem, et al. 2019]. The nodular morphology is very often observed for Ni-B, Ni-B-W and Ni-B-Mo [Sürdem, et al. 2019; Mukhopadhyay et al. 2018; Nemane et al. 2022]. The accumulation of grains over the surface restricts lateral expansion and promotes vertical growth instead. This vertical growth is the reason for columnar structure of the coatings resulting the surface morphology resembling cauliflower [Vitry et al. 2022; Balaraju et al. 2014]. Similar columnar structure may be observed in **Figure 6.1** and the cauliflower like morphology along with closely packed nodules is observed in **Figure 6.2**, **Figure 6.3** and **Figure 6.4** [Aydeniz et al. 2013; Niksefat et al. 2015; Vitry et al. 2022; Balaraju et al. 2014; Nemane et al. 2022]. The nodular surface of Ni-B coatings becomes closely packed with increased concentration. The same trend is also observed due to the inclusion of tungsten and molybdenum individually with ENB. But there are a few cluster formations of nodules found in Ni-B coatings at high level of concentrations as displayed in **Figure 6.4(a)**.

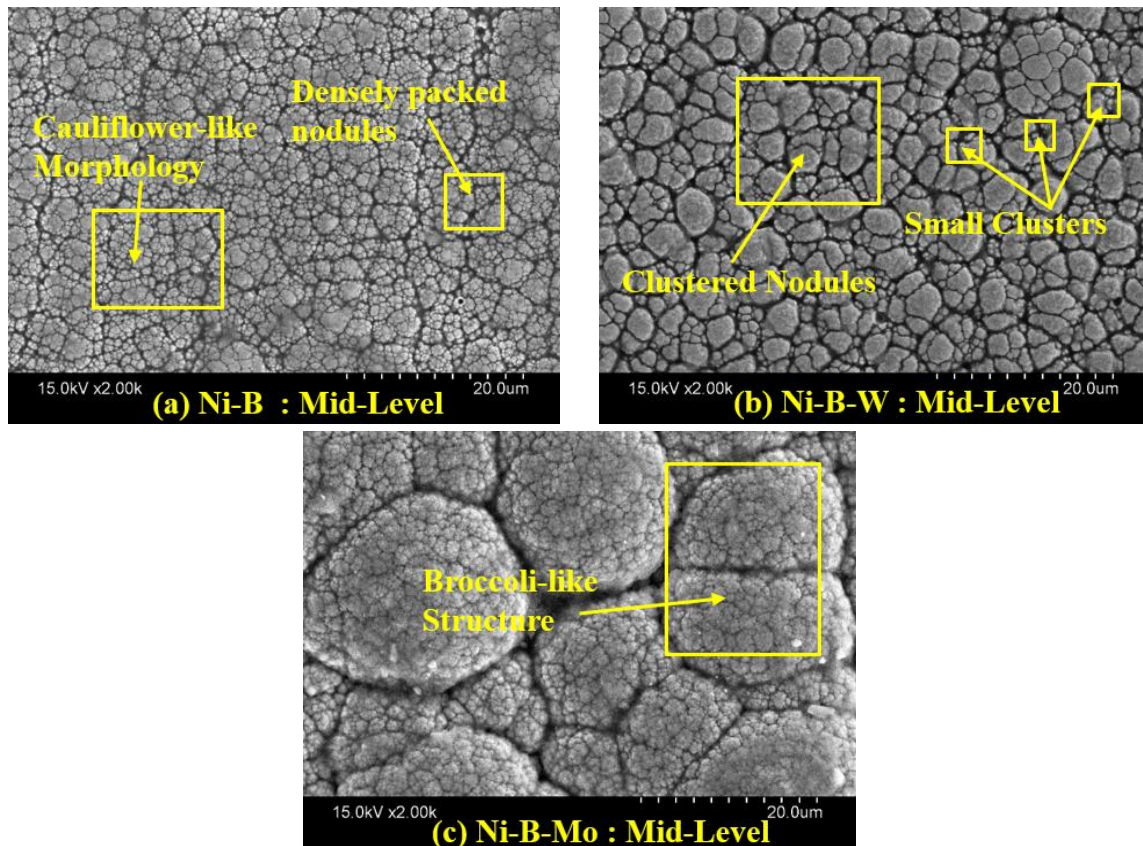


Figure 6.3: Surface Morphology of Electroless Coatings Obtained at Mid Level of Concentrations (a) Ni-B, (b) Ni-B-W, and (c) Ni-B-Mo

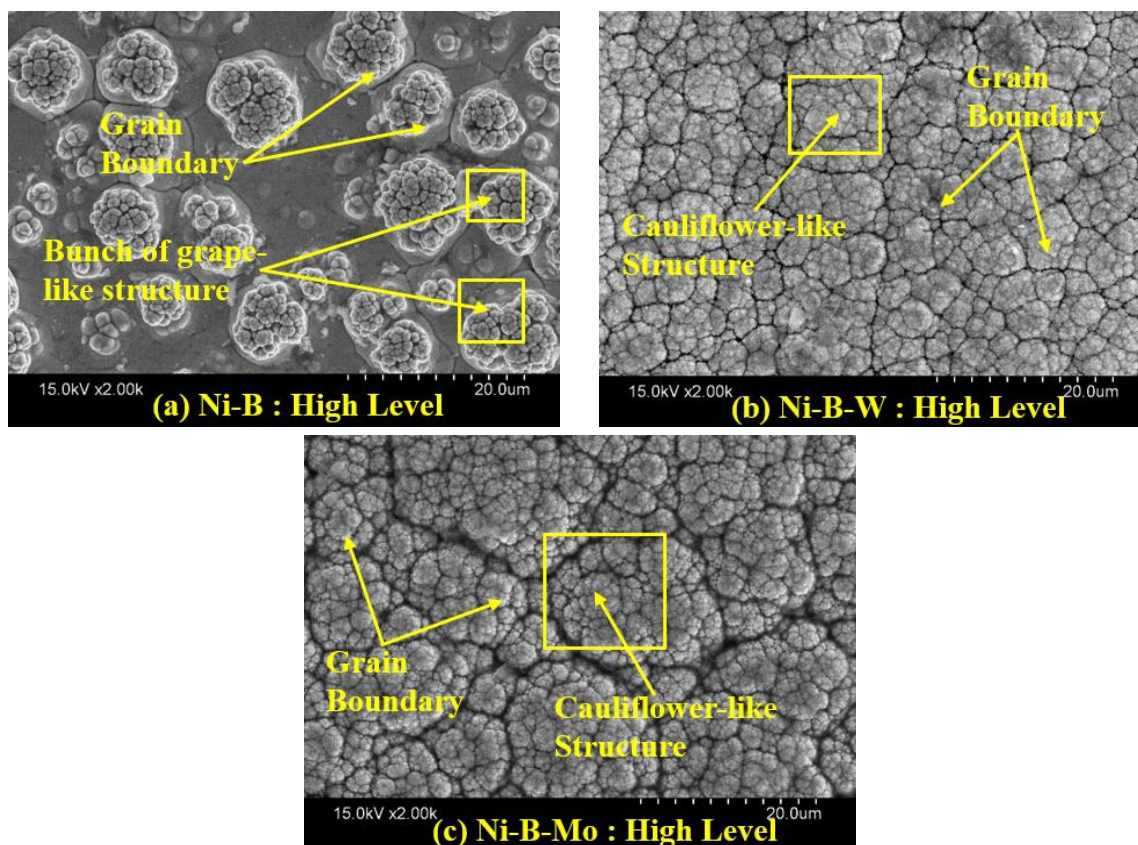


Figure 6.4: Surface Morphology of Electroless Coatings Obtained at High Level of Concentrations (a) Ni-B, (b) Ni-B-W, and (c) Ni-B-Mo

Whereas, the Ni-B-Mo coated surface is observed to possess some visible cracks at low level due to high stress growth and the other variant does not possess any such cracks. The same Ni-B-Mo coated surface is observed to get more uniform and denser with bath level rise. Columnar growth is a common characteristic of ENB coatings. It is familiar for its nature to reduce the actual surface contact area and helps in reducing the COF value. The ENB coated surface is observed to be compact and the nodules are seen to become bigger with bath level concentration which is possibly because of the higher amount of reducing agent [Sürdem, et al. 2019; Vitry et al. 2022]. The deposition of nanograins occurs at various nucleation points near the substrate surface. The deposition of nano-grains on the surface prevents the growth along lateral direction and progresses along the vertical direction leading to cauliflower like surface morphology [Vitry et al. 2010; Nemane and Chatterjee, 2020]. All variant of coatings under study is observed to possess closely packed nodules and cauliflower like morphology.

6.3.3 Chemical Composition

The chemical composition of the coatings is investigated using energy dispersive x-ray analysis (EDAX). The EDAX spectrum of the as-deposited Ni-B, Ni-B-W and Ni-B-Mo coatings may be seen in **Figure 3.4** (Chapter 3), **Figure 4.4** (Chapter 4) and **Figure 5.4** (Chapter 5), respectively. The EDAX spectrums confirms the presence of major coating elements in respective coatings. The minimum concentration of those elements is provided in weight % in **Table 6.4**. The amount of boron in Ni-B-Mo coatings at low level is observed to be more than other variants which is observed to rise with concentration except for Ni-B-W coatings at high level [Mukhopadhyay et al. 2018; Mukhopadhyay et al. 2018; Bonin and Vitry, 2016; Lekka et al. 2018]. The same boron content in Ni-B coatings is found to be highest at mid and high level of concentration.

Table 6.4 Chemical Composition of Coatings

Elements		Ni-B	Ni-B-W	Ni-B-Mo
Nickel	Low Level	93.30±0.80	90.30±0.70	90.20±0.70
	Mid-Level	89.10±0.60	88.40±0.50	87.60±0.50
	High Level	84.90±0.60	86.20±0.60	84.50±0.60
Boron	Low Level	3.30±0.20	3.80±0.30	3.90±0.30
	Mid-Level	6.10±0.40	5.70±0.40	5.80±0.40
	High Level	8.20±0.40	5.10±0.30	6.10±0.40
Tungsten	Low Level	X	2.70±0.20	X
	Mid-Level	X	3.60±0.20	X
	High Level	X	4.40±0.30	X
Molybdenum	Low Level	X	X	3.10±0.30
	Mid-Level	X	X	3.90±0.30
	High Level	X	X	4.50±0.30

The inclusion of tungsten into ENB might have lowered the boron deposition rate slightly at mid-level. The tungsten deposition further dominated the boron deposition in Ni-B-W coatings at high level concentration and decreased the boron content slightly compared to mid-level [Nemane et al. 2022; Agrawal and Mukhopadhyay, 2022;

Bonin and Vitry, 2016; Lekka et al. 2018]. Similar increasing trend of boron may be observed for Ni-B-Mo coatings as well but it remained low compared to Ni-B coatings. Therefore, addition of W or Mo must have dominated the boron deposition and ultimately lowering its concentration in the coated layers. The common trend in NaBH₄ reduced electroless coatings is that the boron content tends to rise with sodium borohydride concentration [**Sürdem, et al. 2019**]. Sodium borohydride serves as a reducing agent, facilitating the extraction of metal ions from the chemicals present in the coating bath solution. The extracted ions are deposited over the substrate surface. The higher concentration of borohydride extracts more metal ions and deposit at faster rate leading to speed up the coating process. Same mechanism is followed for ternary coatings as well but deposition of W and Mo suppressed the boron ion deposition and reduced their concentration slightly. When tungsten and molybdenum are co-deposited with electroless Ni-B, there is further reduction in boron content on the quaternary coatings compared to binary and ternary coatings under investigation. The molybdenum content in the electroless Ni-B-Mo coatings is observed to be slightly more than the tungsten content in the electroless Ni-B-W coatings. Both molybdenum as well as tungsten are found in group 6 of periodic table. However, molybdenum typically exists in the coating bath as MoO₄²⁻, while tungsten exists in a group of complex ions [**Agrawal and Mukhopadhyay, 2022**]. As a result, the molybdenum content is found to deposit in higher percentage relative to tungsten in the ternary coatings. Those metal ions are deposited at higher concentrations like boron but Ni content is reduced against raised bath level. The presence of Ni reduced because of the increase in boron, W, Mo in the coated specimen. These observations align with findings from published reports [**Nemane et al. 2022; Agrawal and Mukhopadhyay, 2022; Bonin and Vitry, 2016; Lekka et al. 2018**].

6.3.4 Phase Structure

The phase transition characteristic of the coatings, as they vary with bath concentrations, is carried out using x-ray diffraction (XRD). The obtained spectrums for various phases for different coating categories are presented through **Figure 6.5**. The XRD pattern of all the coatings in this study possesses a sharp peak with a broad hump at

low level. A broad hump present in XRD spectra indicates the amorphous phase [Sürdem et al. 2019; Pal et al. 2011; Vitry et al. 2022]. A sharp intensity peaks in the XRD pattern signify the presence of crystalline phase [Sürdem et al. 2019; Pal et al. 2011; Vitry et al. 2022]. The XRD pattern contains hump and sharp peak which indicates the presence of amorphous-crystalline phase at low level concentration [Sürdem et al. 2019; Pal et al. 2011]. The coatings with a boron content exceeding 6.5% typically inhibit nuclei formation at nucleation points, particularly at roughness peaks and troughs. This leads to prevention of crystalline phase transformation [Sürdem, et al. 2019; Vitry et al. 2022]. But all types of coated specimens developed in the current study contain boron below 4 wt.%. This lower concentration of boron leads to crystalline phase formation. Therefore, both EDAX and XRD results are in well agreement [Sürdem, et al. 2019; Balaraju et al. 2014; Bonin and Vitry, 2016; Liu et al. 2013]. The boron content on the coated specimens under this study increased with bath concentrations which may encourage the transformation of phase to amorphous phase. The declining trend of sharp intensity peak with coating bath concentration also confirms the phase transformation towards amorphous phase. The shift from the crystalline phase to the amorphous phase is likely attributed to the rise in NaBH_4 [Sürdem, et al. 2019]. Conversely, the existence of either tungsten, molybdenum or both tungsten & molybdenum on the coatings promotes the transition to an amorphous phase [Nemane et al. 2022; Agrawal and Mukhopadhyay, 2022; Bonin and Vitry, 2016; Lekka et al. 2018]. The borohydride reduced coating structure in as-deposited condition is usually controlled by the boron content. The higher concentration of boron prevents the coating crystallization [Nemane and Chatterjee, 2020]. The presence of boron prevents the nucleation of Ni at multiple nucleation points of isolation zones preferably at surface peaks and valleys [Nemane and Chatterjee, 2020; Mukhopadhyay et al. 2018]. Similarly, the presence of tungsten and molybdenum in borohydride reduced coatings also promotes the amorphous phase formation [Yildiz et al. 2017; Aydeniz et al. 2013; Yildiz et al. 2013; Radwan et al. 2015]. The increased concentration of tungsten and molybdenum leads to reduction in boron content which is expected to promote crystalline phase formation.

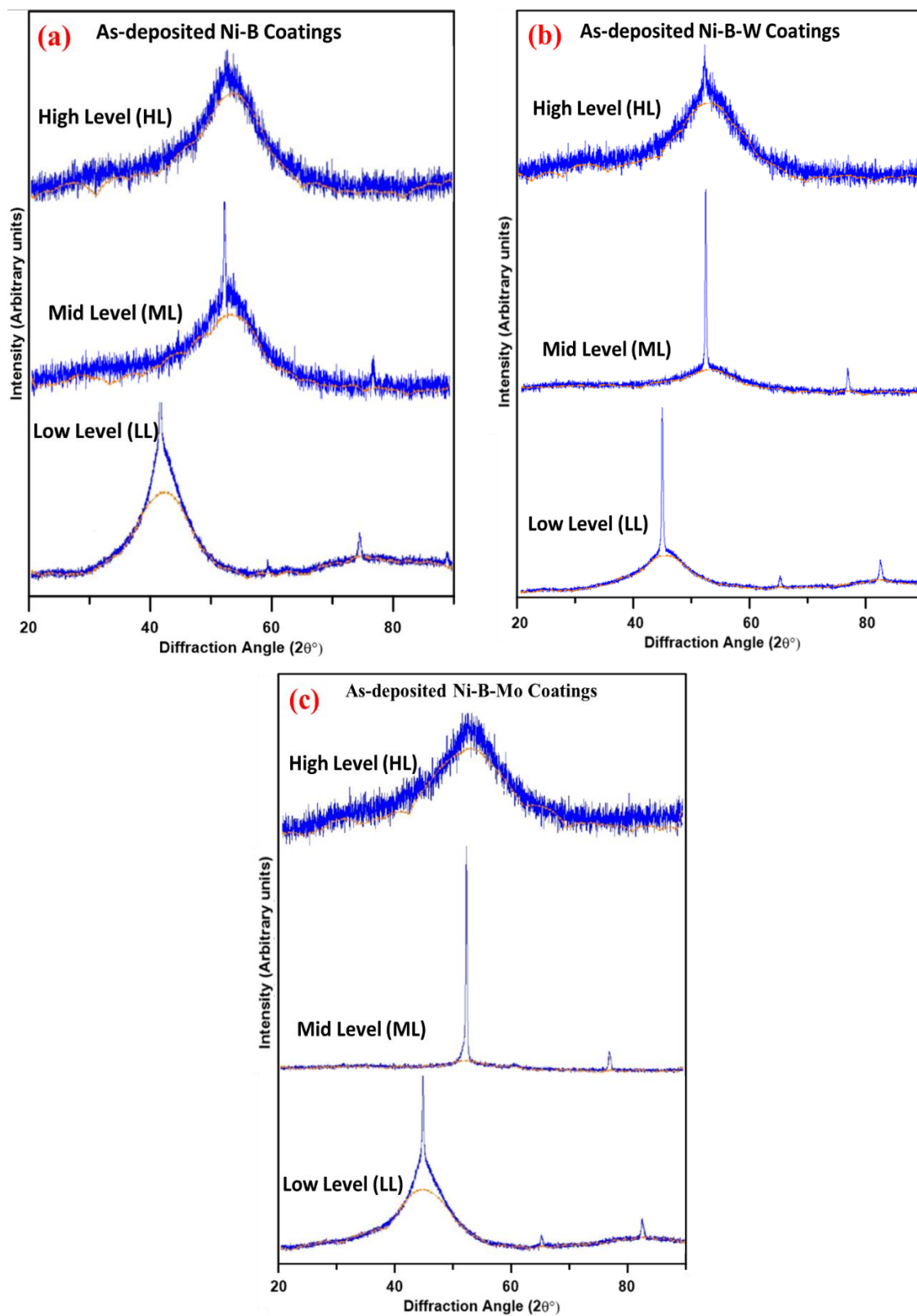


Figure 6.5: XRD Patterns of As-deposited Electroless Coatings (a) Ni-B, (b) Ni-B-W and (c) Ni-B-Mo

Conversely, the increased tungsten and molybdenum content leads to formation of amorphous phase of borohydride reduced binary and ternary coatings. The boron content in all the coatings exhibited a considerable rise with coating composition except for NBW coatings at high level. The XRD pattern of NBW coatings also contains a sharp peak but the intensity is not much. Hence, this can be associated with the slight decrease of boron content in NBW coatings at high level concentration. In NBM coatings, both boron and molybdenum content appear to rise progressively with the bath concentration. Increased trend of boron and Mo, both promotes amorphous phase formation. Hence, the diminishing trend of sharp crystalline peak for NBM coatings may be associated with this rise in boron and Mo.

6.4 Physical and Mechanical Behaviours

6.4.1 Surface Roughness

The specimens coated at low level concentration exhibits smoother surfaces compared to the uncoated ones. The bared specimens have an Ra value of 0.285 μm . **Figure 6.6** represents the change in Ra value of the coated specimens obtained with various compositions and types. **Figure 6.6** also indicates a rise in Ra value with the rise of bath level. The surface roughness value of NaBH_4 based coatings usually depends on the reduction rate. The reduction rate is seen to depend on reducing agent concentration in the coating bath. The surface roughness of these coatings depends on borohydride concentration. Hence, the ion extraction rate depends on reducing agent concentration [Bülbül et al. 2013; Wan et al. 2016; Vitry et al. 2012; Madah et al. 2015]. Sodium borohydride is used as reducing agent under present study. Therefore, the change in Ra value may be correlated with the NaBH_4 concentration for all types of coating in the current study. It is also seen that the ion extraction or reduction reaction do not start at ambient temperature. The chemical reaction starts at around 70°C [Vitry et al. 2014; Balaraju et al. 2014]. The coating bath temperature ranges from 75°C to 95°C, which mean the reduction rate is initially slow and accelerates with temperature rise. The reduced ions begin to deposit near the substrate surface i.e., the peaks and troughs. The supply of metal ions is less at low level concentration due to lesser amount of metal salt present in the coating bath solution and lower coating bath temperature. The lower

concentration of reducing agent also leads to lesser amount of ion extraction. This leads to a slow deposition of metal ions and makes the surface smooth. Conversely, the coating bath solution at high level contain higher amount of reducing agent and coating bath temperature is also high.

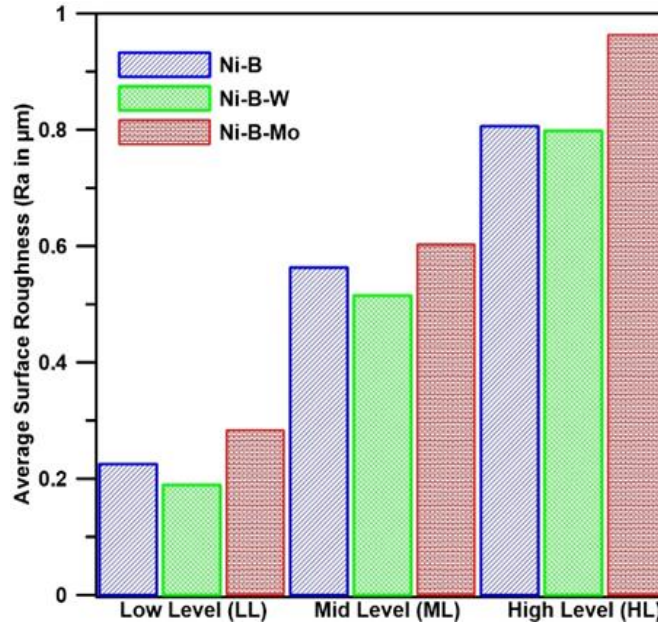


Figure 6.6: Comparative Average Surface Roughness (Ra in μm) Plot

Hence, the reduction of metal ions is also very high which leads to speedy deposition of ions. The rapid extraction of ions causes them to settle haphazardly on the surface, resulting in a rough texture [Vitry et al. 2012]. Consequently, the reduction in surface roughness at low level concentration might be because of a lower reduction rate at lower concentrations of sodium borohydride [Vitry et al. 2012]. The increase in surface roughness could be a result of elevated reduction rate due to higher sodium borohydride concentrations [Sürdem, et al. 2019; Vitry et al. 2012]. The average surface roughness trend with coating bath concentration variation is summarised as follows

Ni-B-Mo > Ni-B > Ni-B-W	at Low Level Concentrations (LLC)
Ni-B-Mo > Ni-B > Ni-B-W	at Mid-Level Concentration (MLC)
Ni-B-Mo > Ni-B > Ni-B-W	at High Level Concentrations (HLC)

Figure 6.6 further represents that the deposition of Ni-B-Mo coatings over the substrate makes the surface rough compared to other variants at low level of bath concentration. However, it is still less compared to substrate at low level. As the bath level rises, the surface roughness of all types of coatings under study is observed to rise. The Ra value of the substrates covered with coated layer consistently maintained the highest value across the examined range. As the reduction rate increases, associated with a rise in sodium borohydride, so does the Ra value [Sürdem, et al. 2019; Vitry et al. 2012]. Therefore, the intensified chemical reaction with sodium borohydride might be the primary cause for this surge in average roughness value [Bülbül et al. 2013; Wan et al. 2016; Vitry et al. 2012]. The inclusion of tungsten into Ni-B matrix makes the surface dense, compact which seemed to have smoothened the surface, leading to a reduction in surface roughness of Ni-B-W coated surface upto mid-level. This pattern aligns with the findings depicted in previous works [Yildiz et al. 2013; Nemané et al. 2022]. Conversely, the incorporation of molybdenum contributes to high stress growth which results in crack formation and consequently a rougher surface is obtained [Mukhopadhyay et al. 2018, Yildiz et al. 2013; Mukhopadhyay et al. 2018; Bonin and Vitry, 2016]. The coarse morphology is another factor contributing to higher surface roughness of Ni-B-Mo coatings. However, the inclusion of tungsten and molybdenum together into Ni-B matrix smoothened the surface relative to the other variants under study.

6.4.2 Nano-indentation Test

The indentation tests are carried out at a constant indentation depth for all the coatings. The loading unloading curves for as-deposited Ni-B, Ni-B-W and Ni-B-Mo coatings are displayed in **Figure 3.7** (Chapter 3), **Figure 4.7** (Chapter 4) and **Figure 5.7** (Chapter 5), respectively. The Figures show the load required for different coatings to indent the same depth. The higher load required for same indentation depth is the indication of higher nanohardness value. The load required for Ni-B is the highest at high level concentration and lowest at low level concentration. The loading unloading curves also show that the applied load is increased with coating bath level for as-deposited coatings which indicates the increasing trend of nanohardness value. The boron content

also increases with coating bath level [Sürdem, et al. 2019; Pal et al. 2018]. Therefore, the Ni-B coating hardness increased with boron content [Sürdem, et al. 2019; Pal et al. 2018]. The same trend may also be observed for as-deposited Ni-B-W and Ni-B-Mo coated specimens. The increase in the presence of hard particles like boron, tungsten or molybdenum in the coated surface has the capability to enhance the hardness of the coatings [Sürdem, et al. 2019; Vitry and Bonin, 2017; Mukhopadhyay et al. 2018]. The EDAX results show that the boron concentration increased for all the coatings. The boron concentration is not same for different categories of coatings. The Ni-B covered samples are observed to possess highest boron content especially at mid-level and high level but the nanohardness of ENB surface is not the highest within the working range. Therefore, nanohardness value doesn't depend solely on boron concentration. **Figure 6.7** represents the average nanohardness value of different coating categories at different levels. The hardness of Ni-B-W specimens is found to improve due to concentration level while the boron content is slightly reduced at high level. On the other hand, the tungsten content is seen to rise till high level concentration. Therefore, the increasing trend of boron as well as tungsten led to increase the nanohardness value [Yildiz et al. 2017; Mukhopadhyay et al. 2018]. The increased amount of tungsten possibly leads to a slight reduction of boron at high-level [Mukhopadhyay et al. 2018]. The hardness of Ni-B-Mo specimens is observed to improve slightly as the boron content increased. But the hardness value remained to be much lower than Ni-B coated specimens. The amount of Mo is observed to increase with bath composition and the addition of Mo leads to formation of cracks surface due to stress growth. On the other hand, addition tungsten like hard particles with electroless Ni-B matrix leads to enhancement in coating hardness. The EDAX result also shows a rise in boron content as well as tungsten content on Ni-B-W coatings though the boron content remained lower than Ni-B coatings. The increased tungsten content in Ni-B-W with bath concentration could have resulted an enhancement of the nanohardness value relative to other three variant of coatings. The specimens with of amorphous phase are found to have higher nanohardness value than the specimens with crystalline phase. The inclusion of tungsten and molybdenum into Ni-B prevents the nucleation which accelerates the development of amorphous phase and improves the

surface hardness. But the cracked surface morphology lowered then nano-hardness value of Ni-B-Mo coatings.

A comparative plot for nano-hardness value is displayed in **Figure 6.7**. The hardness variation trends at different levels are as follows

Ni-B-W > Ni-B > Ni-B-Mo	at Low Level Concentration (LLC)
Ni-B-W > Ni-B > Ni-B-Mo	at Mid-Level Concentration (MLC)
Ni-B-W > Ni-B > Ni-B-Mo	at High Level Concentration (HLC)

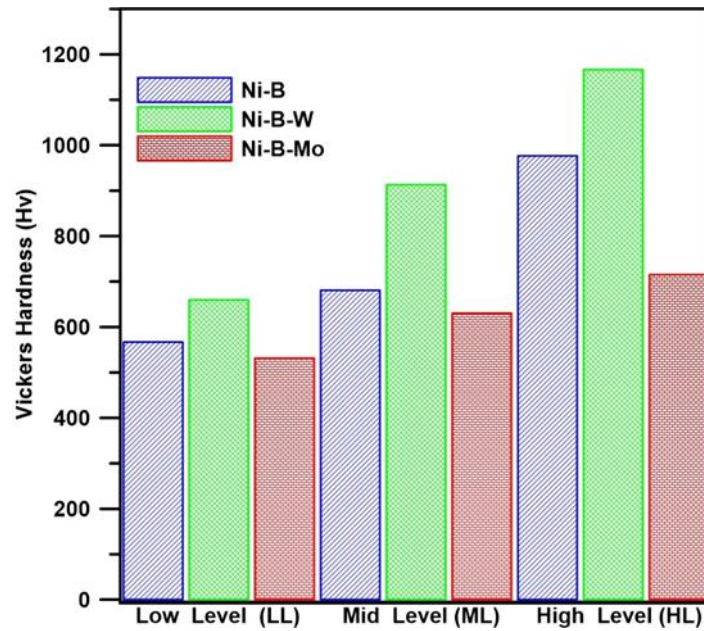


Figure 6.7: Comparative Hardness Plot Obtained from Nano-indentation

All the coatings have a tendency towards the transformation from amorphous-crystalline to amorphous phase with the bath concentration level rise. This trend may be seen from the XRD pattern shown in **Figure 6.5**. This may also be another reason for the improvement in hardness value with bath concentration for all variants. The addition of W into Ni-B matrix improved the hardness of Ni-B-W coated specimens and it is higher than the hardness of Ni-B coated specimens. The coating hardness is also found to vary with grain size [Sürdem, et al. 2019; Dominguez-Rios et al. 2012; Liu et al. 2013; Arias et al. 2019; Pal et al. 2018] which may also be a probable cause of improved hardness. The incorporation of Mo with ENB is expected to improve the hardness. But it promotes the crack development and coarse-grained morphology which may lead to

reduction in nanohardness value. The hardness value of Ni-B-Mo coated specimens is much lower relative to the other variants under the current investigation. The W content in Ni-B-W is raised due to bath composition rise and it is higher than the other variants. The increased amount of W into quaternary coating suppressed the boron deposition slightly [Vitry et al. 2014]. The higher concentration of W is the main reason for highest nano-hardness value of Ni-B-W coated specimens relative to other variants throughout the working range.

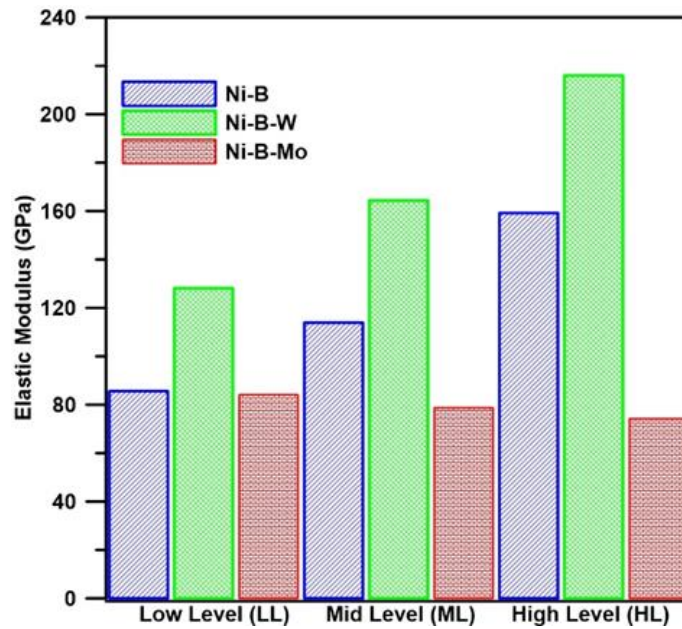


Figure 6.8: Comparative Elastic Modulus Plot Obtained from Nano-indentation

The average of elastic modulus at different bath level is shown in **Figure 6.8**. The trend of elastic modulus variation is summarised as follows.

Ni-B-W > Ni-B > Ni-B-Mo at Low Level Concentration (LLC)

Ni-B-W > Ni-B > Ni-B-Mo at Mid-Level Concentration (MLC)

Ni-B-W > Ni-B > Ni-B-Mo at High Level Concentration (HLC)

The elastic modulus of coated specimens does not depend on surface hardness, rather it is found to depend on grain size [Sürdem, et al. 2019; Dominguez-Rios et al. 2012; Liu et al. 2013; Arias et al. 2019; Pal et al. 2018]. The grain size of Ni-B coated specimens is found to rise with NaBH₄ content in the coating bath solution [Liu et al.

2013]. This rise in grain size due to boron concentration at high level might have increased the elastic modulus of Ni-B coatings. The obtained elastic modulus values are also observed to improve for Ni-B-W coatings like Ni-B coated specimens within the working range. Whereas, it is seen to follow opposite trend for Ni-B-Mo coated specimens. The addition of Mo leads to coarse surface morphology due to high stress growth and crack formation [Mukhopadhyay et al. 2018; Mukhopadhyay et al. 2019] which might have lowered the elastic modulus. But, no specific trend is found for elastic modulus variation under this current study. Hence, the mechanism of elastic modulus variation in this current study cannot be explained. Further detailed investigation is required to understand the mechanism of elastic modulus for electroless borohydride reduced coatings.

6.4.3 Micro-Scratch Test

The coated surfaces are tested for scratch hardness using a scratch hardness tester and the scratches are formed on the different types of coatings obtained at different concentrations. The same scratch marks are measured at ten different locations to calculate the scratch hardness. The average of the calculated scratch hardness values is presented through a comparative plot shown in **Figure 6.9**. The average scratch hardness of the coated specimens obtained at various compositions are shown in **Figure 6.9**. **Figure 6.9** indicates an improvement in scratch hardness by bath level rise for all variants of coatings. This increase in scratch hardness value may be correlated with the variation in composition of the coatings. The EDAX and XRD results also agree with this trend. The rise of boron content and compact surface morphology must have improved the scratch hardness of Ni-B coatings like nanohardness. The boron content increased initially on Ni-B-W coatings and decreased slightly at high concentration level. The tungsten content increased with bath level for Ni-B-W coated specimens. The rise of boron as well as tungsten might have enhanced the scratch hardness of the Ni-B-W coatings like nanohardness. All the coating possesses closely packed nodular surface morphology for whole range of composition [Nemane and Chatterjee, 2020; Aydeniz et al. 2013] which is associated with morphology resembling cauliflower [Vitry and Bonin, 2017; Balaraju et al. 2016; Mukhopadhyay et al. 2018]. The nodular surface of

the coatings seemed to become more compact with bath level rise. The compact surface morphology might have prevented the penetration of stylus tip leading to gradual increase in scratch hardness with concentration level. The Ni-B-W coated specimens are seen to possess highest scratch hardness value for the whole working range. Whereas, the Ni-B-Mo coatings are found to have lowest scratch hardness value similar to nanohardness value. The inclusion of Mo into ENB makes the surface rough and cracked morphology due to high stress growth [Vitry and Bonin, 2017; Balaraju et al. 2016; Mukhopadhyay et al. 2018]. This might have lowered the scratch hardness of NBM surface.

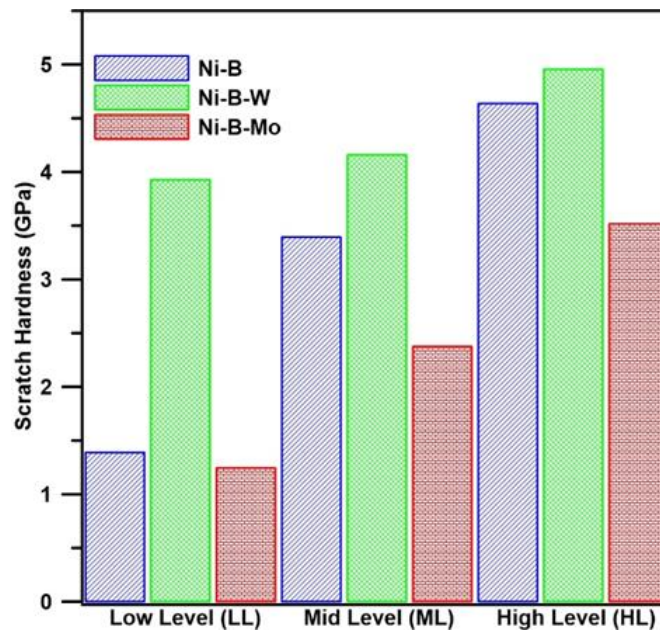


Figure 6.9: Comparative Scratch Hardness Plot

The trend observed for variation in scratch hardness value of the coatings at different levels are as follows

Ni-B-W > Ni-B > Ni-B-Mo at low-level (LL) concentration

Ni-B-W > Ni-B > Ni-B-Mo at Mid-level (ML) concentration

Ni-B-W > Ni-B > Ni-B-Mo at High-level (HL) concentration

6.5 Tribological Test

The variation of friction coefficient (COF) against sliding duration is presented in **Figure 3.11** (Chapter 3), **Figure 4.11** (Chapter 4) and **Figure 5.11** (Chapter 5),

respectively for as-deposited Ni-B, Ni-B-W and Ni-B-Mo coatings, respectively. The COF versus sliding duration plot shows that the COF value increases drastically at the beginning of the test. The friction force increases initially with time and it stables after some time. Generally, the surface roughness peaks are grinded during the sliding. The grinding of roughness peaks makes the surface smooth which leads to a comparatively stable friction. The friction coefficient plot is not smooth like a straight line as the debris comes under the sliding surface which makes friction coefficient fluctuate within a certain range. Similar pattern may be observed for all variant of coatings even though there is a difference between average COF values. The friction coefficient obtained at high level of concentrations is observed to be higher than the low and mid-level concentrations for binary and ternary coatings. Whereas, the friction coefficient plot at mid-level concentration is highest for the quaternary coatings. The increased friction coefficient may be correlated with the increased surface roughness with the increased sodium borohydride concentration [Bülbül et al. 2013; Wan et al. 2016].

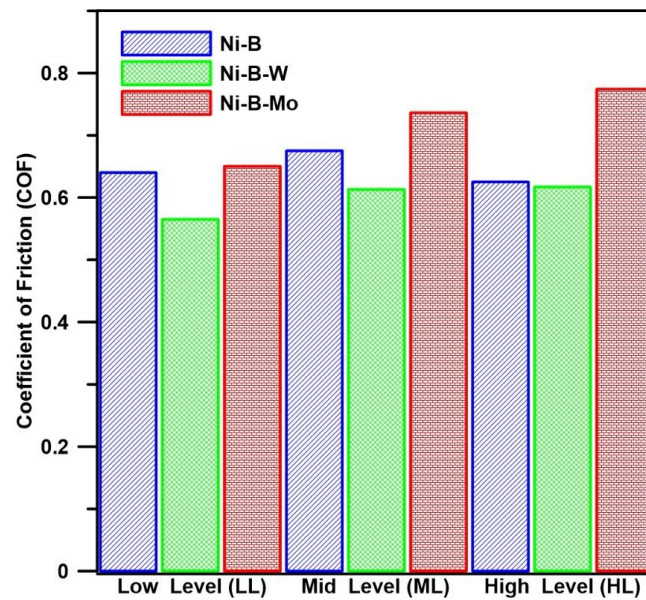


Figure 6.10: Comparative COF Plot at Various Concentration Levels

The grinded debris sometimes comes under the sliding surface and acts as load bearing element resulting a reduction in friction coefficient by reducing the actual contact surface area [Liu et al. 2013]. This may be correlated with the reduction in friction

coefficient of Ni-B-W coatings. The debris containing hard elements like tungsten may sometime entrap in-between mating surfaces and lead to higher friction coefficient value as well. The variation in average COF for the specimens coated with different types and compositions are depicted through **Figure 6.10** for comparative study. Generally, the friction coefficient increases rapidly at the beginning and then it settles down within a certain range. The initial increase in friction is possibly due to the gradual rise of friction force with the applied load. The friction force initially increases because of the breaking of roughness peaks also. After some time, the grinded debris of the coated layers may entrap in-between the sliding surfaces and the sliding friction is converted to rolling friction leading to reduction in COF value. The grinded debris acted as load bearing element. The entrapment of grinded debris in-between sliding surface may also result in unprecedented change in COF value. The COF value initially increases which gets stable after some time possibly due to the conglomeration of worn-out debris beneath the sliding surface and smoothening the surface. The wear debris acted as load bearing surface and smoothening of mating surfaces lead to reduction in COF value relative to initial rise. The average COF value calculated at different bath level concentration is presented separately in **Figure 6.10** to make a comparison of COF values. The uncoated substrate is also tested for tribological behaviour under same test conditions. The average coefficient of friction for the uncoated substrate is found to be 0.63 which is higher than the COF value for the Ni-B-W coated specimens within the working range. The COF value of Ni-B coated specimen is higher than uncoated substrate except at high level of concentration. Whereas, the COF value of Ni-B-Mo coated specimens are higher than substrate throughout the working range.

The trends of average COF values for different coatings at different levels are as follows

Ni-B-Mo > Ni-B > Ni-B-W	at Low Level Concentration
Ni-B-Mo > Ni-B > Ni-B-W	at Mid-Level Concentration
Ni-B-Mo > Ni-B > Ni-B-W	at High Level Concentration

In **Figure 6.10**, the Ni-B-Mo and Ni-B coated specimens are seen to possess almost same COF value at low level concentration. While, Ni-B-Mo possesses highest

COF value within the working range. The Ni-B-Mo coated specimens are known to possess coarse grained and cracked surface which led to highest Ra value compared to other variants. The higher Ra value ultimately leads to higher COF value in-between sliding surfaces. Addition of Mo with ENB coating led to crack formation due to high stress growth and coarse morphology which is the reason for high friction coefficient [Agrawal and Mukhopadhyay, 2022]. The coefficient of friction value of Ni-B-Mo coated surface is the highest, followed by Ni-B and Ni-B-W coated surfaces obtained at low and mid level of concentrations. The coated surface becomes rough with the increased borohydride concentration for Ni-B coatings but it remained slightly lower compared to Ni-B-Mo. The inclusion of tungsten alone into Ni-B matrix i.e., Ni-B-W makes the surface compact and harder. The compact surface morphology and better plastic deformation behavior of Ni-B-W coatings might have reduced the COF value compared to other two variant coatings upto mid-level. The rise of friction coefficient may also be correlated with the adhesiveness of coated surface and the accumulation of wear debris in the wear track. The coefficient of friction value of Ni-B-Mo coated surface remained highest even at high level concentration, followed by Ni-B and Ni-B-W, respectively.

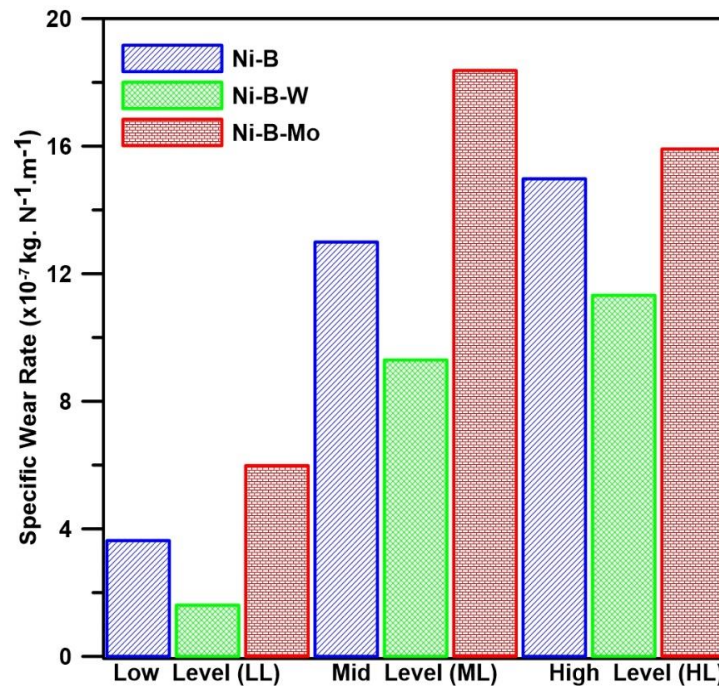


Figure 6.11: Comparative Specific Wear Rate Plot

The specific wear rate of the uncoated substrate is also determined using mass loss method. The wear rate of the uncoated substrate is found to be 13.273×10^{-7} Kg/N.m. The wear rate of the uncoated substrate is higher than the Ni-B-W coated specimens throughout the working range. The wear rate is usually low for the surfaces with higher surface hardness [Madah et al. 2015]. The wear rate under current study agrees well with the surface hardness behaviour of the coatings. The Ni-B coated specimens found to possess better wear resistance upto mid-level than uncoated substrate. The Ni-B-Mo coated specimens possess higher wear rate than uncoated substrate as well as other coating variants.

The summary of wear rate trend is given as

Ni-B-Mo > Ni-B > Ni-B-W	at Low Level Concentrations
Ni-B-Mo > Ni-B > Ni-B-W	at Mid-Level Concentrations
Ni-B-Mo > Ni-B > Ni-B-W	at High Level Concentrations

The specific wear rate plots are displayed in **Figure 6.11**. The wear rate of Ni-B coatings is increased with bath level due to higher surface roughness and crushing of roughness peaks. The Ni-B-Mo coated surfaces possess cracked morphology which raised the Ra value ultimately leading to higher wear rate. The wear rate of Ni-B-Mo is even higher than Ni-B coatings across the examined range. Generally, the surface roughness of borohydride reduced coatings is observed to rise with reduction rate due to increase in borohydride concentration [Vitry and Bonin, 2017]. The roughness asperities are broken and ground down at the time of sliding of tribo pin against counter surface leads to a rise in wear rate. The incorporation of W with ENB makes the coated surface compact and hard ultimately leading to the lowest wear rate at low level concentration. The cracked morphology and segregated nodules of Ni-B-Mo coatings propagates the crack which raises the wear rate. The high adhesive force of repetitive loading-unloading during the sliding of mating surfaces aggravated the wear rate of Ni-B-Mo coated surface further. The wear rate of Ni-B-Mo Coatings is found to be the highest throughout the working range.

The wear mechanism of the Ni-B coatings may be understood from the SEM images displayed in **Figure 6.12(a)**, **Figure 6.13(a)** and **Figure 6.14(a)** in which the

wear debris are observed in the wear tracks. Some pits and prows may also be seen from and the coatings are removed by patches in some cases [Madah et al. 2015; Mukhopadhyay et al. 2018]. These are the indication of adhesive type wear mechanism. Similar wear mechanism is also reported in earlier studies [Madah et al. 2015; Mukhopadhyay et al. 2018].

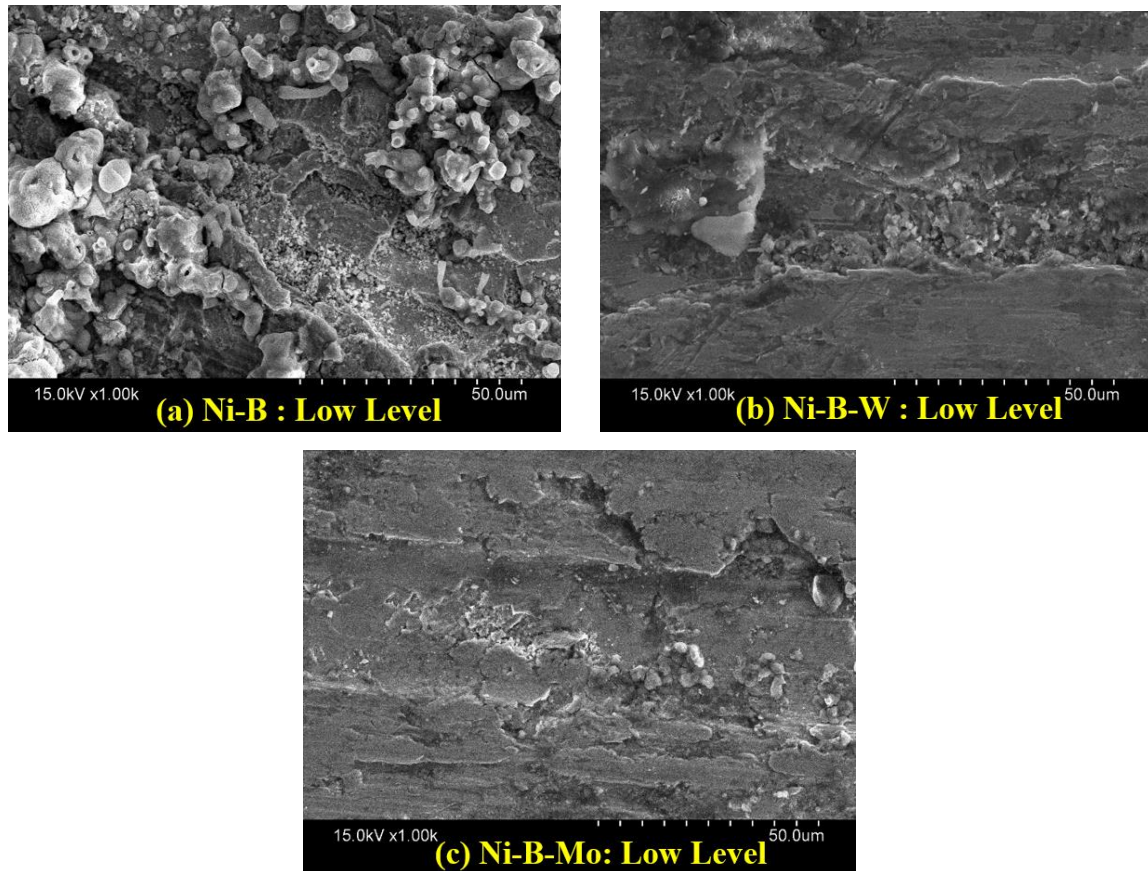


Figure 6.12: SEM Image of Worn-out Surface of As-deposited Coatings Obtained at Low Level Concentrations of (a) Ni-B, (b) Ni-B-W and (c) Ni-B-Mo

The SEM images of worn-out surfaces of Ni-B-W coatings are displayed in **Figure 6.12(b)**, **Figure 6.13(b)** and **Figure 6.14(b)**. The worn-out surfaces reveal that some of the nodules crushed, grinded and some debris remained to be undeformed. This indicates that the coated surface possesses high hardness, good resistance to plastic deformation and high wear resistance [Mukhopadhyay et al. 2018]. The nodules are observed to be crushed and smeared on the worn surface. **Figure 6.13** represents some

grooves formed over the worn-out surface which is formed by the undeformed debris during the sliding test. The undeformed debris might have made the surface coarse and raised the COF value [Mukhopadhyay et al. 2018; Mukhopadhyay et al. 2018]. The undeformed wear debris also bears the load and reduces the wear rate. The worn-out surface exhibits plastic deformation with some shallow scratches in sliding direction.

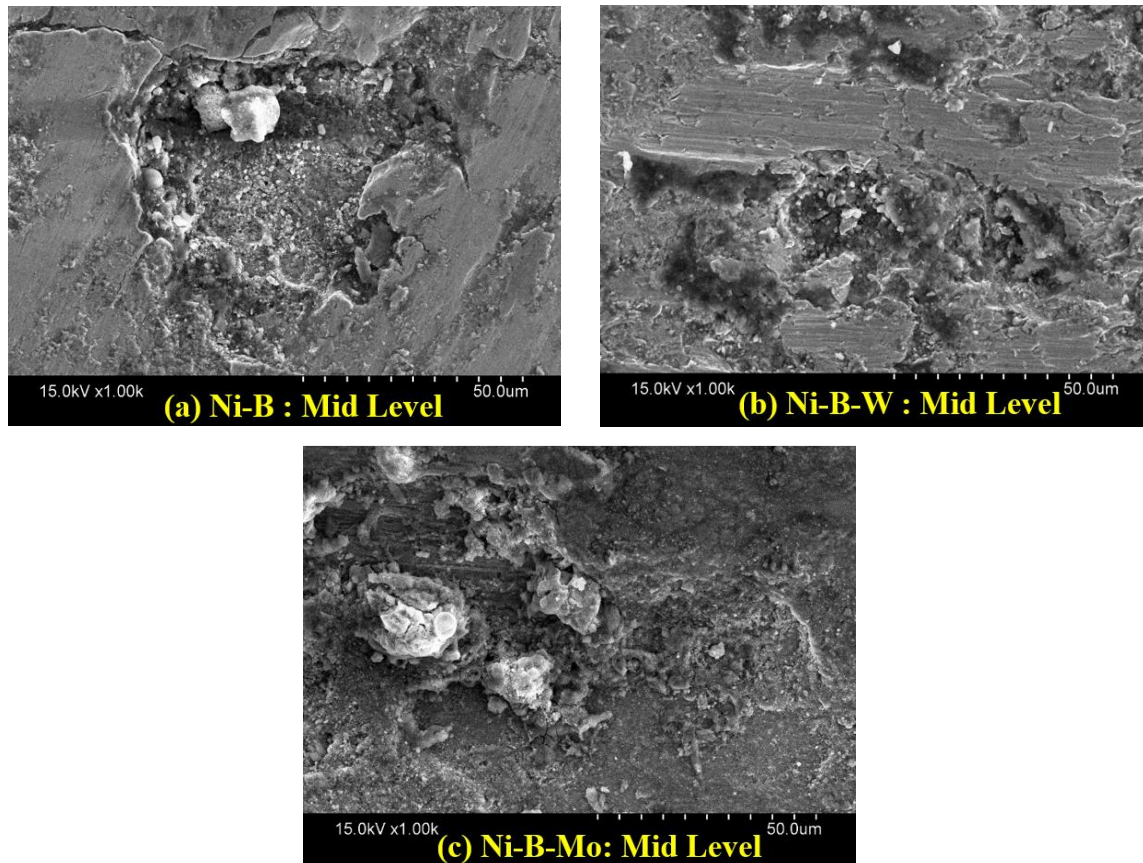


Figure 6.13: SEM Image of Worn-out Surface of As-deposited Coatings Obtained at Mid-Level Concentrations of (a) Ni-B, (b) Ni-B-W and (c) Ni-B-Mo

Besides, some debris are also found to be pressed on the worn surface which shows the adhesiveness of the coatings leading to increase the COF value further. The worn-out surfaces of Ni-B-Mo coatings are presented in **Figure 6.12(c)**, **Figure 6.13(c)** and **Figure 6.14(c)**. It indicates that the surfaces are severely damaged throughout the working range. The nodules formed during the crushing of asperity peaks may be observed to spread over the wear track. The wear cutting as well as delamination of

coatings may be observed which is formed by the strain hardened debris during sliding [Yildiz et al. 2013; Radwan et al. 2015; Arias et al. 2019] leading to higher wear rate. The worn-out surface also possesses some wear cracks due to repetitive loading during sliding and high stress growth. The cracks propagate during the repeated loading which leads to higher wear rate. This type of wear indicates the abrasion type of wear mechanism. On the other hand, some of the coated layers are delaminated during the tribo test which is clearly visible in the **Figure 6.12(c)**, **Figure 6.13(c)** and **Figure 6.14(c)**. This type delamination is the indication of adhesive type wear mechanism. Therefore, the Ni-B-Mo coated layers are worn-out during the tribo test by abrasive and adhesive type of wear mechanism [Miri et al. 2021; Mukhopadhyay et al. 2018].

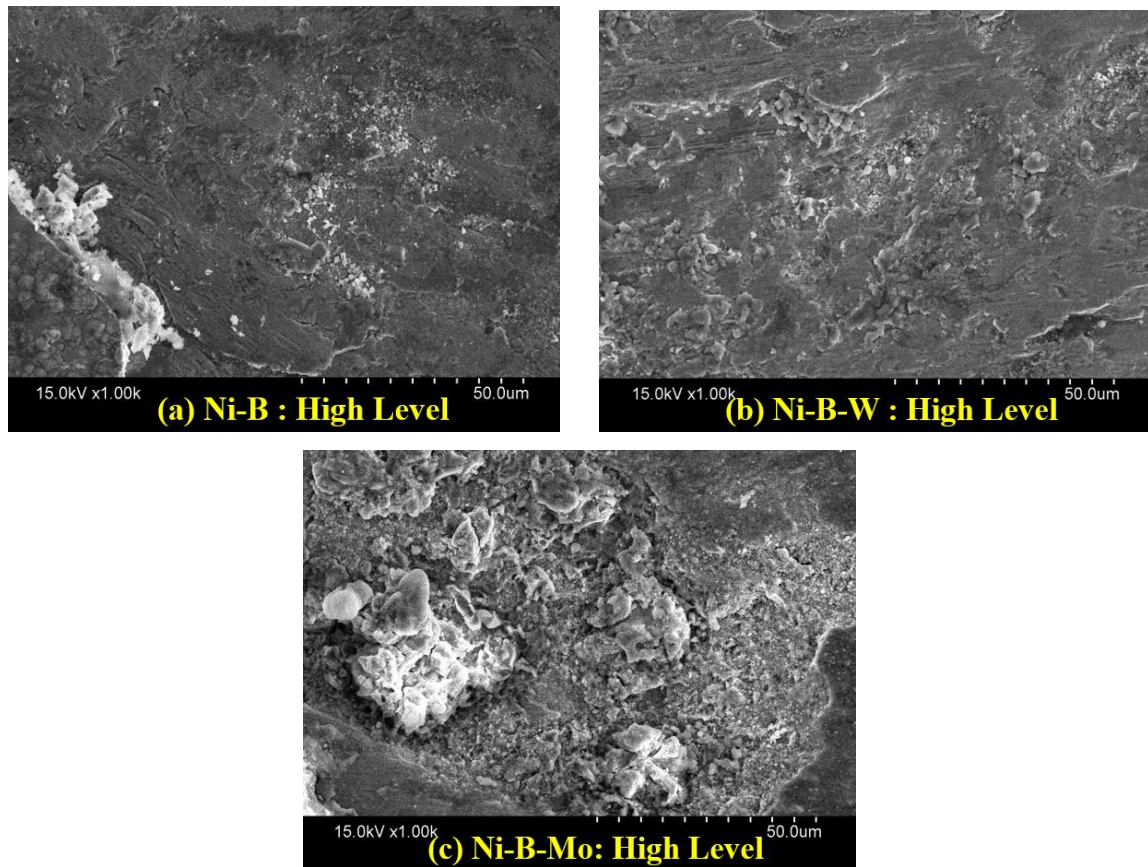


Figure 6.14: SEM Image of Worn-out Surface of As-deposited Coatings Obtained at High Level Concentration of (a) Ni-B, (b) Ni-B-W and (c) Ni-B-Mo

All the worn-out surfaces are further studied through elemental analysis. The chemical composition of the worn-out surfaces is presented in **Figure 6.15**, **Figure 6.16** and **Figure 6.17** for Ni-B, Ni-B-W and Ni-B-Mo, respectively. The presence of the peaks for major coating elements are observed in the EDAX spectrums which confirms their presence in the coated surface. The peaks of Fe and O may be seen along with major elements, but the concentration of Fe and O is very less in most cases. This confirms that the coated layers are not removed completely during tribo test [Mukhopadhyay et al. 2019; Madah et al. 2015; Mukhopadhyay et al. 2018].

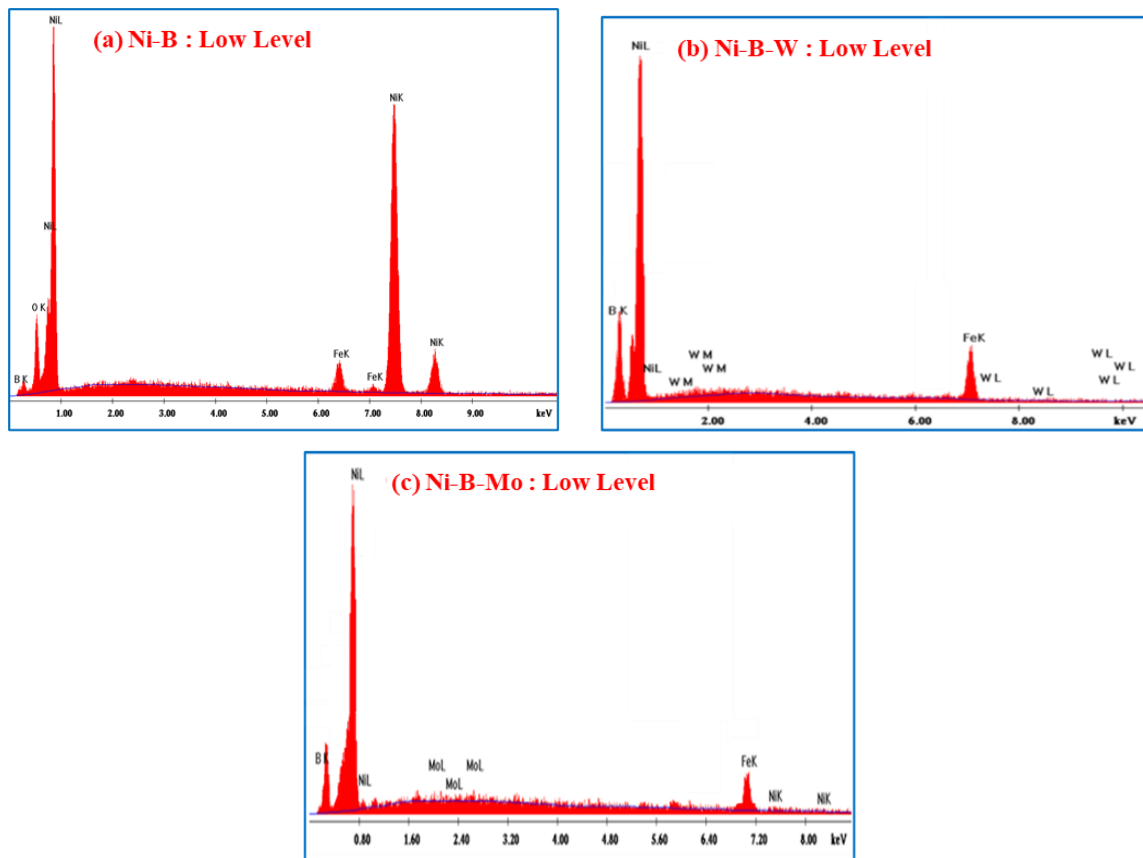


Figure 6.15: EDAX Spectrum of Worn-out Surface of As-deposited Coatings Obtained at Low Level Concentrations of (a) Ni-B, (b) Ni-B-W and (c) Ni-B-Mo

But EDAX spectra of some coatings are also observed to possess few broad peaks of Fe which indicates the presence of large amount of Fe on the worn-out surface. There are some Fe peaks in the EDAX spectrum of the worn-out surfaces of Ni-B-W coatings as well [Correa et al. 2013; Agarwal and Mukhopadhyay, 2022]. The addition of

tungsten into Ni-B matrix leads to a compact surface morphology which leads to an increase in surface hardness. Generally, the coatings with higher surface roughness exhibits lower wear rate [Madah et al. 2015]. The higher surface hardness of as-deposited Ni-B-W coatings may be correlated with the lower wear rate of it. But the debris formed during the sliding contains some hard elements. The hard elements may have entrapped in-between counter surface and the substrate surface.

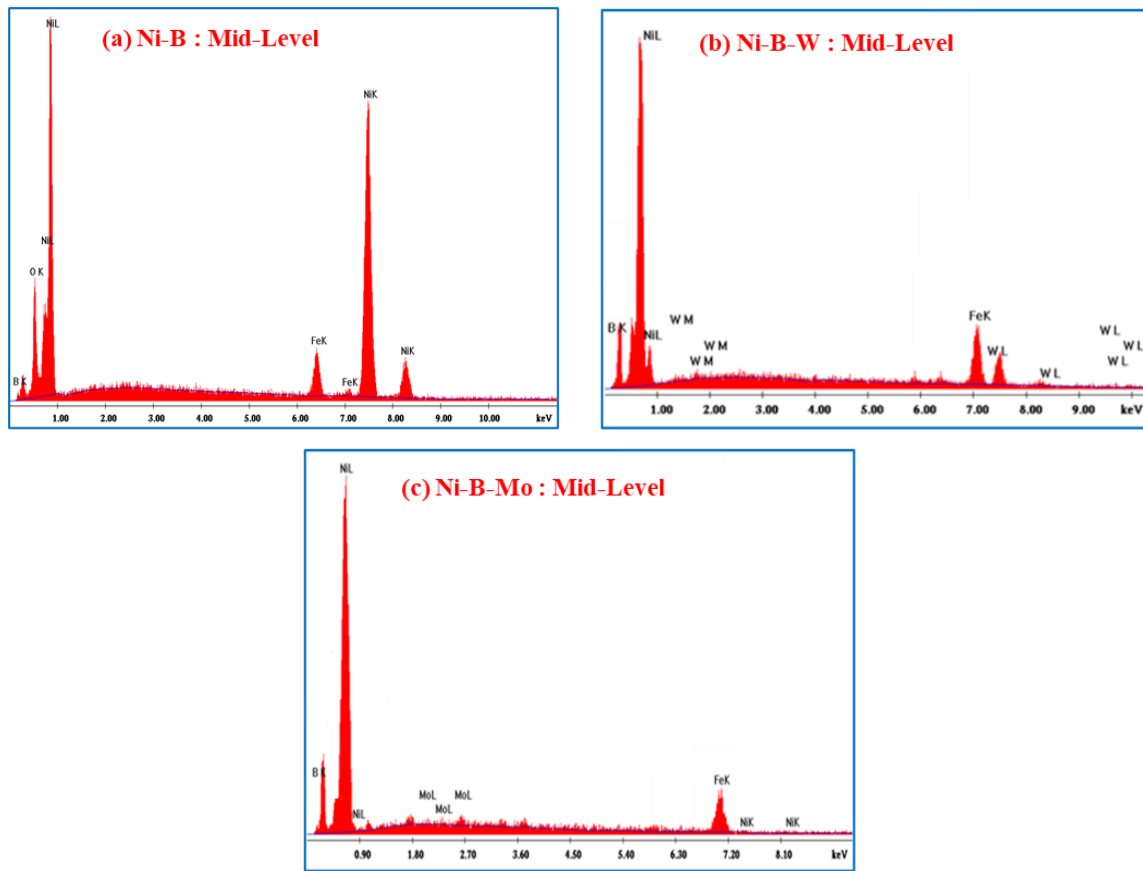


Figure 6.16: EDAX Spectrum of Worn-out Surface of As-deposited Coatings Obtained at Mid-Level Concentrations of (a) Ni-B, (b) Ni-B-W and (c) Ni-B-Mo

The entrapped hard elements are pressed in the substrate surface which might have helped the delamination of coated layers and formed some patches during the sliding. The hard elements might have also removed some portion of the substrate to form wear patches. The portions removed from the substrate are expected to contain Fe which might be the reason for the broad peaks of Fe in the EDAX spectrum. On the other hand, the addition of molybdenum into the Ni-B matrix leads to formation of rough

surface or cracked surface due to high stress growth. The grinding of roughness peaks leads to higher wear rate. The cracked surface morphology may also promote the higher wear rate of the coatings. The worn-out surface appears to possess some delamination or patches formed by the adhesive type of wear mechanism during the repetitive loading unloading at a load of 40 N. The coating layers are expected adhere to the substrate. But the coatings are possibly delaminated during the loading unloading and some of the substrate's patches are removed with delaminated layers. Those patches may be the reason for the Fe peaks present in the EDAX spectrum. The current wear trend of wear rate is in collinear with the surface roughness trend.

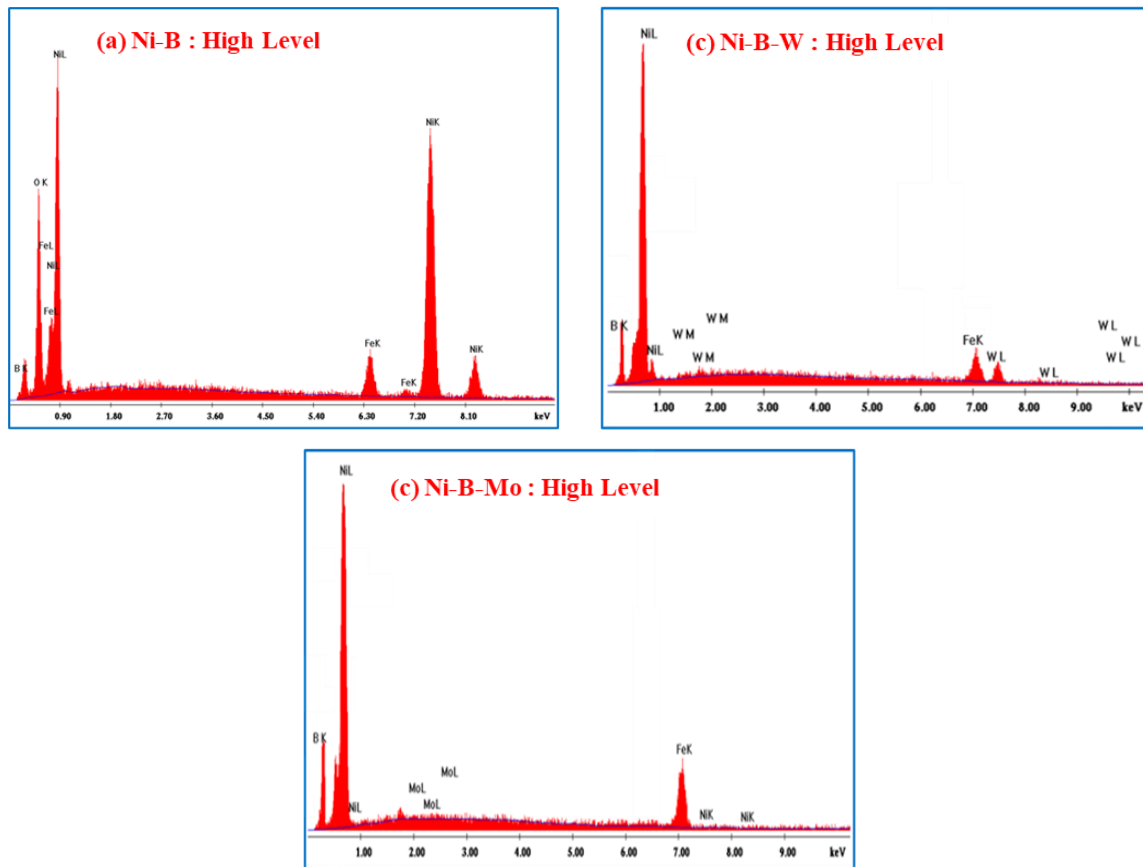


Figure 6.17: EDAX Spectrum of Worn-out Surface of As-deposited Coatings Obtained at High Level Concentrations of (a) Ni-B, (b) Ni-B-W and (c) Ni-B-Mo

The surface hardness of the as-deposited Ni-B-Mo coatings are lower than the other variant of coatings. The lower surface hardness may also be a reason for the higher wear rate of as-deposited Ni-B-Mo coatings. The above-mentioned reason may be one of

reason for the presence of Fe peak in the EDAX spectrum. The second one may be due to the lower coating thickness. The coating thickness of all variants are low at lower concentration level. The coating thickness at the worn-out region is decreased largely even for coatings obtained at high level concentration also at certain regions by wearing action during the sliding and hence the final thickness may be very less on those regions. The coating in the other regions is not completely removed or delaminated. The EDAX analysis method is direct and affected by coating thickness as well as surface roughness [Correa et al. 2013; Mukhopadhyay et al. 2018]. Therefore, this may be another reason for the presence of Fe peak in the EDAX spectrum which is also reported in previous studies [Agarwal and Madah et al. 2015]. The third one or lastly, the Fe peaks observed might appeared due to the debris formed from the counter surface and accumulated into the worn-out surface of the coated specimens.

6.6 Corrosion Resistance Test

The corrosion resistance tests are carried out through EIS and PDP test. The equivalent circuit diagram for EIS test is presented in **Figure 2.22** (Chapter 2). **Figure 2.22(a)** shows the equivalent circuit diagram (ECD) which is suitable for ideal behaviour where single time constant is visible in nyquist plot. The equivalent circuit diagram presented in **Figure 2.22(b)** is suitable for non-ideal cases where two-time constants are visible in nyquist plot. The CPE_{dl} is incorporated into the ECD and it may be utilised for modelling of non-ideal double layer capacitance. The plots are generated using the software provided with the test setup. The tafel plot is obtained from the PDP test and the nyquist plot is obtained from the EIS test. The software uses the data collected in the computer to generate the nyquist plot considering imaginary impedance on the y-axis and real impedance on the x-axis. The bigger semicircle of nyquist plot represents the better corrosion performance of coatings [Miri et al. 2021; Mukhopadhyay et al. 2018] and lower negative value of corrosion current potential (E_{corr}) acquired using tafel plot indicates the improvement in corrosion performance of the coated layers [Anik et al. 2008; Kanta et al. 2010; Kanta et al. 2009]. The performance of coated layers against corrosion is also found to depend on its morphology and phase structure [Kanta et al. 2010; Kanta et al. 2009]. An increment in R_{ct} value obtained from nyquist plot indicates

the improvement in corrosion performance [Anik et al. 2008; Kanta et al. 2010; Kanta et al. 2009]. Corrosion resistance of coatings is found to depend on various factors like surface porosity, microstructure, heterogeneities, columnar growth, phase structure etc. [Yildiz et al. 2013]. The ENB coated layers are found to prevent the steel substrate against corrosion [Bülbül et al. 2013].

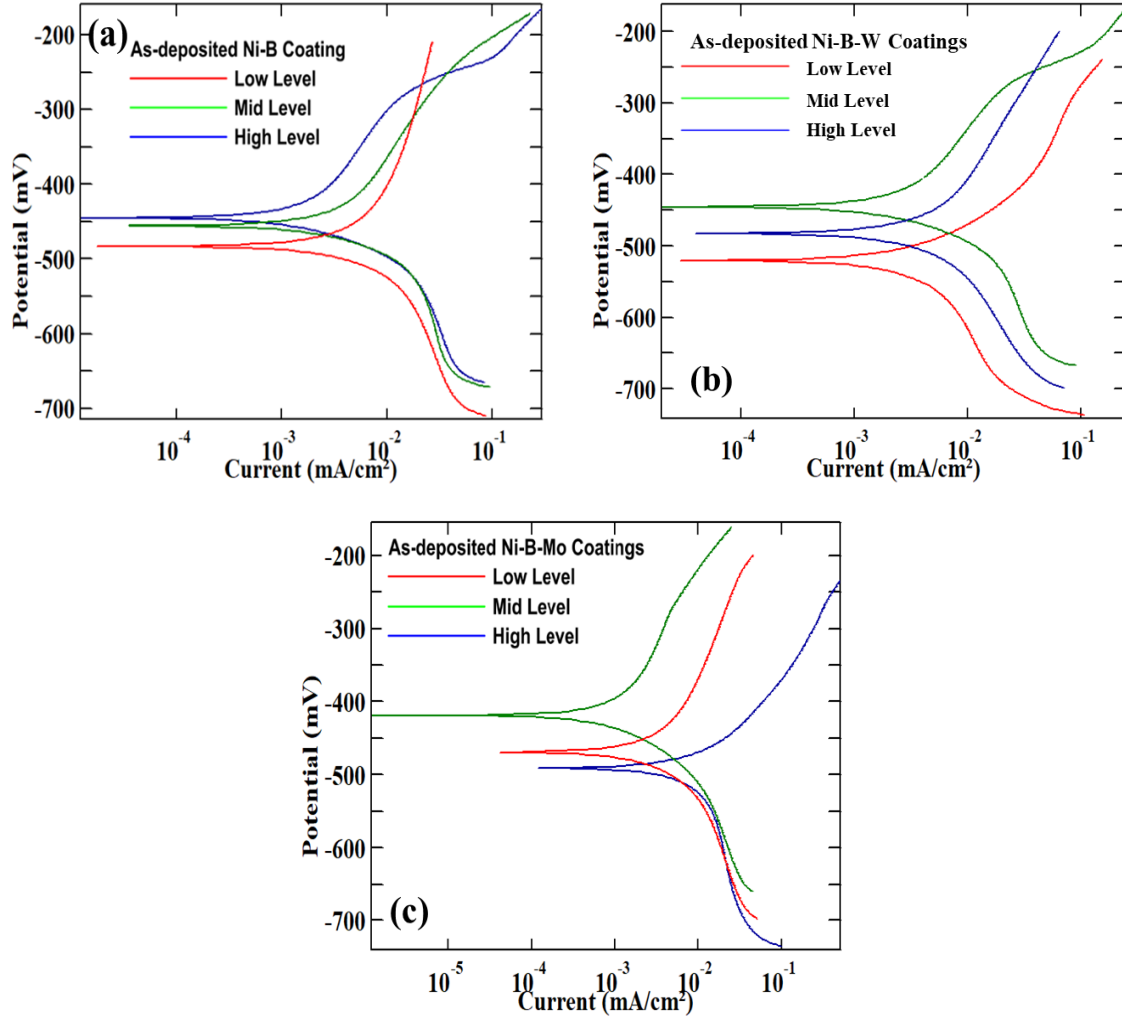


Figure 6.18: Tafel Plot for As-deposited (a) Ni-B, (b) Ni-B-W and (c) Ni-B-Mo Coatings

Figure 6.18 represent the tafel plots obtained for different coatings at different levels. The nyquist plot of the same coatings are displayed in **Figure 6.19**. It may be found from **Figure 6.18(a)** that the negative E_{corr} value is decreased with coating bath

concentration level. The semi-circle loop in **Figure 6.19(a)** also becomes bigger with coating bath concentration level. Therefore, the corrosion resistance of Ni-B coated specimens is increased with bath level. The boron concentration raised with NaBH_4 concentration which ultimately improved the corrosion resistance of Ni-B coated layers [Vitry et al. 2012]. The corrosion resistance of Ni-B coated specimens is seen to improve with boron. The Ra value of the Ni-B coated specimens is raised with borohydride concentration. Generally, the rougher surface is suitable for the corrosive medium to penetrate. But, in this case the higher boron content might have made the surface compact and prevented the corrosive solution to penetrate and improved the corrosion resistance. Hence, the both characterisation and corrosion test results may be correlated with each other. It may be observed from **Figure 6.18** and **Figure 6.19** that the corrosion performance of all variants is enhanced till mid-level concentration. The corrosion test also suggests the same trend. The common observation from the characterisation also suggests that the raised boron concentration is the reason for this improvement in corrosion resistance. Another common trend in characterisation is observed that the coatings possess amorphous-crystalline phase at low level concentration. The same phases are observed to have a tendency to transform towards the amorphous phase at mid-level concentration. The amorphous phase is familiar for better corrosion behaviour compared to crystalline phase [Anik et al. 2008]. Therefore, the rise of boron concentration as well as amorphous phase of the coatings may be the reason for this improvement in corrosion resistance. The corrosion resistance of Ni-B-Mo coated specimens is found to be highest till mid-level concentrations followed by Ni-B and Ni-B-W. The corrosion resistance of Ni-B coated specimens is highest at high level concentration and NBW coatings remained at lowest throughout the working range. The corrosion performance of Ni-B-W coated specimens improved till mid-level concentration with boron content and it is found to decrease as boron content decreased at high level. Therefore, it may be correlated with the variation in boron content. While, the corrosion resistance of Ni-B-W coatings remained low relative to Ni-B. The same trend may be observed in earlier studies as well [Aydeniz et al. 2013]. The surface becomes rough with the addition of Mo in the borohydride reduced electroless coating which is known to deteriorate the corrosion resistance of coating [Dominguez-Rios et al. 2012].

But still the NBM coatings show better corrosion behaviour till mid-level concentration possibly due to increasing trend of boron content till mid-level concentration.

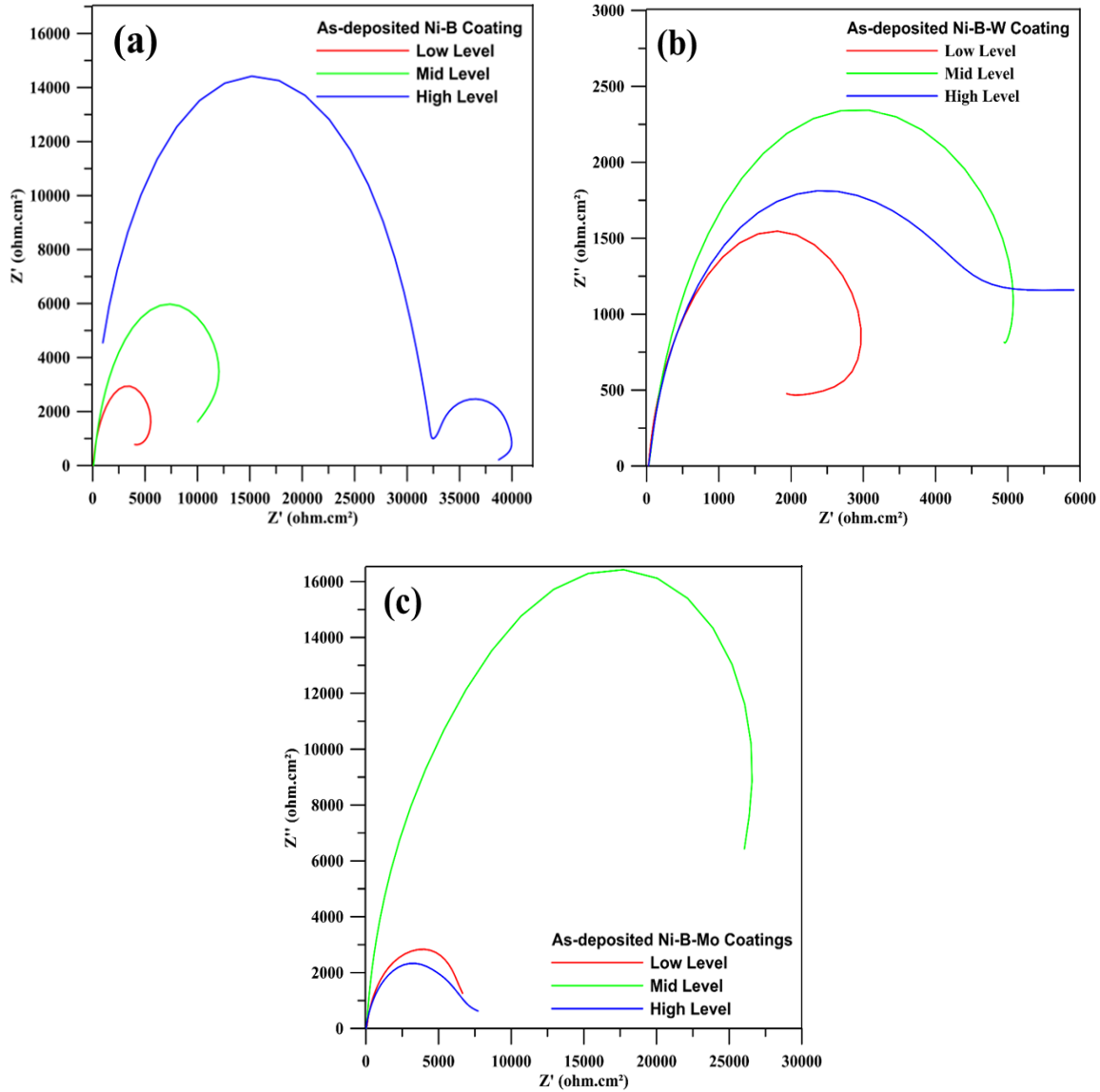


Figure 6.19: Nyquist Plot for As-deposited (a) Ni-B, (b) Ni-B-W and (c) Ni-B-Mo Coatings

Similar trend of higher corrosion resistance may also be seen in earlier articles as well [Serin et al. 2015; Niksefat et al. 2015; Georgiza et al. 2017]. But the corrosion resistance of NBM coated specimens at HLC concentration might have decreased due to the rise in Mo content.

The comparative trend of corrosion resistance of the coated specimens are as follows

Ni-B-Mo > Ni-B > Ni-B-W	at Low Level Concentrations
Ni-B-Mo > Ni-B > Ni-B-W	at Mid-Level Concentrations
Ni-B > Ni-B-Mo > N-B-W	at High Level Concentrations

The substrate underwent corrosion test are further analysed through SEM. The SEM images of the corroded substrates of Ni-B, Ni-B-W and Ni-B-Mo at various concentrations are displayed in **Figure 3.17** (Chapter 3), **Figure 4.17** (Chapter 4.17) and **Figure 5.17** (Chapter 5), respectively. All the corroded surfaces are observed to possess corrosion byproducts deposited over the substrate surface. The accumulation of the corrosion byproducts over the substrate confirms the corrosion attack of the corrosive electrolytes. The SEM images of Ni-B coated surface displayed in **Figure 3.17** and obtained at low level concentration are found to be mostly affected by the corrosion attack and it decreased with bath level increase. This agrees well with the EIS and PDP test results. The corrosion attacks are possibly remained till the outer layers only and only some localised corrosion attacks occurred by the electrolytes which might have penetrated through grain boundaries [Serin et al. 2015; Mukhopadhyay et al. 2018]. The corroded surfaces of Ni-B-W and Ni-B-Mo, presented in **Figure 4.17** and **Figure 5.17**, respectively are also affected by some local corrosion attacks only. **Figure 4.17** also shows Ni-B-W coatings to possess the corrosion compound at its surface in all three level which indicates the penetration of corrosive medium through the grain boundaries [Serin et al. 2015; Mukhopadhyay et al. 2018]. The lower corrosion resistance may be correlated with the decreased boron content as well as the presence of crystalline structure in low and high level of concentrations. **Figure 5.17** shows the corroded surface of NBM coatings deposited at mid-level concentration and it is least effected. The substrate deposited with high level concentration is found to be worst affected. The boron content is increased with level of concentration for Ni-B-Mo coatings which might have led to an improvement the corrosion resistance of Ni-B-Mo coated specimens till mid-level concentration. The phase structure modification from nanocrystalline-amorphous mixture to amorphous may be another reason for this rise. The boron content is increased

further with negligible amount but Mo content increased considerably at high level concentration. The increased amount of Mo content in the coatings makes the surface rough forming some crack or prominent grain boundaries might have created some corrosion attack zone. Those corrosion attack zone might have allowed the electrolytes to penetrate and lead to a reduction in corrosion performance of Ni-B-Mo coated specimens at high level concentration. The corrosion performance of electroless coatings is seen to vary with phase structure as well as surface morphology [Mukhopadhyay et al. 2018; Yazdani et al. 2019]. The nano-crystalline phases are seen to be more corrosion sensitive compared to amorphous phase [Bülbül et al. 2013; Anik et al. 2008; Hamid et al. 2010]. The phase structure of the borohydride reduced coatings also transformed from amorphous-nano-crystalline to amorphous phase structure. It may be another cause of this improvement against corrosion resistance. Therefore, the EIS and PDP test results agrees well with the characterisation results.

6.7 Closure

This chapter contains a comparative study of the borohydride reduced electroless binary and ternary coatings. The suggests that all the coatings under study possess a cauliflower like surface morphology. The coatings may be used to develop smooth surface at lower concentration levels or till mid-level concentrations for certain cases. The amount of major coating elements increased with increased concentration levels of coating bath parameters which contribute to increase the indentation hardness as well as scratch hardness. But the friction coefficient is found to be quite high. But, it is lower than substrate material. On the other hand, high hardness of the coatings leads to an improvement in wear resistance of the coatings except for Ni-B-Mo coatings. The resistance of all variant of coatings increased with coating bath concentration level till mid concentration and it deteriorates upon further rise in concentration level. However, the corrosion resistance behaviour of electroless Ni-B-Mo coatings is found to be better than other variants.

This page is intentionally left blank

Chapter 7: Conclusion and Future Scope

Outline: 7.1. Conclusions, 7.2 Future Scope

7.1 Conclusions

The current study envisages the significance of incorporation of hard particles like tungsten and molybdenum at different concentrations on tribo-mechanical behaviour of electroless nickel based borohydride reduced coatings. Steel substrates are coated using binary and ternary coatings with varying coating bath compositions. The coated specimens are then characterised and tested for different mechanical and tribological tests to understand the impact of those bath element concentrations. The coated specimens are also tested for corrosion resistance. Finally, an attempt has been made to correlate the test results and the following conclusions are drawn from the investigation results.

Electroless Ni-B Alloy Coating

- The coated layer thickness of the electroless Ni-B coatings is increased with the coating bath concentration level. The sodium borohydride increased with bath concentration level which might have accelerated the chemical reaction process and ion reduction ultimately resulting an improvement in coating thickness.
- The surface morphology of the as-deposited coatings is found to be cauliflower like appearance while the grain size of the as-deposited coatings is seen to increase with coating bath concentration level due to increase in sodium borohydride concentration.
- The phase structure of as-deposited Ni-B coatings is seen to depend on boron content. Amorphous and nano-crystalline structure are found to co-exists in as-deposited coatings obtained from low borohydride content coating bath solution which transforms into amorphous structure upon increase in borohydride concentration. This change in phase structure can be attributed with the increase in boron content with NaBH_4 .

- The boron content in the coating is increased with reduction rate due to increase in NaBH_4 concentration and coating bath temperature. The reduction rate increases with rise in NaBH_4 concentration as well as coating bath temperature.
- The increase in boron content due to rise in reduction rate leads to an increase in surface roughness whereas the same is found to decrease with increase in nickel chloride and temperature as the nickel might have smoothened the coated surface.
- The increased surface roughness leads to a rise in COF value. The specific wear rate also increases due to grinding and crushing of roughness peaks during sliding of pin over the counter surface.
- The increase in boron content with sodium borohydride also leads to an increase in surface hardness and scratch hardness. This improvement of surface hardness as well as scratch hardness is possibly due to rise in boron content.
- The increase in bath parameter concentration leads to an improvement in corrosion resistance of as-deposited coatings as well. The increased boron concentration in the coating might have transformed the phase structure from mixture of nano-crystalline and amorphous to amorphous structure which also might have improved the corrosion resistance of electroless Ni-B coatings.

Electroless Ni-B-W Alloy Coatings

- The electroless Ni-B-W coating thickness is increased with the coating bath concentration. The NaBH_4 acts as reducing agent which extracts the metal ions. Hence, the increase in NaBH_4 concentration accelerates the reduction rate and improves the coating thickness with bath concentration level.
- As-deposited electroless Ni-B-W coatings are found to possess compact and uniform surface morphology with closely packed nodular surface within the working range. The coating thickness is observed to increase with bath level concentration.
- The boron and tungsten content are found to increase with bath concentration level which leads to an increase in surface hardness obtained from nano-indentation technique and scratch hardness measured from micro-scratch test. The

compact surface morphology of the coatings also may be a possible reason for the increase in surface hardness.

- The surface roughness of the Ni-B-W coated surface is observed to become 0.185 μm at low concentration of NiBH_4 which is smoother than the substrate having surface roughness of 0.285 μm . The same surface becomes rougher with the increase in NiBH_4 concentration. The addition of sodium tungstate makes the rougher than substrate but it does not vary much with the variation of sodium tungstate.
- The COF of the Ni-B-W coated layer slightly decreases from 0.628 to 0.520 with nickel chloride concentration in the solution which agrees well with the surface roughness trend. The increasing trend of surface roughness with sodium borohydride leads to an increase in COF value from 0.423 to 0.680 within the working range. The COF value also increases slightly from 0.558 to 0.754 with sodium tungstate concentration.
- The corrosion resistance of Ni-B-W coated specimen is also increased from low to mid concentration levels and the same is decreased with further rise in concentration level. The increased surface roughness with tungsten content may be a possible reason for this decrease in corrosion resistance.

Electroless Ni-B-Mo Alloy Coatings

- The electroless Ni-B-Mo coated layer thickness is seen to improve with coating bath level. The concentration of reducing agent increased with bath level and the increased reducing agent accelerates the deposition rate due to accelerated chemical reaction rate.
- The electroless Ni-B-Mo coatings are seen to possess a cauliflower like surface morphology like other borohydride reduced electroless coatings. The coated surface at low concentration possesses a cracked and rough morphology due to high stress growth.
- The EDAX result shows an increase in molybdenum content with increased bath level. The increased molybdenum does not impact the boron content and the boron content is also seen to increase with bath concentration. This increase in

boron and molybdenum leads to an reduction in nickel content in the electroless Ni-B-Mo coatings.

- The average surface roughness of the Ni-B-Mo coated specimens does not change much with the variation of NiCl_2 . It increases with the increase in sodium borohydride concentration as the reduction rate increases with sodium borohydride concentration. The increase in molybdenum concentration accelerates the rough and coarse grain surface formation which results in high roughness value.
- The surface hardness of the coated specimens is observed to improve with nickel chloride because of compact and smoothening of surface while the same increases due to higher boron content in the coated specimens with the higher concentration of sodium borohydride. But the surface hardness decreases with the increased molybdenum concentration due to rough and coarse-grained surface morphology. Similar, trend may also be observed for scratch hardness.
- The addition of molybdenum accelerates the formation of rough and coarse grain surface morphology but the COF value is observed to reduce due to rise in NiCl_2 possibly because of smoothening of surface. The COF value increases with the rise in NaBH_4 and molybdenum concentration in the coatings following the surface roughness trend. The wear rate is also observed to rise with sodium borohydride and sodium molybdate concentration.
- The corrosion resistance of Ni-B-Mo coated surface is seen to increase with bath concentration from low to mid concentration and it decreased upon further rise in concentration level. The increase in corrosion resistance possibly due to the increase in boron content but the higher concentration of molybdenum decreased the corrosion resistance at high level of concentration.

Comparison of Electroless Ni-B, Ni-B-W and Ni-B-Mo Alloy Coatings

- All the coatings possess minimum coating thickness at low level of concentration. The coated layer thickness increased with further rise in coating bath level. This rise in coating thickness may be correlated with the increase in sodium borohydride concentration with the coating bath level. In this case, the sodium

borohydride dominated the reduction reaction and corresponding rise in coating thickness.

- The Ni-B and Ni-B-W coated surface appears to be smooth and bright till mid level concentrations while surfaces become dark and rough in appearance at high level. All the surfaces are seen to exhibit cauliflower like morphology in as-deposited condition and a uniform dispersion of nodules may also be observed over the coated surface. The Ni-B-Mo coated surface appears to possess a cracked and rough surface morphology at low level concentration due to high stress growth.
- The elemental analysis (EDAX) of the coatings confirms a rise in boron content with concentration level for all variant of coatings except for Ni-B-W at high level of concentration. This decrease in boron content of Ni-B-W coatings at high level is possibly due to co-deposition of tungsten with ENB. But, the addition of Mo with ENB does not affect much in boron concentration but it remained to be lower than the boron content in electroless Ni-B coatings.
- All variant (under study) of coated specimens possesses a sharp peak with a hump which is meant to be the presence of crystalline-amorphous phase at low level concentration. The same crystalline peak diminishes with rise in concentration level and phase structure transform into amorphous phase for all variant of coatings with the rise in boron content. The W and Mo also prevents nuclei formation and assists the amorphous phase formation which is also a reason for phase transformation.
- The average surface roughness (Ra) value of the coated specimen tends to increase with bath concentration. The Ni-B-Mo coatings exhibit the highest roughness, attributed to both the elevated borohydride concentration and the inclusion of molybdenum. The presence of molybdenum encourages stress development leading to crack propagation resulting rougher surface.
- The nano-hardness as well as scratch hardness value of the coatings are seen to increase with bath level concentration due to increase in boron, tungsten and molybdenum like hard particles. The Ni-B-W coatings are seen to possess highest scratch-hardness value for the complete working range and highest nano-hardness

throughout the working range. The stress growth and crack formation due to Mo addition into Ni-B matrix leads to lowest the nano-hardness and scratch hardness value for the coatings under study.

- The elastic modulus of all variant of coated specimens are observed to rise with concentration level except for the Ni-B-Mo coated specimens. The elastic modulus of Ni-B-Mo coating is seen to maintain the lowest value within the complete working range in this current study. But, there is no specific trend is observed with different coating bath lement concentration individually.
- The Ni-B-Mo coated specimen is found to exhibit highest friction coefficient as well as highest wear rate due to rough surface and cracked morphology. The Ni-B-W coatings are found to possess lower COF and wear rate for its compact morphology, higher surface hardness as well as better resistance against plastic deformation.
- The corrosion resistance of as-depoisted Ni-B-Mo coated specimens are found to be the better than the other varints till mid level concentration. While Ni-B coated specimens are seen to possess better corrosion resistance at high level concentration due to higher boron content.

Overall, borohydride reduced electroless Ni-B-W coatings shows highest indentation and scratch hardness value compared to other two varints. The wear resistance is also seen to be better for Ni-B-W coatings due to its better surface hardness value. Whereas, the surface smoothening of any substrate may be done by the deposition of Ni-B or Ni-B-W coatings but within mid level concention only. The study also suggets that Ni-B-Mo coating is better choice to acts against corrosive medium but it is at the mid level concentration only. Hence, Ni-B-W coatings may be a better choice for tribological applications and Ni-B-Mo coatings may be a better choice for anti-corrosive applications. Electroless Ni-B coatings may also be a good choice for anti-corrosiive applications at higher concentrations.

7.2 Future scope

Few promising results have been obtained for electroless nickel-based coatings with the addition of boron, tungsten and molybdenum. But it is yet to ensure the industrial applications. Moreover, a lot of work need to be done to make the deposition process eco-friendly. The use of organic and sustainable stabilizers or deposition without stabilizers is at its very early stages. The electroless borohydride reduced coating are to be done at high temperatures. Hence, developing a coating bath for coating deposition at low temperatures is still a challenge. Another challenge in the borohydride reduced coatings is that the deposition coating without the use of ethylenediamine or replacement of ethylenediamine. the industrial application of electroless deposition still faces a major challenge because of the recycling, retreatment, and replenishment of coating baths. The current status of overall study of electroless coatings is not sufficient to ensure the practical feasibility and longevity of the technology. Therefore, it is imperative to conduct further investigation into these aspects to tackle the obstacles and fully explore the capabilities of this technology. Beyond its established role in augmenting resistance to wear and corrosion, electroless nickel-boron coatings hold significant promise for diversifying into various fields. For instance, deeper realization into the influence of the stabilizers on the coating's microstructure and morphology could enable the development of exceptionally smooth and lustrous deposits, rendering them ideal for decorative purposes. Moreover, development of textured surfaces suitable for hydrophobic properties could open avenues in areas such as self-cleaning coatings or biomedical devices.

Furthermore, there has been limited exploration into the conductivity and catalytic potential of electroless Ni-B coatings. These coatings hold promise for various applications like water splitting, supercapacitors, and catalysis. For illustration, exceptional conductivity of electroless Ni-B coatings could position them as excellent candidates for high-performance supercapacitors. On the other hand, their catalytic capabilities could be leveraged across diverse applications, such as hydrogen generation through water splitting. Hence, delving into these novel applications, one can utilize the full potential of electroless Ni-B coatings and make them more versatility for industries.

This page is intentionally left blank

References

- Afroukhteh, S. et al. 2012a. Preparation of Electroless Ni-P Composite Coatings Containing nano-scattered Alumina in Presence of Polymeric Surfactant. *Progress in Natural Science: Materials International*, 22(4), pp. 318-325. <https://doi.org/10.1016/j.pnsc.2012.06.006>.
- Afroukhteh, S. et al. 2012b. Preparation of the Ni-P Composite Coating Co-deposited by Nano TiC Particles and Evaluation of It's Corrosion Property. *Applied Surface Science*, 258(7), pp. 2597-2601. <https://doi.org/10.1016/j.apsusc.2011.10.101>.
- Agrawal, R. and Mukhopadhyay, A. 2022. Development of Ni-B Electroless Coating from Stabilizer Free Bath and Characterization of High Temperature Tribological Behaviour, Scratch and Corrosion Resistance. *Surface Topography: Metrology and Properties*, 10(4), p. 045028. <https://doi.org/10.1088/2051-672X/aca784>.
- Agrawal, R. and Mukhopadhyay, A. 2023. Inclusion of W in Electroless Ni-B Coating Developed from a Stabilizer Free Bath and Investigation of Its Tribological Behaviour. *Journal of the Indian Chemical Society*, 100(4), p. 100966. <https://doi.org/10.1016/j.jics.2023.100966>.
- Agrawal, R. et al. 2023. A Systematic Investigation of Lead-Free Electroless Ni-B-W Coating Properties using Taguchi's Methodology. *Coatings*, 13(9), 1585. <https://doi.org/10.3390/coatings13091585>.
- Alirezai, S. et al. 2005. Effect of Alumina Content on Wear Behaviour of Ni-P-Al₂O₃(α) Electroless Composite Coatings. *Surface Engineering*, 21(1), pp. 60-66. <https://doi.org/10.1179/174329305X23272>.
- Anik, M. et al. 2008. Effect of Coating Bath Composition on the Properties of Electroless Nickel-Boron Films. *Surface and Coatings Technology*, 202(9), pp. 1718-1727. <https://doi.org/10.1016/j.surfcoat.2007.07.031>.
- Araghi, A. and Paydar, M.H. 2010. Electroless Deposition of Ni-P-B₄C Composite Coating on AZ91D Magnesium Alloy and Investigation on Its Wear and Corrosion Resistance. *Materials & Design*, 31(6), pp. 3095-3099. <https://doi.org/10.1016/j.matdes.2009.12.042>.
- Ardakani, S.R. et al. 2017. Characterization of Ni-P-SiO₂-Al₂O₃ Nano-composite Coatings on Aluminum Substrate. *Materials Chemistry and Physics*, 189, pp. 207-214. <https://doi.org/10.1016/j.matchemphys.2016.12.023>.
- Arias, S. et al. 2019. Effect of Heat Treatment on Tribological Properties of Ni-B Coatings on Low Carbon Steel: Wear Maps and Wear Mechanisms. *Journal of Tribology*, 141(9), p. 091601. <https://doi.org/10.1115/1.4043906>.

- Ashassi-Sorkhabi, H. and Es'haghi, M. 2013. Corrosion Resistance Enhancement of Electroless Ni-P Coating by Incorporation of Ultrasonically Dispersed Diamond Nanoparticles. *Corrosion Science*, 77, pp. 185-193. <https://doi.org/10.1016/j.corsci.2013.07.046>.
- Aydeniz, A.I. et al. 2013. Electroless Ni-B-W Coatings for Improving Hardness, Wear and Corrosion Resistance. *Materials and Technology*, 47(6), pp. 803-806. <http://mail.imt.si/izvodi/mit136/aydeniz.pdf>
- Balaraju, J.N. et al. 2014. Nanocrystalline Electroless Nickel Poly-Alloy Deposition: Incorporation of W and Mo. *Transactions of the IMF*, 92(3), pp. 169-176. <https://doi.org/10.1179/0020296713Z.000000000123>.
- Balaraju, J.N. et al. 2016. Hardness and Wear Behaviour of Electroless Ni-B Coatings. *Materials Science and Technology*, 32(16), pp. 1654-1665. <https://doi.org/10.1080/02670836.2015.1137683>.
- Baldwin, C. and Such, T.E. 1968. The Plating Rates and Physical Properties of Electroless Nickel/Phosphorus Alloy Deposits. *Transactions of the IMF*, 46(1), pp. 73-80. <https://doi.org/10.1080/00202967.1968.11870052>.
- Banerjee, S. et al. 2022. Improving Corrosion Resistance of Magnesium Nano-composites by Using Electroless Nickel Coatings. *Facta Universitatis, Series: Mechanical Engineering*, 20(3), pp. 647-663. <https://doi.org/10.22190/FUME210714068B>.
- Barati, Q. and Hadavi, S.M.M. 2020. Electroless Ni-B and Composite Coatings: A Critical Review on Formation Mechanism, Properties, Applications and Future Trends. *Surfaces and Interfaces*, 21, p. 100702. <https://doi.org/10.1016/j.surfin.2020.100702>.
- Barker, D. 1993. Electroless Deposition of Metals. *Transactions of the IMF*, 71(3), pp. 121-124. [https://doi.org/10.1016/0376-4583\(81\)90138-2](https://doi.org/10.1016/0376-4583(81)90138-2)
- Baskaran, I. et al. 2006. Formation of Electroless Ni-B Coatings Using Low Temperature Bath and Evaluation of Their Characteristic Properties. *Surface and Coatings Technology*, 200(24), pp. 6888-6894. <https://doi.org/10.1016/j.surfcoat.2005.10.013>.
- Baudrand, D. and Bengston, J. 1995. Electroless Plating Processes: Developing Technologies for Electroless Nickel, Palladium, and Gold. *Metal Finishing*, 93(9), pp. 55-57. [https://doi.org/10.1016/0026-0576\(95\)99502-2](https://doi.org/10.1016/0026-0576(95)99502-2).

- Bekish, Y.N. et al. 2010. Electrodeposited Ni-B Alloy Coatings: Structure, Corrosion Resistance and Mechanical Properties. *Electrochimica Acta*, 55(7), pp. 2223-2231. <https://doi.org/10.1016/j.electacta.2009.11.069>.
- Berkh, O. et al. 1996. Properties of Electrodeposited NiP-SiC Composite Coatings. *Metal Finishing*, 94(3), pp. 35-40. [https://doi.org/10.1016/0026-0576\(96\)84169-9](https://doi.org/10.1016/0026-0576(96)84169-9).
- Bigdeli, F. and Allahkaram, S.R. 2009. An Investigation on Corrosion Resistance of As-applied and Heat-Treated NiP/nanoSiC Coatings. *Materials & Design*. 30(10), pp. 4450-4453. <https://doi.org/10.1016/j.matdes.2009.04.020>.
- Bonin, L. and Vitry, V. 2016. Mechanical and Wear Characterization of Electroless Nickel Mono and Bilayers and High Boron-Mid Phosphorus Electroless Nickel Duplex Coatings. *Surface and Coatings Technology*, 307, pp. 957-962. <https://doi.org/10.1016/j.surfcoat.2016.10.021>.
- Bonin, L. et al. 2018. Optimization of Electroless NiB Deposition Without Stabilizer, Based on Surface Roughness and Plating Rate. *Journal of Alloys and Compounds*, 767, pp. 276-284. <https://doi.org/10.1016/j.jallcom.2018.06.330>.
- Bonin, L. et al. 2019. The Tin Stabilization Effect on the Microstructure, Corrosion and Wear Resistance of Electroless NiB Coatings. *Surface and Coatings Technology*, 357, pp. 353-363. <https://doi.org/10.1016/j.surfcoat.2018.10.011>.
- Bonin, L. et al. 2020. Inorganic Salts Stabilizers Effect in Electroless Nickel-Boron Plating: Stabilization Mechanism and Microstructure Modification. *Surface and Coatings Technology*, 401, p. 126276. <https://doi.org/10.1016/j.surfcoat.2020.126276>.
- Bonin, L. et al. 2020. Replacement of Lead Stabilizer in Electroless Nickel-Boron Baths: Synthesis and Characterization of Coatings from Bismuth Stabilized Bath. *Sustainable Materials and Technologies*, 23, p. e00130. <https://doi.org/10.1016/j.susmat.2019.e00130>.
- Brenner, A. and Riddell, G.E. 1946. Nickel Plating on Steel by Chemical Reduction. *Journal of Research of the National Bureau of Standards*, 37(1), p. 31. <https://doi.org/10.6028/jres.037.019>.
- Budinski, K.G. 1988. *Surface Engineering for Wear Resistance*. Englewood Cliffs, N.J.: Prentice Hall.
- Bülbül, F. et al. 2012. Tribological and Corrosion Behaviour of Electroless Ni-B Coating Possessing a Blackberry Like Structure. *Metals and Materials International*, 18, pp. 631-637. <https://doi.org/10.1007/s12540-012-4011-1>.

- Bülbül, F. et al. 2013. Investigation of Structural, Tribological and Corrosion Properties of Electroless Ni-B Coating Deposited on 316L Stainless Steel. Proceedings of the Institution of Mechanical Engineers, Part J: Journal of Engineering Tribology, 227(6), pp. 629-639. <https://doi.org/10.1177/1350650112464928>.
- Çelik, İ. et al. 2016. Investigation of Structural and Tribological Properties of Electroless Ni-B Coated Pure Titanium. Proceedings of the Institution of Mechanical Engineers, Part J: Journal of Engineering Tribology, 230(1), pp. 57-63. <https://doi.org/10.1177/1350650115588568>.
- Correa, E. et al. 2013. Tribological Behavior of Electroless Ni-B Coatings on Magnesium and AZ91D Alloy. Wear, 305(1-2), pp. 115-123. <https://doi.org/10.1016/j.wear.2013.06.004>.
- Cullity, B.D. 1956. Elements of X-ray Diffraction. Addison-Wesley Publishing.
- Czagány, M. et al. 2017. The Influence of the Phosphorous Content and Heat Treatment on the Nano-micro-structure, Thickness and Micro-hardness of Electroless Ni-P Coatings on Steel. Applied Surface Science, 423, pp. 160-169. <https://doi.org/10.1016/j.apsusc.2017.06.168>.
- Dadkhah, M. et al. 2016. Thermal Treatment Synthesis of SnO₂ Nanoparticles and Investigation of Its Light Harvesting Application. Applied Physics A, 122, pp. 1-9. <https://doi.org/10.1007/s00339-016-0233-2>.
- Das, S.K. and Sahoo, P. 2011. Tribological Characteristics of Electroless Ni-B Coating and Optimization of Coating Parameters Using Taguchi Based Grey Relational Analysis. Materials & Design, 32(4), pp. 2228-2238. <https://doi.org/10.1016/j.matdes.2010.11.028>.
- De Minjer, C.H. and Brenner, A. 1957. Studies on Electroless Nickel Plating. Plating, 44(12), pp. 1297-1305.
- Delaunois, F. and Lienard, P. 2002. Heat Treatments for Electroless Nickel Boron Plating on Aluminium Alloys. Surface and Coatings Technology, 160(2-3), pp. 239-248. [https://doi.org/10.1016/S0257-8972\(02\)00415-2](https://doi.org/10.1016/S0257-8972(02)00415-2)
- Delaunois, F. et al. 2000. Autocatalytic Electroless Nickel-Boron Plating on Light Alloys. Surface and Coatings Technology, 124, pp. 201-209. [https://doi.org/10.1016/S0257-8972\(99\)00621-0](https://doi.org/10.1016/S0257-8972(99)00621-0).
- Dellasega, D. et al. 2017. Boron Films Produced by High Energy Pulsed Laser Deposition. Materials & Design, 134, pp. 35-43. <https://doi.org/10.1016/j.matdes.2017.08.025>.
- Dervos, C.T. et al. 2004. Vacuum Heat Treatment of Electroless Ni-B Coatings. Materials Letters, 58(5), pp. 619-623. [https://doi.org/10.1016/S0167-577X\(03\)00581-0](https://doi.org/10.1016/S0167-577X(03)00581-0).

- Domínguez-Ríos, C. et al. 2012. Measurement of Mechanical Properties of an Electroless Ni-B Coating Using Nanoindentation. *Industrial and Engineering Chemistry Research*, 51(22), pp. 7762-7768. <https://doi.org/10.1021/ie201760g>.
- Duari, S., et al. 2016. Investigation of Friction and Wear Properties of Electroless Ni-P-Cu Coating under Dry Condition. *Journal of Molecular and Engineering Materials*, 4(04), p. 1640013. <https://doi.org/10.1142/S225123731640013X>.
- Duncan, R.N. 1996. The Metallurgical Structure of Electroless Nickel Deposits: Effect on Coating Properties. *Plating and Surface Finishing*, 83(11), pp. 65-69. <https://www.nmfr.org/pdf/p1196j.pdf>
- Ebrahimian-Hosseinabadi, M. et al. 2006. Wear Behavior of Electroless Ni-P-B₄C Composite Coatings. *Wear*, 260(1-2), pp. 123-127. <https://doi.org/10.1016/j.wear.2005.01.020>.
- Evans, W.T. and Schlesinger, M. 1994. The Effect of Solution pH and Heat-Treatment on the Properties of Electroless Nickel Boron Films. *Journal of the Electrochemical Society*, 141(1), p. 78. <https://doi.org/10.1149/1.2054713>.
- Fan, X. et al. 2012. Improving Stability of Thermal Barrier Coatings on Magnesium Alloy with Electroless Plated Ni-P Interlayer. *Surface and Coatings Technology*, 206(21), pp. 4471-4480. <https://doi.org/10.1016/j.surfcoat.2012.05.004>.
- Farrokhzad, M.A. 2017. High Temperature Oxidation Behaviour of Autocatalytic Ni-P-BN(h) Coatings. *Surface and Coatings Technology*, 309, pp. 390-400. <https://doi.org/10.1016/j.surfcoat.2016.11.089>.
- Fetohi, A.E. et al. 2015. Development of Electroless Ni-P Modified Aluminum Substrates in a Simulated Fuel Cell Environment. *Journal of Industrial and Engineering Chemistry*, 30, pp. 239-248. <https://doi.org/10.1016/j.jiec.2015.05.028>.
- Gadhari, P. and Sahoo, P. 2016. Electroless Nickel-Phosphorus Composite Coatings: A Review. *International Journal of Manufacturing, Materials, and Mechanical Engineering*, 6(1), pp. 14-50. <https://doi.org/10.4018/IJMMME.2016010102>
- Gaevskaya, T.V. et al. 1996. The Effect of Boron on the Microstructure and Properties of Electrodeposited Nickel Films. *Metal Finishing*, 94(6), pp. 100-103. [https://doi.org/10.1016/0026-0576\(96\)83649-X](https://doi.org/10.1016/0026-0576(96)83649-X)
- Gawne, G.T. and Ma, U. 1988. Engineering Properties of Chromium Plating and Electroless and Electroplated Nickel. *Surface Engineering*, 4(3), pp. 239-249. <https://doi.org/10.1179/sur.1988.4.3.239>.

- Gay, P.A. et al. 2007. Characterisation and Mechanical Properties of Electroless NiP-ZrO₂ Coatings. *Surface and Coatings Technology*, 202(4-7), pp. 1167-1171. <https://doi.org/10.1016/j.surfcoat.2007.05.081>.
- Georgiza, E. et al. 2017. Production and Properties of Composite Electroless Ni-B-SiC Coatings. *Surface and Coatings Technology*, 325, pp. 46-51. <https://doi.org/10.1016/j.surfcoat.2017.06.019>.
- Ghaderi, M.M. et al. 2016. Investigation of High Temperature Wear Resistance of Electroless Nickel Coating with Different Contents of Phosphorous. *Protection of Metals and Physical Chemistry of Surfaces*, 52, pp. 538-542. <https://doi.org/10.1134/S2070205116030126>.
- Gilley, K.L. et al. 2012. Heat Treatments Modify the Tribological Properties of Nickel Boron Coatings. *ACS Applied Materials & Interfaces*, 4(6), pp. 3069-3076. <https://doi.org/10.1021/am3004297>.
- Goettems, F.S. and Ferreira, J.Z. 2017. Wear Behaviour of Electroless Heat Treated Ni-P Coatings as Alternative to Electroplated Hard Chromium Deposits. *Materials Research*, 20, pp. 1300-1308. <https://doi.org/10.1590/1980-5373-MR-2017-0347>.
- Goldenstein, A.W. et al. 1957. Structure of Chemically Deposited Nickel. *Journal of The Electrochemical Society*, 104(2), p. 104. <https://doi.org/10.1149/1.2428503>.
- Gorbunova, K.M. et al. 1973. Electroless Deposition of Nickel-Boron Alloys. *Journal of The Electrochemical Society*, 120(5), pp. 613-618. <https://doi.org/10.1149/1.2403514>.
- Gould, A.J. et al. 1981. Phosphorus Distribution in Electroless Nickel Deposits. *Surface Technology*, 12(1), pp. 93-102. [https://doi.org/10.1016/0376-4583\(81\)90140-0](https://doi.org/10.1016/0376-4583(81)90140-0).
- Gutzeit, G. 1955. Industrial Nickel Coating by Chemical Catalytic Reduction. *Transactions of the IMF*, 33(1), pp. 383-423. <https://doi.org/10.1080/00202967.1955.11869708>.
- Gutzeit, G. 1959. Catalytic Nickel Deposition from Aqueous Solution. *Plating and Surface Finishing*, 46, pp. 1158-1164.
- Gutzeit, G. and Mapp, E.T. 1954. 'KANIGEN' Chemical Nickel Plating. *Anti-Corrosion Methods and Materials*, 3(10), pp. 331-336. <https://doi.org/10.1108/eb019232>.
- Hamid, Z.A. et al. 2010. Influence of Deposition Temperature and Heat Treatment on the Performance of Electroless Ni-B Films. 205(7), pp. 2348-2354. <https://doi.org/10.1016/j.surfcoat.2010.09.025>.

Hosseini, M.G. et al. 2019. Pulse Plating of Ni-W-B Coating and Study of Its Corrosion and Wear Resistance. *Metallurgical and Materials Transactions A: Physical Metallurgy and Materials Science*, 50(11), pp. 5510-5524. <https://doi.org/10.1007/s11661-019-05444-1>.

Hsu, C.I. et al. 2015. The Effect of Incorporated Self-lubricated BN(h) Particles on the Tribological Properties of Ni-P/BN(h) Composite Coatings. *Applied Surface Science*, 357, pp. 1727-1735. <https://doi.org/10.1016/j.apsusc.2015.09.207>.

Islam, M. and Shehbaz, T. 2011. Effect of Synthesis Conditions and Post-Deposition Treatments on Composition and Structural Morphology of Medium-Phosphorus Electroless Ni-P Films. *Surface and Coatings Technology*, 205(19), pp. 4397-4400. <https://doi.org/10.1016/j.surfcoat.2011.03.042>.

Islam, M. et al. 2015. Electroless Ni-P/SiC Nanocomposite Coatings with Small Amounts of SiC Nanoparticles for Superior Corrosion Resistance and Hardness. *Journal of Materials Engineering and Performance*, 24, pp. 4835-4843. <https://doi.org/10.1007/s11665-015-1801-X>.

Jappes, J.T.W. et al. 2005. A Study on the Influence of Process Parameters on Efficiency and Crystallinity of Electroless Ni-P Deposits. *Journal of Materials Processing Technology*, 169(2), pp. 308-313. <https://doi.org/10.1016/j.jmatprotec.2005.03.010>.

Kanta et al. 2010. Nickel-Boron Electrochemical Properties Investigations. *Journal of Alloys and Compounds*, 505(1), pp. 151-156. <https://doi.org/10.1016/j.jallcom.2010.05.168>.

Kanta, A.F. et al. 2009a. Wear and Corrosion Resistance Behaviours of Autocatalytic Electroless Plating. *Journal of Alloys and Compounds*, 486(1-2), pp. L21-L23. <https://doi.org/10.1016/j.jallcom.2009.07.038>.

Kanta, A.F. et al. 2009b. Effect of Thermochemical and Heat Treatments on Electroless Nickel-Boron. *Materials Letters*, 63(30), pp. 2662-2665. <https://doi.org/10.1016/j.matlet.2009.09.031>.

Karthikeyan, S. and Ramamoorthy, B. 2014. Effect of Reducing Agent and Nano-Al₂O₃ Particles on the Properties of Electroless Ni-P Coating. *Applied Surface Science*, 307, pp. 654-660. <https://doi.org/10.1016/j.apsusc.2014.04.092>.

Kaya, B. et al. 2008. Preparation and Properties of Electroless Ni-B and Ni-B-nano-Composite Coatings. In *American Institute of Physics Conference Proceedings*, 1127(1), pp. 62-73. <https://doi.org/10.1063/1.3146199>.

- Kreye, V.A. et al. 1986. Barium can Replace Calcium in Calmodulin-Dependent Contractions of Skinned Renal Arteries of the Rabbit. *Pflügers Archiv*, 406, 308-311. <https://doi.org/10.1007/BF00640919>.
- Krishnan, K.H. et al. 2006. An Overall Aspect of Electroless Ni-P Depositions - A Review Article. *Metallurgical and Materials Transactions A*, 37, pp. 1917-1926. <https://doi.org/10.1007/s11661-006-0134-7>.
- Krishnaveni, K. et al. 2005. Electroless Ni-B Coatings Preparation and Evaluation of Hardness and Wear Resistance. *Surface and Coatings Technology*, 190(1), pp. 115-121. <https://doi.org/10.1016/j.surfcoat.2004.01.038>.
- Krishnaveni, K. et al. 2012. Electroless Ni-B-Si₃N₄ Composite Coating: Deposition and Evaluation of Its Characteristic Properties. *Synthesis and Reactivity in Inorganic, Metal-Organic, and Nano-Metal Chemistry*, 42(7), pp. 920-927. <https://doi.org/10.1080/15533174.2011.618475>.
- Kundu, S. et al. 2018. A Parametric Investigation of High Temperature Friction Performance of Electroless Ni-P Deposits. *Materials Today: Proceedings*, 5(2), pp. 8547-8556. <https://doi.org/10.1016/j.matpr.2017.11.552>.
- Lee, J.Y. and Lee, H.K. 2018. Electroless Ni-P Metallization on Palladium Activated Polyacrylonitrile (PAN) Fiber by Using a Drying Process. *Materials Chemistry and Physics*, 204, pp. 257-261. <https://doi.org/10.1016/j.matchemphys.2017.10.048>.
- Lekka, M. et al. 2018. Ni-B Electrodeposits with Low B Content: Effect of DMAB Concentration on the Internal Stresses and the Electrochemical Behaviour. *Surface and Coatings Technology*, 344, pp. 190-96. <https://doi.org/10.1016/j.surfcoat.2018.03.018>.
- Li, D. et al. 2017. Enhancing Structure Integrity and Corrosion Resistance of Mg Alloy by a Two- Step Deposition to Avoid F Ions Etching to Nano-SiO₂ Reinforcement. *Journal of Alloys and Compounds*, 705, pp. 70-78. <https://doi.org/10.1016/j.jallcom.2017.01.204>.
- Liu, X. et al. 2013. Grain Size Effect on the Hardness of Nanocrystal Measured by the Nano-size Indenter. *Applied Surface Science*, 279, pp. 159-166. <https://doi.org/10.1016/j.apsusc.2013.04.062>.
- Liu, Y.Y. et al. 2007. Synthesis and Tribological Behavior of Electroless Ni-P-WC Nanocomposite Coatings. *Surface and Coatings Technology*, 201(16-17), pp. 7246-7251. <https://doi.org/10.1016/j.surfcoat.2007.01.035>.

- Loto, C.A. 2016. Electroless Nickel Plating - A Review. *Silicon*, 8, pp. 177-186. <https://doi.org/10.1007/s12633-015-9367-7>.
- Luo, H. et al. 2015. Development of Electroless Ni-P/nano-WC Composite Coatings and Investigation on Its Properties. *Surface and Coatings Technology*, 277, pp. 99-106. <https://doi.org/10.1016/j.surfcoat.2015.07.011>.
- Ma, C. et al. 2014. Effect of Heat Treatment on Structures and Corrosion Characteristics of Electroless Ni-P-SiC Nano-composite Coatings. *Ceramics International*, 40(7), pp. 9279-9284. <https://doi.org/10.1016/j.ceramint.2014.01.150>.
- Maclean, J.D. and Karten, S.M. 1954. A Practical Application of Electroless Nickel Plating. *Plating*, 41(11), pp. 1284-1287.
- Madah, F. et al. 2015. Investigations on the Wear Mechanisms of Electroless Ni-B Coating During Dry Sliding and Endurance Life of the Worn Surfaces. *Surface and Coatings Technology*, 282, pp. 6-15. <https://doi.org/10.1016/j.surfcoat.2015.09.003>.
- Makkar, P. et al. 2014. Wear Characteristics of Mechanically Milled TiO₂ Nanoparticles Incorporated in Electroless Ni-P Coatings. *Advanced Powder Technology*, 25(5), pp. 1653-1660. <https://doi.org/10.1016/j.appt.2014.05.018>.
- Mallory, G. 1991. The Fundamental Aspects of Electroless Nickel Plating. *Electroless Plating: Fundamentals and Applications*, William Andrew, pp. 1-56.
- Matsubara, H. et al. 2007. Co-deposition Mechanism of Nanodiamond with Electrolessly Plated Nickel Films. *Electrochimica Acta*, 52(9), pp. 3047-3052. <https://doi.org/10.1016/j.electacta.2006.09.043>.
- Miri, T. et al. 2021. Electroless Ni-B-MMT Nanocomposite on Magnesium Alloy. *Surface Engineering*, 37(9), pp. 1194-1205. <https://doi.org/10.1080/02670844.2021.1959287>.
- Mohanty, D. et al. 2019. Characterisation and Corrosion Study of Electroless Nickel-Boron Coating Reinforced with Alumina Nanoparticles. *Materials Today: Proceedings*, 19(2), pp. 317-321. <https://doi.org/10.1016/j.matpr.2019.07.216>.
- Mukhopadhyay, A. 2019. Tribological Characteristics of Electroless Ni-B-W-Mo Coatings under Dry Sliding Condition. *Journal of Manufacturing Technology Research*, 11(1/2), pp. 13-23.
- Mukhopadhyay, A. et al. 2017. Tribological Behavior of Sodium Borohydride Reduced Electroless Nickel Alloy Coatings at Room and Elevated Temperatures. *Surface and Coatings Technology*, 321, pp. 464-476. <https://doi.org/10.1016/j.surfcoat.2017.05.015>

- Mukhopadhyay, A. et al. 2018a. "Effect of Heat Treatment on the Characteristics of Electroless Ni-B, Ni-B-W and Ni-B-Mo Coatings, Materials Today: Proceedings, 5(2), pp. 3306-3315. <https://doi.org/10.1016/j.matpr.2017.11.573>.
- Mukhopadhyay, A. et al. 2018b. Comparative Study of Tribological Behavior of Electroless Ni-B, Ni-B-Mo, and Ni-B-W Coatings at Room and High Temperatures. Lubricants, 6(3), p. 67. <https://doi.org/10.3390/lubricants6030067>.
- Mukhopadhyay, A. et al. 2018c. Effect of Heat Treatment on Microstructure and Corrosion Resistance of Ni-B-W-Mo Coating Deposited by Electroless Method. Surface Review and Letters, 25(08), p. 1950023. <https://doi.org/10.1142/S0218625X19500239>.
- Mukhopadhyay, A. et al. 2018d. Effect of Heat Treatment on the Characteristics of Electroless Ni-B, Ni-B-W and Ni-B-Mo Coatings. Materials Today: Proceedings, 5(2), pp. 3306-3315. <https://doi.org/10.1016/j.matpr.2017.11.573>.
- Mukhopadhyay, A. et al. 2018e. Effect of Heat Treatment on Tribological Behavior of Electroless Ni-B-Mo Coatings at Different Operating Temperatures. Silicon, 10, pp. 1203-1215. <https://doi.org/10.1007/s12633-017-9594-1>.
- Mukhopadhyay, A. et al. 2018f. Effect of Operating Temperature on Tribological Behavior of As-plated Ni-B Coating Deposited by Electroless Method. Tribology Transactions, 61(1), pp. 41-52. <https://doi.org/10.1080/10402004.2016.1271929>.
- Mukhopadhyay, A. et al. 2018g. Tribological Behavior of Electroless Ni-B-W Coating at Room and Elevated Temperatures. Proceedings of the Institution of Mechanical Engineers, Part J: Journal of Engineering Tribology, 232(11), pp. 1450-1466. <https://doi.org/10.1177/1350650118755781>.
- Mukhopadhyay, A. et al. 2018h. Wear and Friction Characteristics of Electroless Ni-B-W Coatings at Different Operating Temperatures. Materials Research Express, 5(2), p. 026526. <https://doi.org/10.1088/2053-1591/aae5a>.
- Mukhopadhyay, A. et al. 2019. Tribological Characteristics of Electroless Ni-B-Mo Coatings at Different Operating Temperatures. Surface Review and Letters, 26(4), p. 1850175. <https://doi.org/10.1142/S0218625X18501755>.
- Mukhopadhyay, A. et al. 2021. Co-deposition of W and Mo in Electroless Ni-B Coating and Its Effect on the Surface Morphology, Structure, and Tribological Behavior. Proceedings of the Institution of Mechanical Engineers, Part L: Journal of Materials: Design and Applications, 235(1), pp. 149-161. <https://doi.org/10.1177/1464420720956270>

- Musil, J. et al. 2002. Relationships Between Hardness, Young's Modulus and Elastic Recovery in Hard Nanocomposite Coatings. *Surface and Coatings Technology*, 154(2-3), pp. 304-313. [https://doi.org/10.1016/S0257-8972\(01\)01714-5](https://doi.org/10.1016/S0257-8972(01)01714-5).
- Narayanan, T.S.N.S. and Seshadri, S.K. 2004. Formation and Characterization of Borohydride Reduced Electroless Nickel Deposits. *Journal of Alloys and Compounds*, 365(1-2), pp. 197-205. [https://doi.org/10.1016/S0925-8388\(03\)00680-7](https://doi.org/10.1016/S0925-8388(03)00680-7).
- Nemane, V. and Chatterjee, S. 2020. Scratch and Sliding Wear Testing of Electroless Ni-B-W Coating. *Journal of Tribology*, 142(2), p. 021705. <https://doi.org/10.1115/1.4045165>.
- Nemane, V. et al. 2022. Tribological Electroless Ternary Ni-B-W Coatings: A Suitable Alternative to Hard Chromium Coatings. *Journal of Tribology*, 144(12), p. 121401. <https://doi.org/10.1115/1.4055409>.
- Niksefat, V. and Ghorbani, M. 2015. Mechanical and Electrochemical Properties of Ultrasonic-Assisted Electroless Deposition of Ni-B-TiO₂ Composite Coatings. *Journal of Alloys and Compounds*, 633, pp. 127-136. <https://doi.org/10.1016/j.jallcom.2015.01.250>.
- Novák, M. et al. 2010. Influence of Heat Treatment on Tribological Properties of Electroless Ni-P and Ni-P-Al₂O₃ Coatings on Al-Si Casting Alloy. *Applied Surface Science*, 256(9), pp. 2956-2960. <https://doi.org/10.1016/j.apsusc.2009.11.057>.
- Oraon, B. et al. 2007. Parametric Optimization and Prediction of Electroless Ni-B Deposition. *Materials & Design*, 28(7), pp. 2138-2147. <https://doi.org/10.1016/j.matdes.2006.05.017>.
- Pal, S. and Jayaram, V. 2018. Effect of Microstructure on the Hardness and Dry Sliding Behavior of Electroless Ni-B Coating. *Materialia*, 4, pp. 47-64. <https://doi.org/10.1016/j.mtla.2018.09.004>.
- Pal, S. et al. 2011. Characterization of Phase Transformation Behaviour and Microstructural Development of Electroless Ni-B Coating. *Materials Science and Engineering A*, 528(28), pp. 8269-8276. <https://doi.org/10.1016/j.msea.2011.07.060>.
- Pal, S. et al. 2018. Characterization of Thermal Stability and High-Temperature Tribological Behavior of Electroless Ni-B Coating. *Metallurgical and Materials Transactions A: Physical Metallurgy and Materials Science*, 49, pp. 3217-3236. <https://doi.org/10.1007/s11661-018-4599-y>.
- Palaniappa, M. and Seshadri, S.K. 2008. Friction and Wear Behavior of Electroless Ni-P and Ni-W-P Alloy Coatings. *Wear*, 265(5-6), pp. 735-740, <https://doi.org/10.1016/j.wear.2008.01.002>.

- Pancrecius, J.K. et al. 2018. Metallic Composite Coatings by Electroless Technique - A Critical Review. *International Materials Reviews*, 63(8), pp. 488-512.
<https://doi.org/10.1080/09506608.2018.1506692>.
- Park, I.C. and Kim, S.J. 2018. Cavitation Erosion Behavior in Seawater of Electroless Ni-P Coating and Process Optimization Using Taguchi Method. *Applied Surface Science*, 477, pp. 37-43. <https://doi.org/10.1016/j.apsusc.2018.02.033>.
- Rabizadeh, T. et al. 2010. An Investigation on Effects of Heat Treatment on Corrosion Properties of Ni-P Electroless Nano-coatings. *Materials & Design*, 31(7), pp. 3174-3179. <https://doi.org/10.1016/j.matdes.2010.02.027>.
- Radwan, A.B. et al. 2015. Improvement in Properties of Ni-B Coatings by the Addition of Mixed Oxide Nanoparticles. *International Journal of Electrochemical Science*, 10(9), pp. 7548-7562. <http://hdl.handle.net/10576/34855>.
- Raju, P.R.M. et al. 2015. Effect of Reinforcement of Nano-Al₂O₃ on Mechanical Properties of Al₂O₃/Ni-B NMMCs. *Materials Today: Proceedings*, 2(4-5), pp. 3712-3717. <https://doi.org/10.1016/j.matpr.2015.07.152>.
- Ranganatha, S. et al. 2012. Process and Properties of Electroless Ni-Cu-P-ZrO₂ Nanocomposite Coatings. *Materials Research Bulletin*, 47(3), pp. 635-645. <https://doi.org/10.1016/j.materresbull.2011.12.024>.
- Rao, Q.L. et al. 2005. Microstructure Evolution of Electroless Ni-B Film During Its Depositing Process. *Applied Surface Science*, 240(1-4), pp. 28-33. <https://doi.org/10.1016/j.apsusc.2004.07.059>.
- Riddle, Y.W. and Bailer, T.O. 2005. Friction and Wear Reduction via an Ni-B Electroless Bath Coating for Metal Alloys. *JOM*, 57(4), pp. 40-45. <https://doi.org/10.1007/s11837-005-0080-7>.
- Riedel, W. 1991. *Electroless Nickel Plating*. Metals Park, Ohio: ASM International, Stevenage, England: Finishing Publications Ltd.
- Romero-Romero, M. et al. 2017. Electroless Ni-B Coating onto TiH₂ Powder: An Approach for a Simplified Surface Preparation. *Surface and Coatings Technology*, 315, pp. 181-187. <https://doi.org/10.1016/j.surfcoat.2017.02.038>.
- Sadreddini, S. and Afshar, A. 2014. Corrosion Resistance Enhancement of Ni-P-nano SiO₂ Composite Coatings on Aluminum. *Applied Surface Science*, 303, pp. 125-130. <https://doi.org/10.1016/j.apsusc.2014.02.109>.

Sadreddini, S. et al. 2017. Corrosion Behavior and Microhardness of Ni-P-SiO₂-Al₂O₃ Nano-composite Coatings on Magnesium Alloy. *Journal of Materials Engineering and Performance*, 26, pp. 2032-2039. <https://doi.org/10.1007/s11665-017-2632-8>.

Sahoo, P. and Das, S.K. 2011. Tribology of Electroless Nickel Coatings - A Review. *Materials & Design*, 32(4), pp. 1760-1775. <https://doi.org/10.1016/j.matdes.2010.11.013>.

Sarret, M. et al. 2006. Electroless NiP Micro- and Nano-composite Coatings. *Surface and Coatings Technology*, 201(1-2), pp. 389-395. <https://doi.org/10.1016/j.surfcoat.2005.11.127>.

Serin, I.G. and Göksenli, A. 2015. Effect of Annealing Temperature on Hardness and Wear Resistance of Electroless Ni-B-Mo Coatings. *Surface Review and Letters*, 22 (5), p. 1550058. <https://doi.org/10.1142/S0218625X15500584>.

Serin, I.G. et al. 2015. Effect of Annealing Temperature on the Corrosion Resistance of Electroless Ni-B-Mo Coatings. *Journal of Materials Engineering and Performance*, 24(8), pp. 3032-3037. <https://doi.org/10.1007/s11665-015-1568-0>.

Sha, W. et al. 2011. 1-Introduction to Electroless Copper and Nickel-Phosphorus (Ni-P) Depositions. *Electroless Copper and Nickel-Phosphorus Plating*, pp. 1-2, Elsevier. <https://doi.org/10.1533/9780857090966.1>.

Shakoor, R.A. et al. 2014. Properties of Electrodeposited Ni-B-Al₂O₃ Composite Coatings. *Materials & Design*, 64, pp. 127-135. <https://doi.org/10.1016/j.matdes.2014.07.026>

Sharma, A. and Singh, A.K. 2013. Electroless Ni-P and Ni-P-Al₂O₃ Nanocomposite Coatings and Their Corrosion and Wear Resistance. *Journal of Materials Engineering and Performance*, 22, pp. 176-183. <https://doi.org/10.1007/s11665-012-0224-1>.

Sharma, S. and Sharma, S. 2016. Co-deposition of Synthesized ZnO Nanoparticles into Ni-P Matrix Using Electroless Technique and Their Corrosion Study. *Journal of Materials Engineering and Performance*, 25(10), pp. 4383-4393. <https://doi.org/10.1007/s11665-016-2292-0>.

Shi, L.T. et al. 2016. Effects of Cobalt Content on Mechanical and Corrosion Properties of Electroless Ni-Co-P/TiN Nanocomposite Coatings. *Materials and Corrosion*, 67(10), pp. 1034-1041. <https://doi.org/10.1002/maco.201608844>.

Soleimani, R. et al. 2015. Development of Mathematical Model to Evaluate Microstructure and Corrosion Behavior of Electroless Ni-P/nano-SiC Coating Deposited on 6061 Aluminum Alloy. *Journal of Industrial and Engineering Chemistry*, 23, pp. 328-337. <https://doi.org/10.1016/j.jiec.2014.09.002>.

- Sribalaji, M. et al. 2016. Nanoindentation and Nanoscratch Behavior of Electroless Deposited Nickel-Phosphorous Coating. *Materials Chemistry and Physics*, 177, pp. 220-228. <https://doi.org/10.1016/j.matchemphys.2016.04.022>.
- Srinivasan, K.N. et al. 2010. Studies on Development of Electroless Ni-B Bath for Corrosion Resistance and Wear Resistance Applications. *Surface Engineering*, 26(3), pp. 153-158. <https://doi.org/10.1179/174329409X409468>.
- Srivastava, A. et al. 1992. Factors Influencing the Deposition Rate of Ni-B Electroless Films. *International Journal of Materials Research*, 83(4), pp. 251-253. <https://doi.org/10.1515/ijmr-1992-830408>.
- Sudagar, J. et al. 2013. Electroless Nickel, Alloy, Composite and Nano Coatings - A Critical Review. *Journal of Alloys and Compounds*, 571, pp. 183-204. <https://doi.org/10.1016/j.jallcom.2013.03.107>.
- Sukackienė, Z. et al. 2020. Electroless Deposition of Nickel Boron Coatings Using Morpholine Borane as a Reducing Agent. *Chemija*, 31(1), pp. 1-10. <https://doi.org/10.6001/chemija.v31i1.4167>.
- Sürdem, S. et al. 2019. A Parametric Study on the Relationship between NaBH_4 and Tribological Properties in the Nickel-Boron Electroless Depositions. *Materials Research Express*, 6(12), 125085. <https://doi.org/10.1088/2053-1591/ab5beb>.
- Szunerits, S. and Thouin, L. 2007. Microelectrode Arrays. *Handbook of Electrochemistry*, Elsevier, pp. 391-428. <https://doi.org/10.1016/B978-044451958-0.50023-9>.
- Taha-Tijerina, J. et al. 2019. Tribological Evaluation of Electroless Ni-B Coating on Metal-Working Tool Steel. *International Journal of Advanced Manufacturing Technology*, 103(5-8), pp. 1959-1964. <https://doi.org/10.1007/s00170-019-03684-4>
- Tomlinson, W.J. and Carroll, M.W. 1990. Substrate Roughness, Deposit Thickness and the Corrosion of Electroless Nickel Coatings. *Journal of Materials Science*, 25, pp. 4972-4976. <https://doi.org/10.1007/BF00580115>.
- Townsend, H.E. 1994. 'ASM Handbook: Vol 05 Surface Engineering, ASM Handbook.' American Society for Metals, Ohio.
- Tsujikawa, S. 2005. Reconstruction of General Scalar-Field dark Energy Models. *Physical Review D*, 72(8), p. 083512. <https://link.aps.org/doi/10.1103/PhysRevD.72.083512>.

- Venkatakrishnan, P.G. and Karthik, V. 2019. Structural, Morphological and Mechanical Properties of Electroless Ni-B Based Alloy Coatings. In *Materials Today: Proceedings*, 27(3), pp. 2360-2363. <https://doi.org/10.1016/j.matpr.2019.09.129>.
- Vitry, V. and Bonin, L. 2017. Increase of Boron Content in Electroless Nickel-Boron Coating by Modification of Plating Conditions. *Surface and Coatings Technology*, 311, pp. 164-171. <https://doi.org/10.1016/j.surfcoat.2017.01.009>
- Vitry, V. et al. 2008. Mechanical Properties and Scratch Test Resistance of Nickel-Boron Coated Aluminium Alloy After Heat Treatments. *Surface and Coatings Technology*, 202(14), pp. 3316-3324. <https://doi.org/10.1016/j.surfcoat.2007.12.001>.
- Vitry, V. et al. 2010. Initiation and Formation of Electroless Nickel-Boron Coatings on Mild Steel: Effect of Substrate Roughness. *Materials Science and Engineering: B*, 175(3), pp. 266-273. <https://doi.org/10.1016/j.mseb.2010.08.003>.
- Vitry, V. et al. 2011. Mechanical and Wear Characterization of Electroless Nickel-Boron Coatings. *Surface and Coatings Technology*, 206(7), pp. 1879-1885. <https://doi.org/10.1016/j.surfcoat.2011.08.008>.
- Vitry, V. et al. 2012. Experimental Study on the Formation and Growth of Electroless Nickel-Boron Coatings from Borohydride-Reduced Bath on Mild Steel. *Applied Surface Science*, 263, pp. 640-647. <https://doi.org/10.1016/j.apsusc.2012.09.126>.
- Vitry, V. et al. 2014. Comparison of Various Electroless Nickel Coatings on Steel: Structure, Hardness and Abrasion Resistance. In *Materials Science Forum*, 783-786, pp. 1405-1413. Trans Tech Publications Ltd. <https://doi.org/10.4028/www.scientific.net/msf.783-786.1405>.
- Vitry, V. et al. 2022. Recent Advances in Electroless Nickel-Boron Coatings. *Surface and Coatings Technology*, 429, p. 127937. <https://doi.org/10.1016/j.surfcoat.2021.127937>
- Wan, Y. et al. 2016. Corrosion and Tribological Performance of PTFE-Coated Electroless Nickel Boron Coatings. *Surface and Coatings Technology*, 307, pp. 316-23. <https://doi.org/10.1016/j.surfcoat.2016.09.001>.
- Wang, H.L. et al. 2014. Effect of Novel Ternary Ligand System on Acidic Electroless Ni-P Plating on AZ91D Magnesium Alloy. *Transactions of Nonferrous Metals Society of China (English Edition)*, 24(9), pp. 3014-3022. [https://doi.org/10.1016/S1003-6326\(14\)63439-7](https://doi.org/10.1016/S1003-6326(14)63439-7).
- Wang, W. et al. 2016. Ductile Electroless Ni-P Coating onto Flexible Printed Circuit Board. *Applied Surface Science*, 367, pp. 528-532. <https://doi.org/10.1016/j.apsusc.2016.01.254>.

- Wang, Y. et al. 2015. Duplex Ni-P-ZrO₂/Ni-P Electroless Coating on Stainless Steel. *Journal of Alloys and Compounds*, 630, pp. 189-194. <https://doi.org/10.1016/j.jallcom.2015.01.064>.
- Wang, Y. et al. 2015. Microstructure and Properties of Sol-enhanced Ni-Co-TiO₂ Nanocomposite Coatings on Mild Steel. *Journal of Alloys and Compounds*, 649, pp. 222-228. <https://doi.org/10.1016/j.jallcom.2015.07.147>.
- Watanabe, T. and Tanabe, Y. 1983. The Lattice Images of Amorphous-like Ni-B Alloy Films Prepared by Electroless Plating Method. *Transactions of the Japan Institute of Metals*, 24(6), pp. 396-404. <https://doi.org/10.2320/matertrans1960.24.396>.
- Wei, P.J. and Lin, J.F. 2005. A New Method Developed to Evaluate Both the Hardness and Elastic Modulus of a Coating-Substrate System. *Surface and Coatings Technology*, 200(7), pp. 2489-2496. <https://doi.org/10.1016/j.surfcoat.2004.09.013>.
- Wu, X. et al. 2015. Improving the Properties of 211Z Al Alloy by Enhanced Electroless Ni-P-TiO₂ Nanocomposite Coatings with TiO₂ Sol. *Surface and Coatings Technology*, 270, pp. 170-174. <https://doi.org/10.1016/j.surfcoat.2015.03.006>.
- Wurtz, M.A. 1844. On the Hydruret of Copper. *The London, Edinburgh, and Dublin Philosophical Magazine and Journal of Science*, 25(164), pp. 154-156. <https://doi.org/10.1080/14786444408644956>
- Xie, Z. and Shan, S. 2018. Nanocontainers-Enhanced Self-healing Ni Coating for Corrosion Protection of Mg Alloy. *Journal of Materials Science*. 53(5), pp. 3744-3755. <https://doi.org/10.1007/s10853-017-1774-2>.
- Xu, H. et al. 2005. Synthesis and Properties of Electroless Ni -P-Nanometer Diamond Composite Coatings. *Surface and Coatings Technology*, 191(2-3), pp. 161-165. <https://doi.org/10.1016/j.surfcoat.2004.03.045>.
- Yazdani, S. and Mahboubi, F. 2019. Comparison Between Microstructure, Wear Behavior, and Corrosion Resistance of Plasma-Nitrided and Vacuum Heat-Treated Electroless Ni-B Coating. *Journal of Bio-and Tribo-Corrosion*, 5, pp. 1-11. <https://doi.org/10.1007/s40735-019-0264-2>.
- Yazdani, S. et al. 2018. Investigation of Wear Behavior of As-plated and Plasma-Nitrided Ni-B-CNT Electroless having Different CNTs Concentration. *Applied Surface Science*, 457, pp. 942-955. <https://doi.org/10.1016/j.apsusc.2018.07.020>.

- Yildiz, R.A. et al. 2013. Effect of Annealing Temperature on the Corrosion Resistance of Electroless Produced Ni-B-W Coatings. *Advanced Materials Research*, 651, pp. 263-268. <https://doi.org/10.4028/www.scientific.net/AMR.651.263>.
- Yildiz, R.A. et al. 2017. Effect of Heat Treatments for Electroless Deposited Ni-B and Ni-W-B Coatings on 7075 Al Alloy. *International Journal of Materials, Mechanics and Manufacturing*, 5(2), pp. 83-86. <https://doi.org/10.18178/ijmmm.2017.5.2.295>.
- Yu, L. 2011. Preparation and Characterization of Ni-P-nanoTiN Electroless Composite Coatings. *Journal of Alloys and Compounds*. 509(10), pp. 4154-4159. <https://doi.org/10.1016/j.jallcom.2011.01.025>.
- Yunacti, M. et al. 2021. Characterization of Electroless Nickel-Boron Deposit from Optimized Stabilizer-Free Bath. *Coatings*, 11(5), p. 576. <https://doi.org/10.3390/coatings11050576>.
- Yunacti, M. et al. 2021. Corrosion Resistance of Electroless Nickel-Boron Coating in a Bath Exempt from Stabilizer. *Materials Proceedings*, 6(1), p. 35. <https://doi.org/10.3390/CMDWC2021-10038>.
- Zhou, Y. et al. 2003. The Effects of Triple Junctions and Grain Boundaries on Hardness and Young's Modulus in Nanostructured Ni-P. *Scripta Materialia*, 48(6), pp. 825-830. [https://doi.org/10.1016/s1359-6462\(02\)00511-0](https://doi.org/10.1016/s1359-6462(02)00511-0).
- Ziyuan, S. et al. 2006. Nanocrystalline Ni-B Coating Surface Strengthening Pure Copper. *Applied Surface Science*, 253(3), pp. 1051-1054. <https://doi.org/10.1016/j.apsusc.2005.12.169>.

This page is intentionally left blank

Publications from the Thesis

This page is intentionally left blank

Materials Research Express



PAPER

Effect of borohydride concentration on tribological and mechanical behavior of electroless Ni-B coatings

RECEIVED
27 September 2019REVISED
13 November 2019ACCEPTED FOR PUBLICATION
18 November 2019PUBLISHED
29 November 2019Manik Barman, Tapan Kumar Barman and Prasanta Sahoo¹

Department of Mechanical Engineering, Jadavpur University, Kolkata 700032, India

¹ Author to whom any correspondence should be addressed.E-mail: psjume@gmail.com

Keywords: electroless Ni-B, COF, wear, nano-indentation, nano-scratch, corrosion

Abstract

Electroless Nickel boron (Ni-B) coatings were deposited over mild steel substrates to study the effect of borohydride concentration on tribological behaviour and mechanical properties. Three different types of coating bath solutions were used to deposit coatings. The as-deposited coatings were characterised based on surface morphology, composition and phase structure using scanning electron microscopy (SEM), energy dispersive spectroscopy (EDS) and x-ray diffraction (XRD), respectively. Friction and wear behaviour of the as-deposited coatings were evaluated by pin-on-disc tribo-tester. Coefficient of friction of the coatings decreases with the increase in borohydride concentration. Surface hardness, elastic modulus and scratch resistance behaviour of the coatings were evaluated using the data obtained by nano-indentation techniques. It is seen that the surface hardness and elastic modulus of the as-deposited coatings increase with the increase in borohydride concentrations. Electrochemical impedance spectroscopy (EIS) and potentiodynamic polarisation tests were conducted to analyse corrosion behaviour of the coatings against a corrosive environment of 3.5% NaCl solution. The corrosion test results displayed an increasing trend of corrosion resistance as the borohydride concentration increases in the coating bath solution.

1. Introduction

Electroless coating is a deposition process by the action of chemical reaction of reducing agents present in the coating bath solution and without the use of electricity. The application of electroless coatings are increasing day by day since the inception of it by Brenner and Riddell in 1946 [1], in the industries for tribological applications due to their excellent physical, mechanical, electrical, corrosion and tribological behaviour. Electroless nickel-boron coatings are widely used in aerospace, chemical and electrical industries due to its high hardness, excellent friction and wear behaviour [2, 3]. Borohydride reduced electroless nickel-boron coating has been developed and characterized based on various parameters like deposition rate, coating thickness, surface morphology, effect of substrate nature etc [4–7]. The properties of the coatings can be modified by varying the bath composition of the coating bath solution [8] and operating conditions [9, 10] according to the requirement which can be further modified with heat treatment [9, 11–13]. It was found that the electroless Ni-B coating can be deposited from a low temperature coating bath with the addition of complexing agent and stabilizer but the deposition rate is less compared to high temperature bath [14]. The coatings obtained at a temperature below 80 °C exhibits amorphous structure which transforms into crystalline structure upon heat treatment [15]. The deposition rate decreases with plating time while it increases with coating bath temperature [14, 15]. The deposition rate of the coating can be improved with the addition of dimethylaminoborane (DMAB) in the coating bath solution [16]. On the other hand, boron content of the electroless Ni-B coatings increases with the increase in plating bath temperature [15] and it also varies with concentration of sodium borohydride present in the coating bath [14]. The properties of the Ni-B coatings mainly depend on the amount of boron present in the coatings and the changes in phase structure as well as surface morphology due to heat treatment [17]. Electroless Ni-B coatings exhibits nano-crystalline structure


This page is intentionally left blank

Effect of Coating Bath Parameters on Properties of Electroless Nickel-Boron Alloy Coatings

Manik Barman, Heritage Institute of Technology, India

Tapan Kumar Barman, Jadavpur University, India

Prasanta Sahoo, Jadavpur University, India

 <https://orcid.org/0000-0002-1538-0646>

ABSTRACT

Electroless nickel-boron binary coatings were obtained with various bath compositions to investigate the effect of bath parameters on tribological and mechanical behaviours of the coating. Characterisation of the coating for surface morphology and phase structure is done using scanning electron microscopy (SEM) and x-ray diffraction (XRD), respectively, whereas tribological behaviour of coatings is evaluated on a pin-on-disc tribo-tester. Elastic modulus and surface hardness of coatings have been obtained using nano-indentation technique, while the scratch behaviour of the coatings has been determined using micro-scratch test. Corrosion resistance of coatings is also determined. It is observed that surface roughness of the coatings increased with increase in sodium borohydride concentration but decreased slightly with increase in nickel chloride concentration. Friction and wear characteristics are found to increase with surface roughness which occurs due to increased boron content. Surface hardness and scratch hardness are also seen to vary with coating bath parameters.

KEYWORDS

Bath Parameter, Corrosion, Electroless Coating, Friction Coefficient, Nano-Indentation, Nickel-Boron, Scratch, Wear

1. INTRODUCTION

The electroless coating developed by Brenner and Riddell in 1946 (Brenner and Riddell 1946) is a plating process in absence of electricity. Electroless coating has become popular gradually since the time of invention for its excellent properties. Electroless nickel-phosphorous coating is well known for its mechanical properties and nickel-boron coating is popular for its tribological properties. The use of electroless coatings can be found in industries like automobile, chemical, oil, gas and aerospace for their excellent mechanical, physical and tribological behaviours. Chemically deposited nickel-boron coatings were analysed based on deposition rate, plating thickness, surface morphology and surface texture etc. (Anik et al. 2008; Kanta et al. 2009; Kanta et al. 2010; Hamid et al. 2010; Bonin et al. 2019; Mohanty et al. 2019; Sukackiene et al. 2020). Coating characteristics depend on the


DOI: 10.4018/IJSEIMS.2022010101

Copyright © 2022, IGI Global. Copying or distributing in print or electronic forms without written permission of IGI Global is prohibited.

This page is intentionally left blank

Effect of heat-treatment temperature and borohydride concentration on corrosion behaviour of ENB coating

Proc IMechE Part C:
J Mechanical Engineering Science
2023, Vol. 237(1) 183–200
© IMechE 2022
Article reuse guidelines:
sagepub.com/journals-permissions
DOI: 10.1177/09544062221117677
journals.sagepub.com/home/pic
SAGE

Manik Barman, Tapan Kumar Barman and Prasanta Sahoo 

Abstract

Electroless Ni-B (ENB) alloy coatings are extensively used due to their good tribological, physical, electrical and mechanical properties. The behaviour of coatings generally depends on the concentration of bath parameters, heat-treatment temperature, as well as heat-treatment duration. The current study was carried out to deposit coatings over steel specimens with various NaBH_4 concentrations and heat-treated at various temperatures to study the significance of NaBH_4 concentration as well as heat-treatment temperature on corrosion resistance of the Ni-B coatings. Ni-B coatings were heat-treated for an hour at different temperatures for example, 350°C, 450°C and 550°C. Electrochemical impedance spectroscopy (EIS) and Potentiodynamic polarization (PDP) test methods were employed to analyse the corrosion behaviour of the as-deposited as well as heat-treated coatings. The tests were conducted against a corrosive environment consisting of 3.5% NaCl solution. It was observed that the as-deposited coatings with low boron content exhibit a mixture of amorphous and nanocrystalline structures. The same gradually becomes amorphous with the rise in sodium borohydride concentration. The increase in boron content with sodium borohydride concentration in the coating bath led to the transformation of phase structure. This amorphous phase structure of as-deposited coatings further transforms into a crystalline structure upon heat treatment. This crystallinity increases with heat-treatment temperature. The as-deposited coatings show cauliflower-like surface morphology at all concentrations of NaBH_4 but the same becomes a coarse-grained structure with clustered aggregates leading to a rough surface. The as-deposited coatings show better corrosion resistance behaviour compared to heat-treated ones, especially at the higher temperature.

Keywords

Electroless Ni-B, heat-treatment, bath composition, EIS, corrosion resistance

Introduction

The coatings are normally used to provide a protective layer over the base metal or to change the surface behaviours of the parent metal. A thin film of coating may improve surface smoothness, tribological behaviour, corrosion resistance, hardness against indentation as well as scratch etc. Therefore, it is better to deposit a coating layer as per the requirement instead of changing the base metal. The soft coatings are used in packaging industries, mobile phone casings, automotive industries for soft touch feeling interior purposes etc. The hard coatings are found to be used in automobile industries like bearings, oil seal valves, cylinder liners, piston rings for tribological applications, gas turbine blades and knife sharpeners against severe conditions. The various coatings are deposited through various deposition techniques like thermal spray coating, PVD, CVD, electrodeposition, electroless coatings etc. The electroless coating deposition

technique is named due to the absence of electricity for coating. The ENB coatings are popular for their tribological and mechanical properties. The borohydrides reduced ENB coatings normally show cauliflower or broccoli-like surface morphology in as-deposited conditions which helps in improving the tribological behaviour by reducing the actual surface contact area.^{1–3} The presence of boron-like hard particles helps to improve the surface hardness of steel substrate due to the addition of an ENB alloy coating layer over it.⁴ The ENB coatings have been studied on the basis of coating deposition rate, surface

Department of Mechanical Engineering, Jadavpur University, Kolkata, India

Corresponding author:

Prasanta Sahoo, Department of Mechanical Engineering, Jadavpur University, 188 Raja S C Malik Road, Kolkata 700032, India.
Emails: psjume@gmail.com; prasanta.sahoo@jadavpuruniversity.in

This page is intentionally left blank

TRIBO-MECHANICAL CHARACTERIZATION OF ENB ALLOY COATINGS: EFFECT OF HEAT-TREATMENT TEMPERATURE AND SODIUM BOROHYDRIDE CONCENTRATION

Manik Barman, Tapan Kumar Barman, Prasanta Sahoo

Department of Mechanical Engineering, Jadavpur University, Kolkata, India

Abstract. *Previously electroless Ni-B (ENB) coatings were analyzed and optimized based on various coating parameters. However, variation of nano-indentation behaviour like nano-hardness, elastic modulus and scratch hardness variation with bath composition and heat treatment temperature has not been reported earlier. An attempt has been made to explore the same in the present study. ENB coating layers are deposited on AISI 1040 steel specimen with varying concentration of sodium borohydride (NaBH_4) and heat-treated at 350°C, 450°C and 550°C to investigate the related effects. Nano-hardness and elastic modulus of as-coated specimens are found to improve with NaBH_4 concentration due to increased boron content and nodule size. Both nano-hardness and elastic modulus are observed to improve further upon heat treatment because of incorporation of various boride phases leading to compact morphology and increased size of the nodules. Scratch hardness value also increases with NaBH_4 concentration and it improves further upon heat treatment and reaches to its maximum at 450°C due to presence of compact and hard Ni_2B phase. Compact homogeneous surface morphology enhances the friction and wear behaviour of the heat-treated coatings even though surface roughness deteriorates after heat treatment.*

Key words: ENB, Heat-treatment, COF, Wear, Nano-hardness, Micro-scratch

1. INTRODUCTION

ENB alloy coatings are known to have improved tribological behaviour due to their cauliflower-like surface morphology which helps to improve frictional behaviour by reducing the real contact area [1, 2]. ENB coatings also enhance the surface hardness of mild steel substrate [3, 4]. The coatings have also been investigated on the basis of different parameters like plating rate, thickness, surface morphology, surface roughness, surface hardness, tribological behaviour etc. [3, 4]. It was observed that the coating's behaviour

Received August 14, 2022 / Accepted October 25, 2022

Corresponding author: Prasanta Sahoo

Department of Mechanical Engineering, Jadavpur University, Kolkata 700032, India

E-mail: psjume@gmail.com; prasanta.sahoo@jadavpuruniversity.in

© 2020 by University of Niš, Serbia | Creative Commons License: CC BY-NC-ND

This page is intentionally left blank



Tribo-Mechanical Characterisation of Borohydride Reduced Ni–B–W Coatings

Manik Barman^{1,2} · Tapan Kumar Barman² ·
Prasanta Sahoo²

Received: 23 January 2023 / Accepted: 16 March 2023
© The Institution of Engineers (India) 2023

Abstract The borohydride reduced electroless coatings are widely used for their excellent tribological, physical and mechanical behaviours. The coating behaviours are dependent on its compositions. The addition of hard particles into Ni–B matrix may alter the coating composition and ultimately lead to modification in coating behaviours. Hence, electroless Ni–B–W coatings were developed on

Keywords Electroless coating · Ni–B–W · Bath parameter · COF · Wear · Elastic modulus · Nano-hardness · Scratch-hardness

Introduction

AISI 1040 steel substrate to understand the significance of tungsten concentration in tribo-mechanical behaviour of the W reinforced ternary coatings. The surface roughness of the coating was seen to increase significantly with sodium borohydride concentration though the surface roughness is lower (0.185) at lower concentrations of sodium borohydride relative to substrate (0.285). But the roughness values did not vary much with nickel chloride concentration as well as sodium tungstate. The SEM results of as-coated specimens reveal the cauliflower-like surface morphology which is useful for the reduction in friction and wear of the coatings. The elemental analysis results obtained from EDAX show an increase in tungsten concentration from 2.8 to 4.2% with the increase in bath level concentration leading to increase in surface hardness obtained from nano-indentation technique and the scratch hardness obtained from micro-scratch tests. The nano-hardness and scratch hardness were also observed to improve with nickel chloride, sodium borohydride concentration in the coating bath solution.

The electroless coatings are generally applied over any substrate to provide some protection or modify the surface behaviour of base metal. The electroless coatings find its wide applicability in chemical, electrical and aerospace industries for its excellent tribo-mechanical behaviours. The borohydride reduced coated specimens usually possess cauliflower-like surface morphology leads to improvement in friction and wear resistance due to the reduction in real contact area [1, 2]. The ENB coatings are also known to enhance the hardness of steel [3–5]. The characteristics of coatings vary with their chemical composition, surface morphology, and phase structure. These further depend on coating process, chemical composition, and coating bath operating conditions. The dependency of coating characteristics on different coatings parameters like plating rate, thickness, surface morphology, and surface roughness effect, etc., have already been studied by many researcher [6–8]. The coating behaviours are also found to change with heat treatment due to modification of surface morphology, phase structure [9, 10]. The chemical content in the coatings also changes with bath composition and the operating temperature, pH, etc. [6, 8, 11, 12]. The coated layers obtained with low sodium borohydride in the solution possess crystalline structure due to low boron content in the as-deposited coatings [8, 13, 14]. It is also found to co-exist the crystalline and amorphous phase structure for coatings obtained from medium level of borohydride concentration which is observed to transform into amorphous phase due to increase in borohydride

✉ Prasanta Sahoo
psjume@gmail.com; prasanta.sahoo@jadavpuruniversity.in

¹ Department of Mechanical Engineering, Heritage Institute of Technology, Kolkata, India

² Department of Mechanical Engineering, Jadavpur University, Kolkata, India

This page is intentionally left blank

Engineering Research Express



PAPER

Tribomechanical behaviour of electroless Ni-B-Mo coatings with varying bath composition

RECEIVED
2 February 2023REVISED
31 May 2023ACCEPTED FOR PUBLICATION
9 June 2023PUBLISHED
21 June 2023Manik Barman^{1,2}, Tapan Kumar Barman² and Prasanta Sahoo^{2,*} ¹ Department of Mechanical Engineering, Heritage Institute of Technology, Kolkata, India² Department of Mechanical Engineering, Jadavpur University, Kolkata, India

* Author to whom any correspondence should be addressed.

E-mail: psjume@gmail.com and prasanta.sahoo@jadavpuruniversity.in

Keywords: electroless coating, Ni-B-Mo, bath composition, COF, wear, nano-indentation, micro-scratch

Abstract

Ni-B-Mo alloy coating layers are developed on steel substrates with various coating bath compositions to investigate the significance of bath parameters on coating characteristics. The as-deposited coatings are characterized based on surface roughness, coating thickness, surface morphology, and phase structure through Surface Roughness Tester, Scanning Electron Microscopy (SEM), and x-ray Diffraction (XRD), respectively. Tribological behaviour of the coated layers is investigated through a pin-on-disc multi-tribo tester under dry condition. Surface hardness and elastic modulus are measured through nano-indentation tests. The scratch-hardness of the coatings is measured using a micro-scratch tester. Coating characteristics are determined and the significance of each coating bath parameter is analysed. It is found that the coating thickness increases with bath parameter concentration level due to increase in borohydride concentration. The increase in molybdenum

concentration increases the surface roughness (R_a) from $0.28 \mu\text{m}$ to $1.05 \mu\text{m}$ and forms coarse grained surface morphology with some visible cracks leading to increase in COF value from 0.24 to 0.77. Nano-hardness and scratch hardness are found to decrease with the addition of molybdenum into the Ni-B matrix though nano-hardness (Hv) value increases from its minimum value of 530 to 971 due to the increase in boron concentration. The elastic modulus value is found to vary from 83 GPa to 197 GPa but no such specific trend may be observed with the variation of bath composition.

1. Introduction

Chemical deposition or electroless coating method is well known to improve the surface behaviour of base metal which helps to achieve required properties in materials to use in different applications. Electroless nickel-boron (ENB) coating possesses good tribological behaviour. Chemically deposited borohydride-reduced ENB coatings generally exhibit dense and compact nodules forming cauliflower-like surface morphology. This helps in the reduction of actual contact area between mating surfaces to improve the tribological behaviour [1, 2]. Borohydride reduced binary alloy coatings are further observed to enhance the hardness of steel specimen with the addition of ENB film [3–6]. The characteristics of coatings vary with their chemical composition, surface morphology, as well as phase structure. These features may be altered as per the requirement by controlling the deposition process, chemical composition, and coating bath operating conditions [3–6]. The dependency of coating characteristics on different coating parameters like plating rate, thickness, surface morphology, surface roughness effect, etc have already been studied in previous works [7–9]. The coating behaviours are also found to change with heat treatment duration and temperature due to modification of surface morphology as well as phase structure after heat treatment [10, 11]. The chemical content in the coating also changes with coating bath composition and operating temperature, pH, etc [7, 9, 12, 13]. The coated layers obtained with low sodium borohydride in the solution possess crystalline structure due to low boron content in the as-deposited condition [9, 14, 15]. It is also found to co-exist the crystalline and amorphous phase structure for coatings obtained from a

This page is intentionally left blank



Corrosion Behaviour of Borohydride Reduced Ni–B, Ni–B–W, Ni–B–Mo, Ni–B–W–Mo Coatings with Varying Composition: A Comparison

Manik Barman^{1,2} · Tapan Kumar Barman² ·
Prasanta Sahoo²

Received: 11 August 2023 / Accepted: 11 October 2023
© The Institution of Engineers (India) 2023

Abstract The borohydride reduced binary (Ni–B), ternary (Ni–B–W, Ni–B–Mo) and quaternary (Ni–B–W–Mo) alloy coatings are deposited by chemical deposition method. The same coatings are used to study the variation in corrosion behaviour of the coatings with the inclusion of W, Mo individually or together. The coatings are deposited over steel substrate with changing bath composition to study the role of coating bath parameters on corrosion resistance behaviour. The coating characterisation based on roughness, morphology and phase structure are performed using stylus type roughness tester, scanning electron microscopy (SEM) and x-ray diffraction (XRD), respectively. A potentiostat is employed to measure corrosion response of the coatings by

potentiodynamic polarisation (PDP) and electrochemical impedance spectroscopy (EIS) test method. The tests are carried out using a corrosive medium of 3.5% NaCl solution. All the coatings are observed to exhibit cauliflower like surface morphology. The roughness of the coatings increases with bath parameter concentration. The corrosion resistance of the Ni–B–Mo coatings are found to be better than other three variants till mid-level of concentrations. The Ni–B coated specimens show higher corrosion resistance at higher level of concentrations compared to the ternary and quaternary coatings.

Keywords Electroless coating · Ni–B · Ni–B–W · Ni–B–Mo · Ni–B–W–Mo · Bath composition · Corrosion resistance

✉ Prasanta Sahoo
psjume@gmail.com

¹ Department of Mechanical Engineering, Heritage Institute of Technology, Kolkata, India

² Department of Mechanical Engineering, Jadavpur University, Kolkata, India

Introduction

The coatings are generally used as a protective layer over a substrate to prevent the base material from harsh environment or to achieve a surface property which the base material does not possess. Different soft coatings are used for packaging, providing soft touch feelings in interior decorations, mobile phone covers etc. The hard coatings are used widely starting from domestic purposes to decorate or as protective layer in automobile industries over the base metal surface to protect against corrosion, abrasion etc. These coatings may be deposited over the base metal using different methods like electrodeposition, PVD, CVD, electroless methods. The

electroless nickel-based coatings are being used widely for their excellent physical, mechanical, and tribological behaviours. Thin film coatings may be developed using chemical deposition process or electroless coating methods. Thin film nickel-based coatings are deposited using electroless method to make smooth surface and improve corrosion behaviour, surface hardness and the wear resistance.

The electroless nickel-boron (ENB) coatings are well known for their tribological behaviour. The ENB coatings are widely known for its friction and wear performance because of its cauliflower like morphology [1–3] and electroless nickel-phosphorous coatings are well known for their mechanical behaviour [4]. The addition of boron or phosphorous like hard elements into coating enhances the hardness of steel specimens [4, 5]. Chemically deposited ENB coated specimens are evaluated for plating rate, thickness, morphology, etc. [4–9]. Coating characteristics are known to vary with composition and operating conditions [1–6]. The coating characteristics may also be altered upon heat treatment [8, 9]. The amorphous phase of coatings in untreated conditions transform into crystalline structure after heat treatment [5–9]. These are also found to depend on coating

This page is intentionally left blank



PAPER

Tribological behavior of electroless Ni-B ternary and quaternary coatings with inclusion of W and Mo

RECEIVED
26 October 2023REVISED
13 December 2023ACCEPTED FOR PUBLICATION
29 December 2023PUBLISHED
10 January 2024Manik Barman^{1,2} , Tapan Kumar Barman² and Prasanta Sahoo^{2,*} ¹ Department of Mechanical Engineering, Heritage Institute of Technology, Kolkata, India² Department of Mechanical Engineering, Jadavpur University, Kolkata, India

* Author to whom any correspondence should be addressed.

E-mail: psjume@gmail.com and prasanta.sahoo@jadavpuruniversity.in

Keywords: electroless Ni-B, W, Mo, surface roughness, COF, wear

Abstract

Electroless nickel coatings help to tailor requisite surface properties in materials for use in various applications. The aim of the present study is to examine the tribological behavior of electroless nickel-boron coatings incorporated with Mo and W. The coated layers are developed over pin samples with various bath compositions. The coated specimens are characterised to assess their basic features. The tribological tests are carried out with the help of a pin-on-disc tribo-tester under dry conditions. The coating characteristics are determined to comprehend the importance of tungsten as well as molybdenum concentration in electroless nickel-boron coatings. In the as-deposited state, all the coated specimens displayed a surface morphology resembling cauliflower. Moreover, the roughness of these coated surfaces in their as-deposited state showed an increase corresponding to the concentration of the bath parameter, resulting in a higher coefficient of friction (COF). The addition of Mo into Ni-B matrix promotes the coarse grained and cracked surface morphology leading to highest friction coefficient value of as-deposited Ni-B-Mo coatings. The highest surface roughness of

Ni-B-Mo coatings also leads to the highest specific wear rate due to breaking and crushing of roughness peaks. The present study reveals the effect of incorporation of W and Mo in electroless Ni-B coatings to control the friction and wear characteristics of the specimens. This will help in deciding the proper electroless bath compositions for specific tribological applications.

1. Introduction

The materials are protected against harsh environments by providing a coating layer over it. There are different types of coatings like soft coating or hard coatings used for different purposes. These coatings are developed using various techniques such as electro-deposition, physical vapour deposition, chemical vapour deposition, chemical deposition technique etc. The thin film coated specimens are developed through chemical deposition process or electroless process to achieve smooth surface, improve corrosion resistance, enhance hardness against indentation or scratch and improve the performance against wear. The chemically deposited Ni-B (ENB) like thin film is popular due to its excellent friction and wear characteristics. The electroless Ni-B coated specimens possess very good tribological behavior due to their surface morphology [1–3]. The surface hardness of uncoated steel substrate gets increased after the Ni-B coating layer deposits over it [4, 5]. The characteristic of ENB coatings, such as deposition rate, thickness, morphology is thoroughly studied [4–9]. The coated specimen behavior is observed to change depending on their composition as well as operating conditions like coating bath temperature, pH [1–5]. The coating characteristics may further be modified with the phase transformation upon heat treatment [8–11]. The morphology as well as phase structure are found to depend on the composition of coatings [7–10]. The changes of coating composition led to change the morphology and phase structure which ultimately altered the surface hardness and wear behavior [5, 6, 8, 12]. These two are further seen to enhance with boron concentration [11, 13] which may further be improved by annealing [8, 14] due to formation of Ni₂B, Ni₃B phases upon annealing [8, 9, 14–16]. The elastic modulus and surface hardness both are found to

This page is intentionally left blank



Effects of W and Mo Concentrations on Mechanical Behaviour of Ni–B Based Coatings—A Comparative Study

Manik Barman^{1,2} · Tapan Kumar Barman² ·
Prasanta Sahoo²

Received: 16 January 2024 / Accepted: 6 March 2024
© The Institution of Engineers (India) 2024

Abstract The coatings are utilised on any materials as a protective layer. The coating characteristics are dependent on their composition, phase structure and surface morphology. In this current investigation, the coated specimens are developed by chemical deposition method with the incorporation of tungsten (W) and molybdenum (Mo) either

alone or jointly into Ni–B matrix. The coatings are studied to make a comparative analysis on mechanical behaviours of the as-deposited coatings to understand the impact of bath parameters. Steel made square samples are coated with borohydride reduced coatings with various compositions. The coating characterisations are carried out for the elemental analysis of the coated specimens as well as their surface morphology. The coated layer thicknesses are found to rise due to rise in concentration for all types of coatings under study. The nanoindentation tests are conducted to determine elastic modulus and nanohardness. The scratch hardness tests are carried out using a micro-scratch tester. The boron concentration is found to increase with chemical solution element concentrations which contribute to increase the nanohardness. The nanohardness of Ni–B–W–Mo coatings is found to be better than untreated binary and ternary coatings at higher compositions. The scratch hardness of untreated Ni–B–W coatings is observed to possess its maximum value across the examined range due to the presence of boron and tungsten. The nanohardness and scratch hardness of untreated Ni–B–Mo coatings

increase with concentration level in the coating bath but remained lower than other variants.

Keywords Ni–B · W · Mo · Composition · Nanoindentation · Elastic modulus · Scratch hardness

Abbreviations

BM	Electroless Ni–B–Mo coating
BW	Electroless Ni–B–W coating
BWM	Electroless Ni–B–W–Mo coating
EDAX	Energy dispersive X-ray analysis
HL	Higher level
LL	Lower level
ML	Middle level
NB	Electroless Ni–B coating
SEM	Scanning electron microscopy
XRD	X-ray diffraction

Introduction

The coatings are used for the purpose of surface modification of any material if it does not have the required characteristics. There are various coatings like soft coatings, hard coatings. The soft coatings are usually used for interior decoration purpose or aesthetic modifications to have a soft touch feeling etc. The hard coatings find their applications in industrial uses like anticorrosion, to prevent scratch or indentation, abrasion etc. The soft or hard coatings may be developed by various methods such as electroplating, electroless plating, CVD, PVD, thermal spray. The electroless coating deposition process is also a similar process which uses chemical reaction without electricity. The electroless nickel-based coated specimens are known to possess good physical, mechanical, and tribological

✉ Prasanta Sahoo
psjume@gmail.com; prasanta.sahoo@jadavpuruniversity.in

¹ Department of Mechanical Engineering, Heritage Institute of Technology, Kolkata, India

² Department of Mechanical Engineering, Jadavpur University, Kolkata, India

Manik Barman
16/07/24

This page is intentionally left blank